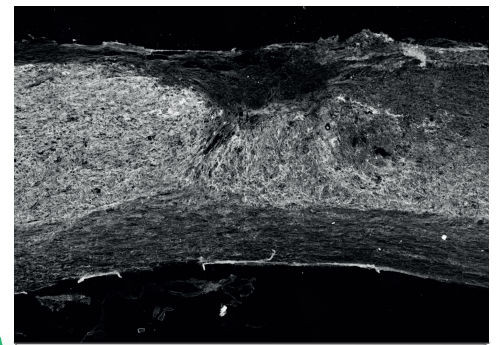
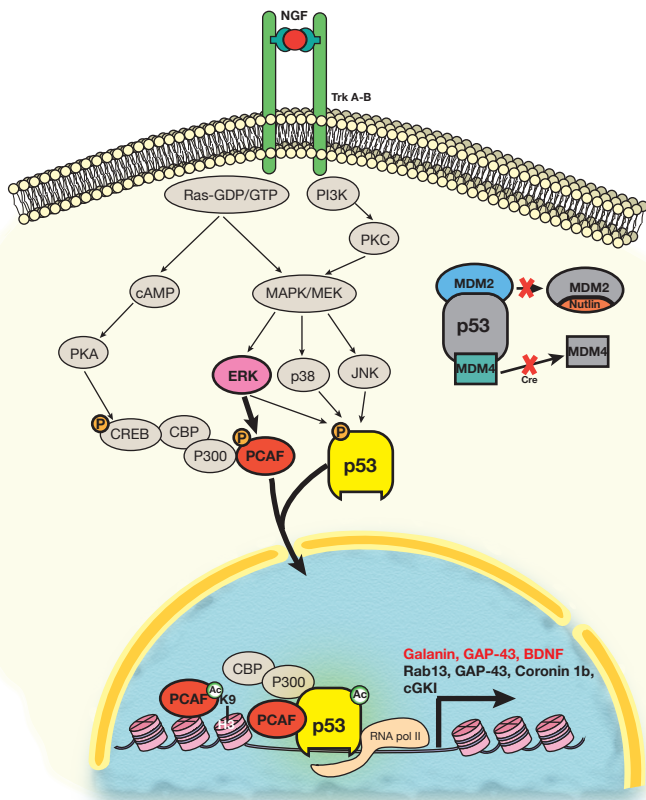


# Promoting Regeneration and Functional Recovery following SCI through Transcriptional Regulation



Marília Grando Sória

Promoting Regeneration and Functional Recovery following SCI  
through Transcriptional Regulation

Dissertation

zur Erlangung des Grades eines  
Doktors der Naturwissenschaften

der Mathematisch-Naturwissenschaftlichen Fakultät  
und  
der Medizinischen Fakultät  
der Eberhard-Karls-Universität Tübingen

vorgelegt

von

**Marília Grando Sória**  
aus Cascavel (Paraná), Brasilien

August - 2015





Tag der mündlichen Prüfung: .....

Dekan der Math.-Nat. Fakultät: Prof. Dr. W. Rosenstiel

Dekan der Medizinischen Fakultät: Prof. Dr. I. B. Autenrieth

1. Berichterstatter: Prof. Dr. Simone Di Giovanni

2. Berichterstatter: Prof. Dr. Burkhard Schlosshauer

Prüfungskommission: Prof. Dr. Simone Di Giovanni

Dr. Jing Hu

Prof. Dr. Burkhard Schlosshauer

PD Dr. Andrea Wizenmann

**Erklärung / Declaration:**

Ich erkläre, dass ich die zur Promotion eingereichte Arbeit mit dem Titel:

„Promoting Regeneration and Functional Recovery following SCI through Transcriptional Regulation“

selbständig verfasst, nur die angegebenen Quellen und Hilfsmittel benutzt und wörtlich oder inhaltlich übernommene Stellen als solche gekennzeichnet habe. Ich versichere an Eides statt, dass diese Angaben wahr sind und dass ich nichts verschwiegen habe. Mir ist bekannt, dass die falsche Abgabe einer Versicherung an Eides statt mit Freiheitsstrafe bis zu drei Jahren oder mit Geldstrafe bestraft wird.

*I hereby declare that I have produced the work entitled “Promoting Regeneration and Functional Recovery following SCI through Transcriptional Regulation”, submitted for the award of a doctorate, on my own (without external help), have used only the sources and aids indicated and have marked passages included from other works, whether verbatim or in content, as such. I swear upon oath that these statements are true and that I have not concealed anything. I am aware that making a false declaration under oath is punishable by a term of imprisonment of up to three years or by a fine.*

Tübingen, den .....

Datum / Date

.....

Unterschrift /Signature

## ABSTRACT

Spinal cord injury (SCI) is a devastating condition due to the permanent neurological deficits it causes, and the abruptness these impairments take place. To date there is no curative therapy for SCI, therefore finding efficient treatment candidates for clinical translation is a compelling need.

The deficits associated to SCI result from the disruption of the normal anatomy followed by a complex cascade of events involving excitotoxicity, ischemia and inflammation. This leads to death of neurons, oligodendrocytes and demyelination. Moreover, reactive glial cells proliferate in the attempt to restrain the spread of damage, building up a physical and molecular barrier – the glial scar. However, the glial scar also represents an obstacle to axonal regrowth. Furthermore, in contrast to neurons in the periphery, adult central neurons do not normally regenerate due to an intrinsic inability to reactivate the growth machinery.

With the purpose of promoting regeneration and functional recovery after SCI in adult mice, in this work we addressed different but interdependent molecular mechanisms to awake the intrinsic growth machinery of central neurons and to modulate the extrinsic environment within the injury site.

Firstly, we performed the first systematic screening comparing epigenetic regulatory mechanisms between the PNS and CNS after injury. As a result, we showed that the injury-driven retrograde signaling controls the activation of the acetyltransferase PCAF in the dorsal root ganglia system. PCAF in turn leads to chromatin remodeling and activation of genes associated to nerve regeneration. This successful regenerative response promoted sprouting of dorsal column fibers only when the SCI was preceded by a peripheral branch injury. Most importantly, forced expression of PCAF in dorsal root ganglia neurons led to axon growth after SCI, mimicking the effects of a preconditioning injury.

It was already known that PCAF also forms a multiprotein complex with CBP/P300 and p53, a pleiotropic factor, to drive the transcription of several regeneration associated genes. p53 is indeed a key orchestrator of CNS regeneration, playing a pivotal role in activating the intrinsic regenerative capacity of post-mitotic CNS neurons in addition to modulate the extrinsic environment. Thus, our second strategy was to manipulate p53 in order to enhance the p53-dependent regenerative response and improve functional recovery. By

disrupting the p53 interaction with its main negative regulators MDM2 or MDM4, either by local Nutlin-3a inhibition or conditional deletion in SMC neurons, respectively, we enhanced p53 transactivation. This led in fact to increased sprouting of descending tracts and improved locomotor behavior of adult mice after SCI without increasing cell death. Furthermore, we showed for the first time that these pro-regenerative effects of p53 are dependent on IGF1 signaling.

In the p53 studies, Nutlin-3a, a potent MDM2 inhibitor, was employed as a drug of choice. Nutlin-3a is already under scrutiny in clinical trials for cancer therapy and might be clinically available in the near future. Therefore this work opens an exciting possibility to bring a new candidate for translation in the SCI clinical context.

## LIST OF FIGURES

<b>Figure I.</b> Spinal cord injury by WHO Global Regions from traumatic causes 1959–2011	2
<b>Figure II.</b> Pathophysiology of SCI	4
<b>Figure III.</b> Schematic representation of the injury site following CNS trauma	8
<b>Figure IV.</b> Increased nuclear PCAF and H3K9ac following SNA but not DCA	14
<b>Figure V.</b> ERK retrograde signalling controls PCAF activation	16
<b>Figure VI.</b> PCAF is required for conditioning-dependent axonal regrowth after SCI	18
<b>Figure VII.</b> PCAF overexpression induces spinal axonal regeneration	19
<b>Figure VIII.</b> p53-mediated decision-making processes in neurons	25
<b>Figure IX.</b> Control of p53 stability by Mdm2 homo-oligomers and Mdm2–Mdmx hetero-oligomers	29
<b>Figure X.</b> Infection and labeling of SMC layer-V neurons	30
<b>Figure XI.</b> Conditional deletion of MDM4 in the sensorimotor cortex enhances corticospinal tract sprouting following T9 dorsal hemisection in MDM4 <sup>fl</sup> mice	32
<b>Figure XII.</b> Schematic illustration of the osmotic minipump/intrathecal catheter system	33
<b>Figure XIII.</b> Spinal cord immunoblotting after Nutlin-3 or vehicle delivery	34
<b>Figure XIV.</b> MDM2/p53 inhibition via Nutlin-3 delivery enhances neurological recovery and corticospinal tract regeneration following T9 dorsal hemisection	37
<b>Figure XV.</b> MDM2/p53 inhibition via Nutlin-3 delivery enhances 5-HT axonal sprouting and functional recovery via IGF1 following T9 dorsal hemisection	37
<b>Figure XVI.</b> Nutlin-3 reduces the size of the fibronectin-positive core scar area and the density of CD11b <sup>+</sup> cells at the injury site	38
<b>Figure XVII.</b> Restoration of function after spinal cord injury might arise from anatomical plasticity of damaged or spared connections	44

## LIST OF ABBREVIATIONS

<b>5-HT</b>	5-hydroxytryptamine	<b>GAP-43</b>	Growth associated protein 43
<b>AAV</b>	Adeno-associated virus	<b>GAPDH</b>	Glyceraldehyde-3-phosphate dehydrogenase
<b>AKT</b>	Protein kinase B	<b>GFAP</b>	Glial fibrillary acidic protein
<b>APAF</b>	Apoptotic protease activating factor	<b>GFP</b>	Green fluorescent protein
<b>ARF-BP1/ Mule</b>	HECT, UBA And WWE domain containing 1, E3 ubiquitin protein ligase	<b>GNAT</b>	GCN5-related N-acetyltransferase
<b>ATF</b>	Activating transcription factor	<b>H3</b>	Histone H3
<b>BAX</b>	BCL2-associated X protein	<b>HAT</b>	Histone acetyltransferase
<b>BBB</b>	Blood brain barrier	<b>HDAC</b>	Histone deacetylase
<b>Bcl2</b>	B-cell CLL/lymphoma 2	<b>IGF1</b>	Insulin-like growth factor
<b>BDA</b>	Biotin dextran tetramethylrhodamine	<b>IGF1R</b>	IGF-1 receptor
<b>BDNF</b>	Brain-derived neurotrophic factor	<b>IHC</b>	Immunohistochemistry
<b>BMP4</b>	Bone morphogenetic protein 4	<b>JAK</b>	Janus kinase
<b>BMS</b>	Basso Mouse Scale	<b>JNK</b>	c-Jun N-terminal kinase
<b>C/EBP</b>	CCAAT-enhancer-binding protein	<b>KLF</b>	Kruppel-like factor
<b>cAMP</b>	Cyclic adenosine monophosphate	<b>L1CAM</b>	L1 cell adhesion molecule
<b>CAP-23</b>	Brain abundant, membrane attached signal protein 1	<b>LINGO-1</b>	Leucine rich repeat and Ig domain containing 1
<b>CBP</b>	CREB-binding protein	<b>LPS</b>	Lipopolysaccharide
<b>CGI</b>	CpG island	<b>MAG</b>	Myelin-associated glycoprotein
<b>cGKI</b>	cGMP-dependent protein kinase type I	<b>MDM2</b>	Mouse double minute 2
<b>cGMP</b>	Cyclic guanosine monophosphate	<b>MDM4</b>	Mouse double minute 4
<b>ChiP</b>	Chromatin immunoprecipitation	<b>MEK</b>	Mitogen-activated protein kinase kinase
<b>CNS</b>	Central nervous system	<b>mTOR</b>	Mammalian target of rapamycin
<b>CORO1B</b>	Coronin, actin binding protein, 1B	<b>NCAM</b>	Neural cell adhesion molecule
<b>CPG</b>	Central pattern generator	<b>NG2</b>	Chondroitin sulfate proteoglycan 4
<b>CREB</b>	cAMP response element-binding protein	<b>NGF</b>	Nerve growth factor
<b>CSPG</b>	Chondroitin sulphate proteoglycan	<b>NgR</b>	Nogo receptor
<b>CST</b>	Corticospinal tract	<b>NT</b>	Neurotrophin
<b>Ctip2</b>	B-cell CLL/lymphoma 11B	<b>OEC</b>	Olfactory ensheathing cell
<b>DAB</b>	3,3'-Diaminobenzidine	<b>OMgp</b>	Oligodendrocyte-myelin glycoprotein
<b>DCA</b>	Dorsal column axotomy	<b>ONC</b>	Optic nerve crush
<b>DRG</b>	Dorsal root ganglia	<b>OPC</b>	Oligodendrocyte progenitor cell
<b>Erk</b>	Extracellular-signal-regulated kinases	<b>p300</b>	E1A-associated protein p300
<b>GADD45</b>	Growth arrest and DNA damage-inducible 45	<b>p38MAPK</b>	Mitogen-activated protein kinase
		<b>PBS</b>	Phosphate buffered saline
		<b>PCAF</b>	P300/CBP-associated factor
		<b>PI3K</b>	Phosphatidylinositol-4,5-bisphosphate 3-kinase
		<b>PNS</b>	Peripheral nervous system
		<b>PPP</b>	Picropodophyllin

<b>PSN</b>	Propriospinal neuron	<b>Smad</b>	MAD homolog
<b>PTEN</b>	Phosphatase and tensin homolog	<b>SMC</b>	Sensorimotor cortex
<b>PTM</b>	Post-translational modification	<b>SNA</b>	Sciatic nerve axotomy
<b>PTP<math>\sigma</math></b>	Protein tyrosine phosphatase sigma	<b>SNAP-25</b>	Synaptosomal-associated protein 25
<b>Rab13</b>	Ras-related protein Rab-13	<b>SOCS</b>	Suppressor of cytokine signaling
<b>RAF</b>	Ras-activated rapidly accelerated fibrosarcoma	<b>SPRR</b>	Small proline-rich protein
<b>RAG</b>	Regeneration associated gene	<b>STAT</b>	Signal transducer and activator of transcription
<b>RAR<math>\beta</math></b>	Retinoic acid receptor beta	<b>Syd</b>	Sunday Driver
<b>RGC</b>	Retinal ganglion cell	<b>Trk</b>	Tyrosine kinase receptor
<b>Rho</b>	Ras homolog gene	<b>TROY</b>	Tumor necrosis factor receptor superfamily member 19
<b>ROCK</b>	Rho-associated protein kinase	<b>Tuj1</b>	Neuron-specific class III beta-tubulin
<b>SC</b>	Schwann cell	<b>WT</b>	Wild type
<b>SCI</b>	Spinal cord injury		
<b>Sema4D/CD100</b>	Semaphorin-4D		



## CONTENTS

<b>SYNOPSIS</b>	<b>1</b>
1 Spinal cord injury overview and rationale	1
2 Pathophysiology of SCI	3
2.1 THE ROLE OF THE EXTRINSIC ENVIRONMENT IN THE CNS REGENERATIVE FAILURE	5
2.2 NEURONAL INTRINSIC MECHANISMS OF CNS REGENERATION FAILURE	8
2.2.1 <i>How does the cell body sense the injury?</i>	10
2.2.2 <i>How the epigenetic landscape influences the growth machinery? The role of PCAF.</i>	12
2.2.3 <i>How transcription factors drive the regenerative response? Letting p53 work.</i>	21
3 Considerations on neuroplasticity to promote functional recovery after SCI	40
4 Conclusion remarks and perspectives	45
5 References	48
<b>PUBLICATIONS AND STATEMENT OF CONTRIBUTIONS</b>	<b>64</b>
1 The MDM4/MDM2-p53-IGF1 axis controls axonal regeneration, sprouting and functional recovery after CNS injury	65
2 PCAF-dependent epigenetic changes promote axonal regeneration in the central nervous system	121
APPENDIX – Calculations of Nutlin-3a mass rate infusion and concentration	151
<b>ACKNOWLEDGMENTS</b>	<b>153</b>
<b>CURRICULUM VITAE</b>	<b>154</b>

## SYNOPSIS

### 1 Spinal cord injury overview and rationale

Injury to the spinal cord disrupts the descending or ascending pathways of the central nervous system, often resulting in different levels of irreversible sensory, motor and/or autonomic deficits. These include complete or incomplete tetraplegia or paraplegia, spasticity, anesthesia, paresthesia or dysesthesia; pain syndromes like neuropathic, visceral and musculoskeletal pain; urinary, bowel and sexual dysfunction; and life-threatening conditions like autonomic dysreflexia. As a result, impairments compromise daily activities and the overall quality of life.

Up to 90% of the spinal cord injury (SCI) cases are traumatic in origin, usually due to road traffic accidents and self-harm/violence (WHO and ISCOS, 2013). The World Health Organization in collaboration with the International Spinal Cord Society estimated that in 2011 236 to 4187 per million of people were living with traumatic SCI worldwide, depending upon the global region that was analyzed (Lee et al., 2014), with approximately 250.000-500.000 new cases from traumatic and non-traumatic etiology yearly (WHO and ISCOS, 2013). The majority of patients affected by this condition are young males (18-32 years of age in developing or developed countries) (Lee et al., 2014) and otherwise economically active people (Figure I). However, as a result of global ageing, there has been an increase in the incidence of SCI affecting people with 60 or more years of age, a stronger tendency in countries of Western Europe, where the population is older (WHO and ISCOS, 2013; Lee et al., 2014); falls are the main cause of SCI in this group, followed by traffic accidents and non-traumatic causes like neoplasms, degenerative conditions of the spinal column, and vascular and autoimmune disorders (WHO and ISCOS, 2013).

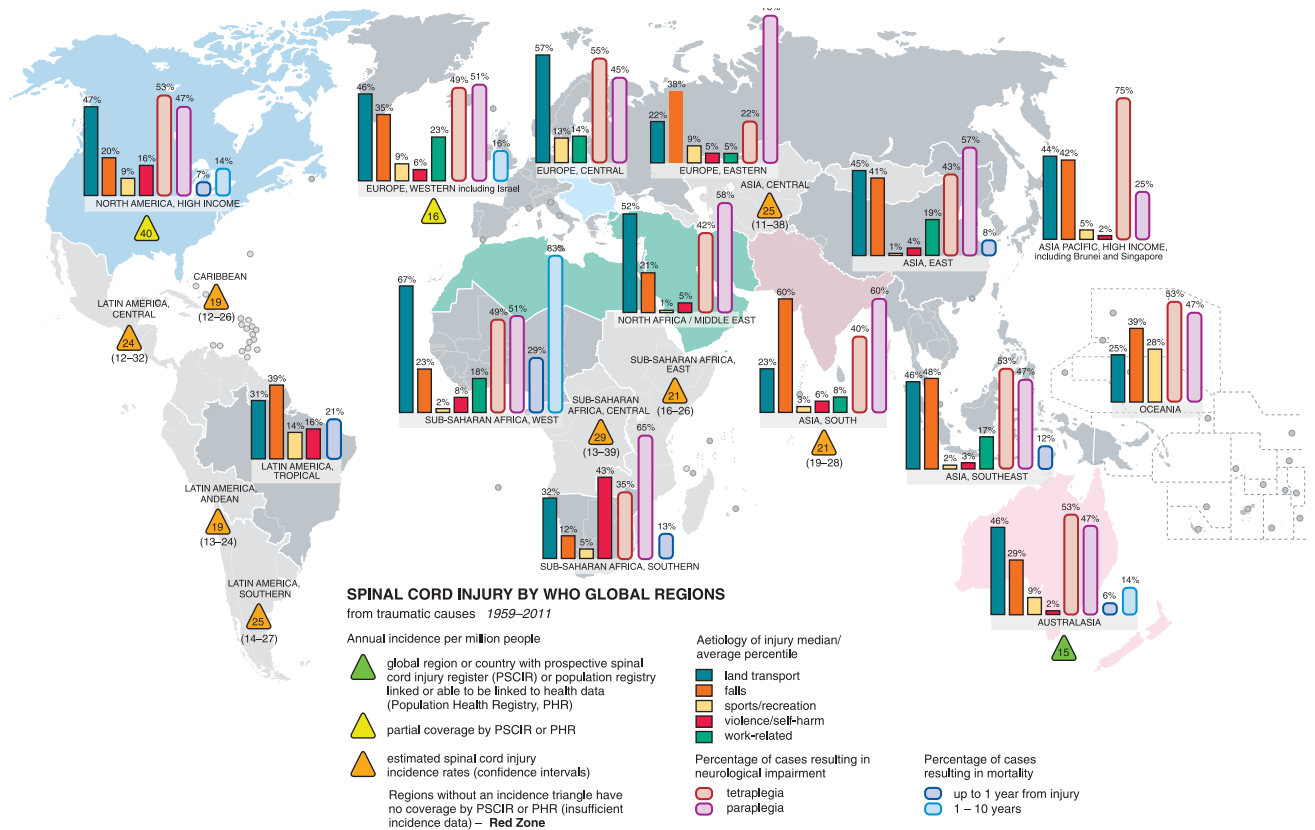


**Figure I. Spinal cord injury by WHO Global Regions from traumatic causes 1959–2011.** (Reproduced from Lee B et al., page 112, *Spinal Cord* 2014; 52:110–116.)

During their lives, patients with SCI usually will have to deal with bladder dysfunction and consequently recurrent urinary tract infections, they are more prone to have pneumonia, pulmonary emboli, decubitus ulcers and septicemia (Donovan, 2007). Therefore, the loss of working force, the reduction of life expectancy and the treatment of SCI comorbidities are not only a personal burden, but also incur in high costs for the society as a whole (Cannon, 2013; WHO and ISCOS, 2013).

In view of the reasons mentioned above, and given that SCI is usually a sudden and unexpected condition with extensive disabling consequences, there is a great effort to find medical therapies to restore the neurological functions of the affected patients. Although the incidence of spinal cord injuries is considered relatively low, the financial burden for the long lasting care and rehabilitation of often young patients makes the discovery of strategies that foster the recovery of function in SCI both ethically and financially compelling. This may perhaps motivate profit organizations to invest in SCI research to accelerate clinical translation.

## 2 Pathophysiology of SCI

The neurological deficits associated with SCI result mainly from damage to spinal neurons and white matter tracts. This damage occurs in two phases (McDonald and Sadowsky, 2002). The primary injury is due to the trauma itself, because mechanical forces compress and pull the cord. Blood vessels are severed, axons are distracted and cell membranes are ruptured. Micro-hemorrhages in the gray matter take place within minutes and spread out radially and axially. The spinal cord swells and ischemia occurs when swelling exceeds the blood pressure (McDonald and Sadowsky, 2002; Norenberg et al., 2004). Neurogenic shock also contributes to the hypoperfusion. The gray matter, due to higher metabolic rates, is particularly sensitive to ischemia. The hypoperfusion reaches the surrounding white matter, contributing to the conduction block and, therefore, to the characteristic areflexia or hyporeflexia of the spinal shock (Ditunno et al., 2004).

Edema, ischemia, inflammation and a variety of factors released by ruptured cells trigger a secondary injury cascade. Glutamate promotes excitotoxicity by flooding the damaged spinal neurons, axons and astrocytes to overexcite neighboring neurons that in turn let in waves of calcium ions. This calcium triggers the production of free radicals that ultimately kill healthy neurons and oligodendrocytes. Unsevered neurons therefore undergo demyelination, exacerbating the spinal shock (McDonald and Sadowsky, 2002). Nevertheless, calcium is essential to mount a regenerative response, as described later.

Moreover, within one to three days after the injury, dendrites of spinal neurons retract and many synapses degenerate (Llewellyn-Smith and Weaver, 2001; Ditunno et al., 2004). Days to weeks after the initial insult, oligodendrocytes also undergo apoptosis, affecting as many as four segments from the trauma site, exacerbating the post-injury demyelination (Beattie et al., 2000). Interestingly, the secondary injury is actually responsible for most of the pathological changes seen in the human injured spinal cord (Norenberg et al., 2004). Figure II summarizes the pathophysiological events following SCI.

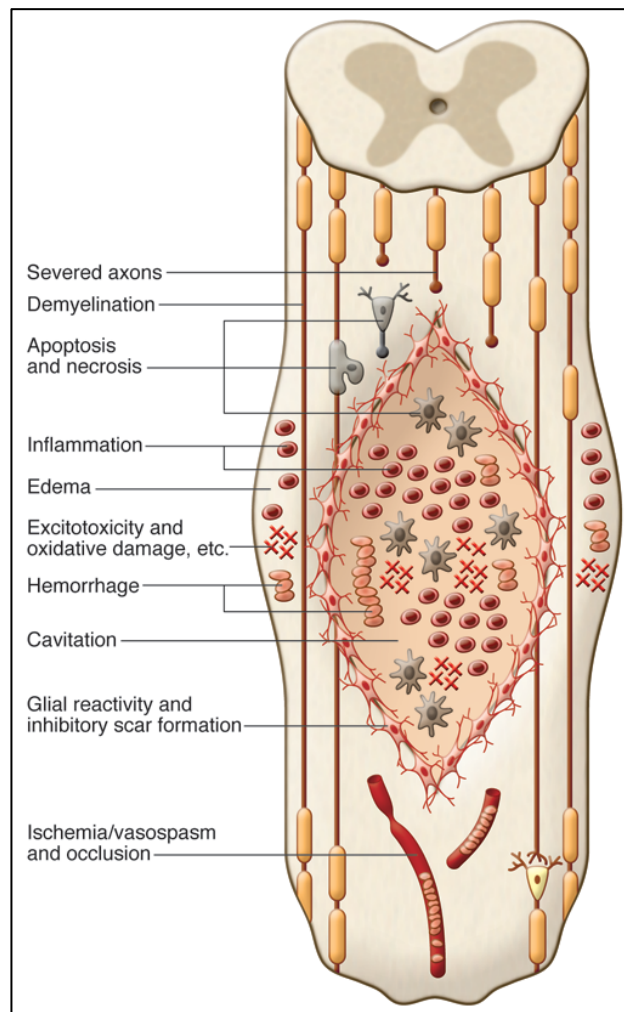


**Figure II. Pathophysiology of SCI.** The primary and secondary injury mechanisms involve edema, hemorrhage, inflammation, apoptosis, necrosis, excitotoxicity, lipid peroxidation, electrolyte imbalance, ischemia/vasospasm, and blood vessel occlusion. Oligodendrocytes and neurons die, resulting in axonal demyelination and disruption of synaptic transmission. In the subacute and chronic phases, a fluid-filled cavity or cyst forms in the center of the cord, with surrounding hypertrophic astrocytes and macrophages. These and other cells secrete extracellular matrix and inhibitory molecules, such as chondroitin sulphate proteoglycans (CSPGs), which compose the glial scar, resulting in a physical and chemical barrier to regeneration. (Reproduced from *Mothe and Tator*, page 3825, *J Clin Invest* 2012;122:3824–3834.)

In humans, following the areflexia/hyporeflexia phase of the spinal shock, that lasts for 24 hours after the injury, reflexes commence to return in days 1 to 3 as a result of denervation supersensitivity to neurotransmitters. The early and late phases of hyperreflexia take place from 1 to 4 weeks and until 12 months after injury, respectively, as a result of neuronal plasticity. If there is significant spared motor descending input, sprouting can lead to functional recovery. If there is minimal sparing, however, growth of segmental reflex inputs might instead contribute to spasticity and less voluntary motor recovery (Ditunno et al., 2004). For the cases in which the neurological deficits are permanent, full restoration of

functions would not only imply sprouting, but also regeneration of severed axons to reinnervate their original or novel targets.

In contrast to the peripheral nervous system (PNS), however, axons of the central nervous system (CNS) have a very limited regenerative response. It was initially thought that this inability to mount an efficient regenerative response relied on extrinsic cues pertaining to the CNS environment, since ground-breaking work from Aguayo and colleagues (Richardson et al., 1980, 1984; Aguayo et al., 1981) demonstrated that axons could grow into peripheral nerve grafts bridging the injury site in the spinal cord of rodents. Indeed, a robust endogenous regeneration response occurs solely in about 30% of dorsal column transected axons 6-24 hours after injury in mice, but the axons fail to grow back to or beyond the lesion scar (Kerschensteiner et al., 2005).

Notwithstanding, experimental blockade of extrinsic inhibitory activities has so far failed to achieve the expected axonal regeneration, pointing to an intrinsic inability of neurons to activate a regrowth program (Fournier et al., 2003; Sivasankaran et al., 2004; Zheng et al., 2005). Moreover, not all types of neurons are able to grow into peripheral nerve grafts, with the corticospinal tract (CST) axons showing the greatest refractoriness to experimental interventions (Richardson et al., 1984; Bregman et al., 1989). These extrinsic and intrinsic properties of the CNS will be briefly reviewed in order to contextualize the original contributions of this work. Even though they were examined separately, they are in fact interdependent, since the transcriptional growth machinery is active in the permissive adult PNS, but not in the adult CNS (Lindner et al., 2013).

## 2.1 THE ROLE OF THE EXTRINSIC ENVIRONMENT IN THE CNS REGENERATIVE FAILURE

In order to restore the blood brain barrier (BBB) and avoid the spread of damage to the remaining fragile central nervous system tissue, a glial scar is formed to wall off zones of intense inflammation within the injury site (Faulkner et al., 2004). Nevertheless, it also represents a physical and molecular barrier to axonal regeneration.

The glial reaction to injury results in the recruitment of microglia, oligodendrocyte progenitor cells (OPCs), meningeal cells and astrocytes to the lesion site (Yiu and He, 2006). Perivascular fibroblasts deposit fibronectin in the injury site (Zhu et al., 2015), while astro-

cytes proliferate around this fibronectin-positive epicenter (Camand et al., 2004). These reactive astrocytes upregulate the production of tenascin, semaphorin 3, ephrin-B2, slit proteins, and CSPGs (Fitch and Silver, 2008). A large fluid-filled cavity or cyst forms in the center of the cord, surrounded by a subpial rim containing some preserved axons, many of which are demyelinated (Figure II), a scar morphology that is often observed in humans (Bunge et al., 1993) and rats (Sroga et al., 2003) after SCI. By contrast, in mice a dense fibrotic tissue without cavitation predominates (Sroga et al., 2003).

Aggrecan, brevican, neurocan, versican, phosphacan and NG2 belong to the CSPG class of extracellular matrix molecules. Proteoglycans are upregulated in areas of gliosis following traumatic injuries in the brain and spinal cord. They are typically enhanced in regions of BBB breakdown (Fitch and Silver, 1997) and at high concentration in the lesion center that gradually diminishes into the penumbra, forming an inhibitory gradient to axonal growth (Yiu and He, 2006). The protein tyrosine phosphatase  $\sigma$  (PTP $\sigma$ ) (Shen et al., 2009), the phosphatase leukocyte common antigen-related (LAR) (Fisher et al., 2011) and the Nogo receptors (NgR) 1 and 3 (Dickendesher et al., 2012) are receptors for the inhibitory glycosylated side chains of CSPGs. It has been recently shown that PTP $\sigma$  is implicated in converting growth cones into a dystrophic state by stabilizing them within CSPG-rich substrates (Lang et al., 2014). Severed axons also interact with NG2<sup>+</sup>-OPCs at the lesion core, which entrap their dystrophic ends, and though counteracting dieback, prevent their elongation (Busch et al., 2010). Moreover, there is enhanced CSPGs production within the perineuronal nets, which has been implicated in reactive glial changes by denervated target regions distant from the lesion site, thus limiting potential plasticity from surviving inputs (Massey et al., 2006).

The myelin also contributes to the growth inhibitory environment of the CNS. Damaged axons are initially exposed to various myelin-associated inhibitors from oligodendrocytes and myelin debris. These inhibitors include the Nogo member of the reticulon family of proteins and its isoforms Nogo-A, -B, -C (Prinjha et al., 2000), the myelin-associated glycoprotein (MAG) (McKerracher et al., 1994), the oligodendrocyte-myelin glycoprotein (OMgp) (Wang et al., 2002b), the transmembrane semaphorin 4D (Sema4D/CD100) (Moreau-Fauvarque et al., 2003) and ephrin B3 (Benson et al., 2005). All the three Nogo isoforms have a common 66 amino acid loop (Nogo-66) (Prinjha et al., 2000), which is recognized by NgR (Fournier et al., 2001), a receptor that is expressed in many types of CNS

neurons and can also bind with high affinity to MAG (Liu et al., 2002) and OMgp (Wang et al., 2002b). Nogo-A is highly expressed in oligodendrocytes (Huber et al., 2002) and promotes growth cone collapse through the binding of Nogo-66 to NgR1 (Fournier et al., 2001). NgR1 forms a complex with the transmembrane proteins LINGO-1 (Mi et al., 2004), p75 (Wang et al., 2002a) or TROY (Park et al., 2005), that are present in the growth cone of the nerve cell (Schwab, 2010). This triggers the activation of RhoA and ROCK (Niederöst et al., 2002), leading to the phosphorylation of cofilin by LIM kinase to destabilize the actin cytoskeleton of damaged axons, culminating in growth cone collapse (Hsieh et al., 2006). Moreover, Sema4D/CD100 is expressed by oligodendrocytes, can be induced by injury and triggers growth cone collapse (Moreau-Fauvarque et al., 2003).

The inflammatory response may also contribute to the regenerative failure in the CNS. Like astrocytes, resident microglia respond rapidly to injury, extending cellular processes or migrating toward the lesion site, where they take part in the scar formation (Davalos et al., 2005). Within 30 minutes, they form a dense border to seal the lesion and avoid the spread of damage (Davalos et al., 2005). Approximately 2 days after the injury, blood monocytes migrate into the lesion (Pineau et al., 2010) where they differentiate into tissue macrophages (Mawhinney et al., 2012). Both monocyte-derived macrophages and fully activated microglia express high levels of CD45, therefore are no longer distinguishable and are referred as microglia/macrophages (David and Kroner, 2011).

The role of microglia/macrophages to the regeneration failure is rather controversial. While they act as scavengers, cleaning debris at the injury site, and helping to restrain the damage, they also produce pro-inflammatory cytokines, proteases and other factors that are cytotoxic (David and Kroner, 2011) and contribute to delayed axonal dieback (Evans et al., 2014). Different types of macrophage activation may explain this dual *modus operandi*. The “classically” activated or M1 phenotype of macrophages is driven by exposure to interferon- $\gamma$  or tumor necrosis factor- $\alpha$  and display a neurotoxic phenotype (Gordon and Taylor, 2005; Kigerl et al., 2009), although in some circumstances (e.g. via zymosan or LPS inflammatory induction) it may also enhance axonal regeneration in the lesioned PNS or CNS (Yin et al., 2003; Boivin et al., 2007). The “alternatively activated” or M2 is induced by interleukins 4 or 13 and downregulates the expression of pro-inflammatory cytokines, promotes more robust neurite outgrowth and stimulates remyelination (Gordon and Taylor, 2005; Miron et al., 2013). The M1 phenotype predominates after SCI, while M2 markers are only transiently



expressed (Kigerl et al., 2009; Gensel and Zhang, 2015). M2 is indeed the phenotype of resting microglia in the uninjured CNS (Ponomarev et al., 2007).

Taken together, the environment of the lesioned spinal cord site is not permissive to axonal regeneration. Whilst the severed axon tip struggles to advance a new growth cone, myelin-derived inhibitory factors promotes its collapse, CSPGs turn it into a dystrophic state, and in the sequence it suffers the attack of M1 macrophages, which were paradoxically supposed to clean the harmful debris in first place (Silver et al., 2015) (Figures II and III).

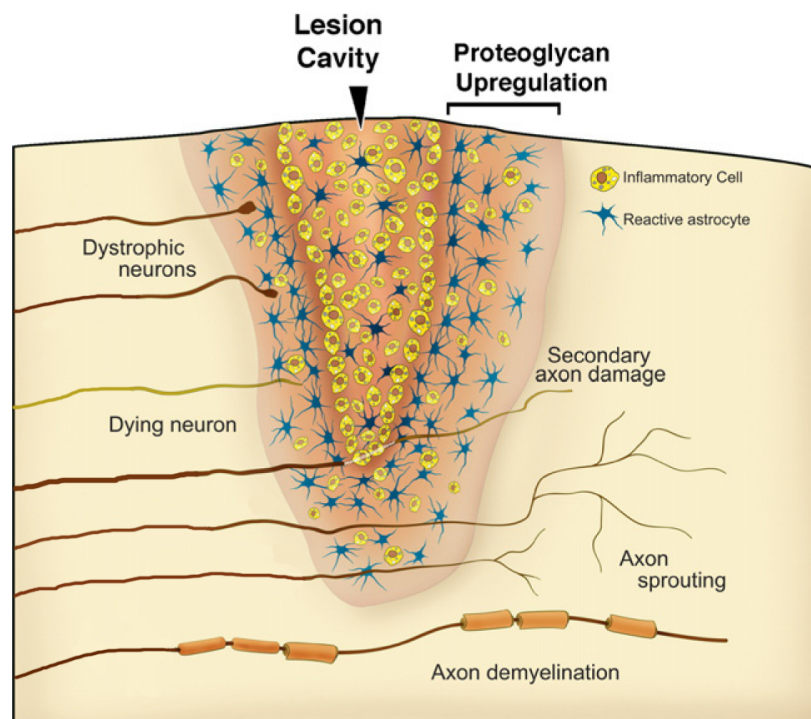


**Figure III. Schematic representation of the injury site following CNS trauma.** The lesion cavity expands as inflammatory cells interact with the surrounding reactive astrocytes and other reactive glial cells. This intense inflammatory response leads to a cascade of secondary damage to axons initially spared from direct trauma, and demyelination of adjacent axons. The gradient of inhibitory molecules upregulated in the areas of intense inflammation provides an environment that is non-permissive for regeneration, and dystrophic neurons develop the classically described sterile end-balls with clubbed endings that are characteristic of abortive attempts at regeneration. If experimental interventions render the scar environment more permissive and/or reactivate the intrinsic neuronal growth program, axons may eventually sprout or regenerate past the lesion site. (Adapted from Fitch MT and Silver J, page 298, *Exp Neurol* 2008;209:294-301.)

## 2.2 NEURONAL INTRINSIC MECHANISMS OF CNS REGENERATION FAILURE

At the beginning of last century, Ramon Y Cajal proposed that injured adult central axons were not capable of regeneration. In his own words: "(...) *In adult centres, the nerve paths are something fixed, ended, immutable. Everything may die, nothing may be regen-*

erated. (...)” (Page 750, Ramón y Cajal, 1928). In fact, after injury to the adult mammalian CNS, most of the axons retract from the injury site. In mice, thirty minutes after the SCI, the proximal and distal segments of severed dorsal column axons undergo dieback by acute axonal degeneration, followed by later (>30 hours) Wallerian degeneration of the distal stump (Kerschensteiner et al., 2005). Only the minority of the remaining proximal axonal segments are able to sprout, doing so by a millimeter or less, and terminating in dystrophic growth cones that halt elongation (Bradke et al., 2012). Today we know that experimental interventions are able to awaken the intrinsic growth machinery of adult neurons after CNS injury. Even though much progress has been done in unraveling this machinery, especially by studying injury models in the PNS, the nervous system in development and of lower invertebrates, there is still lack of information on how signaling pathways are activated or inactivated, and how they interact to promote restoration of the CNS, therefore hindering concrete clinical translation.

In order to mount an effective regenerative response, an injured neuron has to sense that the damage has happened, inform its nucleus what and where it has occurred, in turn the nucleus has to alter gene transcription to ultimately assemble a new competent growth cone and promote axonal elongation toward its original targets. While these events are well orchestrated in the PNS, where regeneration does take place, many signaling pathways appear to be defective in the CNS (Tedeschi, 2012).

The differences between the PNS and CNS responses to injury have been extensively studied in the dorsal root ganglia (DRG) system. DRG neurons are pseudo-unipolar cells with a peripheral branch bringing in sensory input and a central branch travelling into the dorsal columns to relay the sensory information to higher centers. This anatomy provides a unique opportunity to track changes to central or peripheral injuries converging in the same nucleus. Indeed, injuries to the peripheral but not the central branch are able to trigger a regenerative response (Schreyer and Skene, 1991). Of special interest, a previous injury to the peripheral branch, the so-called “preconditioning injury”, primes the cell to a regenerative state, consequently improving regeneration after a subsequent peripheral injury, and even promoting axonal outgrowth after a central injury (Richardson and Issa, 1984; Neumann and Woolf, 1999).

In the present work, specific intrinsic mechanisms involving gene expression were unraveled and experimentally manipulated to achieve axonal outgrowth and functional recov-

ery after SCI. Briefly, we discovered that the acetylation of lysine 9 of histone H3 (H3K9Ac) by a specific histone acetyltransferase (HAT), the P300/CBP-associated factor (PCAF), drives the expression of regeneration associated genes (RAGs) after PNS injury. RAGs are genes differentially induced between the regenerating PNS and the non-regenerating CNS, whose protein products include transcription factors such as c-JUN, CREB, STAT3, ATF3, RAR  $\beta$ , and p53; cytoskeleton and growth cone associated proteins such as  $\alpha$ -tubulin, Coronin 1b and Rab13, MAP-1, GAP-43, CAP-23; cell adhesion molecules like NCAM, L1CAM, and TAG1; cytokines and extracellular matrix components, including SNAP-25, CPG15/neuritin, Galectin-1, Galanin and SPRR1; and the neurotrophin brain-derived neurotrophic factor (BDNF) (Di Giovanni, 2009). More importantly, forcing the expression of PCAF in DRG neurons promoted growth of dorsal column axons after SCI, mimicking a preconditioning injury (Puttagunta and Tedeschi et al., 2014). Our work provided the first systematic screening comparing epigenetic regulatory mechanisms between the PNS and CNS after injury. Moreover, we showed that the retrograde signaling is implicated in the modulation of the chromatin landscape following injury.

In another set of experiments aiming to promote functional recovery following SCI, we released the transcription factor p53 of its constitutively inhibition by the ubiquitin ligases mouse double minute 2 and 4 (MDM2 and MDM4). For the first time, we demonstrated that enhancing p53 transactivation leads to sprouting of serotonergic (5-HT) and corticospinal fibers and functional recovery in mice. Furthermore, we provided a novel mechanistic insight on CNS regeneration, by showing that these pro-regenerative p53 effects depend upon the insulin-like growth factor 1 receptor (IGF-1R) signaling (Joshi and Sória et al., 2015).

Next, I will summarize the main events known so far to prompt an intrinsic regenerative response in injured neurons, focusing on the mechanisms that I contributed to discovering.

### 2.2.1 *How does the cell body sense the injury?*

Axotomy provokes depolarization of the cell membrane that is sufficient to activate voltage-gated calcium channels, leading to calcium influx in the neuron and propagation of

the response to the soma via activation of voltage-dependent sodium channels. The spiking activity causes a sodium load, activation of transient calcium currents, and inversion of the sodium–calcium exchanger, providing an additional mean of entry for calcium (Mandolesi et al., 2004). The calcium current propagates along the axon reaching the cell body, therefore constituting rapid retrograde signaling (Rishal and Fainzilber, 2010), and is essential to seal the cut axonal membrane (Spira et al., 1993), to drive cytoskeletal changes necessary for the formation of a new growth cone (Ziv and Spira, 1997; Spira et al., 2003), to activate the long-range retrograde molecular signaling (Perlson et al., 2005) and local protein translation (Yudin et al., 2008).

The successful assembly of a new growth cone is crucial to drive axonal regeneration. In fact, severed CNS axons are only able to produce retraction bulbs, which are dystrophic growth cones, pointing to an intrinsic regenerative failure already in the initial steps (Bradke et al., 2012). This is probably a result of the characteristic microtubule depolymerization that occurs at the CNS-injured axonal stump and consequently impairs the advancement of the growth cone (Ertürk et al., 2007).

The fast signaling calcium wave leads to export of histone deacetylase 5 (HDAC5) from the nucleus in a protein kinase C $\mu$  dependent manner (Cho et al., 2013). Nuclear export of HDAC5 increases acetylation of histones to help in the activation of a pro-regenerative gene expression program. Moreover, it seems to prime the neuronal cell body to receive a second slower signaling wave of information, that rely on retrograde transport of molecular motors along the axon microtubules (Cho et al., 2013; Doron-Mandel et al., 2015). In the uninjured neuron, neurotrophic factors are constantly retrograde transported (Bronfman et al., 2007), and the drastic reduction in the amount of these factors arriving to the soma after axonal injury may inform the cell body about the damage (Rishal and Fainzilber, 2010).

Active retrograde transport is mediated by the dynein complex from plus to minus ends of microtubules (Cosker et al., 2008). Importin  $\alpha$  and  $\beta$  are major components of the nuclear import complex. Some of the local signals produced at the injury site contain a nuclear localization signal (NLS). NLS-bearing proteins are bound to importin  $\alpha/\beta$  heterodimers and the complex is attached to dynein to be transported to the nucleus (Yudin et al., 2008). One such cargo is the type III intermediate filament vimentin, which is locally translated after injury, and cleaved by the calcium-activated protease calpain. The vimentin proteolysis products bind to both phosphorylated extracellular-signal-regulated kinases (pErks)

and importin  $\beta$  1, therefore linking pErks to the dynein retrograde motor (Perlson et al., 2005). Other cargo involved in alerting the soma to initiate a regeneration response include the c-Jun N-terminal kinase (JNK)-Sunday Driver (Syd) complex (Cavalli et al., 2005).

Once these signals arrive at the soma, they need to reach the nucleus to alter gene transcription. However, accessibility to gene promoters additionally requires chromatin remodeling to be in a more relaxed state.

### 2.2.2 *How the epigenetic landscape influences the growth machinery? The role of PCAF.*

Epigenetic modifications initiate the regulatory changes to drive or repress transcription depending on the environmental context. They are essential during embryological development, when strict temporal and spatial regulation of gene expression is required (Lindner et al., 2013). Furthermore, it has been shown that chromatin modifications play a fundamental role in adult neurogenesis, cognition, vision, learning and memory, neurodegenerative and psychiatric disorders (Feng and Fan, 2009; Day and Sweatt, 2010; Ma et al., 2010). More recent experimental data suggest that epigenetic modifications regulate axonal outgrowth and regeneration in post-mitotic adult CNS neurons (Gaub et al., 2010, 2011; Iskandar et al., 2010; Trakhtenberg and Goldberg, 2012; Cho et al., 2013; Cho and Cavalli, 2014).

The classical components of the epigenome include DNA methylation and histone post-translational modifications (PTMs). DNA methylation is mediated by DNA methyltransferase enzymes, which catalyze the covalent binding of the methyl group to the C5 position of the cytosine residue of CpG dinucleotides (Feng and Fan, 2009). The canonical methylated CpG (5mCpG) serves as an attachment site for members of the family of methylated CpG binding domain (MBD) proteins. The binding of MBD proteins to methylated DNA sites in gene promoters leads to the recruitment of histone-modifying enzymes, deacetylation of histone protein tails, and chromatin condensation around the gene promoter resulting in transcriptional repression (Sharma et al., 2005). On the other hand, histone PTMs are mostly regulated by histone acetyltransferases (HATs), histone deacetylases (HDACs), histone methyltransferases, and histone lysine demethylases, which form large multiprotein complexes in the proximity of gene regulatory regions (Yang and Seto, 2007).

Specific combinations of acetylated and methylated sites (i.e. the “histone code”) are associated with “open” or “closed” chromatin formations. This “code” mediates protein-protein interactions contributing to short- and long-term regulation of transcription, representing a specific form of cellular memory (Sharma et al., 2005). Transcriptionally active chromatin predominates in early embryogenesis and in the growth-active developing nervous system (Reik, 2007), whereas global DNA methylation levels are higher in the adult brain than in comparison to other tissues (Goto et al., 1994).

Acetylated histone H3 at lysine residues 9, 14, 18 and 27 (H3K9/14/18/27 ac) and acetylated H4 are often associated to active promoter regions and close to transcription start sites. Moreover, not only does histone acetylation imply a more relaxed chromatin state at gene promoters, but also so does methylation of histone H3-K4 and K36 (Kouzarides, 2007). The acetylation of lysines is highly dynamic and regulated by the opposing action of histone acetyltransferases (HATs) and histone deacetylases (HDACs) (Bannister and Kouzarides, 2011). Type A members compose the largest family of HATs, they are nuclear enzymes usually found in multiprotein complexes and can be classified in three categories: GCN5-related N-acetyltransferases (GNATs), MYST, and CREB-binding protein (CBP)/P300 families (Hodawadekar and Marmorstein, 2007; Bannister and Kouzarides, 2011). Of these, well characterized are PCAF, which belongs to the GNATs family, and the complex CBP/P300. PCAF acetylates the core histones H3 at lysines 9, 14 and 18, and H4, whereby it is the primary HAT for H3K9. Its transcriptional activation repertoire also includes acetylation of transcription factors as a co-activator (Jin et al., 2011).

In Puttagunta and Tedeschi et al. (2014), we sought to find an epigenetic “orchestrator of gene regulation” linking the retrograde signaling to the transcription of RAGs. For that, we performed equidistant PNS and CNS injuries in mice, respectively by sciatic nerve crush (SNA) and dorsal column axotomy (DCA), and submitted L4-L6 DRG from both conditions to DNA methylation arrays and screening of histone modifications at the proximal promoters of RAGs by quantitative chromatin immunoprecipitation (ChIP) assays.

We found no differences in DNA methylation of RAGs between SNA and DCA, thus promoter and CGI DNA methylation are probably not essential to the differential regenerative response between the PNS and CNS. Of the histone modifications related to activation of gene transcription (H3K9ac, H3K18ac and H3K4me2) or gene repression (H3K9me2 and H3K27me3) (Wang et al., 2008), only H3K9ac and H3K9me2 were differentially enriched at

the promoters of the specific upregulated RAGs *GAP-43*, *Galanin* and *BDNF* following 1-7 days after SNA in the mouse. Moreover, PCAF was also enriched at these promoters, which is with H3K9ac usually found in the proximity of transcription start sites of active transcribing genes (Wang et al., 2008). Conversely, H3K9me2 was reduced at the same promoters after SNA, but increased after DCA. Furthermore, the nuclear expression of H3K9ac and PCAF was increased in SNA in comparison to DCA (Figure 3, Puttagunta and Tedeschi et al., 2014, reproduced below as Figure IV). Taken together, these histones modifications portray an active expression state of specific essential upregulated RAGs after SNA, whilst a repressive state is depicted after DCA (Figure 1a,b,c; Puttagunta and Tedeschi et al., 2014).

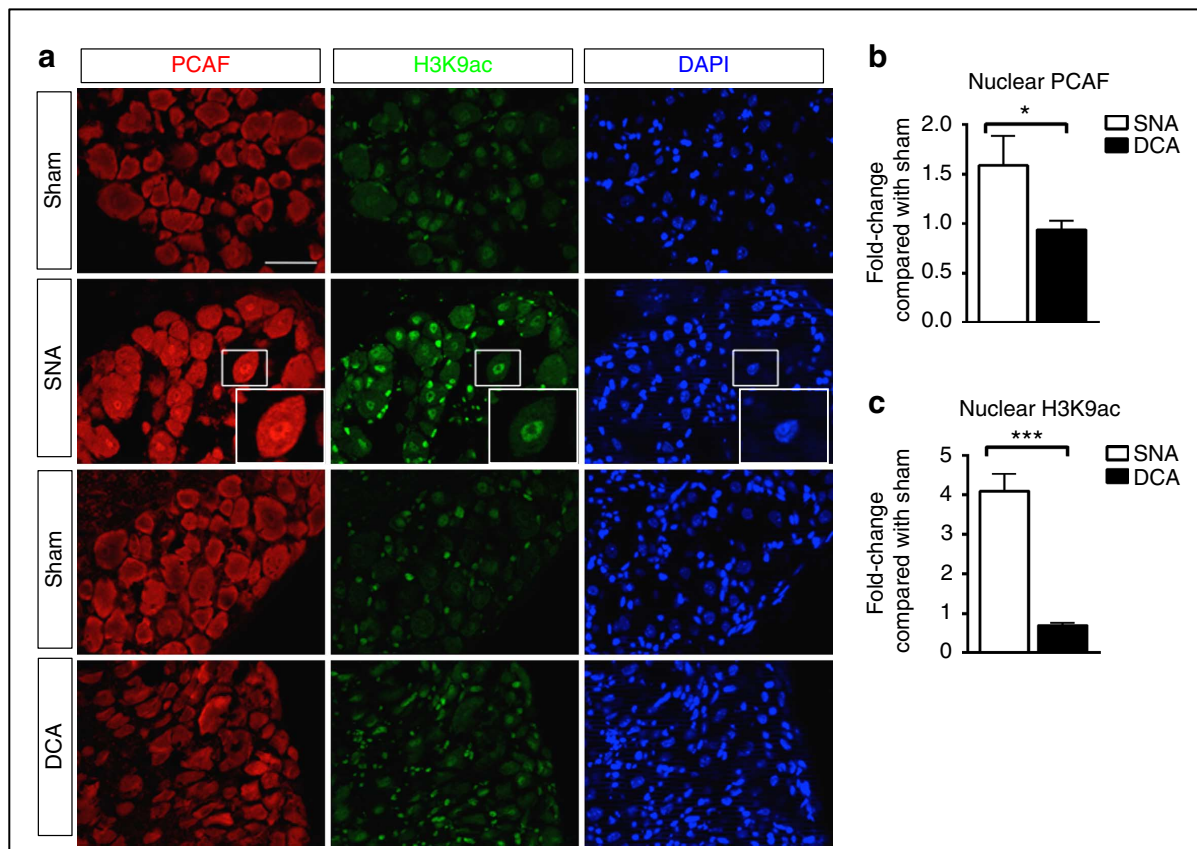


**Figure IV. Increased nuclear PCAF and H3K9ac following SNA but not DCA.** (a) IHC co-staining with PCAF and H3K9ac of L4-L6 DRG following Sham/SNA or Sham/DCA. Insert shows high nuclear expression of PCAF and H3K9ac after SNA. Scale bar, 50  $\mu$ m. (b) IHC intensity density analysis reveals an increase in nuclear PCAF following SNA/Sham but not DCA/Sham. (c) Intensity density analysis of IHC stained with H3K9ac reveals a significant fold increase following SNA but not DCA when compared with respective Sham. Student's t-test, error bars, s.e., \* $P < 0.05$ , \*\*\* $P < 0.001$ ,  $N = 3$  per group, performed in triplicate. (Reproduced from Puttagunta and Tedeschi et al., page 5, *Nat Commun* 2014;5:3527.)

To address how the activation of PCAF might occur after PNS injury, we postulated that retrograde signaling could be implicated. For that, we exposed adult primary DRG neu-

ronal cultures to nerve growth factor (NGF) or to NGF together with PD98059 (PD), the Erk kinase (MEK) inhibitor. NGF is a neurotrophin that is induced after sciatic nerve injury (Rush, 1995); it activates the Erk signaling and promotes neurite outgrowth (Averill et al., 2001); and induces PCAF nuclear localization and activation of its acetyltransferase activity in PC12 cells (Wong et al., 2004). NGF increased the expression of pErk, nuclear PCAF and H3K9ac, while PD abrogated their induction. Similar results were obtained *in vivo*, with SNA promoting an Erk-activation-dependent raise in pErk expression, acetylation of H3K9, and PCAF nuclear translocation in DRG neurons. Inhibition of Erk activation also led to decrease in gene expression of *GAP-43*, *Galanin* and *BDNF* as well as reduced PCAF and H3K9ac promoter occupancy for these genes (Figure 4, Puttagunta and Tedeschi et al., 2014, reproduced below as Figure V).



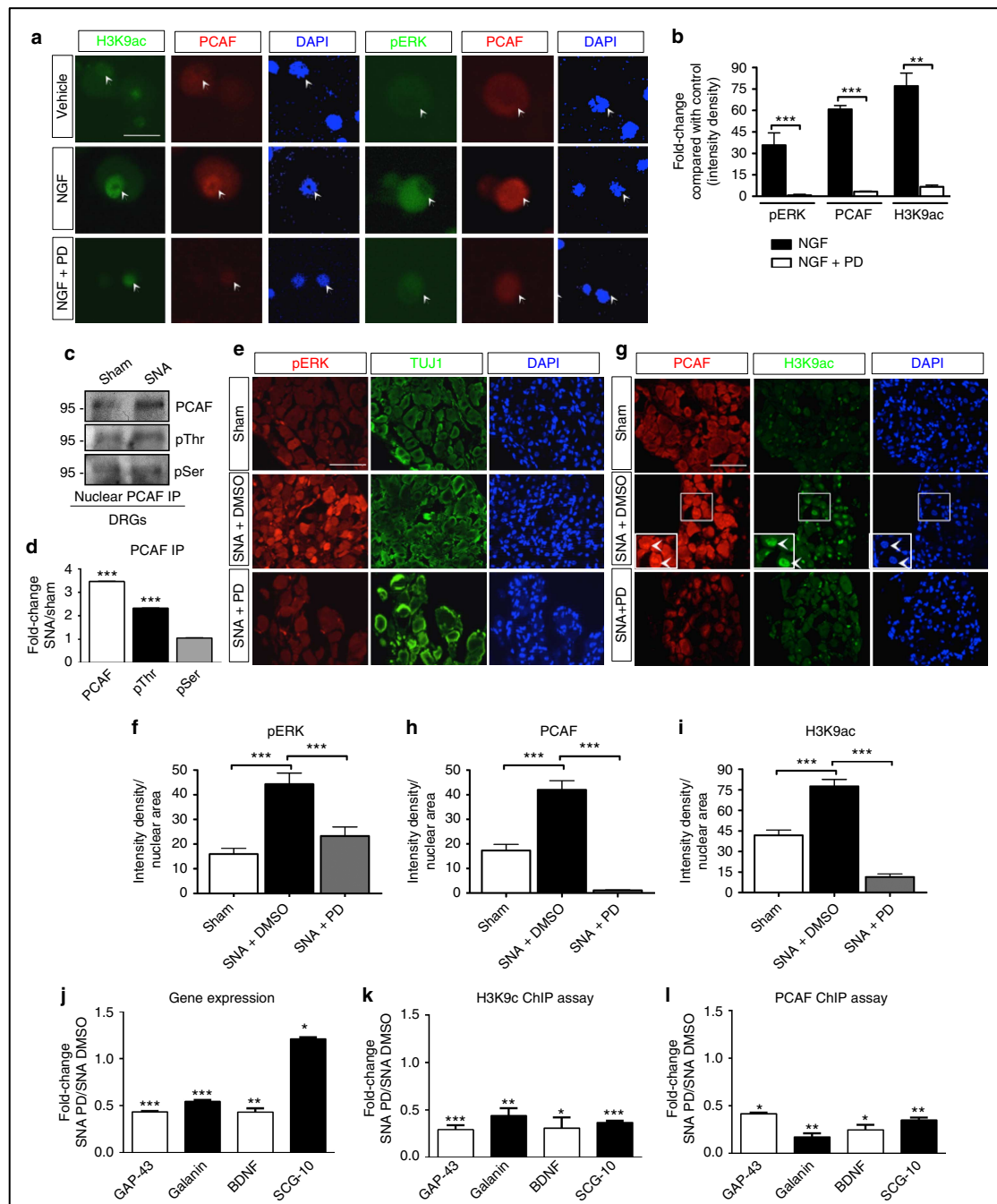


**Figure V. ERK retrograde signalling controls PCAF activation.** (a,b) NGF stimulates pERK, PCAF and H3K9ac expressions in adult DRG cultures after 3-h treatment, which is abrogated by the ERK kinase inhibitor PD98059 (PD), ICC (a) and fold change analysis of intensity density (b). Scale bar, 20 mm,  $N = 3$  per group, performed in triplicate. (c,d) Nuclear PCAF immunoprecipitation from in vivo L4-L6 DRG 24 h following Sham or SNA reveals an increase in PCAF expression and threonine phosphorylation following SNA but not serine phosphorylation, immunoblot (c) and fold change of density analysis (d).  $N = 5$  per group, performed in triplicate. (e–i) In L4-L6 DRG, 24 h following SNA we observe an increase in pERK (e,f), PCAF (g,h) and H3K9ac (g,i) expression, which is significantly decreased by ERK inhibition with PD at the nerve stump. Insert shows high nuclear expression of PCAF and H3K9ac after SNA. Scale bars, 75 μm,  $N = 3$  per group, performed in triplicate. (j–l) PD also inhibits gene expression (Q-PCR,  $N = 3$  per group) (j) as well as H3K9ac (k) and PCAF (l) at the promoters of GAP-43, Galanin and BDNF 24 h following SNA (ChIPs).  $N = 6$  per group, performed in triplicate. Error bars, s.e. (b,f,h,i),  $P < 0.0001$ , ANOVA, Bonferroni *post hoc* tests,  $**P < 0.001$  and  $***P < 0.001$ , (d,j–l) Student's *t*-test,  $*P < 0.05$ ,  $**P < 0.001$  and  $***P < 0.001$ . Original immunoblot images are shown in Supplementary Fig. 12. (Reproduced from Puttagunta and Tedeschi et al., page 6, Nat Commun 2014;5:3527.)

Interestingly, a preconditioning injury (i.e. SNA 7 days before DCA) led to an increase in *GAP-43*, *Galanin* and *BDNF* expression and promoter occupancy by PCAF in the L4-L6 DRG 24 hours after DCA (Figure 1d,e, Puttagunta and Tedeschi et al., 2014). This observation motivated us to test whether PCAF overexpression in DRG could mimic the preconditioning injury. Indeed, PCAF overexpression increased neurite outgrowth in permissive and non-permissive substrates (Figure 5, Puttagunta and Tedeschi et al., 2014). In *ex vivo* experiments, pharmacological inhibition of PCAF and PCAF<sup>-/-</sup> repressed H3K9ac and abolished neurite outgrowth following SNA, respectively, and inhibition of Erk phenocopied the loss of PCAF (Figures 5 and 6, Puttagunta and Tedeschi et al., 2014). In the *in vivo* setting, preconditioning-injured PCAF<sup>-/-</sup> mice showed reduced sprouting of dorsal columns after DCA in a way that they resembled non-conditioned wild-type mice, and reduced expression of *GAP-43*, *Galanin* and *BDNF* in DRG following SCI (Figure 7, Puttagunta and Tedeschi et al., reproduced below as Figure VI). Strikingly, overexpression of PCAF in the DRG of wild type mice enhanced regeneration of the dorsal columns across and up to 1 mm rostral to the DCA site mimicking the enhancement of the growth potential following a preconditioning injury (Figure 8, Puttagunta and Tedeschi et al., 2014, reproduced below as Figure VII).

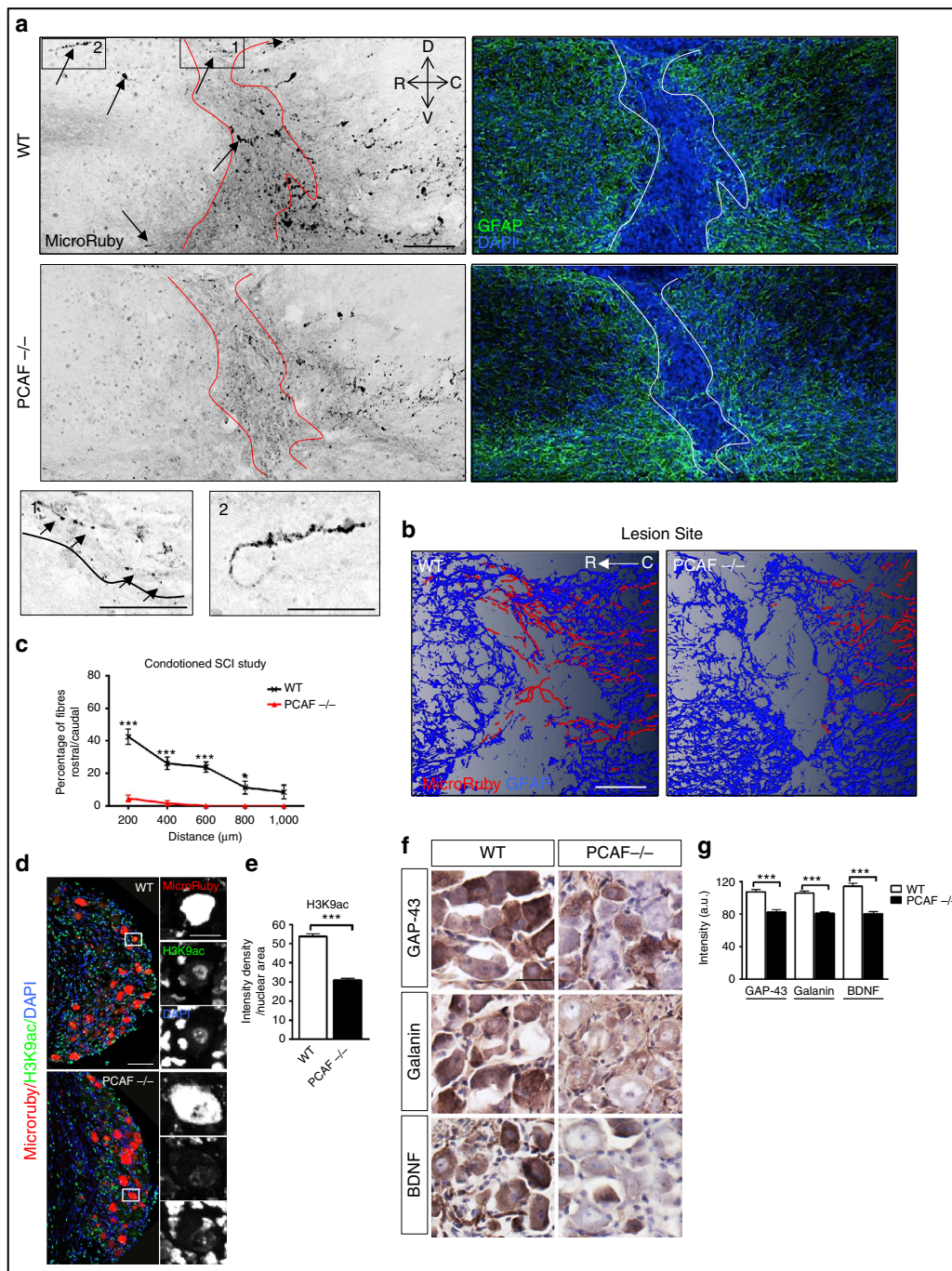


**Figure VI. PCAF is required for conditioning-dependent axonal regrowth after SCI.** (a) MicroRuby tracing of the dorsal columns shows regenerating fibres invading into and past the lesion site (upper) in WT but not in PCAF<sup>-/-</sup> (lower) after conditioning injury (SNA followed by DCA; left panels). The red dotted lines indicate the lesion site. Insets (1 and 2) show higher magnification of regenerating axons. D-R-C-V: anatomical coordinates, dorsal-rostral-caudal-ventral. Right panels show the lesion site. Arrows indicate axonal sprouts. Scale bar, 100 μm. (b) Amira 3D reconstruction of regenerating dorsal column axons and glial scar in a sagittal projection (~25 μm) of the lesion site from WT and PCAF<sup>-/-</sup> mice. (c) Quantification of regenerating axons,  $N = 6$  (WT),  $N = 6$  (PCAF<sup>-/-</sup>), Welch's  $t$ -test,  $*P < 0.05$  and  $***P < 0.001$ . (d,e) Lack of CNS regeneration correlates with a significant decrease in H3K9ac expression in L4-L6 PCAF<sup>-/-</sup> traced DRG neurons when compared with WT, IHC (d), bar graphs (e). Inset shows high nuclear expression of H3K9ac in WT but not PCAF<sup>-/-</sup> traced DRG neurons. Student's  $t$ -test, error bars, s.e.,  $***P < 0.001$ ,  $N = 6$ , performed in triplicate. (f,g) IHC and 3,3'-Diaminobenzidine (DAB) intensity analysis of L4-6 DRG neurons shows a decrease in GAP-43, BDNF and Galanin expression in PCAF<sup>-/-</sup> DRG neurons when compared with WT after SNA followed by SCI. Scale bar, 25 μm. Student's  $t$ -test,  $***P < 0.001$ ,  $N = 4$  per group, performed in triplicate. (Reproduced from Puttagunta and Tedeschi et al., page 9, Nat Commun 2014;5:3527.)



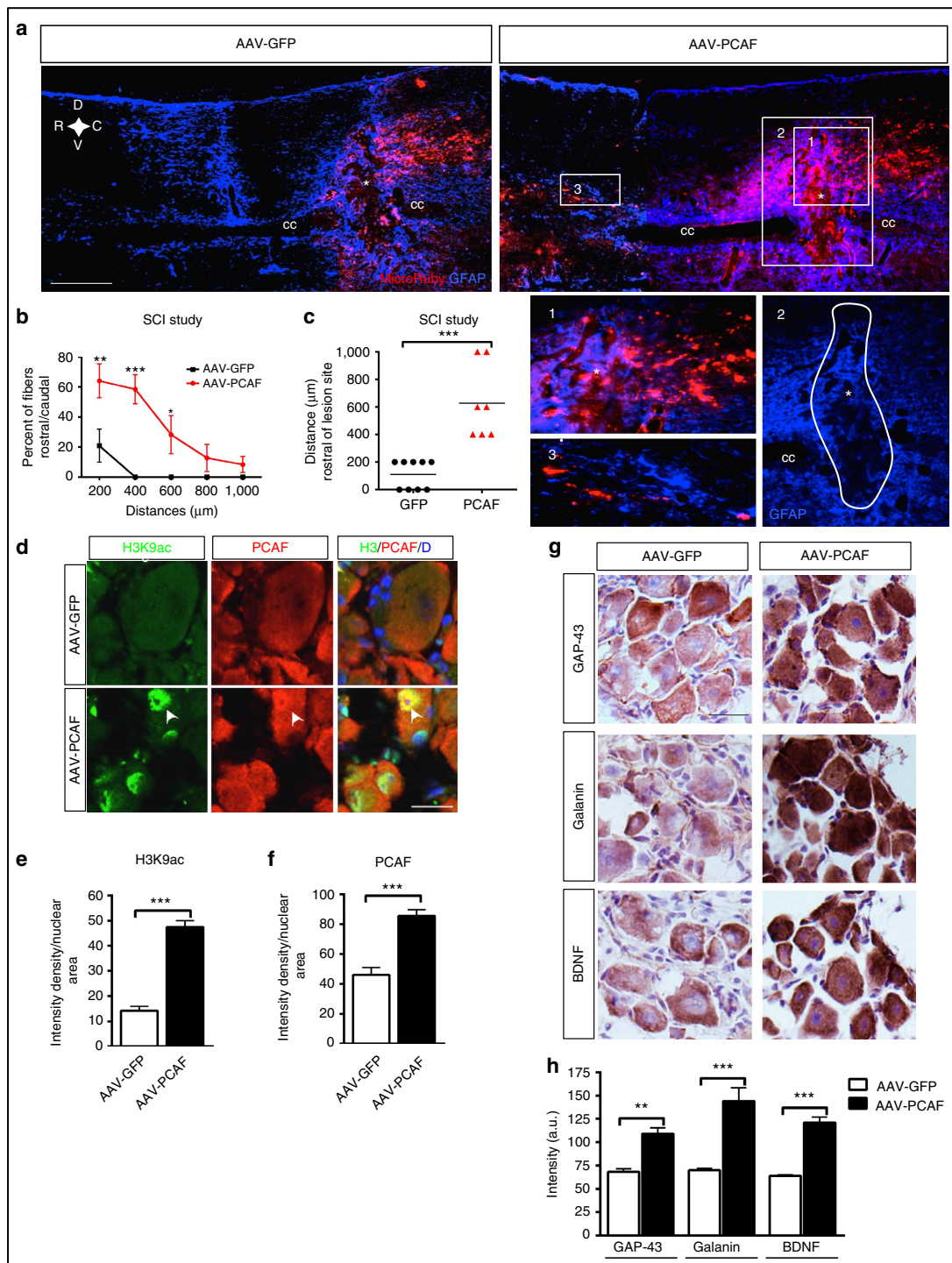


**Figure VII. PCAF overexpression induces spinal axonal regeneration.** (a) MicroRuby tracing of the dorsal columns shows regenerating fibres invading into and past the lesion site after AAV-PCAF overexpression (upper right) versus a control AAV-GFP virus (upper left). Insets show higher magnification of regenerating axons. D-R-C-V: anatomical coordinates, dorsal-rostral-caudal-ventral. cc: central canal. Scale bar, 250  $\mu\text{m}$ . (b) Quantification of regenerating axons,  $N = 9$  (AAV-GFP),  $N = 7$  (AAV-PCAF). (c) Quantification of longest regenerating axon per animal. (d-f) Overexpression of AAV-PCAF in the SCI study promotes H3K9ac (8 weeks post infection; arrow-heads) as shown by IHC (d). Nuclear intensity density analysis of H3K9ac (e) and PCAF (f) show enhanced PCAF and H3K9ac after PCAF overexpression. (g,h) GAP-43, Galanin and BDNF IHC analysis of corresponding L4-L6 DRG from infected AAV-PCAF and AAV-GFP animals show an increase in GAP-43, Galanin and BDNF expression, IHC (g) and DAB intensity analysis (h). Scale bars, 25  $\mu\text{m}$ . Error bars, s.e., (b) Welch's  $t$ -test,  $*P < 0.05$ ,  $**P < 0.01$  and  $***P < 0.001$ . (c,h)  $P < 0.0001$ , ANOVA, Bonferroni *post hoc* tests,  $**P < 0.01$  and  $***P < 0.001$ , (e,f) Student's  $t$ -test,  $***P < 0.001$ ,  $N = 3$ , performed in triplicate. (Reproduced from Puttagunta and Tedeschi *et al.*, page 10, *Nat Commun* 2014;5:3527.)

In conclusion, we discovered that PCAF is an essential “orchestrator of gene expression” after PNS injury, linking the Erk dependent retrograde signaling to expression of specific RAGs (*GAP-43*, *Galanin* and *BDNF*) via changes in the chromatin landscape (acetylation of H3K9). Moreover, we showed that PCAF is essential for the activation of the CNS regeneration program following a preconditioning injury, therefore providing a potential mechanism to be explored in SCI translational medicine.

In Puttagunta and Tedeschi et al. (2014), I performed several surgical procedures (SNA and DCA), including applying PD or vehicle onto sciatic nerves. Moreover, I worked on the fixation and frozen-sectioning of DRG; performed and developed several protocols for DRG staining: fluorescent immunohistochemistry for PCAF, H3K9ac, pErk 1/2 and Tuj1 (Figures 3a, 4e,g and 8d,g); and DAB staining for GAP-43, BDNF and Galanin (Figures 7f and 8d,g).

Furthermore, I created a method to specifically quantify the nuclear intensity density (ID) of H3K9ac, PCAF and pErk in DRG-stained sections. For that, photomicrographs were taken with an Axio Imager.Z1/ Apotome (Zeiss) microscope as 0,800 mm Z-stacks at x40 magnification and processed with the software AxioVision (Zeiss). In order to determine the nuclear ID of pixels, Image J (Fiji) was used. First of all, the Z-stack that contained the highest intensity of pixels was chosen for analysis. After that, each neuronal nuclear area was selected in the DAPI channel (about 25 nuclei/picture). The same selection was then used to delineate the nuclei in the other channels. The threshold of the nuclear area was set for each different channel, and based on that the pixel ID of the nucleus was determined and divided by its nuclear area. Triplicates of each treatment were analyzed. The respective quantifications are shown in bar graphs of Figures 3b,c, 4f,h,i and 8e,f.

Moreover, I worked in all steps of on the NGF/PD *in vitro* assay, including DRG cultures, NGF or NGF+PD administration, fixation, fluorescent immunocytochemistry for PCAF, H3K9ac and pErk and respective intensity density quantifications (Figure 4a,b). Finally, I acquired and arranged the representative pictures of my experiments that were published in Figures 3, 4, 7 and 8 of Puttagunta et al. (2014).

Having demonstrated how the chromatin environment has to be prepared to allow gene expression in the injured neuron, and knowing that histone modifiers like PCAF and CBP/P300 work in multiprotein complexes, I will next explore some of the other players in

transcriptional complexes that are necessary to activate the intrinsic neuronal regenerative capacity, focusing on the transcription factor p53.

### 2.2.3 *How transcription factors drive the regenerative response? Letting p53 work.*

During development, the axons of nervous cells elongate for long distances thanks to an active growth program related to gene transcription, that couple cytoskeletal changes to extrinsic cues. Once these cells reach their post-synaptic partners, however, the growth cone differentiates into a pre-synaptic terminal and the growth program is switched off (Caroni and Becker, 1992). Accordingly, through developmental stages of the CNS, there is a gradual decline in the expression of factors that promote axon growth, such as the B-cell CLL/lymphoma 2 (Bcl-2) (Chen et al., 1997) and the mammalian target of rapamycin (mTOR) (Park et al., 2008; Liu et al., 2010), while growth repressive factors like the Kruppel-like factors (KLFs) 4 and 9 increase (Moore et al., 2009), highlighting the loss of regenerating capacity of the CNS.

In the injured adult PNS, an intrinsic successful regenerative response is mounted by means of transcription activation or repression associated to key signaling pathways, while in the CNS negative regulators of growth pathways predominate (Liu et al., 2011). Gene transcription is a tightly regulated process, in which transcription factors and co-factors work together to recruit RNA polymerase to specific DNA regulatory regions upstream to the transcription start site (Tedeschi, 2012).

Intuitively, many factors involved in PNS regeneration and in the preconditioning effect have been experimentally manipulated in CNS injury models with the purpose to replicate the PNS successful regenerative response. These factors and their related pathways will now be briefly considered.

In the PNS, axon growth is dependent on neurotrophins (NTs), which include NGF, BDNF, NT-3 and NT-4 acting on correspondingly tyrosine kinase receptors (TrkA for NFG, TrkB for BDNF and NT-4, and TrkC for NT-3) or on the common receptor p75 (Reichardt, 2006). While the reduction of retrograde transported neurotrophins after injury functions as a damage alarm, Schwann cells increase their production and release to support the regenerative response (Seijffers and Benowitz, 2008). The binding of neurotrophins to their recep-

tors triggers various intracellular pathways. The most important ones for axon growth are the phosphoinositide 3-kinases (PI3K)/serine/threonine/protein kinase B (AKT) and the Ras-activated rapidly accelerated fibrosarcoma (RAF)/Erk kinase cascade. The PI3K/AKT pathways seem to regulate the cytoskeleton (Kimpinski and Mearow, 2001), while Erk not only mediates the PCAF-dependent chromatin remodeling, but also activates many transcription factors necessary for regeneration, such as CREB and STAT3, and exerts local effects on microtubule assembly (Gao et al., 2004; Goold and Gordon-Weeks, 2005; Qiu et al., 2005).

Following PNS injury, cyclic AMP (cAMP) levels increase activating the protein kinase A, which phosphorylates the cAMP response element-binding protein (CREB). CREB participates in axon growth by upregulating the expression of Arginase I, which synthesizes polyamines that may interact with cytoskeletal elements and overexpression of CREB promotes regeneration of the dorsal columns after SCI (Gao et al., 2004). Nevertheless, the effects of cAMP elevation are only partially responsible for the potency of conditioning lesions on central axonal regeneration. Compared to cAMP modulation, conditioning lesions initiate far more extensive regenerative responses in DRG neurons, leading to long-lasting changes in gene expression and superior axonal regeneration in vivo (Blesch et al., 2012). Indeed, we showed that cAMP signaling in adult DRG neuronal cultures did not induce nuclear PCAF translocation as opposed by a preconditioning lesion (Puttagunta and Tedeschi et al., 2014, Supplementary Figure 5).

After peripheral injury, local release of neurotrophic cytokines, such as leukemia-inhibitory factor (Banner and Patterson, 1994), interleukin-6 (Cao et al., 2006) and ciliary neurotrophic factor (Xu et al., 2009), activates the JAK/STAT3 pathway. JAKs phosphorylate STAT3, which is then retrograde transported to the nucleus (Liu et al., 2005), complexes with CBP/P300 (Paulson et al., 1999) and drives the expression of RAGs like GAP-43 and *SPRR1A* (Qiu et al., 2005; Wu et al., 2007). Sustained STAT3 delivery results in sprouting in injured dorsal columns (Bareyre et al., 2011).

Other factors induced after PNS injury include the members of the BMP4/Smad1, JNK/c-Jun and the ATF-3 transcription pathways, which provide another point of crosstalk of signaling pathways (Tedeschi, 2012). While forced activation of the Smad1-dependent BMP signaling promoted dorsal column regeneration (Parikh et al., 2011), the induction of the JNK/c-Jun (Carulli et al., 2002) and ATF-3 (Seijffers et al., 2007) pathways was not able to overcome the intrinsic CNS inhibition for axon outgrowth.

Some factors have been directly studied in the CNS, such as KLF4, suppressor of cytokine signaling 3 (SOCS3) and phosphatase and tensin homolog (PTEN) signaling pathways (Liu et al., 2011). Inhibition of these factors promoted regeneration in specific subsets of CNS neurons. *KLF4* is a potent inhibitory gene for axon growth of embryonic hippocampal neurons and retinal ganglion cells (RGCs) (Moore et al., 2009). SOCS3 is a negative regulator of the JAK/STAT pathway and its deletion promoted robust optic nerve regeneration in adult mice (Smith et al., 2009).

In 2008, Park and colleagues had a remarkable discovery. They injected adeno-associated viruses expressing Cre (AAV-Cre) or a control virus into the vitreous body of different adult floxed mice (*Rb<sup>ff</sup>*, *p53<sup>ff</sup>*, *Smad4<sup>ff</sup>*, *Dicer<sup>ff</sup>*, *LKB1<sup>ff</sup>* or *PTEN<sup>ff</sup>*) and performed optic nerve crush (ONC) at later time points. Using this approach, they were able to conditionally and individually delete these genes and observe their effects on retinal ganglion cells (RGCs) regeneration. Among the mouse lines studied, those that had deletion of *PTEN* exhibited the largest effects on both neuronal survival and axon regeneration of RGCs, with some regenerating fibers reaching the optic chiasm 4 weeks after injury (Park et al., 2008).

Nevertheless, such regrowth tapered off within 2 weeks after injury, a similar outcome observed after *SOCS3* deletion (Park et al., 2008; Smith et al., 2009). Simultaneous *PTEN* and *SOCS3* deletion in RGCs, however, enabled robust (more than tenfold increase in the number of regenerating axons compared with deletion of either gene alone) and sustained axon regeneration after optic nerve injury (up to 4 weeks when the double-deletion was performed before the injury, or up to 3 weeks when the double-deletion was performed after injury) (Sun et al., 2011). Gene expression profiling revealed that *PTEN/SOCS3* double deletion triggers differential expression of several pro-regeneration genes, among which two encode critical positive mTOR regulators, namely small GTPase Rheb and insulin-like growth factor 1 (IGF1) (Sun et al., 2011). Sustained regeneration would be critical in the clinical setting, in which regenerating axons would need to surpass the hurdle of much greater distances imposed by adult organisms to reinnervate their original targets.

Investigators also tested whether neonatal *PTEN* conditional deletion in neurons of the sensorimotor cortex (SMC) would also promote CST regeneration following unilateral pyramidotomy, T8 dorsal hemisection or T8 complete crush in the adult (Liu et al., 2010). In fact, this resulted in extensive trans-midline sprouting from the intact CST into the denervated (pyramidotomized) site, and unprecedented regeneration of adult CST axons in both SCI



models up to 3 mm caudal to the injury site (Liu et al., 2010). These regenerating CST axons were able to form synapses caudal to the lesion (Liu et al., 2010), but functional recovery was unexpectedly only modest, as reported in another cohort of experiments, in which short-hairpin RNA (shRNA) was employed to suppress PTEN expression (Zukor et al., 2013). PTEN is an antagonist of PI3K activity, and *PTEN* deletion leads to AKT activation, consequently triggering mTOR, which controls cell growth and size by regulating cap-dependent protein translation initiation (Guertin and Sabatini, 2007; Park et al., 2010), therefore it is likely that neuronal growth competence is dependent on the capability of new protein synthesis, which provides building blocks for axonal regrowth.

In the past decade, another factor that emerged as a prominent candidate for controlling axon regeneration pathways is the transcription factor p53. p53 is at the hub of numerous signaling pathways that are triggered in response to particular stresses, all of which can leave their mark on p53 by way of diverse post-translational modifications (phosphorylation, acetylation, sumoylation and neddylation) and interactions with cofactors. The precise combination of these marks dictates the behavior of p53 in any given situation (Murray-Zmijewski et al., 2008).

p53 is activated mainly after genotoxic and oxidative stress and depending upon the level of DNA damage, it determines cell fate. Moderate damage leads to p53-dependent G1 cell cycle arrest to repair the DNA (Sengupta and Harris, 2005; Okorokov, 2014), whereas high dose damage inflicts apoptosis to restrain tumor formation (Okorokov, 2014). p53-downstream effectors of these responses are *p21* and *GADD45* for cell cycle arrest (Taylor and Stark, 2001), or pro-death genes including *BAX*, *NOXA*, *PUMA*, *FAS*, *DR5* and *APAF-1* (Harms et al., 2004; Murray-Zmijewski et al., 2008). Therefore, p53 is recognized as the genome gatekeeper and has been widely explored in cancer medicine for its tumor suppressor properties.

But p53 is a pleiotropic factor that governs many other aspects of the cell life, including angiogenesis, senescence and cell growth (Green and Chipuk, 2006; Riley et al., 2008). In the nervous system, it was demonstrated that p53 is involved in cell survival, proliferation and differentiation of the developing CNS (Armesilla-Diaz et al., 2009; Tedeschi and Di Giovanni, 2009; Quadrato and Di Giovanni, 2012). And as demonstrated by key experiments summarized in the next paragraphs, it also plays a definite role in the regeneration of the nervous system. In fact, the p53-dependent decision-making process that results either

in neuronal death or survival during development is similar to the one that drives axonal retraction or outgrowth in the injured adult nervous system (Tedeschi and Di Giovanni, 2009). Again, post-translational modifications of p53 are at the forefront of this decisive process, with phosphorylation of specific serine and threonine residues being often associated with increased neuronal death following genotoxic stress, while acetylation of specific lysine residues are implicated in outgrowth and differentiation of neural cells (Figure VIII) (Tedeschi and Di Giovanni, 2009).

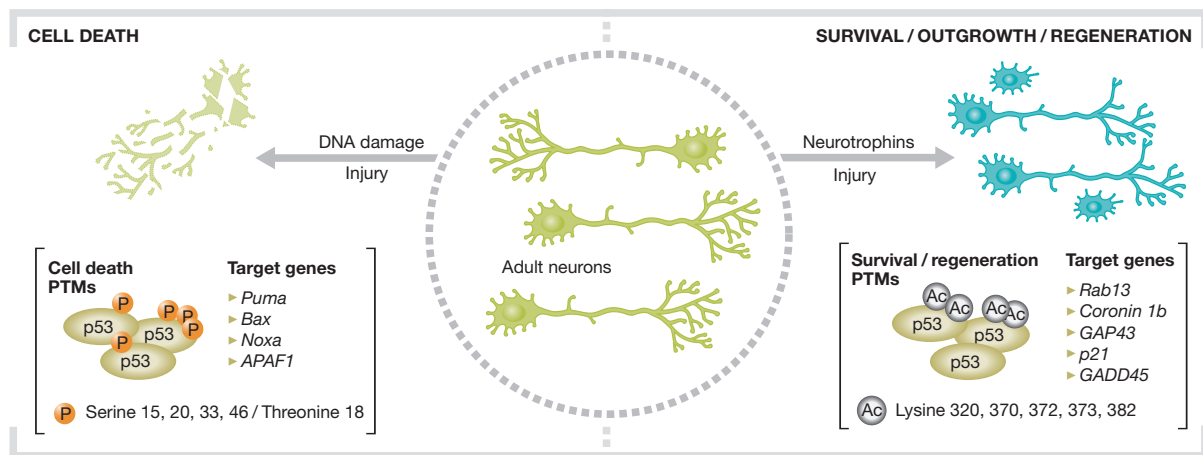


**Figure VIII. p53-mediated decision-making processes in neurons.** p53 PTMs and related target genes involved in cell death or survival/outgrowth/regeneration after lesion in the adult nervous system. (Adapted from Tedeschi and Di Giovanni, page 579, *EMBO Rep* 2009; 10(6):576-83.)

By employing temporal gene expression profile after SCI, Di Giovanni and colleagues (Di Giovanni et al., 2005) identified a cluster of induced genes whose proteins promote neurite outgrowth, including the actin-binding protein Coronin 1b and the small GTPase Rab13. They also showed that these proteins are co-expressed with GAP-43 in axons in the spinal cord after injury. By investigating a possible common transcription factor driving the expression of these genes, they found that Coronin 1b and Rab13 share multiple p53 transcription binding sites (Di Giovanni et al., 2006). In fact, they showed that p53 is required for neurite outgrowth in cultured cells including primary neurons as well as for axonal regeneration after facial axotomy in mice (Di Giovanni et al., 2006).

Furthermore, a specific PTM in p53, the acetylation of lysine 320 (K320), provokes the binding of p53 to Coronin 1b and Rab13 promoters to drive their expression, and p53 also induced the expression of the pro-regenerative protein GAP-43 (Di Giovanni et al.,

2006). Interestingly, PCAF specifically acetylates p53 at K320 (Knights et al., 2006), and overexpression of PCAF increased the binding of acetylated p53 to the promoters of Coroin 1b and Rab13 (Di Giovanni et al., 2006). Therefore, a new function was added to the vast p53 repertoire, showing that it was able to coordinate the regenerative response of adult neural cells. In fact, p53 can be activated by NGF (Eizenberg et al., 1996), which lead to PTMs in p53 via the kinases Erk1/2 and 2, p38MAPK, JNK1-2 and the acetyltransferase PCAF (Di Giovanni and Rathore, 2012), evidencing the crosstalk of p53 with other established intrinsic neuroregenerative pathways.

Further investigation of the interaction between p53 and GAP-43, a prototypical protein for axon growth, which is highly expressed in the developing nervous system and in the PNS and CNS following injury, revealed that p53 forms a transcriptional complex with CBP/P300 in a chromatin environment. This complex specifically acetylates p53 at lysines 372, 373 and 382 (K372-3-82) and is then recruited to the GAP-43 promoter to drive the expression of GAP-43 (Tedeschi et al., 2009a). This was also demonstrated *in vivo*, where both CBP and p53 K372-3-82 were induced following facial motor neurons axotomy and the p53/GAP-43 transcriptional module was essential to promote facial nerve regeneration (Tedeschi et al., 2009a).

p53 also drives the expression of the cGMP-dependent protein kinase type I (cGKI) during neuronal maturation, which counteracts Semaphorin 3A-induced growth cone collapse (Tedeschi et al., 2009b). Moreover, it has been shown that p53 is present in the growth cones of primary hippocampal neurons, where it prevents their collapse by inhibiting the Rho kinase activity (Qin et al., 2009). Furthermore, Semaphorin 3A-mediated growth cone collapse results partially from calpain-mediated truncation of phosphorylated p53, leading to Rho kinase activation and cytoskeleton reorganization (Qin et al., 2010), while Semaphorin 3F downregulates p53 expression to promote growth cone collapse (Yang et al., 2012). These findings indicate that p53 operates either by transcriptional activation of specific RAGs or locally at the growth cone, the structure that is crucial for successful axon regeneration and proper synaptic formation.

In line with the previous mentioned p53 studies in neural regeneration based on chromatin remodeling and formation of transcription complexes, *in vitro* hyperacetylation driven by HDAC inhibition enhanced the acetylation of CBP/P300 and PCAF promoter, forming a positive feedback loop to increase the expression of these HATs, which led to

H3K9 acetylation to relax the chromatin environment and facilitate p53 occupancy of specific promoters. In its turn, p53 acetylation activated the transcription of RAGs, thereby promoting neurite outgrowth and preventing growth cone collapse of cerebellar granule neurons not only in permissive, but also in non-permissive substrates. Interestingly, in untreated (normally acetylated) cells the expression of CBP/P300 and PCAF was reduced by exposure to myelin (Gaub et al., 2010), linking extrinsic cues to the intrinsic machinery failure of central neurons to reactivate a pro-growth program. In an *in vivo* paradigm, HDAC inhibition induced CBP expression and retinal ganglion cells (RGCs) survival but not regeneration following optic nerve crush (ONC) in adult rats. Overexpression of P300, however, was able to promote axon regeneration after ONC as a result of H3 acetylation-dependent chromatin remodeling and acetylation of the pro-growth transcription factors p53 and C/EBP, direct promoter acetylation and occupancy of *GAP-43*, *CORO1B* and *SPRR1A*, and transcription activation of several other RAGs (Gaub et al., 2011).

*In vivo* studies in spinal cord injured-adult p53<sup>-/-</sup> mice showed that in the absence of p53 corticospinal spinal axons had increased dieback, greater number of retraction bulbs and less sprouting in comparison to wild type animals. Reduced sprouting was also observed in serotonergic fibers (Floriddia et al., 2012). Strikingly, p53<sup>-/-</sup> mice also exhibited an enhanced scarring reaction at the lesion site, as evidenced by increased areas of fibronectin deposition and reactive GFAP<sup>+</sup> astrocytes. Moreover, these mice showed a greater number of active microglia/macrophages, but the M1/M2 ratio was similar between p53 null and wild-type mice at the injury site, with M1 cells predominating in both genetic backgrounds. Coupled with these findings, p53<sup>-/-</sup> mice displayed less functional recovery in locomotor tests (Floriddia et al., 2012). Gain of function experiments were able to rescue CST sprouting above the lesion and neurite outgrowth of primary cortical neurons *in vitro* (Floriddia et al., 2012).

These results indicate that p53 is a key orchestrator of CNS regeneration, playing a pivotal role in activating the intrinsic regenerative capacity of post-mitotic CNS neurons in addition to modulate the extrinsic environment where these neurons lie in, thus motivating us to test whether enhancing p53 activation would increase regeneration and functional recovery after SCI. The first strategy was to force p53 expression in the layer V neurons of the mouse sensorimotor cortex, which gives rise to the CST, using viral vectors carrying p53 constructs that mimic p53 acetylation at lysines K320-72-3-82 in its C-terminus (K320-72-3-

82Q), which had already proven to be efficient to promote neurite outgrowth *in vitro* on a non-permissive substrate (Gaub et al., 2010). However, p53 overexpression did not enhance CST sprouting (Simone Di Giovanni's personal communication), suggesting that other molecular players were probably compensating the p53 overexpression to hinder its activity.

After all, p53 regulates cell survival and death decisions, therefore its levels and activation must be tightly regulated to maintain tissue homeostasis. This is achieved by a number of ubiquitin ligases, including MDM2 (Momand et al., 1992), MDM4 (also known as MDMX) (Shvarts et al., 1996), ARF-BP1/Mule (Chen et al., 2005), COP1 (Dornan et al., 2004) and Pirh2 (Leng et al., 2003), that control p53 protein levels and subcellular compartmentalization. Particularly, MDM2 and MDM4 are partners of a sophisticated feedback system to keep p53 in check. In a resting cell, p53 is kept at low levels owing to the E3 ubiquitin-ligase activity of MDM2, which catalyzes p53 polyubiquitylation that targets it for proteasomal degradation, while MDM4 inactivates p53 by occluding its transactivation domain (Toledo and Wahl, 2006). In this scenario, MDM2-dependent monoubiquitylation of p53 also promotes the translocation of p53 from the nucleus to cytoplasm (Wade et al., 2010). Furthermore, both MDM2 and MDM4 are able to inhibit CBP/P300-mediated p53 acetylation (Sabbatini and McCormick, 2002). Upon stress, MDM2 and MDM4 are degraded to transiently allow p53 transactivation, but once the stress is relieved, they accumulate to inactivate and reduce p53 back to its low basal levels (Figure IX) (Toledo and Wahl, 2006; Wade et al., 2010). Specifically, MDM4 inhibits p53 transactivation in overexpression studies (Shvarts et al., 1996), which may explain why overexpression of wild type p53 in the sensorimotor cortex, in the eye, or in the spinal cord after axonal injury did not result in reactivation of the axonal growth program (not shown, data from Simone Di Giovanni's laboratory).

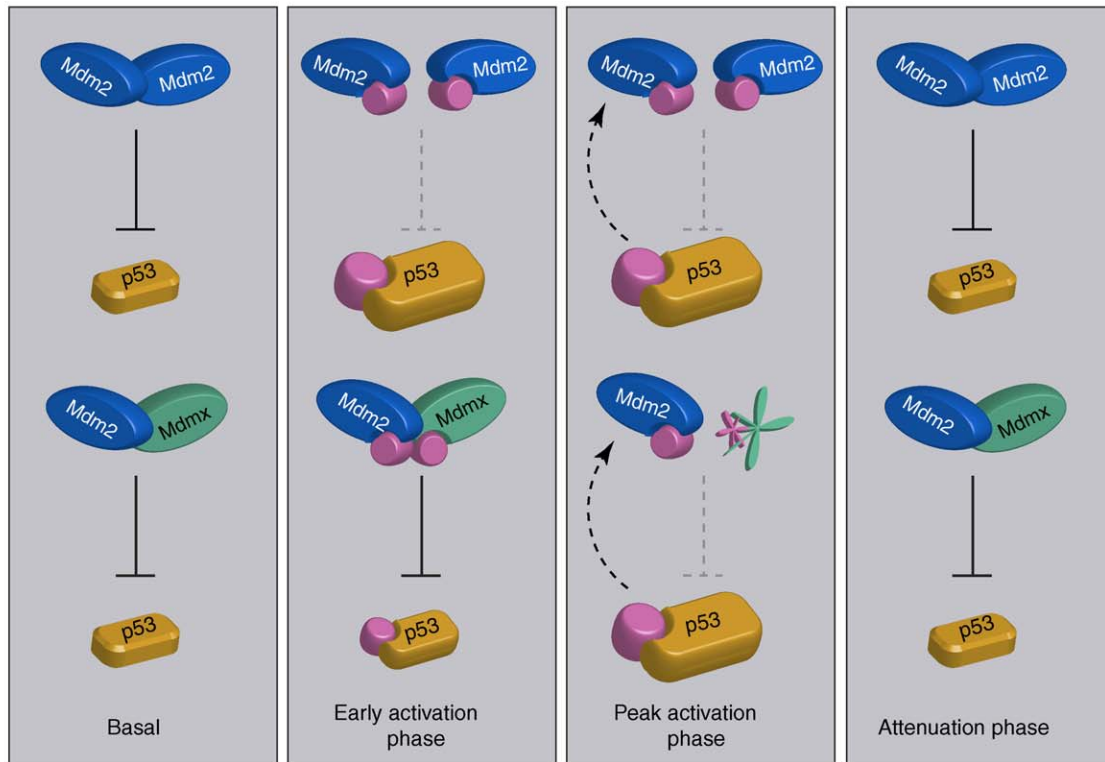


**Figure IX. Control of p53 stability by Mdm2 homo-oligomers and Mdm2-Mdmx hetero-oligomers.** Basal p53 levels are regulated by both Mdm2 homo-oligomers and Mdm2/Mdmx hetero-oligomers. Immediately following DNA damage, during the early activation phase, Mdm2 is destabilized, and phosphorylated at residues outside the RING domain, destabilizing Mdm2 oligomers, leading to increased p53 levels. At the peak activation phase, Mdm2 degrades itself and Mdmx, which removes Mdm2-Mdm2 and Mdm2-Mdmx oligomers, leading to maximal p53 accumulation. During the activation phase, p53 also transactivates the Mdm2 gene (dashed arrow). The attenuation phase begins when DNA damage signaling abates. Kinase inhibition and phosphatase activation removes the pool of phosphorylated Mdm2 and Mdmx, leading to their stabilization. As a result, the homo- and hetero-oligomers regain p53 ubiquitin ligase activity, reducing p53 to basal levels. In addition to regulation of Mdm2 and Mdmx, phosphorylation of p53 during the damage response also contributes to p53 activation by decreasing the affinity for negative regulators, and increasing the affinity for transcriptional co-factors. (Adapted from Wade et al., page 303, *Trends Cell Biol* 2010; 20(5):299-309.)

We therefore decided to experimentally disturb the interaction of p53 with MDM2 or MDM4 to enhance p53 transactivation in two models of CNS injury in mice, SCI and ONC, as we recently reported in Joshi and Sória et al. (2015). For this work, I performed all the SCI and behavioral experiments, while my colleague Y. Joshi was in charge of the ONC model. Firstly, we tested whether the conditional genetic deletion of *MDM4* in corticospinal neurons would aid in p53 transactivation to stimulate the growth program after CST transection. For that, we used homozygous adult *MDM4* floxed mice (*MDM4<sup>fl/fl</sup>*), in which *MDM4* is flanked by loxP sites and can be excised by Cre recombinase. To delete *MDM4* specifically in neurons giving rise to the CST, I stereotactically injected in layer V neurons of the SMC an adeno-associated virus type I (AAV1), which is the optimal serotype to infect corticospinal

neurons (Hutson et al., 2012), encoding a green fluorescent protein (GFP)/Cre recombinase fusion protein (AAV1-CreGFP), or AAV1-GFP in controls. Infected cells express GFP, therefore infection can be ascertain by immunohistochemistry. I monitored the infection specificity of layer V cortical neurons by co-staining GFP with Ctip2 (Supplementary Figure 4, Joshi and Sória et al., 2015, reproduced below as Figure X), a marker expressed by layer V and VI neurons (Lickiss et al., 2012).

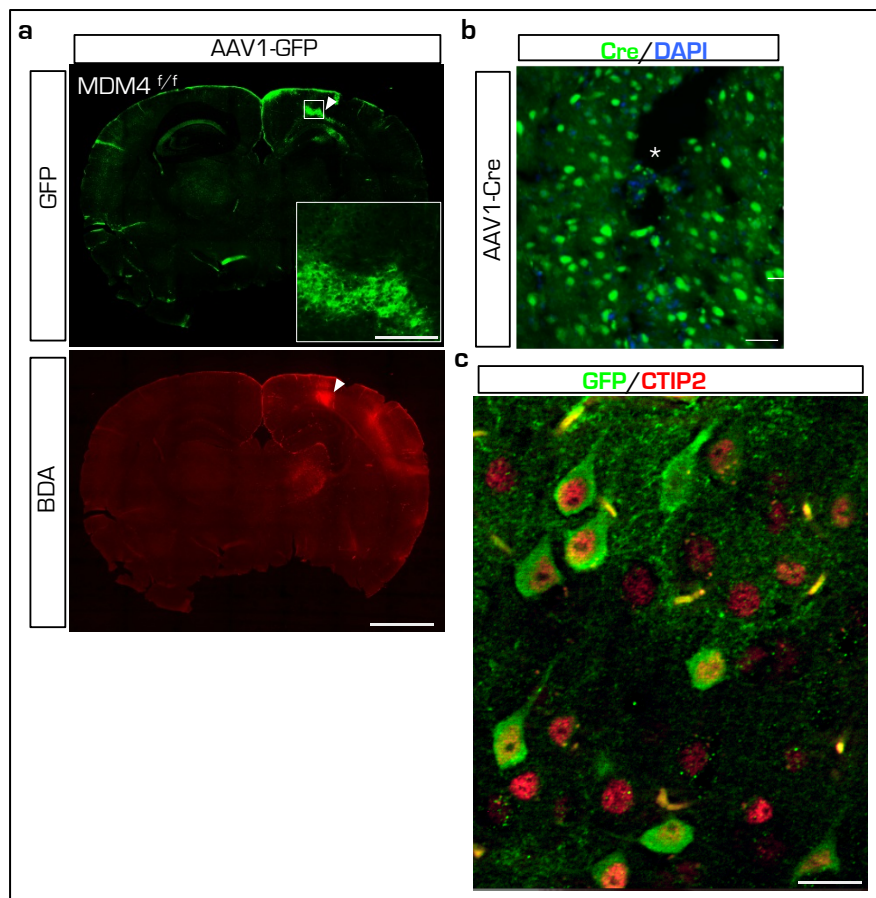


**Figure X. Infection and labeling of SMC layer-V neurons.** (a) Shown are GFP and BDA labeling of the sensorimotor cortex after stereotaxic delivery of AAV-GFP or BDA. Inset shows layer V in the sensorimotor cortex. Scale bar 500  $\mu$ m. (b) Shown are cre-positive cells after anti-cre immunostaining in proximity of the injection site (asterisk) of AAV-cre in the sensorimotor cortex. Scale bar 50  $\mu$ m. (c) Immunostaining for GFP and CTIP2 (layer V neurons marker) show AAV-GFP infection of layer V neurons in the sensorimotor cortex. Scale bar 20  $\mu$ m. (Reproduced from Joshi and Sória et al., *Brain* 2015;138(Pt 7):1843-62.)

Five weeks after the viral injections, at the time when the AAV1 infection rate should be close to peak levels (Mason et al., 2010), I performed T9 spinal cord dorsal hemisections for both groups, a lesion that transects the dorsal and lateral CSTs. Two weeks later, the CST fibers were traced with fluorescent biotin dextran tetramethylrhodamine (BDA). Comparative stereological analysis of the corticospinal axons showed that in animals injected



with AAV1-CreGFP there was a significant increase of sprouting not only rostral, but also caudal to the lesion site extending up to 1 centimeter (Figure 2, reproduced below as Figure XI, and Supplementary Figure 5, Joshi and Sória et al., 2015). These results showed that releasing p53 of the MDM4 inhibitory influence allowed p53 to enhance the regenerative capacity of the otherwise refractory CST axons.

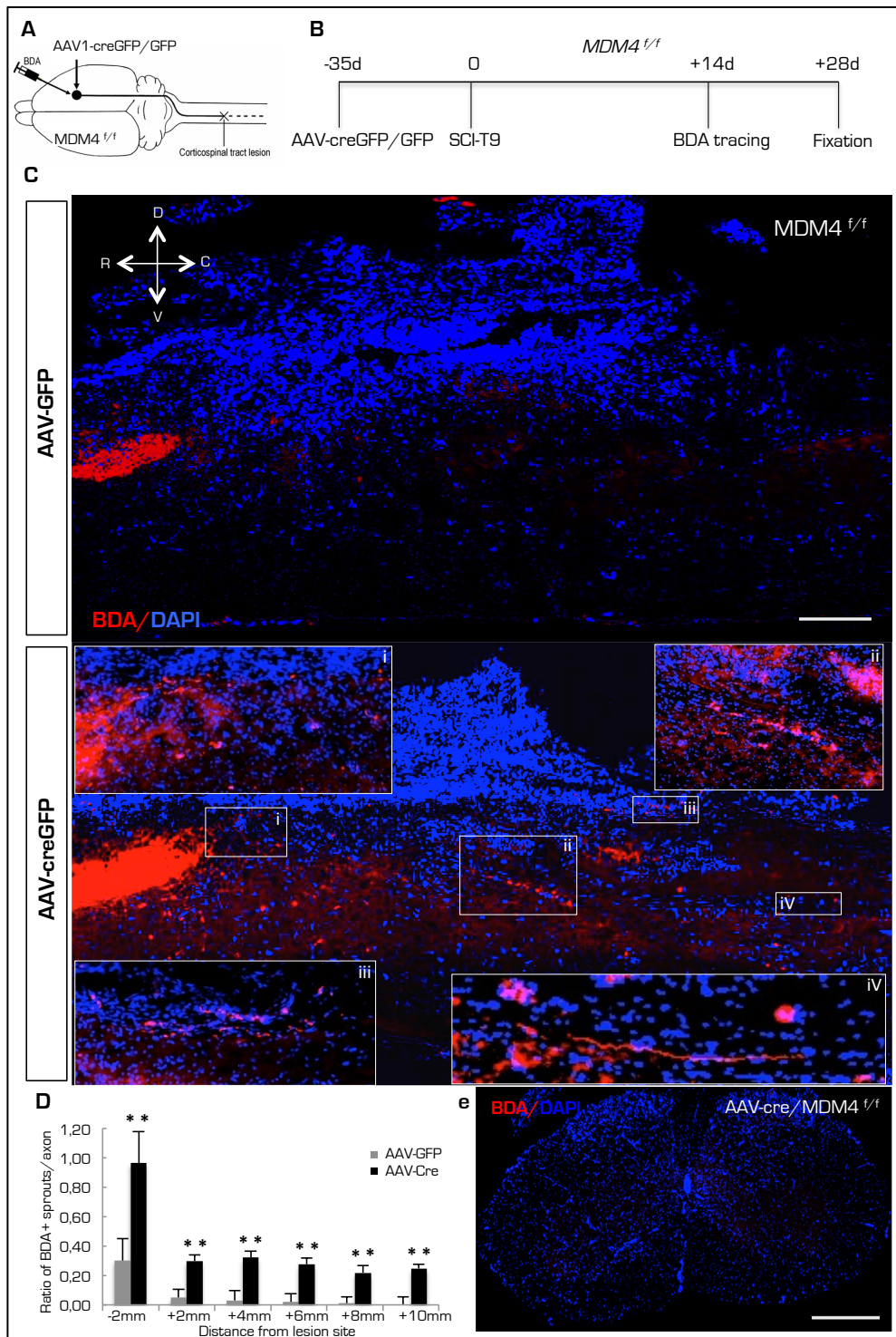




**Figure XI. Conditional deletion of MDM4 in the sensorimotor cortex enhances corticospinal tract sprouting following T9 dorsal hemisection in MDM4<sup>fl/fl</sup> mice.** (A and B) Schematic diagrams summarizing the experimental design. AAV-CreGFP/AAV-GFP particles were injected in the sensorimotor cortex of adult MDM4<sup>fl/fl</sup> mice 5 weeks before T9 dorsal hemisection. BDA for corticospinal tract labelling was injected 14 days before sacrificing the animal. (C) Representative images of sagittal sections from MDM4<sup>fl/fl</sup> mice after cortical AAV-GFP/AAV-CreGFP infection. The corticospinal tract was traced by BDA injection (red) in the cortex. Spinal cord sections were also stained with DAPI (blue). High magnification images (insets) show the sprouting axons past the lesion site, in the AAV-CreGFP infected mice. Scale bar = 500  $\mu$ m. (D) Quantification of the BDA-labelled sprouting corticospinal tract in the spinal cord rostral and distal to the lesion site. (Mann Whitney test, \*\* $P < 0.001$ ,  $N = 10$  for AAV-GFP and  $N = 9$  for AAV-CreGFP, number of cords analyzed). (E) Coronal section of a spinal cord 15 mm caudal to the lesion site showing completeness of the lesion with lack of BDA positive corticospinal tract labelling after AAV-Cre infection in the sensorimotor cortex of MDM4<sup>fl/fl</sup> mice (5 weeks post-spinal cord injury). Scale bar = 500  $\mu$ m. (Reproduced from *Joshi and Sória et al., page 1851, Brain 2015;138(Pt 7):1843-62.*)

Next, we decided to test whether inhibiting MDM2 would also enhance regeneration after SCI. This time, instead of employing genetic manipulation, we decided to use a more clinically applicable approach by inhibiting the MDM2-p53 interaction pharmacologically. The drug of choice was Nutlin-3a, the most potent enantiomer of Nutlin-3, which belongs to a class of selective small-molecule antagonists of MDM2. These compounds are cis-imidazoline analogs that bind MDM2 in the p53 binding pocket and activate the p53 pathway in cancer cells (Vassilev et al., 2004). One of the Nutlin compounds, RG7112, is currently in Phase II clinical trials for cancer therapy (Biswas et al., 2014), and therefore is a real candidate for future clinical application.

For the experiments with Nutlin-3a, we employed adult C57BL/6 wild type mice. I delivered the drug or vehicle via osmotic minipump (model 2002, Alzet, USA) connected to an intrathecal catheter, and performed the T9 spinal cord dorsal hemisection during the same surgical procedure for implantation of the minipump/catheter system. In the day preceding the surgeries, the minipumps were primed, i.e. incubated overnight in saline at 37 °C to assure immediate drug or vehicle delivery after implantation, as indicated by the manufacturer. I placed the catheter in a way to have its tip just caudal to the lesion site (Figure XII). With this system, 4  $\mu$ M/day of Nutlin-3a diluted in 8,6% ethanol/PBS or homologous vehicle were delivered at 0,43  $\mu$ l/hour at the injury site (for details on the mathematic calculations, please refer to the Appendix).

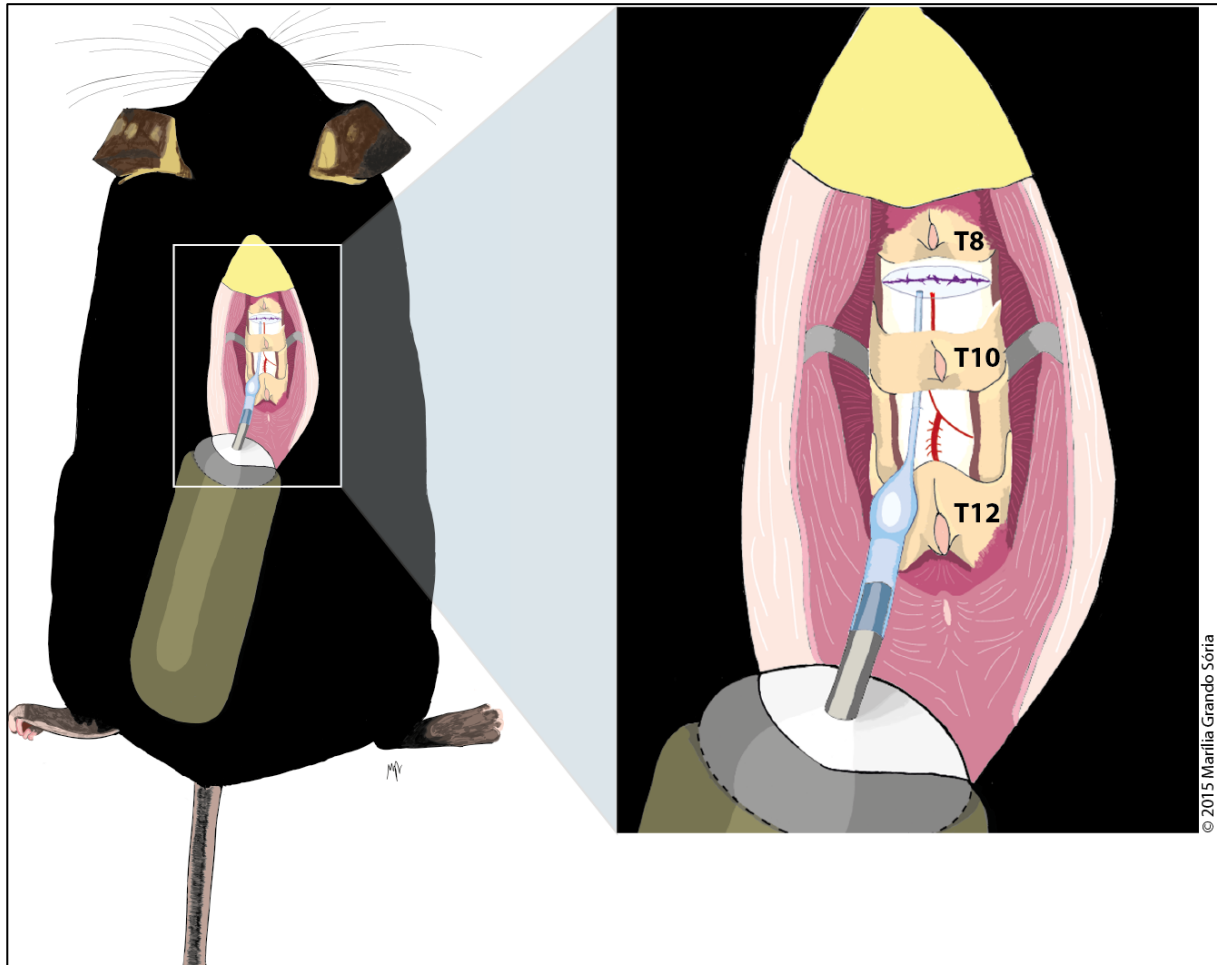


**Figure XII. Schematic illustration of the osmotic minipump/intrathecal catheter system.** After exposing the spinal processes from T8 until T12, laminectomies at the T9 and T11 vertebral levels exposed the spinal cord underneath. A polyethylene 32 G intrathecal catheter (external diameter of  $0,025 \pm 0,0038$  cm) was subdurally inserted at T11 and driven until T9. Its caudal extremity was fixed at T12 with a cyanoacrylate glue and attached to the flow moderator of the pump. The pump was lodged in the subcutaneous tissue of the back of the animal. In order to strength the fixation, a muscular “tunnel” involving the catheter was created by suturing the cut extremities of the superficial muscle layers (in light rose, right panel) at the midline on top of the catheter (from T10 until T12, not shown). With the catheter tied in place, the dorsal hemisection was performed at T9, in a way that the upper extremity of the catheter was just apposed to the injury site. Finally, the above muscles and skin were sutured. (Original illustration by Sória MG, 2015.)

Three days later, in animals receiving Nutlin-3a, immunoblotting of the spinal cord comprising the injury site and two adjacent vertebral segments, one above and other below, revealed that acetylated p53 and its prototypic target p21 were induced, while not increasing cleaved caspase-3, a classic apoptotic marker (Supplementary Figure 10, Joshi and Sória et al., 2015, reproduced below as Figure XIII), suggesting that Nutlin-3a was *de facto* leading to p53 transactivation. Furthermore, in cultured cerebellar granular neurons Nutlin-3a induced several axon growth associated and p53 target genes, without leading to apoptosis (Supplementary Figure 8, Joshi and Sória et al., 2015).

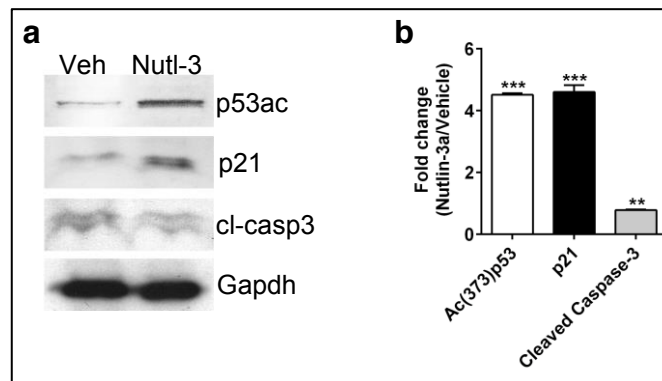


**Figure XIII. Spinal cord immunoblotting after Nutlin-3 or vehicle delivery.** (a) Representative immunoblotting from a spinal cord 72 hours after Nutlin-3 or vehicle delivery with osmotic minipump and spinal cord T9 hemisection. Shown is enhancement of active acetylated p53 (p53ac) and of the prototypical p53 target gene p21 after Nutlin-3 versus vehicle. Classical cell death pathways were also not induced by Nutlin-3 as shown by cl-caspase 3 expression. (b) Bar graphs show densitometry analysis (arbitrary units) expressed as fold change of Nutlin3 versus vehicle.  $N = 3$ . Student's unpaired two-tailed  $t$ -test  $**P < 0.01$  or  $***P < 0.001$ . (Reproduced from Joshi and S3ria et al., *Brain* 2015;138(Pt 7):1843-62.)

Having confirmed the effectiveness of Nutlin-3a delivery and activity in our tissue, we extended the drug or vehicle delivery further to 2 weeks after SCI, and assessed the locomotor behavior weekly until 35 days after injury. During this period, treatment and control groups did not show differences in health outcomes, and Nutlin-3a seemed to be well tolerated. We employed two tests for behavioral assessment, the Basso Mouse Scale (BMS) and the grid walk. The BMS was specifically developed to evaluate mice that suffered a midthoracic SCI at T9 (Basso et al., 2006). It assesses features of locomotion that should be progressively reacquired by injured mice during their recovery period, if the injury type or the treatment provided permit recovery from paraplegia at all. Initially, mice reacquire ankle movements, followed by an intermediate phase when they recover the weight support of the hindlimbs evolving to stepping. In the late phase of recovery, fine details of locomotion are assessed, including forelimb-hindlimb coordination, paw position during stance, and the extent of trunk stability. The BMS main score consists of 9 points, ranging from no ankle movement (0) to normal or nearest normal behavior (9), while the BMS subscore is also cumulative (from 0 to 11) and is useful to discriminate differences in the fine details of locomotion that may not be apparent in the main score (Basso et al., 2006).

The grid walk is a more challenging behavioral task and thereby more sensitive to residual deficits (Bresnahan et al., 1987), therefore only animals able to frequently or consistently plantar step (BMS  $\geq 5$ ) were tested in this modality. To perform well on this examina-

tion, the animals must demonstrate normal limb coordination, which is mediated by ventrolateral tracts, have an intact reticulospinal system for initiation of stepping rhythm, and possess voluntary motor control, which is mediated by corticospinal and rubrospinal systems (Metz et al., 2000).

In our experiments, animals treated with Nutlin-3a performed better in both behavioral modalities in comparison to controls, having significantly higher punctuations on the BMS main and subscores as of the second week (Figure 7, Joshi and Sória et al., 2015, reproduced below as Figure XIV). In the grid walk, Nutlin-3a-treated mice also missed significantly fewer steps than controls from the third week on. Moreover, the majority of the animals showing enough recovery for grid walk assessment belonged to the Nutlin-3a group for all time points after injury (Figure 7, Joshi and Sória et al., 2015, reproduced below as Figure XIV). After the last behavioral tests (35 days after SCI), BDA was injected in the right SMC of the animals to trace the CST. Ten days later they were sacrificed and the spinal cords processed for histology. Stereological analysis revealed a significant increase of CST sprouting above and below the lesion in Nutlin-3a-treated animals in comparison to controls (Figure 7, Joshi and Sória et al., 2015, reproduced below as Figure XIV). These animals also displayed increased sprouting of serotonergic fibers below the lesion (Figure 8, Joshi and Sória et al., 2015, reproduced below as Figure XV).

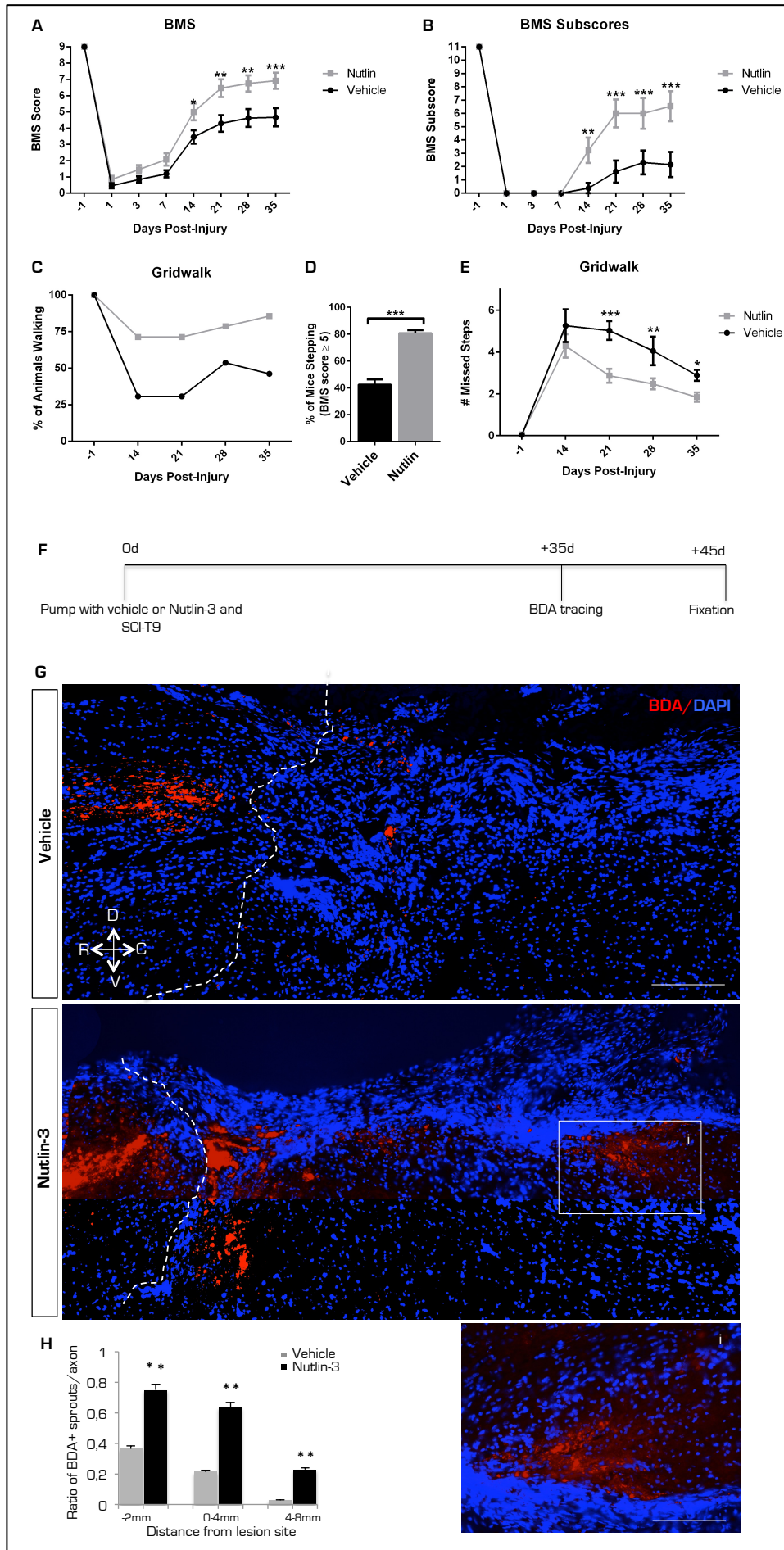




**Figure XIV. MDM2/p53 inhibition via Nutlin-3 delivery enhances neurological recovery and corticospinal tract regeneration following T9 dorsal hemisection.** (A) Basso Mouse Scale score and subscore (B) show significant improvement in locomotion in Nutlin-3 treated mice (Nutlin-3 or vehicle were delivered via osmotic minipump connected to an intrathecal catheter in proximity of a T9 dorsal hemisection for 14 days post-injury). (C) Percentage of mice able to walk on a gridwalk is much higher after Nutlin-3 treatment versus vehicle. (D) Percentage of mice with a Basso Mouse Scale score  $\geq 5$  from 14 days after injury. (E) Number of missteps on a gridwalk is significantly reduced by Nutlin-3 treatment (two-way ANOVA with Sidak's multiple comparisons,  $***P < 0.001$ ;  $**P < 0.01$ ;  $*P < 0.05$ ,  $N = 13$  (vehicle),  $N = 13$  (Nutlin)). (F) Schematic diagram summarizing the experimental design. BDA for corticospinal tract labelling was injected 10 days before sacrifice. SCI = spinal cord injury. (G) Representative images of sagittal cord sections of mice treated with Nutlin-3 or vehicle. The corticospinal tracts were traced by BDA injection (red) in the cortex. Spinal cord sections were also stained with DAPI (blue). Visible are sprouting axons past the lesion site in the Nutlin-3 treated mice. Scale bar = 500  $\mu\text{m}$ . Inset (i) showing sprouting corticospinal tract fibers at higher power. (H) Quantification of the BDA labelled sprouting corticospinal tract axons in the spinal cord rostral and distal to the lesion site. (Mann Whitney test,  $**P < 0.01$ ,  $N = 7$ ). (Reproduced from Joshi and Sória et al., page 1859, *Brain* 2015;138(Pt 7):1843-62.)

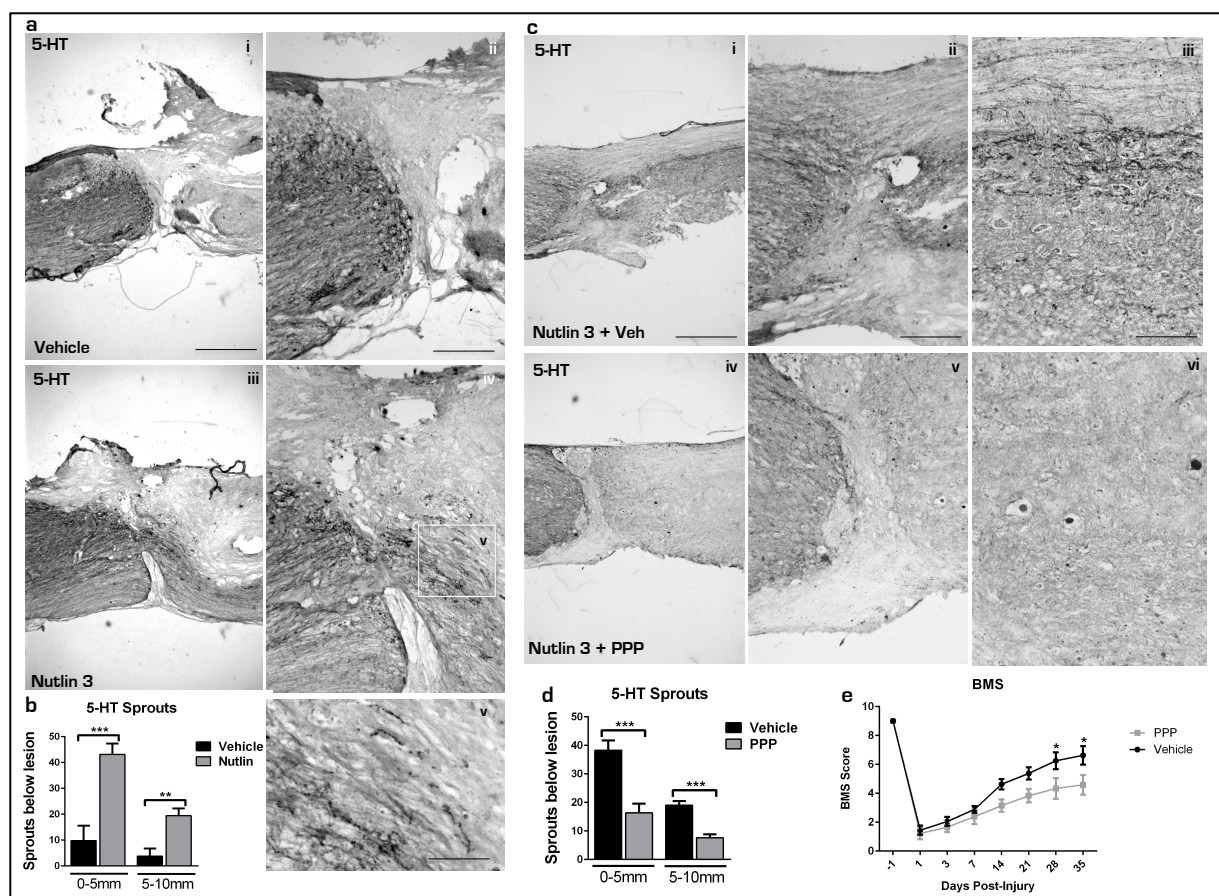


**Figure XV. MDM2/p53 inhibition via Nutlin-3 delivery enhances 5-HT axonal sprouting and functional recovery via IGF1 following T9 dorsal hemisection.** (A) Representative images of sagittal cord sections of mice treated with Nutlin-3 or vehicle (Nutlin-3 or vehicle were delivered via osmotic minipump connected to an intrathecal catheter in proximity of a T9 dorsal hemisection for 14 days post-injury). Raphe-spinal fibres were labelled with an anti-5-HT antibody (immunoperoxidase). Visible are parasagittal cord sections with numerous sprouting axons past the lesion site in the Nutlin-3 treated mice (45 days post-injury). (i and iii) Scale bar = 2,5 mm. (ii and iv) Scale bar = 750  $\mu\text{m}$ . Inset (v): sprouting fibers at higher power. Scale bar = 50  $\mu\text{m}$ . (B) Quantification of the 5-HT-positive fibers in the spinal cord distal to the lesion site. (Unpaired Student's *t*-test,  $***P < 0.001$ ;  $**P < 0.01$ ,  $N = 7$ ). (C) Representative images of sagittal cord sections of mice treated with Nutlin-3 via osmotic mini-pump and intraperitoneal delivery of picropodophyllin (PPP) or vehicle (for 14 days post-spinal injury). Raphe-spinal fibres were labelled with an anti-5-HT antibody (immunoperoxidase). Visible are parasagittal cord sections with numerous sprouting axons past the lesion site in the Nutlin-3 and vehicle treated mice, while only a few are visible after picropodophyllin (35 days post-injury). (i and iv) Scale bar = 2,5 mm; (ii and v) Scale bar =

750  $\mu\text{m}$ ; (iii and vi) Sprouting fibres at high power. Scale bar = 60  $\mu\text{m}$ . (D) Quantification of the 5-HT positive fibres in the spinal cord distal to the lesion site. (Unpaired Student's *t*-test,  $***P < 0.001$ ;  $**P < 0.01$ ,  $N = 7$ ). (E) Basso Mouse Scale score shows significant reduction in locomotion performance in Nutlin-3 and picropodophyllin treated mice versus Nutlin-3 and vehicle (two-way ANOVA with Sidak's multiple comparisons,  $*P < 0.05$   $N = 10$ ). (Reproduced from Joshi and Sória et al., page 1860, *Brain* 2015;138(Pt 7):1843-62.)

At the injury site, Nutlin-3a-treated animals displayed less fibronectin deposition and decreased number of activated microglia/macrophages (Figure XVI).

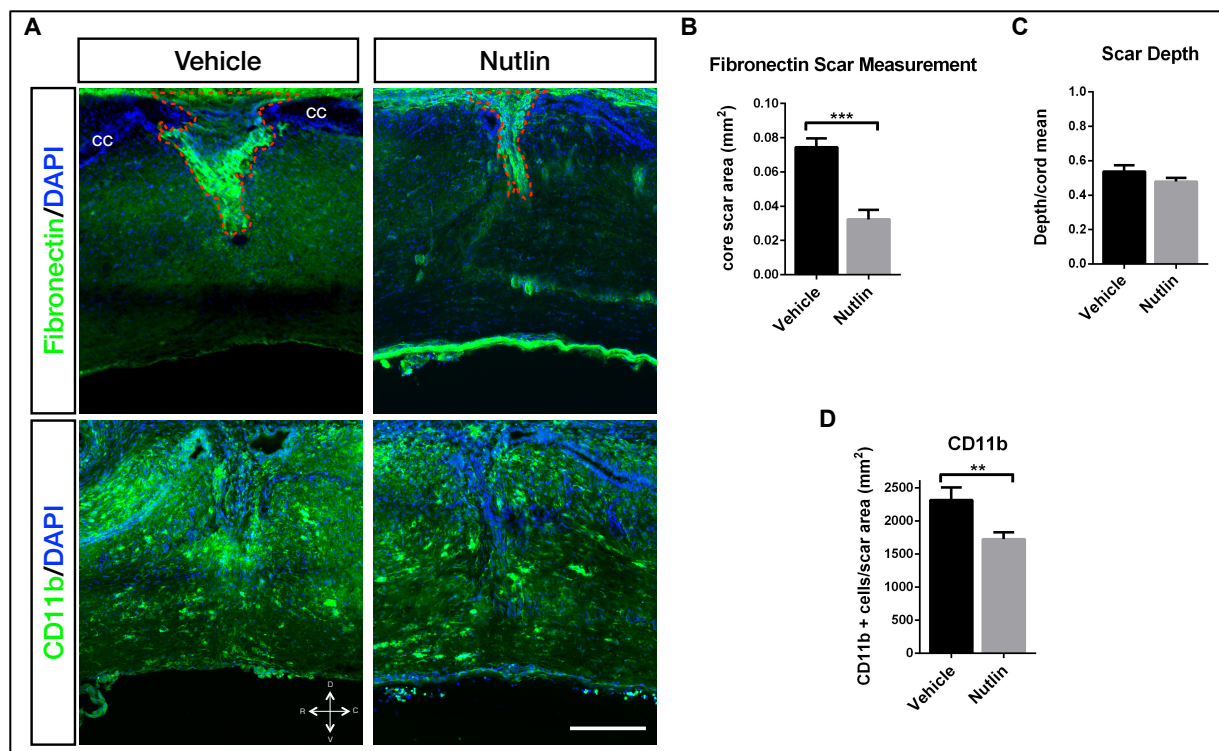


**Figure XVI. Nutlin-3 reduces the size of the fibronectin-positive core scar area and the density of CD11b<sup>+</sup> cells at the injury site.** (A) Representative photomicrographs of spinal cord injury sections of vehicle- or Nutlin-3-treated animals 45 days after T9 dorsal hemisection stained for fibronectin or CD11b. The pictures depict the injury site (R, rostral; C, caudal; D, dorsal; V, ventral; cc, central canal), scale bar 350  $\mu\text{m}$ . (B) In Nutlin-3 samples, there was a significant reduction in the fibronectin core scar area (unpaired two-tailed Student's *t*-test,  $***P < 0,001$ ,  $N = 12$  for Nutlin-3 and  $N = 5$  for vehicle, performed in triplicate), while the scar depth was similar between groups (C), an evidence that the surgeon could consistently reproduce the lesion between animals and groups. (D) Nutlin-3 samples also exhibited significantly fewer activated microglia/macrophages (i.e. CD11b<sup>+</sup> cells) at the injury site (unpaired two-tailed Student's *t*-test,  $**P < 0,01$ ,  $N = 7$  for Nutlin-3 and  $N = 5$  for vehicle, performed in triplicate).

Altogether, these results show that increasing p53 transactivation by disrupting the MDM2-p53 interaction enhances the intrinsic regenerative capacity of CNS neurons, as demonstrated by the increased sprouting of corticospinal and serotonergic axons, as well as contributes to modifying the scarring process to render the extrinsic environment more permissive to axonal outgrowth. The amelioration observed in the behavioral tests likely

resulted from p53-dependent modulation of both intrinsic and extrinsic cues, most probably as a local effect at the injury site and vicinity. Even though it is conjecturable that Nutlin-3a was transported through the CSF and reached the brain parenchyma to transactivate p53 in the cell bodies, in the praxis the redistribution of intrathecal drugs throughout the neural axis has proven uneven (Hayek and Hanes, 2014). Specifically with slow infusion rates involving an intrathecal catheter system, it seems that the delivered agents tend to stay close to the site of infusion (Loomis et al., 1987; Bernardis, 2006). Therefore, I postulate that the increased CST and 5-HT sprouting observed in Nutlin-3a-treated animals probably resulted from local p53 transactivation counteracting growth cone collapse, allied to nuclear transactivation in second-order neurons and interneurons to enhance local plasticity.

Next, we wanted to check what could possibly be the molecular signature of the MDM4-MDM2/p53 complex disruption. Genome wide analysis of FACS sorted RGCs after optic nerve crush revealed that MDM4 conditional deletion was associated with the enhancement of transcripts involved in cytoskeleton remodeling, axonal development and signaling, including genes involved in neuronal maturation, supporting the reactivation of the growth program also in the SCI model. Of special interest was the induction of the insulin growth factor-1 (IGF-1) and receptor signaling pathways in MDM4 deleted cells (Figure 4, Joshi and Sória et al., 2015). Insulin and insulin-like growth factors stimulate neurite initiation and elongation in DRG neurons and augment the effects of NGF when administered together (Fernyhough et al., 1993). IGF-1 is a critical positive mTOR regulator that is triggered by *SOCS3/PTEN* co-deletion in RGCs (Sun et al., 2011), and activation of IGF-1 receptor signaling is also necessary for regeneration of RGCs (Dupraz et al., 2013). Downstream targets of IGF1-receptor activation are PI3K (Bondy and Cheng, 2004) and JAK/STAT3 (Staerk et al., 2005), which are essential for axonal regeneration, as discussed above.

Finally, to address the role of the IGF-1 signaling in our SCI model, we antagonized the IGF-1 receptor by employing picropodophyllin (PPP), a specific IGF-1R inhibitor (Girmita et al., 2004). For that, we conducted experiments in which mice receiving Nutlin-3a via osmotic minipump/intrathecal catheter were concurrently injected for 2 weeks with PPP (20 mg/Kg, 12/12 hours, intraperitoneal route) or vehicle. As a result, in animals co-treated with PPP sprouting of serotonergic fibers was reduced and they displayed impaired functional recovery (Figure 8, Joshi and Sória et al., 2015, reproduced above as Figure XV), thus con-



firming the dependency of p53 transactivation on IGF-1 signaling to promote axon outgrowth after SCI.

### **3 Considerations on neuroplasticity to promote functional recovery after SCI**

Even though much effort has been concentrated in promoting growth of axons to rewire interrupted pathways after SCI, experimental data have shown that this may not be enough to provide functional recovery, as prolific regeneration of CST fibers driven by PTEN inhibition, which formed synaptic contacts below the lesion, was not associated with functional improvement (Zukor et al., 2013). It has already been recognized that mechanisms underlying beneficial functional outcomes in single-treatment approaches might, in fact, include spontaneous rearrangements of spared axons rather than regeneration of lesioned axons (Blesch and Tuszynski, 2009). Moreover, it is likely that several studies reporting “regeneration” of lesioned axons of adult CNS are in reality eliciting axonal sprouting (Blesch and Tuszynski, 2009), since the distinction of types of axon growth may be misleading (Tuszynski and Steward, 2012).

As a matter of fact, several other reports have demonstrated that sprouting of CST fibers (Weidner et al., 2001; Bareyre et al., 2004) and other descending motor tracts, like the rubrospinal (Weishaupt et al., 2013), reticulospinal (Ballermann and Fouad, 2006) and serotonergic tracts (Perrin et al., 2010), do correlate with amelioration of neurological motor functions. Moreover, when as little as 1–2% of the CST was spared in adult rats that underwent electrolytic lesions of the spinal cord, the animals exhibited recovery in the performance of a forepaw reaching task (Li et al., 1997), while as little as 10% of spinal white matter tracts were sufficient to permit spontaneous walking without support in adult cats (Windle et al., 1958). In humans patients that had large portions of spinal tracts transected owing to intractable cancer pain, transection of more than 50% of the spinal cord resulted in only weak or transitory effects on locomotion (Nathan, 1994). Altogether, these observations imply that regeneration of a small percentage of axons could potentially lead to a significant recovery of function. Therefore, the relatively modest growth of CST and 5-HT fibers induced by Nutlin-3a might have aided in the observed functional recovery of the animals in our experiments.

This phenomenon may be explained by synaptic plasticity, that are modifications in synapsis strength in pre-existing pathways, and by anatomical plasticity, which refers to the formation of new circuits of damaged or spared fibers through sprouting and anatomical reorganization, including growth of axonal branches and dendrites. Synaptic and anatomic plasticity may contribute to the limited functional improvement frequently experienced by subjects with incomplete SCI (Raineteau and Schwab, 2001), which is the type of lesion of the majority of spinal cord injured-patients. Even when the injury is neurologically considered complete, there is usually about 1-10% of spared white matter bridging the lesion gap in humans (Kakulas, 1999). The reorganization processes might occur at cortical and subcortical motor centers, in the spinal cord below the lesion, and in the spared fiber tracts that connect these centers. Nevertheless, the information that passes through these new connections is usually fragmentary and distorted, leading to additional dysfunctions, such as chronic pain and spasticity (Raineteau and Schwab, 2001). Most importantly, spontaneous plasticity can be potentiated by activity, as well as by specific experimental manipulations. The challenge is to direct these new connections properly to propitiate meaningful functional recovery and, at the same time, to avoid detrimental effects.

Theoretically, to mediate functional recovery, sprouting of transected descending supraspinal tract systems like the CST must fulfill 2 requirements: (1) transected CST fibers must contact spared intraspinal neuronal tracts that bridge the lesion; (2) these intraspinal neurons must form synaptic contacts on the original targets of the transected CST (Figure XVII) (Bareyre et al., 2004). Bareyre et al. (2004) demonstrated that these processes indeed take place after midthoracic dorsal hemisection in adult rats. They showed that hindlimb CST collaterals spontaneously sprouted into the cervical gray matter where they contact descending propriospinal neurons (PSNs). Long PSNs arborized on lumbar motor neurons, creating a new and functional intraspinal circuit relaying cortical input to its original spinal targets, which was responsible for the partial locomotor recovery experienced by the animals, as CST re-lesion significantly decreased the hindlimb placing response (Bareyre et al., 2004). Even though spontaneous reorganization does occur, strategies that take advantage of this phenomenon and potentiate sprouting of transected tracts are usually paralleled by enhancement of functional recovery in comparison to the more limited recovery observed in control groups, as demonstrated by several experimental interventions (reviewed by Onifer

et al., 2011; Ruff et al., 2012; Burnside and Bradbury, 2014; Fujita and Yamashita, 2014; Schwab and Strittmatter, 2014), including our work (Joshi and Sória et al., 2015).

Perhaps the most striking experiments showing that plasticity is fundamental for functional recovery are the ones involving functional training, which seems to be the most effective approach to direct and enhance plasticity as a means to recover motor function (Dietz and Fouad, 2014). More than 30 years ago, classical experiments demonstrated that the mammalian spinal cord can generate locomotor output in the absence of input from the brain by central pattern generation (Grillner and Zangger, 1979). Adult cats with complete transection of the spinal cord (spinalized cats) could stand and step when sensory input (e.g. standing on a moving treadmill) was provided to the lumbosacral pattern generator circuitry (de Leon et al., 1998). In adult paralyzed rats as a result of complete spinal cord transections, combinations of serotonergic agonists and epidural electrical stimulation were able to acutely transform spinal networks from nonfunctional to highly functional and adaptive states as early as 1 week after injury, which enabled full weight-bearing treadmill locomotion that was almost indistinguishable from voluntary stepping (Courtine et al., 2009). These results show that neuronal circuits for locomotion in the spinal cord can “learn” by training independently of the connection to the brain (Dietz and Fouad, 2014), leading to functional recovery of stepping, and that the spinal cord contains circuits that can produce stereotyped locomotor patterns. The mechanisms underlying this training-induced plasticity include the adaptation of neurotransmitter systems within the spinal cord, the upregulation of BDNF and enhanced collateral sprouting (Fouad and Tetzlaff, 2012).

But the restoration of supraspinal control in this context can be even more beneficial, as elegantly demonstrated by the Courtine group (van den Brand et al., 2012). In their experiments, adult rats received a left lateral over-hemisection at T7 and a right lateral hemisection at T10, which completely abolished hindlimb function, but left an intervening gap of intact tissue in order to simulate a clinically complete human SCI. In addition to systemic administration of serotonin and dopamine receptor agonists, epidural stimulation over L1 and S2 spinal segments and treadmill training, animals aided by a robotic postural interface were encouraged to perform active overground locomotion. As a result, these animals were capable of initiating and sustaining full weight-bearing bipedal locomotion, sprinting up stairs and avoiding obstacles, which was paralleled by anatomical and synaptic plasticity in cortex- and brainstem-derived axonal systems. In contrast, rats that received treadmill-

restricted step training under electrochemically enabled states failed to initiate overground locomotion and did not exhibit remodeling of descending pathways (van den Brand et al., 2012).

Promising results related to functional training and electrical stimulation were already reported in humans. In patients with neurologically complete spinal cord injuries, treadmill training led to the return of rhythmic locomotor muscle activation patterns and a decrease in spasticity (Dietz et al., 1994). In another cohort with incomplete para- and tetraplegic patients, the locomotor improvement resulting from treadmill training allowed 92% of these subjects to become independent walkers, in contrast to only 50% of the ones treated with conventional therapy (Wernig et al., 1995), with follow-up studies showing that the capability of walking persisted or further improved 6 months to 6 years in initially acute patients (Wernig et al., 1998). More recently, 4 young adult chronic spinal cord-injured patients, including 2 with complete SCI, were implanted with a 16-electrode array epidural stimulator over the L1-S1 cord segments and received intensive rehabilitation (including weight-supported treadmill and standing training) before and after implantation (Harkema et al., 2011; Angeli et al., 2014). With continuous stimulation, they were able to stand independently with full weight-bearing for several minutes and move their legs, and some patients even regained partial autonomic control; unlike motor function, these autonomic improvements became independent of stimulation (Harkema et al., 2011; Angeli et al., 2014).

Although these results may provoke enthusiasm, it is still too early for generalizations. The mechanisms underlying plasticity after SCI are still poorly understood and the recovery of functions associated to this phenomenon is still limited. Nevertheless, these studies encourage further investigation to potential clinical translation. Finally, it is likely that treatments that promote anatomical and synaptic plasticity may be potentiated by functional training, since newly formed projections might be fine tuned and stabilized by activity-dependent mechanisms.

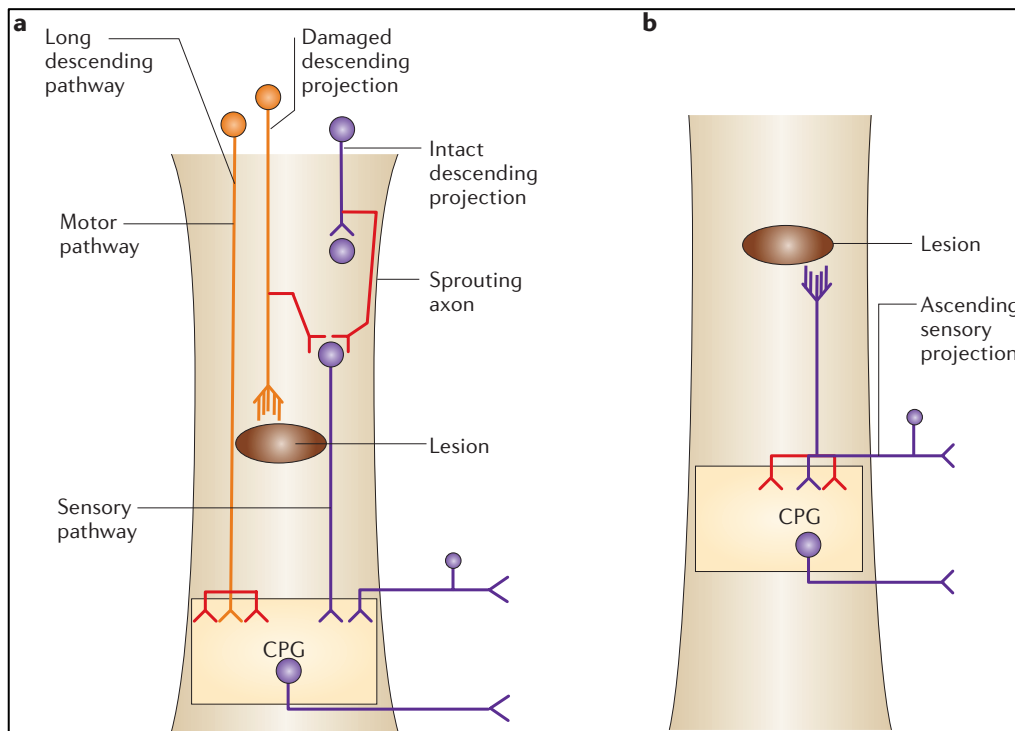


**Figure XVII. Restoration of function after spinal cord injury might arise from anatomical plasticity of damaged or spared connections. (a)** Collateral sprouts (illustrated in red) might form from long descending pathways that bypass the lesion site and activate spinal circuits more effectively or activate novel circuits, or from damaged or intact descending projections that activate local propriospinal neurons that bypass the injury site and form a novel descending system. **(b)** Ascending sensory projections might also form collateral sprouts, which activate spinal circuits more effectively. CPG, central pattern generator. (Reproduced from *Bradbury and MacMahon*, page 649, *Nat Rev Neurosc* 2006;7(8):644-53)

#### 4 Conclusion remarks and perspectives

For millennia SCI was considered an “ailment not to treat”. The first scientific known records of spinal cord injuries date to approximately 2.500 B.C. in the Ancient Egypt, as revealed by the Edwin Smith Surgical Papyrus in 1930 (Hughes, 1988). The papyrus contains six cases of injuries involving the cervical spine, two of them are clearly spinal cord injuries. For these two cases, the author states that no treatment could be provided (Hughes, 1988; Donovan, 2007). This nihilism toward SCI prevailed until last century, when pioneers of the rehabilitative approach for spinal cord-injured patients decided to establish the first SCI care units. Together with the latest advances in surgical and clinical medicine and neuroimaging it was possible to improve the quality of life and reduce the mortality of these patients (Donovan, 2007). Nevertheless, treatments to provide recovery of the neurological functions are still very limited. Most of them are at the bench side, but some hold the promise for clinical translation in the near future.

Ramer et al. (2014) classified the strategies to treat SCI according to the clinical target in three categories: **R**escue, **R**eactivate and **R**ewire. Rescue encompasses early interventions that prevent the spread of damage beyond the initial site of injury, like surgical decompression, cooling or hypothermia, and interventions targeting a specific biological event (e.g. inflammation). Reactivate refers to how spared systems, which are nearly always present in clinical SCI, can be exploited through rehabilitation, pharmacological or electrical stimulation of spinal networks, or remyelination of denuded axons. Finally, rewire aims the regrowth of injured axons or re-purposing of spared ones, with strategies targeting the intrinsic growth capacity of injured neurons or reducing inhibitors of axon growth (Ramer et al., 2014).

In this setting, our proposal to treat SCI by pharmacological transactivation of p53 may target these three fronts simultaneously. We showed that p53 is able to positively modulate the extrinsic environment, reducing inflammation and scar extension, thus reducing the spread of damage. p53 may also foster the reactivation of spared systems to increase compensatory sprouting and, in the same line, help transected axons to grow to rewire lost connections, without increasing apoptosis. These actions represent a solid substratum to explain the amelioration in locomotor recovery experienced by the mice in our experiments.

As a pleiotropic factor, p53 may exert its positive actions by fine tuning various molecular pathways rather than introducing drastic changes in the components that produce the SCI pathological picture. In this way, p53 may shift the balance to a reparative state at the injury site. Radical interventions targeting single components of the injury *milieu* may indeed be harmful. As an example, the attempt to reduce the glial scar by depleting proliferating astrocytes results in impaired BBB repair, decreased remyelination, increased leukocyte infiltration, neuronal degeneration, and increased motor deficits (White and Jakeman, 2008). Similarly, selective ablation of proliferative microglial cells exacerbates lesion pathology and decreases IGF-1 levels (Lalancette-Hébert et al., 2007).

In accordance to our observations with p53 transactivation, other interventions reinforce the importance of modulation of glial cells to enhance functional recovery after SCI. For instance, systemic minocycline administration after SCI in adult rats resulted in reduced density of activated microglia/macrophages remote as well as at the lesion site, which was associated to both diminished CST dieback and lesion size, and improved functional outcome (Stirling et al., 2004). In the same line, studies with transplantation of different types of neuroprotective glial cells at the injury site also reported varied degrees of success in promoting functional recovery. When transplanted into adult acutely spinal cord injured-rats, human embryonic stem cell-derived oligodendrocyte progenitor cells enhance remyelination and promote substantial amelioration in locomotor ability (Keirstead et al., 2005). Grafting of Schwann cells (SCs), which are required for PNS regeneration, results in reduction of lesion cavities, as well as abundant sensory and propriospinal axon growth across the SC-filled lesion and substantial myelination of axons, but supraspinal axons fail to penetrate SC grafts. In animal models of SCI, functional recovery and improvement in axon growth can only be achieved if SCs grafts are combined with other factors (chondroitinase ABC, neurotrophins or cAMP) (Bunge and Wood, 2012). Olfactory ensheathing cells (OECs), unique glia found only in the olfactory system that retain exceptional plasticity and support olfactory neurogenesis, have already been tested in different models of acute and chronic SCI. These cells can stimulate tissue sparing and neuroprotection, enhance sprouting of descending tracts, activate angiogenesis, change the response status of endogenous glia after lesion, remyelinate axons and promote functional recovery (Richter and Roskams, 2008).

At the molecular level, in this work we addressed the molecular mechanisms that link the retrograde signaling to PCAF-dependent chromatin remodeling, a HAT that is known to

form a multiprotein complex with CBP/P300 and p53 itself. This complex activates gene transcription via a multifunctional effector, the protein p53, that drives the transcription of several RAGs. Furthermore, disrupting the negative regulation of MDM2 and MDM4 increases p53 transactivation, which we showed to depend on IGF-1 signaling to exert its pro-growth effects. In this setting, a further step to be tested would be a combinatorial approach by simultaneous promoting PCAF induction and p53 nuclear transactivation in central neurons. This may perhaps lead to greater functional recovery after SCI.

Overall, this work opens an exciting possibility to bring a new candidate for SCI treatment. A pharmacological approach holds the potential for faster clinical translation, an urgent need in the spinal cord clinical context, in comparison to other more complex strategies like cell therapy. Nutlin-3a is already under scrutiny in clinical trials for cancer therapy and therefore may be clinically available in the near future.

However, care has to be taken to extrapolate the results obtained in mice to humans. For example, while corticospinal connections are highly important for motor control in humans, they probably play a minor role in the initiation of limb movement in non-primate mammals (Sengul and Watson, 2012). To address this question, experiments with Nutlin-3a should be repeated in other animal models that are more similar to humans in terms of lesion morphology and neurophysiology. Additional experiments should also try to elucidate the exact mechanism of interaction of p53 and IGF1 signaling. Since both molecules govern several signaling pathways, knowing how they influence each other may reveal more details on how nerve regeneration is orchestrated and pave the way to more specific molecular manipulation. At last but not the least, Nutlin-3a should be tested in combination with other potential therapies for SCI. The spinal cord involves complex systems and multiplicity of cells, therefore successful recovery of functions will probably be achieved with combinatorial strategies targeting different aspects of this *milieu*.



## 5 References

- Aguayo AJ, David S, Bray GM (1981) Influences of the glial environment on the elongation of axons after injury: transplantation studies in adult rodents. *J Exp Biol* 95:231–240.
- Angeli C a., Edgerton VR, Gerasimenko YP, Harkema SJ (2014) Altering spinal cord excitability enables voluntary movements after chronic complete paralysis in humans. *Brain* 137:1394–1409.
- Armesilla-Diaz A, Bragado P, Del Valle I, Cuevas E, Lazaro I, Martin C, Cigudosa JC, Silva A (2009) p53 regulates the self-renewal and differentiation of neural precursors. *Neuroscience* 158:1378–1389.
- Averill S, Delcroix JD, Michael GJ, Tomlinson DR, Fernyhough P, Priestley J V (2001) Nerve growth factor modulates the activation status and fast axonal transport of ERK 1/2 in adult nociceptive neurones. *Mol Cell Neurosci* 18:183–196.
- Ballermann M, Fouad K (2006) Spontaneous locomotor recovery in spinal cord injured rats is accompanied by anatomical plasticity of reticulospinal fibers. *Eur J Neurosci* 23:1988–1996.
- Banner LR, Patterson PH (1994) Major changes in the expression of the mRNAs for cholinergic differentiation factor/leukemia inhibitory factor and its receptor after injury to adult peripheral nerves and ganglia. *Proc Natl Acad Sci USA* 91:7109–7113.
- Bannister AJ, Kouzarides T (2011) Regulation of chromatin by histone modifications. *Cell Res* 21:381–395.
- Bareyre FM, Garzorz N, Lang C, Misgeld T, Büning H, Kerschensteiner M (2011) In vivo imaging reveals a phase-specific role of STAT3 during central and peripheral nervous system axon regeneration. *Proc Natl Acad Sci U S A* 108:6282–6287.
- Bareyre FM, Kerschensteiner M, Raineteau O, Mettenleiter TC, Weinmann O, Schwab ME (2004) The injured spinal cord spontaneously forms a new intraspinal circuit in adult rats. *Nat Neurosci* 7:269–277.
- Basso DM, Fisher LC, Anderson AJ, Jakeman LB, McTigue DM, Popovich PG (2006) Basso Mouse Scale for locomotion detects differences in recovery after spinal cord injury in five common mouse strains. *J Neurotrauma* 23:635–659.
- Beattie MS, Farooqui AA, Bresnahan JC (2000) Review of Current Evidence for Apoptosis After Spinal Cord Injury. *J Neurotrauma* 17:915–925.
- Benson MD, Romero MI, Lush ME, Lu QR, Henkemeyer M, Parada LF (2005) Ephrin-B3 is a myelin-based inhibitor of neurite outgrowth. *Proc Natl Acad Sci USA* 102:10694–10699.
- Bernards CM (2006) Cerebrospinal fluid and spinal cord distribution of baclofen and bupivacaine during slow intrathecal infusion in pigs. *Anesthesiology* 105:169–178.

Biswas S, Killick E, Jochemsen AG, Lunec J (2014) The clinical development of p53-reactivating drugs in sarcomas - charting future therapeutic approaches and understanding the clinical molecular toxicology of Nutlins. *Expert Opin Investig Drugs* 23:629–645.

Blesch A, Lu P, Tsukada S, Alto LT, Roet K, Coppola G, Geschwind D, Tuszynski MH (2012) Conditioning lesions before or after spinal cord injury recruit broad genetic mechanisms that sustain axonal regeneration: Superiority to camp-mediated effects. *Exp Neurol* 235:162–173.

Blesch A, Tuszynski MH (2009) Spinal cord injury: plasticity, regeneration and the challenge of translational drug development. *Trends Neurosci* 32:41–47.

Boivin A, Pineau I, Barrette B, Filali M, Vallières N, Rivest S, Lacroix S (2007) Toll-like receptor signaling is critical for Wallerian degeneration and functional recovery after peripheral nerve injury. *J Neurosci* 27:12565–12576.

Bondy CA, Cheng CM (2004) Signaling by insulin-like growth factor 1 in brain. *Eur J Pharmacol* 490:25–31.

Bradke F, Fawcett JW, Spira ME (2012) Assembly of a new growth cone after axotomy: the precursor to axon regeneration. *Nat Rev Neurosci* 13:183–193.

Bregman BS, Kunkel-Bagden E, McAtee M, O'Neill A (1989) Extension of the critical period for developmental plasticity of the corticospinal pathway. *J Comp Neurol* 282:355–370.

Bresnahan JC, Beattie MS, Todd FD, Noyes DH (1987) A behavioral and anatomical analysis of spinal cord injury produced by a feedback-controlled impaction device. *Exp Neurol* 95:548–570.

Bronfman FC, Escudero CA, Weis J, Kruttgen A (2007) Endosomal transport of neurotrophins: roles in signaling and neurodegenerative diseases. *Dev Neurobiol* 67:1183–1203.

Bunge MB, Wood PM (2012) Realizing the maximum potential of Schwann cells to promote recovery from spinal cord injury. *Handb Clin Neurol* 109:523–540.

Bunge RP, Puckett WR, Becerra JL, Marcillo A, Quencer RM (1993) Observations on the pathology of human spinal cord injury. A review and classification of 22 new cases with details from a case of chronic cord compression with extensive focal demyelination. *Adv Neurol* 59:75–89.

Burnside ER, Bradbury EJ (2014) Manipulating the extracellular matrix and its role in brain and spinal cord plasticity and repair. *Neuropathol Appl Neurobiol* 40:26–59.

Busch S a, Horn KP, Cuascut FX, Hawthorne AL, Bai L, Miller RH, Silver J (2010) Adult NG2+ cells are permissive to neurite outgrowth and stabilize sensory axons during macrophage-induced axonal dieback after spinal cord injury. *J Neurosci* 30:255–265.

Camand E, Morel MP, Faissner A, Sotelo C, Dusart I (2004) Long-term changes in the molecular composition of the glial scar and progressive increase of serotonergic fibre sprouting after hemisection of the mouse spinal cord. *Eur J Neurosci* 20:1161–1176.

Cannon B (2013) Sensation and loss. *Nature* 503:S2–S3.

Cao Z, Gao Y, Bryson JB, Hou J, Chaudhry N, Siddiq M, Martinez J, Spencer T, Carmel J, Hart RB, Filbin MT (2006) The cytokine interleukin-6 is sufficient but not necessary to mimic the peripheral conditioning lesion effect on axonal growth. *J Neurosci* 26:5565–5573.

Caroni P, Becker M (1992) The downregulation of growth-associated proteins in motoneurons at the onset of synapse elimination is controlled by muscle activity and IGF1. *J Neurosci* 12:3849–3861.

Carulli D, Buffo A, Botta C, Altruda F, Strata P (2002) Regenerative and survival capabilities of Purkinje cells overexpressing c-Jun. *Eur J Neurosci* 16:105–118.

Cavalli V, Kujala P, Klumperman J, Goldstein LSB (2005) Sunday Driver links axonal transport to damage signaling. *J Cell Biol* 168:775–787.

Chen D, Kon N, Li M, Zhang W, Qin J, Gu W (2005) ARF-BP1/Mule is a critical mediator of the ARF tumor suppressor. *Cell* 121:1071–1083.

Chen DF, Schneider GE, Martinou JC, Tonegawa S (1997) Bcl-2 promotes regeneration of severed axons in mammalian CNS. *Nature* 385:434–439.

Cho Y, Cavalli V (2014) HDAC signaling in neuronal development and axon regeneration. *Curr Opin Neurobiol* 27:118–126.

Cho Y, Sloutsky R, Naegle KM, Cavalli V (2013) Injury-Induced HDAC5 nuclear export is essential for axon regeneration. *Cell* 155:894–908.

Cosker KE, Courchesne SL, Segal RA (2008) Action in the axon: generation and transport of signaling endosomes. *Curr Opin Neurobiol* 18:270–275.

Courtine G, Gerasimenko Y, van den Brand R, Yew A, Musienko P, Zhong H, Song B, Ao Y, Ichiyama RM, Lavrov I, Roy RR, Sofroniew M V, Edgerton VR (2009) Transformation of nonfunctional spinal circuits into functional states after the loss of brain input. *Nat Neurosci* 12:1333–1342.

Davalos D, Grutzendler J, Yang G, Kim J V, Zuo Y, Jung S, Littman DR, Dustin ML, Gan W-B (2005) ATP mediates rapid microglial response to local brain injury in vivo. *Nat Neurosci* 8:752–758.

David S, Kroner A (2011) Repertoire of microglial and macrophage responses after spinal cord injury. *Nat Rev Neurosci* 12:388–399.

Day JJ, Sweatt JD (2010) DNA methylation and memory formation. *Nat Neurosci* 13:1319–1323.

De Leon RD, Hodgson JA, Roy RR, Edgerton VR (1998) Locomotor capacity attributable to step training versus spontaneous recovery after spinalization in adult cats. *J Neurophysiol* 79:1329–1340.

Di Giovanni S (2009) Molecular targets for axon regeneration: focus on the intrinsic pathways. *Expert Opin Ther Targets* 13:1387–1398.

Di Giovanni S, De Biase A, Yakovlev A, Finn T, Beers J, Hoffman EP, Faden AI (2005) In vivo and in vitro characterization of novel neuronal plasticity factors identified following spinal cord injury. *J Biol Chem* 280:2084–2091.

Di Giovanni S, Knights CD, Rao M, Yakovlev A, Beers J, Catania J, Avantaggiati ML, Faden AI (2006) The tumor suppressor protein p53 is required for neurite outgrowth and axon regeneration. *EMBO J* 25:4084–4096.

Di Giovanni S, Rathore K (2012) P53-Dependent Pathways in Neurite Outgrowth and Axonal Regeneration. *Cell Tissue Res* 349:87–95.

Dickendeshler TL, Baldwin KT, Mironova Y a, Koriyama Y, Raiker SJ, Askew KL, Wood A, Geoffroy CG, Zheng B, Liepmann CD, Katagiri Y, Benowitz LI, Geller HM, Giger RJ (2012) NgR1 and NgR3 are receptors for chondroitin sulfate proteoglycans. *Nat Neurosci* 15:703–712.

Dietz V, Colombo G, Jensen L (1994) Locomotor activity in spinal man. *Lancet (London, England)* 344:1260–1263.

Dietz V, Fouad K (2014) Restoration of sensorimotor functions after spinal cord injury. *Brain* 137:654–667.

Ditunno JF, Little JW, Tessler a, Burns a S (2004) Spinal shock revisited: a four-phase model. *Spinal Cord* 42:383–395.

Donovan WH (2007) Donald Munro Lecture. Spinal cord injury--past, present, and future. *J Spinal Cord Med* 30:85–100.

Dornan D, Wertz I, Shimizu H, Arnott D, Frantz GD, Dowd P, O'Rourke K, Koeppen H, Dixit VM (2004) The ubiquitin ligase COP1 is a critical negative regulator of p53. *Nature* 429:86–92.

Doron-Mandel E, Fainzilber M, Terenzio M (2015) Growth control mechanisms in neuronal regeneration. *FEBS Lett* 589:1669–1677.

Dupraz S, Grassi D, Karnas D, Nieto Guil AF, Hicks D, Quiroga S (2013) The Insulin-Like Growth Factor 1 Receptor Is Essential for Axonal Regeneration in Adult Central Nervous System Neurons. *PLoS One* 8:1–8.

Eizenberg O, Faber-Elman A, Gottlieb E, Oren M, Rotter V, Schwartz M (1996) p53 plays a regulatory role in differentiation and apoptosis of central nervous system-associated cells. *Mol Cell Biol* 16:5178–5185.

Ertürk A, Hellal F, Enes J, Bradke F (2007) Disorganized microtubules underlie the formation of retraction bulbs and the failure of axonal regeneration. *J Neurosci* 27:9169–9180.

Evans T a., Barkauskas DS, Myers JT, Hare EG, You JQ, Ransohoff RM, Huang AY, Silver J (2014) High-resolution intravital imaging reveals that blood-derived macrophages but not resident microglia facilitate secondary axonal dieback in traumatic spinal cord injury. *Exp Neurol* 254:109–120.

Faulkner JR, Herrmann JE, Woo MJ, Tansey KE, Doan NB, Sofroniew M V (2004) Reactive astrocytes protect tissue and preserve function after spinal cord injury. *J Neurosci* 24:2143–2155.

Feng J, Fan G (2009) The role of DNA methylation in the central nervous system and neuropsychiatric disorders. *Int Rev Neurobiol* 89:67–84.

Fernyhough P, Willars GB, Lindsay RM, Tomlinson DR (1993) Insulin and insulin-like growth factor I enhance regeneration in cultured adult rat sensory neurones. *Brain Res* 607:117–124.

Fisher D, Xing B, Dill J, Li H, Hoang HH, Zhao Z, Yang X-L, Bachoo R, Cannon S, Longo FM, Sheng M, Silver J, Li S (2011) Leukocyte common antigen-related phosphatase is a functional receptor for chondroitin sulfate proteoglycan axon growth inhibitors. *J Neurosci* 31:14051–14066.

Fitch MT, Silver J (1997) Activated macrophages and the blood-brain barrier: inflammation after CNS injury leads to increases in putative inhibitory molecules. *Exp Neurol* 148:587–603.

Fitch MT, Silver J (2008) CNS injury, glial scars, and inflammation: Inhibitory extracellular matrices and regeneration failure. *Exp Neurol* 209:294–301.

Floriddia EM, Rathore KI, Tedeschi a., Quadrato G, Wuttke a., Lueckmann J-M, Kigerl K a., Popovich PG, Di Giovanni S (2012) p53 Regulates the Neuronal Intrinsic and Extrinsic Responses Affecting the Recovery of Motor Function following Spinal Cord Injury. *J Neurosci* 32:13956–13970.

Fouad K, Tetzlaff W (2012) Rehabilitative training and plasticity following spinal cord injury. *Exp Neurol* 235:91–99.

Fournier AE, GrandPre T, Strittmatter SM (2001) Identification of a receptor mediating Nogo-66 inhibition of axonal regeneration. *Nature* 409:341–346.

Fournier AE, Takizawa BT, Strittmatter SM (2003) Rho kinase inhibition enhances axonal regeneration in the injured CNS. *J Neurosci* 23:1416–1423.

Fujita Y, Yamashita T (2014) Axon growth inhibition by RhoA/ROCK in the central nervous system. *Front Neurosci* 8:338.

Gao Y, Deng K, Hou J, Bryson JB, Barco A, Nikulina E, Spencer T, Mellado W, Kandel ER, Filbin MT (2004) Activated CREB is sufficient to overcome inhibitors in myelin and promote spinal axon regeneration in vivo. *Neuron* 44:609–621.

Gaub P, Joshi Y, Wuttke A, Naumann U, Schnichels S, Heiduschka P, Di Giovanni S (2011) The histone acetyltransferase p300 promotes intrinsic axonal regeneration. *Brain* 134:2134–2148.

Gaub P, Tedeschi a, Puttagunta R, Nguyen T, Schmandke a, Di Giovanni S (2010) HDAC inhibition promotes neuronal outgrowth and counteracts growth cone collapse through CBP/p300 and P/CAF-dependent p53 acetylation. *Cell Death Differ* 17:1392–1408.

Gensel JC, Zhang B (2015) Macrophage activation and its role in repair and pathology after spinal cord injury. *Brain Res* 1619:1–11.

Girnita A, Girnita L, Prete F (2004) Cyclolignans as Inhibitors of the Insulin-Like Growth Factor-1 Receptor and Malignant Cell Growth. *Cancer Res* 64:236–242.

Goold RG, Gordon-Weeks PR (2005) The MAP kinase pathway is upstream of the activation of GSK3beta that enables it to phosphorylate MAP1B and contributes to the stimulation of axon growth. *Mol Cell Neurosci* 28:524–534.

Gordon S, Taylor PR (2005) Monocyte and macrophage heterogeneity. *Nat Rev Immunol* 5:953–964.

Goto K, Numata M, Komura JI, Ono T, Bestor TH, Kondo H (1994) Expression of DNA methyltransferase gene in mature and immature neurons as well as proliferating cells in mice. *Differentiation* 56:39–44.

Green DR, Chipuk JE (2006) p53 and Metabolism: Inside the TIGAR. *Cell* 126:30–32.

Grillner S, Zangger P (1979) On the central generation of locomotion in the low spinal cat. *Exp Brain Res* 34:241–261.

Guertin D a., Sabatini DM (2007) Defining the Role of mTOR in Cancer. *Cancer Cell* 12:9–22.

Harkema S, Gerasimenko Y, Hodes J, Burdick J, Angeli C, Chen Y, Ferreira C, Willhite A, Rejc E, Grossman RG, Edgerton VR (2011) Effect of epidural stimulation of the lumbosacral spinal cord on voluntary movement, standing, and assisted stepping after motor complete paraplegia: a case study. *Lancet (London, England)* 377:1938–1947.

Harms K, Nozell S, Chen X (2004) The common and distinct target genes of the p53 family transcription factors. *Cell Mol Life Sci* 61:822–842.

Hayek SM, Hanes MC (2014) Intrathecal therapy for chronic pain: current trends and future needs. *Curr Pain Headache Rep* 18:388.

Hodawadekar SC, Marmorstein R (2007) Chemistry of acetyl transfer by histone modifying enzymes: structure, mechanism and implications for effector design. *Oncogene* 26:5528–5540.

Hsieh SH-K, Ferraro GB, Fournier AE (2006) Myelin-associated inhibitors regulate cofilin phosphorylation and neuronal inhibition through LIM kinase and Slingshot phosphatase. *J Neurosci* 26:1006–1015.

Huber AB, Weinmann O, Brösamle C, Oertle T, Schwab ME (2002) Patterns of Nogo mRNA and protein expression in the developing and adult rat and after CNS lesions. *J Neurosci* 22:3553–3567.

Hughes JT (1988) The Edwin Smith Surgical Papyrus: an analysis of the first case reports of spinal cord injuries. *Paraplegia* 26:71–82.

Hutson TH, Verhaagen J, Yáñez-Muñoz RJ, Moon LDF (2012) Corticospinal tract transduction: a comparison of seven adeno-associated viral vector serotypes and a non-integrating lentiviral vector. *Gene Ther* 19:49–60.

Iskandar BJ, Rizk E, Meier B, Hariharan N, Bottiglieri T, Finnell RH, Jarrard DF, Banerjee R V., Skene JHP, Nelson A, Patel N, Gherasim C, Simon K, Cook TD, Hogan KJ (2010) Folate regulation of axonal regeneration in the rodent central nervous system through DNA methylation. *J Clin Invest* 120:1603–1616.

Jin Q, Yu L-R, Wang L, Zhang Z, Kasper LH, Lee J-E, Wang C, Brindle PK, Dent SYR, Ge K (2011) Distinct roles of GCN5/PCAF-mediated H3K9ac and CBP/p300-mediated H3K18/27ac in nuclear receptor transactivation. *EMBO J* 30:249–262.

Joshi Y, Sória MG, Quadrato G, Inak G, Zhou L, Hervera A, Rathore KI, Elnaggar M, Magali C, Marine JC, Puttagunta R, Di Giovanni S (2015) The MDM4/MDM2-p53-IGF1 axis controls axonal regeneration, sprouting and functional recovery after CNS injury. *Brain* 138(Pt 7):1843–1862.

Kakulas BA (1999) A review of the neuropathology of human spinal cord injury with emphasis on special features. *J Spinal Cord Med* 22:119–124.

Keirstead HS, Nistor G, Bernal G, Totoiu M, Cloutier F, Sharp K, Steward O (2005) Human embryonic stem cell-derived oligodendrocyte progenitor cell transplants remyelinate and restore locomotion after spinal cord injury. *J Neurosci* 25:4694–4705.

Kerschensteiner M, Schwab ME, Lichtman JW, Misgeld T (2005) In vivo imaging of axonal degeneration and regeneration in the injured spinal cord. *Nat Med* 11:572–577.

Kigerl KA, Gensel JC, Ankeny DP, Alexander JK, Donnelly DJ, Popovich PG (2009) Identification of two distinct macrophage subsets with divergent effects causing either neurotoxicity or regeneration in the injured mouse spinal cord. *J Neurosci* 29:13435–13444.

Kimpinski K, Mearow K (2001) Neurite growth promotion by nerve growth factor and insulin-like growth factor-1 in cultured adult sensory neurons: Role of phosphoinositide 3-kinase and mitogen activated protein kinase. *J Neurosci Res* 63:486–499.

Knights CD, Catania J, Di Giovanni S, Muratoglu S, Perez R, Swartzbeck A, Quong A a., Zhang X, Beerman T, Pestell RG, Avantaggiati ML (2006) Distinct p53 acetylation cassettes differentially influence gene-expression patterns and cell fate. *J Cell Biol* 173:533–544.

Kouzarides T (2007) Chromatin Modifications and Their Function. *Cell* 128:693–705.

Lalancette-Hébert M, Gowing G, Simard A, Weng YC, Kriz J (2007) Selective ablation of proliferating microglial cells exacerbates ischemic injury in the brain. *J Neurosci* 27:2596–2605.

Lang BT, Cregg JM, DePaul M a., Tran AP, Xu K, Dyck SM, Madalena KM, Brown BP, Weng Y-L, Li S, Karimi-Abdolrezaee S, Busch S a., Shen Y, Silver J (2014) Modulation of the proteoglycan receptor PTP $\sigma$  promotes recovery after spinal cord injury. *Nature* 518:404–408.

Lee BB, Cripps R a, Fitzharris M, Wing PC (2014) The global map for traumatic spinal cord injury epidemiology: update 2011, global incidence rate. *Spinal Cord* 52:110–116.

Leng RP, Lin Y, Ma W, Wu H, Lemmers B, Chung S, Parant JM, Lozano G, Hakem R, Benchimol S (2003) Pirh2, a p53-induced ubiquitin-protein ligase, promotes p53 degradation. *Cell* 112:779–791.

Li Y, Field PM, Raisman G (1997) Repair of adult rat corticospinal tract by transplants of olfactory ensheathing cells. *Science* 277:2000–2002.

Lickiss T, Cheung AFP, Hutchinson CE, Taylor JSH, Molnár Z (2012) Examining the relationship between early axon growth and transcription factor expression in the developing cerebral cortex. *J Anat* 220:201–211.

Lindner R, Puttagunta R, Di Giovanni S (2013) Epigenetic Regulation of Axon Outgrowth and Regeneration in CNS Injury: The First Steps Forward. *Neurotherapeutics* 10:771–781.

Liu BP, Fournier A, GrandPré T, Strittmatter SM (2002) Myelin-associated glycoprotein as a functional ligand for the Nogo-66 receptor. *Science* 297:1190–1193.

Liu K, Lu Y, Lee JK, Samara R, Willenberg R, Sears-Kraxberger I, Tedeschi A, Park KK, Jin D, Cai B, Xu B, Connolly L, Steward O, Zheng B, He Z (2010) PTEN deletion enhances the regenerative ability of adult corticospinal neurons. *Nat Neurosci* 13:1075–1081.



Liu K, Tedeschi A, Park KK, He Z (2011) Neuronal intrinsic mechanisms of axon regeneration. *Annu Rev Neurosci* 34:131–152.

Liu L, McBride KM, Reich NC (2005) STAT3 nuclear import is independent of tyrosine phosphorylation and mediated by importin- $\alpha$ 3. *Proc Natl Acad Sci U S A* 102:8150–8155.

Llewellyn-Smith IJ, Weaver LC (2001) Changes in synaptic inputs to sympathetic preganglionic neurons after spinal cord injury. *J Comp Neurol* 435:226–240.

Loomis CW, Milne B, Cervencko FW (1987) Determination of cross tolerance in rat spinal cord using intrathecal infusion via sequential mini-osmotic pumps. *Pharmacol Biochem Behav* 26:131–139.

Ma DK, Marchetto MC, Guo JU, Ming G, Gage FH, Song H (2010) Epigenetic choreographers of neurogenesis in the adult mammalian brain. *Nat Neurosci* 13:1338–1344.

Mandolesi G, Madeddu F, Bozzi Y, Maffei L, Ratto GM (2004) Acute physiological response of mammalian central neurons to axotomy: ionic regulation and electrical activity. *FASEB J* 18:1934–1936.

Mason MRJ, Ehlert EME, Eggers R, Pool CW, Hermening S, Huseinovic A, Timmermans E, Blits B, Verhaagen J (2010) Comparison of AAV serotypes for gene delivery to dorsal root ganglion neurons. *Mol Ther* 18:715–724.

Massey JM, Hubscher CH, Wagoner MR, Decker JA, Amps J, Silver J, Onifer SM (2006) Chondroitinase ABC digestion of the perineuronal net promotes functional collateral sprouting in the cuneate nucleus after cervical spinal cord injury. *J Neurosci* 26:4406–4414.

Mawhinney LA, Thawer SG, Lu W-Y, Rooijen N van, Weaver LC, Brown A, Dekaban GA (2012) Differential detection and distribution of microglial and hematogenous macrophage populations in the injured spinal cord of lys-EGFP-ki transgenic mice. *J Neuropathol Exp Neurol* 71:180–197.

McDonald JW, Sadowsky C (2002) Spinal-cord injury. *Lancet* 359:417–425.

McKerracher L, David S, Jackson DL, Kottis V, Dunn RJ, Braun PE (1994) Identification of myelin-associated glycoprotein as a major myelin-derived inhibitor of neurite growth. *Neuron* 13:805–811.

Metz GA, Merkler D, Dietz V, Schwab ME, Fouad K (2000) Efficient testing of motor function in spinal cord injured rats. *Brain Res* 883:165–177.

Mi S, Lee X, Shao Z, Thill G, Ji B, Relton J, Levesque M, Allaire N, Perrin S, Sands B, Crowell T, Cate RL, McCoy JM, Pepinsky RB (2004) LINGO-1 is a component of the Nogo-66 receptor/p75 signaling complex. *Nat Neurosci* 7:221–228.

Miron VE, Boyd A, Zhao J-W, Yuen TJ, Ruckh JM, Shadrach JL, van Wijngaarden P, Wagers AJ, Williams A, Franklin RJM, French-Constant C (2013) M2 microglia and macrophages drive oligodendrocyte differentiation during CNS remyelination. *Nat Neurosci* 16:1211–1218.

Momand J, Zambetti GP, Olson DC, George D, Levine AJ (1992) The mdm-2 oncogene product forms a complex with the p53 protein and inhibits p53-mediated transactivation. *Cell* 69:1237–1245.

Moore DL, Blackmore MG, Hu Y, Kaestner KH, Bixby JL, Lemmon VP, Goldberg JL (2009) KLF family members regulate intrinsic axon regeneration ability. *Science* 326:298–301.

Moreau-Fauvarque C, Kumanogoh A, Camand E, Jaillard C, Barbin G, Boquet I, Love C, Jones EY, Kikutani H, Lubetzki C, Dusart I, Chédotal A (2003) The transmembrane semaphorin Sema4D/CD100, an inhibitor of axonal growth, is expressed on oligodendrocytes and upregulated after CNS lesion. *J Neurosci* 23:9229–9239.

Mothe AJ, Tator CH (2012) Advances in stem cell therapy for spinal cord injury. *J Clin Invest* 122:3824–3834.

Murray-Zmijewski F, Slee EA, Lu X (2008) A complex barcode underlies the heterogeneous response of p53 to stress. *Nat Rev Mol Cell Biol* 9:702–712.

Nathan PW (1994) Effects on movement of surgical incisions into the human spinal cord. *Brain* 117(Pt 2):337–346.

Neumann S, Woolf CJ (1999) Regeneration of dorsal column fibers into and beyond the lesion site following adult spinal cord injury. *Neuron* 23:83–91.

Niederöst B, Oertle T, Fritsche J, McKinney RA, Bandtlow CE (2002) Nogo-A and myelin-associated glycoprotein mediate neurite growth inhibition by antagonistic regulation of RhoA and Rac1. *J Neurosci* 22:10368–10376.

Norenberg MD, Smith J, Marcillo A (2004) The pathology of human spinal cord injury: defining the problems. *J Neurotrauma* 21:429–440.

Okorokov AL (2014) p53 in a Crosstalk Between DNA Repair and Cell Cycle Checkpoints. *Cell Cycle* 2:232–234.

Onifer SM, Smith GM, Fouad K (2011) Plasticity after spinal cord injury: relevance to recovery and approaches to facilitate it. *Neurotherapeutics* 8:283–293.

Parikh P, Hao Y, Hosseinkhani M, Patil SB, Huntley GW, Tessier-Lavigne M, Zou H (2011) Regeneration of axons in injured spinal cord by activation of bone morphogenetic protein/Smad1 signaling pathway in adult neurons. *Proc Natl Acad Sci USA* 108:E99–E107.

Park JB, Yiu G, Kaneko S, Wang J, Chang J, He XL, Garcia KC, He Z (2005) A TNF receptor family member, TROY, is a coreceptor with Nogo receptor in mediating the inhibitory activity of myelin inhibitors. *Neuron* 45:345–351.

Park KK, Liu K, Hu Y, Kanter JL, He Z (2010) PTEN/mTOR and axon regeneration. *Exp Neurol* 223:45–50.

Park KK, Liu K, Hu Y, Smith PD, Wang C, Cai B, Xu B, Connolly L, Kramvis I, Sahin M, He Z (2008) Promoting axon regeneration in the adult CNS by modulation of the PTEN/mTOR pathway. *Science* 322:963–966.

Paulson M, Pisharody S, Pan L, Guadagno S, Mui AL, Levy DE (1999) Stat protein transactivation domains recruit p300/CBP through widely divergent sequences. *J Biol Chem* 274:25343–25349.

Perlson E, Hanz S, Ben-Yaakov K, Segal-Ruder Y, Seger R, Fainzilber M (2005) Vimentin-dependent spatial translocation of an activated MAP kinase in injured nerve. *Neuron* 45:715–726.

Perrin FE, Boniface G, Serguera C, Lonjon N, Serre A, Prieto M, Mallet J, Privat A (2010) Grafted human embryonic progenitors expressing neurogenin-2 stimulate axonal sprouting and improve motor recovery after severe spinal cord injury. *PLoS One* 5:e15914.

Pineau I, Sun L, Bastien D, Lacroix S (2010) Astrocytes initiate inflammation in the injured mouse spinal cord by promoting the entry of neutrophils and inflammatory monocytes in an IL-1 receptor/MyD88-dependent fashion. *Brain Behav Immun* 24:540–553.

Ponomarev ED, Maresz K, Tan Y, Dittel BN (2007) CNS-derived interleukin-4 is essential for the regulation of autoimmune inflammation and induces a state of alternative activation in microglial cells. *J Neurosci* 27:10714–10721.

Prinjha R, Moore SE, Vinson M, Blake S, Morrow R, Christie G, Michalovich D, Simmons DL, Walsh FS (2000) Inhibitor of neurite outgrowth in humans. *Nature* 403:383–384.

Puttagunta R, Tedeschi A, Sória MG, Hervera A, Lindner R, Rathore KI, Gaub P, Joshi Y, Nguyen T, Schmandke A, Laskowski CJ, Boutillier A-L, Bradke F, Di Giovanni S (2014) PCAF-dependent epigenetic changes promote axonal regeneration in the central nervous system. *Nat Commun* 5:3527.

Qin Q, Baudry M, Liao G, Noniyev A, Galeano J, Bi X (2009) A novel function for p53: regulation of growth cone motility through interaction with Rho kinase. *J Neurosci* 29:5183–5192.

Qin Q, Liao G, Baudry M, Bi X (2010) Role of calpain-mediated p53 truncation in semaphorin 3A-induced axonal growth regulation. *Proc Natl Acad Sci USA* 107:13883–13887.

- Qiu J, Cafferty WBJ, McMahon SB, Thompson SWN (2005) Conditioning injury-induced spinal axon regeneration requires signal transducer and activator of transcription 3 activation. *J Neurosci* 25:1645–1653.
- Quadrato G, Di Giovanni S (2012) Gatekeeper between quiescence and differentiation: p53 in axonal outgrowth and neurogenesis. *Int Rev Neurobiol* 105:71–89.
- Raineteau O, Schwab ME (2001) Plasticity of motor systems after incomplete spinal cord injury. *Nat Rev Neurosci* 2:263–273.
- Ramer LM, Ramer MS, Bradbury EJ (2014) Restoring function after spinal cord injury: towards clinical translation of experimental strategies. *Lancet Neurol* 13:1241–1256.
- Ramón y Cajal S (1928) *Degeneration and Regeneration of the Nervous System*. London: Oxford University Press.
- Reichardt LF (2006) Neurotrophin-regulated signalling pathways. *Philos Trans R Soc Lond B Biol Sci* 361:1545–1564.
- Reik W (2007) Stability and flexibility of epigenetic gene regulation in mammalian development. *Nature* 447:425–432.
- Richardson PM, Issa VM (1984) Peripheral injury enhances central regeneration of primary sensory neurones. *Nature* 309:791–793.
- Richardson PM, Issa VM, Aguayo AJ (1984) Regeneration of long spinal axons in the rat. *J Neurocytol* 13:165–182.
- Richardson PM, McGuinness UM, Aguayo a J (1980) Axons from CNS neurons regenerate into PNS grafts. *Nature* 284:264–265.
- Richter MW, Roskams AJ (2008) Olfactory ensheathing cell transplantation following spinal cord injury: hype or hope? *Exp Neurol* 209:353–367.
- Riley T, Sontag E, Chen P, Levine A (2008) Transcriptional control of human p53-regulated genes. *Nat Rev Mol Cell Biol* 9:402–412.
- Rishal I, Fainzilber M (2010) Retrograde signaling in axonal regeneration. *Exp Neurol* 223:5–10.
- Ruff CA, Wilcox JT, Fehlings MG (2012) Cell-based transplantation strategies to promote plasticity following spinal cord injury. *Exp Neurol* 235:78–90.
- Rush R (1995) The regulation of nerve growth factor synthesis and delivery to peripheral neurons. *Pharmacol Ther* 65:93–123.
- Sabbatini P, McCormick F (2002) MDMX inhibits the p300/CBP-mediated acetylation of p53. *DNA Cell Biol* 21:519–525.

Schreyer DJ, Skene JH (1991) Fate of GAP-43 in ascending spinal axons of DRG neurons after peripheral nerve injury: delayed accumulation and correlation with regenerative potential. *J Neurosci* 11:3738–3751.

Schwab ME (2010) Functions of Nogo proteins and their receptors in the nervous system. *Nat Rev Neurosci* 11:799–811.

Schwab ME, Strittmatter SM (2014) Nogo limits neural plasticity and recovery from injury. *Curr Opin Neurobiol* 27:53–60.

Seiffers R, Benowitz L (2008) Intrinsic determinants of axon regeneration. In: *CNS Regeneration - Basic Science and Clinical Advances*, 2nd ed. (Kordower JH, Tuszynski MH, eds), pp 1–39. Academic Press.

Seiffers R, Mills CD, Woolf CJ (2007) ATF3 increases the intrinsic growth state of DRG neurons to enhance peripheral nerve regeneration. *J Neurosci* 27:7911–7920.

Sengul G, Watson C (2012) Spinal Cord. In: *The Mouse Nervous System*, pp 424–458. Elsevier Inc.

Sengupta S, Harris CC (2005) p53: traffic cop at the crossroads of DNA repair and recombination. *Nat Rev Mol Cell Biol* 6:44–55.

Sharma RP, Grayson DR, Guidotti A, Costa E (2005) Chromatin, DNA methylation and neuron gene regulation - The purpose of the package. *J Psychiatry Neurosci* 30:257–263.

Shen Y, Tenney AP, Busch S a, Horn KP, Cuascut FX, Liu K, He Z, Silver J, Flanagan JG (2009) PTPsigma is a receptor for chondroitin sulfate proteoglycan, an inhibitor of neural regeneration. *Science* 326:592–596.

Shvarts A, Steegenga WT, Riteco N, van Laar T, Dekker P, Bazuine M, van Ham RC, van der Houven van Oordt W, Hateboer G, van der Eb AJ, Jochemsen AG (1996) MDMX: a novel p53-binding protein with some functional properties of MDM2. *EMBO J* 15:5349–5357.

Silver J, Schwab ME, Popovich PG (2015) Central nervous system regenerative failure: role of oligodendrocytes, astrocytes, and microglia. *Cold Spring Harb Perspect Biol* 7:a020602.

Sivasankaran R, Pei J, Wang KC, Zhang YP, Shields CB, Xu X-M, He Z (2004) PKC mediates inhibitory effects of myelin and chondroitin sulfate proteoglycans on axonal regeneration. *Nat Neurosci* 7:261–268.

Smith PD, Sun F, Park KK, Cai B, Wang C, Kuwako K, Martinez-Carrasco I, Connolly L, He Z (2009) SOCS3 Deletion Promotes Optic Nerve Regeneration In Vivo. *Neuron* 64:617–623.

Spira ME, Benbassat D, Dormann A (1993) Resealing of the proximal and distal cut ends of transected axons: electrophysiological and ultrastructural analysis. *J Neurobiol* 24:300–316.

Spira ME, Oren R, Dormann A, Gitler D (2003) Critical calpain-dependent ultrastructural alterations underlie the transformation of an axonal segment into a growth cone after axotomy of cultured *Aplysia* neurons. *J Comp Neurol* 457:293–312.

Sroga JM, Jones TB, Kigerl K a, McGaughy VM, Popovich PG (2003) Rats and mice exhibit distinct inflammatory reactions after spinal cord injury. *J Comp Neurol* 462:223–240.

Staerk J, Kallin A, Demoulin J-B, Vainchenker W, Constantinescu SN (2005) JAK1 and Tyk2 activation by the homologous polycythemia vera JAK2 V617F mutation: cross-talk with IGF1 receptor. *J Biol Chem* 280:41893–41899.

Stirling DP, Khodarahmi K, Liu J, McPhail LT, McBride CB, Steeves JD, Ramer MS, Tetzlaff W (2004) Minocycline treatment reduces delayed oligodendrocyte death, attenuates axonal dieback, and improves functional outcome after spinal cord injury. *J Neurosci* 24:2182–2190.

Sun F, Park KK, Belin S, Wang D, Lu T, Chen G, Zhang K, Yeung C, Feng G, Yankner B a., He Z (2011) Sustained axon regeneration induced by co-deletion of PTEN and SOCS3. *Nature* 480:372–375.

Taylor WR, Stark GR (2001) Regulation of the G2/M transition by p53. *Oncogene* 20:1803–1815.

Tedeschi A (2012) Tuning the Orchestra: Transcriptional Pathways Controlling Axon Regeneration. *Front Mol Neurosci* 4:1–12.

Tedeschi A, Di Giovanni S (2009) The non-apoptotic role of p53 in neuronal biology: enlightening the dark side of the moon. *EMBO Rep* 10:576–583.

Tedeschi A, Nguyen T, Puttagunta R, Gaub P, Di Giovanni S (2009a) A p53-CBP/p300 transcription module is required for GAP-43 expression, axon outgrowth, and regeneration. *Cell Death Differ* 16:543–554.

Tedeschi A, Nguyen T, Steele SU, Feil S, Naumann U, Feil R, Di Giovanni S (2009b) The tumor suppressor p53 transcriptionally regulates cGKI expression during neuronal maturation and is required for cGMP-dependent growth cone collapse. *J Neurosci* 29:15155–15160.

Toledo F, Wahl GM (2006) Regulating the p53 pathway: in vitro hypotheses, in vivo veritas. *Nat Rev Cancer* 6:909–923.

Trakhtenberg EF, Goldberg JL (2012) Epigenetic regulation of axon and dendrite growth. *Front Mol Neurosci* 5:24.

Tuszynski MH, Steward O (2012) Concepts and Methods for the Study of Axonal Regeneration in the CNS. *Neuron* 74:777–791.

- Van den Brand R, Heutschi J, Barraud Q, DiGiovanna J, Bartholdi K, Huerlimann M, Friedli L, Vollenweider I, Moraud EM, Duis S, Dominici N, Micera S, Musienko P, Courtine G (2012) Restoring Voluntary Control of Locomotion after Paralyzing Spinal Cord Injury. *Science* 336:1182–1185.
- Vassilev LT, Vu BT, Graves B, Carvajal D, Podlaski F, Filipovic Z, Kong N, Kammlott U, Lukacs C, Klein C, Fotouhi N, Liu E a (2004) In vivo activation of the p53 pathway by small-molecule antagonists of MDM2. *Science* 303:844–848.
- Wade M, Wang Y V., Wahl GM (2010) The p53 orchestra: Mdm2 and Mdmx set the tone. *Trends Cell Biol* 20:299–309 Available at: <http://dx.doi.org/10.1016/j.tcb.2010.01.009>.
- Wang KC, Kim JA, Sivasankaran R, Segal R, He Z (2002a) P75 interacts with the Nogo receptor as a co-receptor for Nogo, MAG and OMgp. *Nature* 420:74–78.
- Wang KC, Koprivica V, Kim JA, Sivasankaran R, Guo Y, Neve RL, He Z (2002b) Oligodendrocyte-myelin glycoprotein is a Nogo receptor ligand that inhibits neurite outgrowth. *Nature* 417:941–944.
- Wang Z, Zang C, Rosenfeld JA, Schones DE, Barski A, Cuddapah S, Cui K, Roh T-Y, Peng W, Zhang MQ, Zhao K (2008) Combinatorial patterns of histone acetylations and methylations in the human genome. *Nat Genet* 40:897–903.
- Weidner N, Ner a, Salimi N, Tuszynski MH (2001) Spontaneous corticospinal axonal plasticity and functional recovery after adult central nervous system injury. *Proc Natl Acad Sci USA* 98:3513–3518.
- Weishaupt N, Hurd C, Wei DZ, Fouad K (2013) Reticulospinal plasticity after cervical spinal cord injury in the rat involves withdrawal of projections below the injury. *Exp Neurol* 247:241–249.
- Wernig A, Müller S, Nanassy A, Cagol E (1995) Laufband therapy based on “rules of spinal locomotion” is effective in spinal cord injured persons. *Eur J Neurosci* 7:823–829.
- Wernig A, Nanassy A, Müller S (1998) Maintenance of locomotor abilities following Laufband (treadmill) therapy in para- and tetraplegic persons: follow-up studies. *Spinal Cord* 36:744–749.
- White RE, Jakeman LB (2008) Don’t fence me in: harnessing the beneficial roles of astrocytes for spinal cord repair. *Restor Neurol Neurosci* 26:197–214.
- WHO, ISCOS (2013) International perspectives on spinal cord injury (Bickenbach J, Bodine C, Brown D, Burns A, Campbell R, Cardenas D, Charlifue S, Chen Y, Gray D, Li L, Officer A, Post M, Shakespeare T, Sinnott A, von Groote P, Xiong X, Xiong, eds). World Health Organization.
- Windle WF, Smart JO, Beers JJ (1958) Residual function after subtotal spinal cord transection in adult cats. *Neurology* 8:518–521.

- Wong K, Zhang J, Awasthi S, Sharma A, Rogers L, Matlock EF, Van Lint C, Karpova T, McNally J, Harrod R (2004) Nerve growth factor receptor signaling induces histone acetyltransferase domain-dependent nuclear translocation of p300/CREB-binding protein-associated factor and hGCN5 acetyltransferases. *J Biol Chem* 279:55667–55674.
- Wu D, Zhang Y, Bo X, Huang W, Xiao F, Zhang X, Miao T, Magoulas C, Subang MC, Richardson PM (2007) Actions of neuropoietic cytokines and cyclic AMP in regenerative conditioning of rat primary sensory neurons. *Exp Neurol* 204:66–76.
- Xu J, Chen E, Lu C, He C (2009) Recombinant ciliary neurotrophic factor promotes nerve regeneration and induces gene expression in silicon tube-bridged transected sciatic nerves in adult rats. *J Clin Neurosci* 16:812–817.
- Yang G, Qu X, Zhang J, Zhao W, Wang H (2012) Sema3F downregulates p53 expression leading to axonal growth cone collapse in primary hippocampal neurons. *Int J Clin Exp Pathol* 5:634–641.
- Yang X-J, Seto E (2007) HATs and HDACs: from structure, function and regulation to novel strategies for therapy and prevention. *Oncogene* 26:5310–5318.
- Yin Y, Cui Q, Li Y, Irwin N, Fischer D, Harvey AR, Benowitz LI (2003) Macrophage-derived factors stimulate optic nerve regeneration. *J Neurosci* 23:2284–2293.
- Yiu G, He Z (2006) Glial inhibition of CNS axon regeneration. *Nat Rev Neurosci* 7:617–627.
- Yudin D, Hanz S, Yoo S, Iavnilovitch E, Willis D, Gradus T, Vuppalanchi D, Segal-Ruder Y, Ben-Yaakov K, Hieda M, Yoneda Y, Twiss JL, Fainzilber M (2008) Localized Regulation of Axonal RanGTPase Controls Retrograde Injury Signaling in Peripheral Nerve. *Neuron* 59:241–252.
- Zheng B, Atwal J, Ho C, Case L, He X, Garcia KC, Steward O, Tessier-Lavigne M (2005) Genetic deletion of the Nogo receptor does not reduce neurite inhibition in vitro or promote corticospinal tract regeneration in vivo. *Proc Natl Acad Sci USA* 102:1205–1210.
- Zhu Y, Soderblom C, Trojanowsky M, Lee D-HH, Lee JK (2015) Fibronectin Matrix Assembly after Spinal Cord Injury. *J Neurotrauma* 32:1158–1167.
- Ziv NE, Spira ME (1997) Localized and Transient Elevations of Intracellular Ca<sup>2+</sup> Induce the Dedifferentiation of Axonal Segments into Growth Cones. *J Neurosci* 17:3568–3579.
- Zukor K, Belin S, Wang C, Keelan N, Wang X, He Z (2013) Short hairpin RNA against PTEN enhances regenerative growth of corticospinal tract axons after spinal cord injury. *J Neurosci* 33:15350–15361.



## PUBLICATIONS AND STATEMENT OF CONTRIBUTIONS

### 1. The MDM4/MDM2-p53-IGF1 axis controls axonal regeneration, sprouting and functional recovery after CNS injury

Yashashree Joshi\*, **Marília Grando Sória\***, Giorgia Quadrato, Gizem Inak, Luming Zhou, Arnau Hervera, Khizr I. Rathore, Mohamed Elnaggar, Magali Cucchiarini, Jeanne Christophe Marine, Radhika Puttagunta and Simone Di Giovanni

*Brain* 138(Pt 7):1843–1862, 2015.

Research designed by: **M.G.S.**, Y.J., S.D.G.

Experiments performed by: **M.G.S.**, Y.J., G.Q., G.I., L.Z., A.H., K.R., M.E.

Data analyzed by: **M.G.S.**, Y.J., R.P., S.D.G., A.H.

Support and feedback: R.P., M.C., J.C.M.

Manuscript written by: **M.G.S.**, Y.J., SDG

\* *These authors contributed equally to this work.*

### 2. PCAF-dependent epigenetic changes promote axonal regeneration in the central nervous system

Radhika Puttagunta<sup>§</sup>, Andrea Tedeschi<sup>§</sup>, **Marília Grando Sória**, Arnau Hervera, Ricco Lindner, Khizr I. Rathore, Perrine Gaub, Yashashree Joshi, Tuan Nguyen, Antonio Schmandke, Claudia J. Laskowski, Anne-Laurence Boutillier, Frank Bradke, Simone Di Giovanni

*Nature Communications* 5:3527, 2014.

Research designed by: S.D.G.

Experiments performed by: R.P., A.T., **M.G.S.**, A.H., R.L., K.I.R., P.G., Y.J., T.N., A.S., C.J.L.

Data analyzed by: R.P., A.T., **M.G.S.**, A.H., R.L.

Mice provided by: A.L.B.

Support and feedback: F.B.

Manuscript written by: R.P., S.D.G.

§ *These authors contributed equally to this work.*

# The MDM4/MDM2-p53-IGF1 axis controls axonal regeneration, sprouting and functional recovery after CNS injury

Yashashree Joshi,<sup>1,2,3,\*</sup> Marília Grando Sória,<sup>1,2,\*</sup> Giorgia Quadrato,<sup>1</sup> Gizem Inak,<sup>1,2</sup> Luming Zhou,<sup>1,4</sup> Arnau Hervera,<sup>4</sup> Khizr I. Rathore,<sup>1</sup> Mohamed Elnaggar,<sup>1,2</sup> Magali Cucchiarini,<sup>5</sup> Jeanne Christophe Marine,<sup>6</sup> Radhika Puttagunta<sup>1</sup> and Simone Di Giovanni<sup>1,4</sup>

\*These authors contributed equally to this work.

Regeneration of injured central nervous system axons is highly restricted, causing neurological impairment. To date, although the lack of intrinsic regenerative potential is well described, a key regulatory molecular mechanism for the enhancement of both axonal regrowth and functional recovery after central nervous system injury remains elusive. While ubiquitin ligases coordinate neuronal morphogenesis and connectivity during development as well as after axonal injury, their role specifically in axonal regeneration is unknown. Following a bioinformatics network analysis combining ubiquitin ligases with previously defined axonal regenerative proteins, we found a triad composed of the ubiquitin ligases MDM4, MDM2 and the transcription factor p53 (encoded by *TP53*) as a putative central signalling complex restricting the regeneration program. Indeed, conditional deletion of MDM4 or pharmacological inhibition of MDM2/p53 interaction in the eye and spinal cord promote axonal regeneration and sprouting of the optic nerve after crush and of supraspinal tracts after spinal cord injury. The double conditional deletion of MDM4-p53 as well as MDM2 inhibition in p53-deficient mice blocks this regenerative phenotype, showing its dependence upon p53. Genome-wide gene expression analysis from *ex vivo* fluorescence-activated cell sorting in MDM4-deficient retinal ganglion cells identifies the downstream target IGF1R, whose activity and expression was found to be required for the regeneration elicited by MDM4 deletion. Importantly, we demonstrate that pharmacological enhancement of the MDM2/p53-IGF1R axis enhances axonal sprouting as well as functional recovery after spinal cord injury. Thus, our results show MDM4-MDM2/p53-IGF1R as an original regulatory mechanism for CNS regeneration and offer novel targets to enhance neurological recovery.

- 1 Laboratory for NeuroRegeneration and Repair, Centre for Neurology, Hertie Institute for Clinical Brain Research, University of Tuebingen, Tuebingen, Germany
- 2 Graduate School for Cellular and Molecular Neuroscience, University of Tuebingen, Tuebingen, Germany
- 3 German Centre for Neurodegenerative Diseases (DZNE), Tuebingen, Germany
- 4 Molecular Neuroregeneration, Division of Brain Sciences, Department of Medicine, Imperial College London, London, UK
- 5 Centre of Experimental Orthopaedics, Saarland University Medical Centre, Homburg/Saar, Germany
- 6 Laboratory for Molecular Cancer Biology, Department of Molecular and Developmental Genetics, VIB-K.U.Leuven, Leuven, Belgium

Correspondence to: Simone Di Giovanni, MD, PhD  
Division of Brain Sciences  
Imperial College London  
Hammersmith Hospital Campus  
Imperial College London

Du Cane Road, W12 0NN, UK  
E-mail: s.di-giovanni@imperial.ac.uk

**Keywords:** MDM4; MDM2; IGF1R; p53; optic nerve; spinal cord injury, regeneration

**Abbreviations:** BDA = fluorescent biotin dextran tetramethylrhodamine; CtB = cholera toxin subunit B; RGC = retinal ganglion cell

## Introduction

The adult mammalian CNS is unable to regenerate following axonal injury due to the presence of glial inhibitory environment as well as the lack of a neuronal intrinsic regenerative potential. Research over the past two decades has elucidated several key molecular mechanisms and pathways that limit axonal sprouting and regeneration following CNS axonal injury, including myelin or proteoglycan-dependent inhibitory signalling (Yiu and He, 2006; Giovanni, 2009; Bradke *et al.*, 2012). More recently, accumulating evidence suggests that the modulation of the neuronal intrinsic potential via the manipulation of selected genes in specific neuronal populations may enhance axonal regeneration in the injured CNS (Park *et al.*, 2008; Moore *et al.*, 2009; Smith *et al.*, 2009; Sun *et al.*, 2011). More often, these are developmentally regulated pathways that contribute to locking the adult CNS neurons in a non-regenerative mode. Remarkably, deletion of phosphatase and tensin homolog (PTEN) in retinal ganglion cells (RGCs) or in corticospinal tract axons enhances mTOR activity and leads to robust axonal regeneration after optic nerve or corticospinal tract injury, respectively (Park *et al.*, 2008; Liu *et al.*, 2010), which is further enhanced with conditional co-deletion of SOCS3 (Sun *et al.*, 2011). Furthermore, modifications of the developmentally regulated neuronal transcriptional program can lead to increased axonal regeneration after optic nerve crush or spinal cord injury as demonstrated by the deletion of kruppel-like factor 4 (KLF4), the overexpression of p300 (encoded by *EP300*) in RGCs (Moore *et al.*, 2009; Gaub *et al.*, 2011) as well as the overexpression of KLF7 (Blackmore *et al.*, 2012) or retinoic acid receptor beta (RARβ) in corticospinal neurons (Puttagunta and Di Giovanni, 2011; Puttagunta *et al.*, 2011).

Ubiquitin ligases and ubiquitin ligase-like proteins, including neuronal precursor cell-expressed developmentally downregulated protein (NEDDs), Smad ubiquitin regulatory factor (SMURFs) and murine double minute 2 and 4 (MDM2 and MDM4), coordinate neuronal morphogenesis and connectivity both during development and after axonal injury. Moreover, they regulate the turnover, localization and activity of a number of proteins and transcription factors involved in the axonal regeneration program, including PTEN, p300, KLFs, Smads, p21 and p53 (Yamada *et al.*, 2013). Ubiquitin ligases and ubiquitin ligase-like proteins may therefore represent a regulatory hub controlling the regenerative neuronal response

following injury. However, their role in axonal regeneration remains unaddressed. Therefore, to functionally rank ubiquitin ligase dependent control of the regeneration programme, we systematically analysed protein networks using the *STRING* bioinformatic tool including proteins previously described to be involved in axonal regeneration and sprouting in the CNS and the corresponding ubiquitin ligases. This had the goal to identify central protein networks that control the regeneration program that may have positive implications for functional recovery.

This analysis showed that MDM4, in association with MDM2, and p53 constitutes a central regulatory complex, potentially involved in repressing axonal regeneration. The ubiquitin ligase-like MDM4 and MDM2 can form inhibitory protein complexes with at least four key proteins involved in axonal outgrowth: SMAD1/2, p300, p53 (Kadakia *et al.*, 2002; Markey, 2011). Strikingly, MDM4 and MDM2 expression is developmentally regulated in the retina reaching its maximal levels in adulthood (Vuong *et al.*, 2012), potentially keeping the post-injury RGC growth program in check. Therefore, MDM4 and MDM2 appear to be strong candidates for limiting axonal regeneration in the CNS, particularly in the injured optic nerve.

We investigated whether disruption of MDM4 and MDM2-dependent regulation would affect the axonal regeneration program. Indeed, we found that MDM4 and MDM2 restrict axonal regeneration after optic nerve crush. In fact, conditional MDM4 deletion in RGCs leads to axonal regeneration and sprouting of RGC axons following optic nerve crush. Additionally, conditional co-deletion of MDM4 and its target protein p53 in RGCs after optic nerve crush blocks nerve regeneration elicited by MDM4 deletion alone. Similarly, pharmacological inhibition of the interaction between the MDM4 co-factor MDM2 and p53 via the MDM2/p53 antagonist Nutlin-3a also enables regeneration after optic nerve crush, which is abolished in p53 deficient mice. Further, genome-wide gene expression analysis from a pure RGC population after conditional deletion of MDM4 showed enhancement of IGF1R expression suggesting IGF1 signalling as a downstream effector of the MDM4 deletion. Indeed, co-inhibition of MDM4 and IGF1 signalling after optic nerve crush via a specific IGF1R antagonist impairs axonal regeneration, while viral overexpression of IGF1 in the eye enhances it. Finally, we demonstrate that MDM4/2-p53-IGF1 regulation is critical for axonal sprouting and neurological recovery after spinal cord injury. Both conditional deletion of MDM4 and Nutlin-3 delivery after spinal

cord dorsal hemisection in mice enhance axonal sprouting of supraspinal descending fibres and functional recovery, which is blocked when IGF1R signalling is inhibited.

Together, this work portrays the MDM4-MDM2/p53-IGF1R axis as a novel molecular target for axonal regeneration and neurological recovery after spinal injury.

## Materials and methods

### Mice

All experimental procedures were performed according to the animal protocols approved by the Regierungspräsidium Tübingen. Mice were housed in a colony maintained at 24°C with a 12 h dark/light cycle and *ad libitum* food and water. For all surgeries, mice were anaesthetized with xylazine (10 mg/kg of body weight) and ketamine (100 mg/kg of body weight), and eye ointment bepanthen was applied to protect corneas during surgery.

### Intravitreal injections

For intravitreal injections, pulled glass capillaries attached to a Hamilton syringe via a connector were inserted into the peripheral retina. A volume of vitreal fluid equal to the volume to be injected was removed to avoid intravitreal pressure elevation. The micropipette was deliberately angled in a way to avoid lens injury. Fundoscopic inspection was done after every intravitreal injection to check for any damage to the lens. Animals with lens injury were excluded from the study. For performing the optic nerve injury, the left optic nerve was exposed intraorbitally and crushed for 10 s, 1 mm from the optic disc with forceps (Dumont 5, FST). Care was taken not to injure the ophthalmic artery to avoid retinal ischaemia. Animals with injury to the ophthalmic artery were excluded from the study. For anterograde tracing of the RGC axons, 1 µl cholera subunit B (CtB) conjugated to Alexa Fluor® 555 (Invitrogen) was injected intravitreally at least 2 days before sacrificing the mice. Mice were killed with a lethal dose of anaesthesia and transcardially perfused with ice cold 0.1 M phosphate-buffered saline (PBS) followed by 4% paraformaldehyde. Optic nerves and eyes were dissected and post fixed for 1 h at 4°C, before cryoprotecting them with 30% sucrose solution.

### AAV-cre in MDM4<sup>ff</sup> mice and Nutlin-3a administration

MDM4<sup>ff</sup> mice were a gift from the J.C.M lab and were produced as described previously (Grier *et al.*, 2006). Primers used for genotyping of the MDM4 mice were: a- (forward) - 5'-gggtccttgaaacttgctgtgtagaa-3'; b-(exon2 reverse) - 5'-ctggcgaggtggaatgtgatgt-3'; c-(reverse) - 5'-tatccagtgctcctcttggctt-3'. One microlitre of the adeno-associated virus expressing GFP (AAV GFP) or AAV CreGFP were intravitreally injected in male mice aged postnatal Day 21 and optic nerve crush was performed 14 days later (at postnatal Day 35). Twenty-six days post-optic nerve crush, CtB (Invitrogen, 2 µg/ul) was intravitreally injected in the eye, 2 days before sacrifice

by transcardial perfusion (28 days). One microlitre of 100 nm Nutlin-3a or vehicle were intravitreally injected in C57/BL6 (Charles River) male mice aged postnatal Day 35 and optic nerve crush was performed on the same day. Another intravitreal dose of Nutlin-3a was given 7 days post-optic nerve crush. Twenty-six days later, CtB (Invitrogen, 2 µg/µl) was intravitreally injected, and mice were sacrificed by transcardial perfusion 28 days post-optic nerve crush. Both wild-type and p53<sup>-/+</sup> mice were used for Nutlin-3a experiments.

### Experiments with MDM4<sup>ff</sup>/p53<sup>ff</sup> mice

MDM4<sup>ff</sup> were crossed with P53<sup>ff</sup> mice (Strain name: B6.129P2-Trp53tm1Brn/J, Stock Number: 008462, Jackson Labs) to generate MDM4<sup>ff</sup>/p53<sup>ff</sup> mice. The same experimental design including AAV delivery and optic nerve crush was conducted in MDM4<sup>ff</sup>/p53<sup>ff</sup> as in MDM4<sup>ff</sup>.

### Adeno-associated virus preparation and purification

Details about production of adeno-associated virus 2 (AAV2-GFP/AAV2-CreGFP) has been described elsewhere (Berton *et al.*, 2006; Grieger *et al.*, 2006). Plasmid vector for AAV-GFP and AAV-CreGFP production were a gift from Dr Eric J. Nestler. Briefly, GFP (control) or an N terminal fusion of GFP to Cre were cloned into a recombinant AAV-2 vector containing the human immediate early cytomegalovirus promoter with a splice donor acceptor sequence and polyadenylation signal from the human-globin gene. Cloning of the AAV-2 vector carrying a human IGF1 cDNA sequence was previously described (PMID 22160392). The vector was produced using a triple-transfection, helper-free method. The final purified virus was stored at -80°C. The titre was evaluated after infection in HeLa cells and successful infection was also tested *in vivo*. AAV used were in the range of 1–3 × 10<sup>13</sup> vector genomes (vg)/ml.

### Immunoprecipitation

Whole retinas were collected 72 h after sham or optic nerve crush surgeries and flash frozen in liquid nitrogen. Upon thawing, total proteins were extracted with RIPA lysis buffer (Thermo Inc.) plus protease and phosphatase inhibitors cocktails (Roche). Ten micrograms of protein were diluted in 200 µl of RIPA buffer, and 5 µg of anti-MDM4 antibody (Sigma-Aldrich) was added and incubated for 1 h on a rotating wheel at room temperature. Mouse normal IgG (Santa Cruz) was used as negative control. The immunocomplexes were collected by adding 40 µl of protein G magnetic beads (Cell Signaling), and incubated for 15 min on a rotating wheel at room temperature. Beads were collected with a magnetic separation rack (Cell Signaling), and washed three times with 500 µl of RIPA buffer. Proteins were then eluted with 10 µl of 4× loading buffer (Tris HCl 0.25 M, SDS 4%, glycerol 40%, 0.5% Bromphenol blue, 1× reducing agent) and heated for 5' at 96°C. Beads were separated with the magnetic separation rack, and supernatants onto 4% stacking/10% separating SDS polyacrylamide gels. The proteins were electrophoretically transferred onto nitrocellulose membranes, blocked with PBST + 5% non-fat dried milk, and subsequently



incubated overnight at 4°C with antibodies against p53 (rabbit, 1:1000, Santa Cruz) or MDM2 (mouse, 1:1000, Novus). The proteins were detected by horseradish peroxidase-conjugated secondary antibodies (Thermo) and visualized by chemiluminescence reagents provided with the ECL kit (Thermo) and exposure onto hyperfilm (GE Healthcare).

## Whole mount retinal staining

After perfusion, uninjured and injured eyes were dissected and post-fixed for 1 h in paraformaldehyde. Flat retinæ were plated on a dish in PBS and then stained for Tuj1 to detect surviving RGCs and with DAPI to detect nuclei. The uninjured retinæ were used as a control. The retinæ were mounted with single coverslips with mounting medium (Dako). At least 10 fields were imaged at  $\times 25$  oil magnification specifically from the retinal ganglion cell layer using Zeiss Apotome. The number of Tuj1+ cells was counted with the help of ImageJ. RGCs were quantified by an observer blind to the treatment. At least 15 high magnification images were taken from different parts of each retina and the total viable RGC number was obtained by multiplying the average number per field of Tuj1+ cells in the ganglion cell layer by the retinal area.

## Immunostaining of retina sections

Post-fixed and cryoprotected eyes were snap frozen and then cryosectioned longitudinally (10  $\mu$ m). Standard immunostaining procedures were followed. Antibody specificity was confirmed by using secondary antibody alone for each staining. The details of the antibodies are as follows: anti-p53 (1:200, Leica); anti-MDM4 (1:50, Sigma); anti-MDM2 (1:200, Novus Biologicals); anti-Cre (1:500, Novus Biologicals); anti-Tuj1 (1:1000, Covance and Promega), anti-GFP (1:500, Abcam); anti-p53ac 373 (1:200, Millipore), anti-GFAP (1:1000, Millipore). Detailed protocols are available upon request.

## Retinal ganglion cell densitometry analysis

A high-resolution image was obtained at  $\times 400$  magnification using the Zeiss Axioplan Microscope (Axiovert 200, Zeiss Inc.). Images for the same antigen groups were processed with the same exposure time. Assessment of fluorescence intensity was performed using AlphaEaseFC 4.0.1 software by measuring the intensities specifically from retinal ganglion cells. Care was taken that the area analysed for each cell was the same for each set, 100 cells from at least six sections per condition were quantified. The intensity values of each cell were normalized to the 4',6'-diamidino-2-phenylindole signal and mean values of intensities were calculated for each animal (at least three animals per condition) (Gaub *et al.*, 2011).

## Evaluation of optic nerve regenerating axons

Regenerating axons were counted as described previously (Leon *et al.*, 2000; Park *et al.*, 2008). Longitudinal sections of nerves were mounted and imaged at  $\times 400$ . Every fourth section and at least four sections per animal were quantified by drawing lines perpendicular to the crush site at a distance of

200, 300, 500, 750, 1000 and 1500  $\mu$ m from the crush site. CtB+ axons between these sections were counted and the cross-sectional width of every nerve was also measured. An observer blind to the treatment counted the regenerating fibres. The number of axons per millimetre was calculated and averaged over all the sections  $\Sigma ad$ , the total number of axons extending distance  $d$  in a nerve having a radius of  $r$ , was estimated by summing over all sections having a thickness  $t$  (10  $\mu$ m)  $\Sigma ad = \pi r^2 \times [\text{average axons} / \text{mm}] / t$ .

## Cerebellar granule neuron culture

Cerebellar granule neurons were prepared from cerebella of post-natal Day 7 MDM4<sup>fl/fl</sup> mice as described previously (Gaub *et al.*, 2010; Bradke *et al.*, 2012). Briefly, the minced cerebella were incubated for 15 min at 37°C in an ionic medium with 0.025% trypsin and 0.05% DNase I (Sigma). Then trypsin inhibitor (0.04%, Sigma) was added followed by centrifugation. The pellet was triturated, centrifuged and suspended in the growth medium [basal Eagle's medium supplemented with 10% bovine calf serum, 25 mM KCl, 4 mM glutamine and gentamycin (100 ng/ml)]. Cells were plated at a density of  $10^5$  cells on PDL/myelin (4  $\mu$ g/cm<sup>2</sup>) coated plates followed by infection with adenovirus 5 (AV5)-GFP/AV5-Cre ( $2 \times 10^{10}$  vg/ml). Cells were then fixed with 4% paraformaldehyde 24 h later followed by staining with anti-Tuj1 and anti-Cre. At least 100 single transduced cells per condition ( $n = 4$ ) were traced manually with NeuroLucida software.

## Viral injections into the sensorimotor cortex

Four-week-old MDM4<sup>fl/fl</sup> mice were anaesthetized with ketamine and xylazine and then placed on a stereotactic frame. To infect layer V neurons, AAV1-GFP or AAV1-CreGFP under CMV promoter were injected with a 5  $\mu$ l Hamilton syringe in the right sensorimotor cortex 5 weeks before spinal cord injury. The viruses were injected after craniotomy in a total of four sites [0.8  $\mu$ l/site of AAV1-GFP or AAV1-CreGFP ( $3.1 \times 10^9$  vg/ml) (SignaGen)]. The coordinates used were 1.0 mm lateral, 0.6 mm deep, and +0.5, -0.2, -0.7, and -1 mm with respect to bregma (Steward *et al.*, 2008).

## Quantitative reverse transcriptase polymerase chain reaction

Total RNA was extracted from cerebellar granule neuron cells 24 h after transduction with TRIzol<sup>®</sup> Reagent (Invitrogen). Complementary DNA was synthesized from 1  $\mu$ g of RNA using oligo dT and SuperScript<sup>®</sup> II Reverse Transcriptase kit (Invitrogen). Complementary DNA (1  $\mu$ l of 1:5 dilution) was used in a reverse transcriptase PCR (RT-PCR) using Master Mix (Invitrogen) and for quantitative RT-PCR, SYBR<sup>®</sup> GreenER<sup>™</sup> (ThermoScientific) was used. *Rpl13a* or *18S* RNA were used as controls. Melting curve analysis ensured single amplified products. Primers sequences have been summarized in Supplementary Table 5.

## Retinal ganglion cell culture

Dissociated retinal ganglion cell culture has been described previously (Gaub *et al.*, 2011). Briefly, post-natal Day 7 eyes were dissected, and retinae were incubated in Dulbecco's modified Eagle's medium with Papain (Worthington) and L-cysteine (Sigma) for 40 min. After incubation, retinae were dissociated in Dulbecco's modified Eagle's medium with B27 (Life Technologies) and penicillin/streptomycin (Sigma). Cells were plated at a density of  $10^6$  cells per  $2\text{ cm}^2$ . Plated cells were immediately infected with AV-GFP and AV-Cre at 100 multiplicity of infection. Following incubation, cells were fixed with 4% paraformaldehyde for 20 min. Cells were then blocked with 8% bovine serum albumin, 0.1% Triton<sup>TM</sup> X-100 in PBS and finally incubated with the primary antibodies overnight at 4°C: mouse anti-Tuj1 (1:1000, Promega). Cells were then washed with PBS and incubated with appropriate secondary antibodies (1:1000, Invitrogen) for 1 h at room temperature. At least 10 images taken at  $\times 200$  magnification with Axioplan inverted microscope (Zeiss) were automated analysed for neurite outgrowth with ImageJ, NeuriteTrace plugin.

## Immunoblotting

For immunoblotting, entire retinae were collected 6 h after Nutlin-3a injection and optic nerve crush and flash frozen or 72 h after sham surgery or optic nerve crush. For spinal cord tissue, spinal cord segments corresponding to the injury site (3 mm rostral and 3 mm caudal to the lesion) were harvested and flash frozen in liquid nitrogen. On thawing, proteins were extracted with RIPA buffer (50 mM Tris., 150 mM NaCl, 2 mM EDTA, 1% NP-40, 0.1% SDS, 0.1 mM PMSF,  $1 \times$  Protease inhibitor (Roche),  $1 \times$  PhosphoStop (Roche)). A portion of the lysate (30–50 mg of protein) was then fractionated by SDS-polyacrylamide gel electrophoresis, and the separated proteins were transferred to a nitrocellulose membrane and following blocking, probed for different antigens, as follows: rabbit anti-p53 (1:1000, Santa-Cruz), mouse anti-MDM4 (1:1000, Sigma), rabbit anti-MDM2 (1:1000, Novus); rabbit anti-acetylated p53 (lysine 373) (1:500, Millipore), rabbit anti-cleaved caspase-3 (1:1000, Cell Signaling) or rabbit anti-p21 (1:500, Abcam). Mouse anti-b-actin (1:5000, Sigma) was used as a loading and transfer control. Immune complexes were detected with appropriate secondary antibodies (goat anti-rabbit IgG, goat anti-mouse IgG, label with horseradish peroxidase (Thermo Scientific) and chemiluminescence reagents (Pierce ECL Western blotting Substrate).

## Retrograde labelling of retinal ganglion cells for FACS and Affymetrix gene expression analysis

DiI (Molecular Probes, Invitrogen, 2% in dimethyl formamide) was injected in the superior colliculus of post-natal Day 28 mice. Anaesthetized mice were placed in a stereotaxic holder and  $\sim 2\ \mu\text{l}$  DiI was then injected directly into the superficial superior colliculus (4.5 mm caudal to Bregma, 0.5 mm lateral to sagittal suture and 1–2 mm deep to brain surface) using a  $10\ \mu\text{l}$  gas tight syringe (Hamilton) connected to an automated nano-injector. Seven days after superior colliculus injection, the optic nerve crush was performed. Three days

(72 h) after crush, retinae were dissected and incubated in digestion solution (20 U/ml papain, Worthington; 1 mM L-cysteine HCl; 0.004% DNase; 0.5 mM EDTA in Neurobasal<sup>®</sup>) for 25–40 min at 37°C, with gentle shaking every 5 min. Digestion was stopped by adding ovomucoid solution before trituration. Retinae were then passed through a  $40\ \mu\text{m}$  filter. The obtained suspensions of the retinae were then processed using fluorescence-activated cell sorting (FACS). For microarray, total RNA was isolated from the FACS sorted RGCs using PureLink RNA micro kit (Invitrogen) according to manufacturer's instructions. Affymetrix Mouse Genome 430 2.0 Array from triplicate samples was performed at the Microarray Genechip Facility at Universitätsklinikum, Tübingen. Data processing and analysis was performed according to standard procedures (GC-RMA, RMA, MAS5). Genes differentially expressed were selected based upon a 2-fold change cut-off and significant statistical difference (ANOVA with Bonferroni correction). The microarray data analysis was carried out by Ingenuity Pathway Analysis software (Ingenuity System Inc). Cluster analysis for selected probe sets was performed in R 3.0.1. Signal intensities were scaled and centred and the distance between two expression profiles was calculated using Euclidian distance measure. Hierarchical cluster analysis was performed with average linkage for genes. Heat maps were generated with the Bioconductor package *gplots*.

## Drugs

Nutlin-3a (Cayman) was diluted in 8.6% ethanol in DPBS (vehicle). Before use in osmotic mini-pumps. Picropodophyllin (Medkoo Biosciences) was diluted in 1:10 dimethyl sulphoxide:cottonseed oil (vehicle). The oil was dry-heat sterilized at 150°C for 1 h, before use for i.p. (intraperitoneal) delivery.

## Spinal cord injury surgical procedure, BDA tracing and postoperative care

The experimental procedure followed for spinal cord injury has been described previously (Floriddia *et al.*, 2012). Briefly, anaesthetized wild-type or *Mdm4<sup>fl/fl</sup>* mice (ketamine/xylazine) were kept on a heating pad to maintain the body temperature at 37°C during the whole procedure. An incision was made on the thoracic area after shaving and cleaning with Softasep<sup>®</sup> N (Braun). Muscle tissue right below the incision was dissected to expose laminae T8–T10. A dorsal hemisection at T9 until the central canal was performed with a microknife (FST). To ensure that the lesion was complete, the microknife was passed throughout the dorsal part of the spinal cord several times. This kind of injury damages the dorsal and lateral corticospinal tract, the dorsal columns, the rubrospinal, the dorsal and lateral raphe-spinal, and part of the reticulospinal tracts.

For spinal surgeries with Nutlin-3 delivery by osmotic minipumps (Alzet 2002) 12-week-old C57BL/6 mice (Charles River, Germany) mice were used. A customized 32 G-polyethylene IT catheter (ReCathCo) was placed subdurally until T9. Once placed, the caudal tip of the catheter was glued to the T12 bone with a drop of cyanoacrylate glue (Cyano Veneer, Hager&Werken). The pump was placed in the subcutaneous space on the back of the animal caudal to the surgical incision. All the surgical procedures were performed in an unbiased blind fashion, i.e. the surgeon did not know

the content of the pumps (vehicle versus drug). After 2 weeks pumps were removed under 2% isoflurane/0.8% O<sub>2</sub> and mice were injected with the non-steroidal anti-inflammatory carprofen (Carprieve, Norbrook, 5 mg/kg subcutaneously). The pump was freed from the subcutaneous tissue and removed. The IT catheter, however, was left in place to avoid a secondary injury to the spinal cord. The skin was closed with suture clips. During the surgical procedure, animals were kept warm at 37°C.

After surgery, mice were placed back in their cages and warmed up with an infrared light to prevent hypothermia. Mice underwent daily check for general health, mobility within the cage, wounds, swelling, infections, or autophagy of the toes throughout the experiment. They were injected subcutaneously with 1 ml of 0.9% saline twice daily for 3 days and once daily from Days 4 to 7 after surgery. Pain was managed with injections of 0.05–0.1 mg/kg subcutaneous buprenorphine twice daily (12/12 h) for the first 3 days after the spinal cord injury surgery and 5 mg/kg/day subcutaneous of carprofen for Days 4–7. To prevent urinary infection, enrofloxacin was injected at 5 mg/kg once daily in the first 5 days after surgery. If the animal developed signs of urinary infection in the chronic phase, it received enrofloxacin 10 mg/kg/day subcutaneously for 14 days, and 1 ml of 0.9% saline solution subcutaneously daily until the urine was clear. Animals also received Nutrical as food supplement after the spinal cord injury surgery. Bladders were manually expressed twice daily until needed. Ten to 14 days before sacrifice, the animals were injected with 1.4 µl of a 10% (w/v) solution of BDA (fluorescent biotin dextran tetramethylrhodamine; 10 000 MW, Molecular Probes, 10% w/v in PBS) into four injection sites of the right sensorimotor cortex of the hind limb region to trace the corticospinal tract as previously described (Simonen *et al.*, 2003).

## Quantification of corticospinal tract sprouting

Two weeks following tracer injection mice were perfused transcardially with 0.1 M PBS, pH 7.4, and 4% paraformaldehyde in PBS, pH 7.4 under deep anaesthesia. For each animal, at least three consecutive most medial parasagittal cryosections (18 µm) using the central canal as landmark were chosen and analysed with the software Stereo-Investigator 7 (MBF Bioscience) to count axons and sprouts. The quantification of the sprouting index of the dorsomedial corticospinal tract was performed proximal to the lesion site at rostral and caudal level. For each section, the BDA-labelled sprouts and axons were counted live. The sum of the total number of labelled axons and axon sprouts was normalized to the total number of labelled axons above the lesion site counted in all the analysed sections for each animal, obtaining an inter-animal comparable ratio considering the individual tracing variability (Schnell and Schwab, 1993; Steward *et al.*, 2008). Sprouts and regrowing fibres were defined following the anatomical reported criteria (Joosten and Bar, 1999; Steward *et al.*, 2003; Hill *et al.*, 2004; Erturk *et al.*, 2007). Cords showing spared fibres were excluded by monitoring BDA labelling in coronal sections from 15 mm below the lesion site.

## Immunohistochemistry of brain and spinal cord sections

Animals were intracardially perfused with cold 0.1 M PBS, pH 7.4, followed by fixation with cold 4% paraformaldehyde in 0.1 M PBS, pH 7.4. The spinal cords and brains were dissected and post-fixed with 4% paraformaldehyde for 2 h in ice, then cryoprotected in 30% saccharose and kept at 4°C. After 5–7 days, the tissues were frozen in liquid nitrogen and kept at –80°C until sectioning. The spinal cords and the brains were embedded in Tissue-Tek O.C.T. compound. The cords were sectioned in the sagittal plane at 18 µm thickness, including the injury site. Coronal sections of the cords 1.0 cm rostral and 1.5 cm caudal to the injury site were also included. Brains were sectioned at 40 µm in the coronal plane and the sections were collected in cryoprotectant solution. The tissues were kept at –20°C until staining. For all the stainings performed, the antibody specificity was tested by incubating samples only with the secondary antibody. Primary antibodies for spinal cord sections: anti-fibronectin (1:500, Sigma), anti-GFAP (1:500, Millipore). Coronal sections from brains (40 µm) were processed and stained in free-floating to detect GFP signal in the sensorimotor cortex. GFP signal was also enhanced using chicken anti-GFP antibody (1:500, Abcam). Sections were also stained with anti-Ctip2 antibody (1:500, Abcam) to mark layer V neurons.

Immunohistochemistry anti-fibronectin allowed visualizing of the core of the lesion site. Immunohistochemistry anti-GFAP allowed defining the size of the spinal lesions in all of the experiments performed including treatment versus vehicle. The GFAP-positive immunolabelling delimiting the lesion site was measured in triplicate sections centred around the central canal for each cord. The lesion size was comparable between experimental and control conditions, therefore not affecting the assessment of axonal sprouting.

For 5-HT immunostaining we followed a protocol as previously described (Floriddia *et al.*, 2012). Briefly, spinal cord sections were post-fixed in 0.1% glutaraldehyde in 4% paraformaldehyde. Then quenched with ethanol peroxide and transferred to 0.2% sodium borohydride. They underwent antigen retrieval in 0.1 M citrate buffer, pH 4.5, and microwave irradiation at 98°C for 2 min. The sections were incubated with rabbit anti-5-HT (1:8000, ImmunoStar) in 4% normal goat serum in 0.3% Tris-buffered saline–Triton™ X-100 for 4 days at 4°C. After that, the sections were further blocked in avidin and biotin (avidin-biotin blocking kit, Vector Labs), then were incubated in biotinylated goat anti-rabbit antibody (1:200, Vector Labs) in 2% normal goat serum in 0.3% Tris-buffered saline–Triton™ X-100 followed by incubation in ABC elite complex (Vector Labs). The signal was further amplified by incubation in biotinylated tyramide and revealed with diaminobenzidine tetrahydrochloride (Vector Labs). The sections were dehydrated and coverslipped.

## 5-HT sprouting

5-HT sprouting was evaluated by quantitative measurement of 5-HT-positive axons caudally to the lesion site. The number of 5-HT-positive fibres was counted live with a ×40 objective on parasagittal sections across the left, middle and right segments of the cord from at least three representative sections per cord.



Measurements were conducted blind to the experimental conditions.

## Behavioural assessments

Mice were gently handled daily for five to seven sessions. Thereafter they were acclimatized to the Basso Mouse Scale (Basso *et al.*, 2006) open field platform and to the grid walk apparatus daily for another five to seven sessions. The investigators that participated in the behavioural ratings were blind to the pump content (Nutlin-3a or vehicle) or to the solution the animals were being injected intraperitoneally (picropodophyllin or vehicle). Only animals with a histological proof of hemisection until the central canal, excluding the ones with occurrence of spared fibres below the lesion or with a total hemisection, were taken into account.

### Basso Mouse Scale

Briefly, a mouse walked on the platform for 4 min during which its motor behaviour was rated by two investigators in terms of ankle movement, paw placement, stepping and paw position of the hindlimbs, coordination, trunk stability and tail position. The Basso Mouse Scale main score and subscore were given. Animals were tested 1 day before, then 1, 3, 7, 14, 21, 28 and 35 days after injury.

### Grid walk

The grid walk consists of a 50 cm × 3 cm metal grid placed between two vertical 40 cm high wood blocks. The metal mesh is formed by 1 cm × 1 cm spaces. Only animals able to frequent or consistently step (Basso Mouse Scale ≥ 5) were also tested on the grid walk. The mice were video recorded for 3 min while running on the grid in both directions. The videos were later analysed by a blind investigator, who counted the number of missteps. A misstep occurs when the animal fails to place the paw on the grid and the paw slips down in the 1 cm × 1 cm space. Only animals that had at least three compliant runs were considered for statistical analysis. A compliant run was defined as a run comprising at least ¾ of the grid length in consistent speed. The animals were tested in the grid walk 1 day before the injury and 14, 21, 28 and 35 days afterwards.

To ensure that surgical procedures did not interfere with the behavioural assessments, animals were tested in the Basso Mouse Scale and grid walk in the same day but before the pump was removed (14 days post-injury) and before the tracer was injected (35 days post-injury).

Experiments were performed by the surgeons blinded to the content of either the minipumps or the syringes containing virus or drug. Another researcher organized the groups at random allowing for equal group sizes on each day of surgery; however, the order and treatment were withheld from both the surgeons and the researchers performing behavioural and histological analysis. The treatment order was randomized at the level of the animal such that within a day post-injury, drug treated or control treated animals were interspersed at random. Animals were excluded from analysis in the case of spared fibres (see above) or when we observed a total transection with the fibronectin positive scar spanning the entire depth of the spinal cord. These animals were rejected from analysis by someone blinded to their treatment allocation. A detail description of the experimental designs can be found in

Supplementary Tables 3 and 4, according to ARRIVE guidelines and the Minimal Information about a Spinal Cord Injury Experiment reporting standards.

## STRING bioinformatics analysis

STRING functional protein interaction analysis online tool based upon the work by Jensen *et al.* (2009) was used to identify cluster of axonal regeneration regulatory protein central to the whole protein network. Fifteen regulatory protein networks for genes involved in the axonal regeneration program within the CNS were included in the analysis. They include: STAT3, SMAD1, SMAD2, KLF4, KLF7, KLF9, jun, p53, p300, PTEN, SOCS1, SOCS3, RARB, CREB and SOX11. The interactions include direct (physical) and indirect (functional) association. All of the interactions reported have *P*-values < 0.001, while K-means based clustering was used.

## Results

### MDM4 conditional deletion stimulates optic nerve regeneration and corticospinal tract axonal sprouting

Initially, we performed a protein network analysis with *STRING* network and protein interaction algorithms to determine whether ubiquitin ligases and ubiquitin-like ligases may be linked to known transcriptional and protein synthesis regulators of axonal regeneration in CNS axons (see ‘Materials and methods’ section for detail). Given their central positioning in the protein network, we identified a protein complex composed of MDM4-MDM2 and p53 potentially restricting the regenerative program (Supplementary Fig. 1A). To examine our hypothesis in an *in vivo* model of non-regenerating axons after injury, we used the optic nerve crush method in mice, where the injured optic nerve does not regenerate. First, we established by co-immunoprecipitation experiments that MDM4, MDM2 and p53 form a protein complex in the retina both before and after optic nerve crush (Supplementary Fig. 1B). Importantly, these three proteins are highly expressed in retinal ganglia cells (Supplementary Fig. 2). Next, we asked whether disruption of this complex would enhance axonal regeneration. To this end, we performed conditional deletion of MDM4 specifically in RGCs by intravitreal injection of AAV2-CreGFP virus in MDM4<sup>fl/fl</sup> mice 2 weeks before optic nerve crush, while an AAV2-GFP vector was used as a control (Fig. 1). AAV2 infects RGCs rather efficiently and specifically due to the physical proximity (Supplementary Fig. 3A), although ~5–10% of other neuronal populations can also be infected. Following AAV2-cre mediated infection (Supplementary Fig. 3A) and conditional deletion we could confirm a strong reduction of MDM4 expression in infected cells (Supplementary Fig. 3B). Additionally, AAV-cre mediated genetic deletion of MDM4 in primary



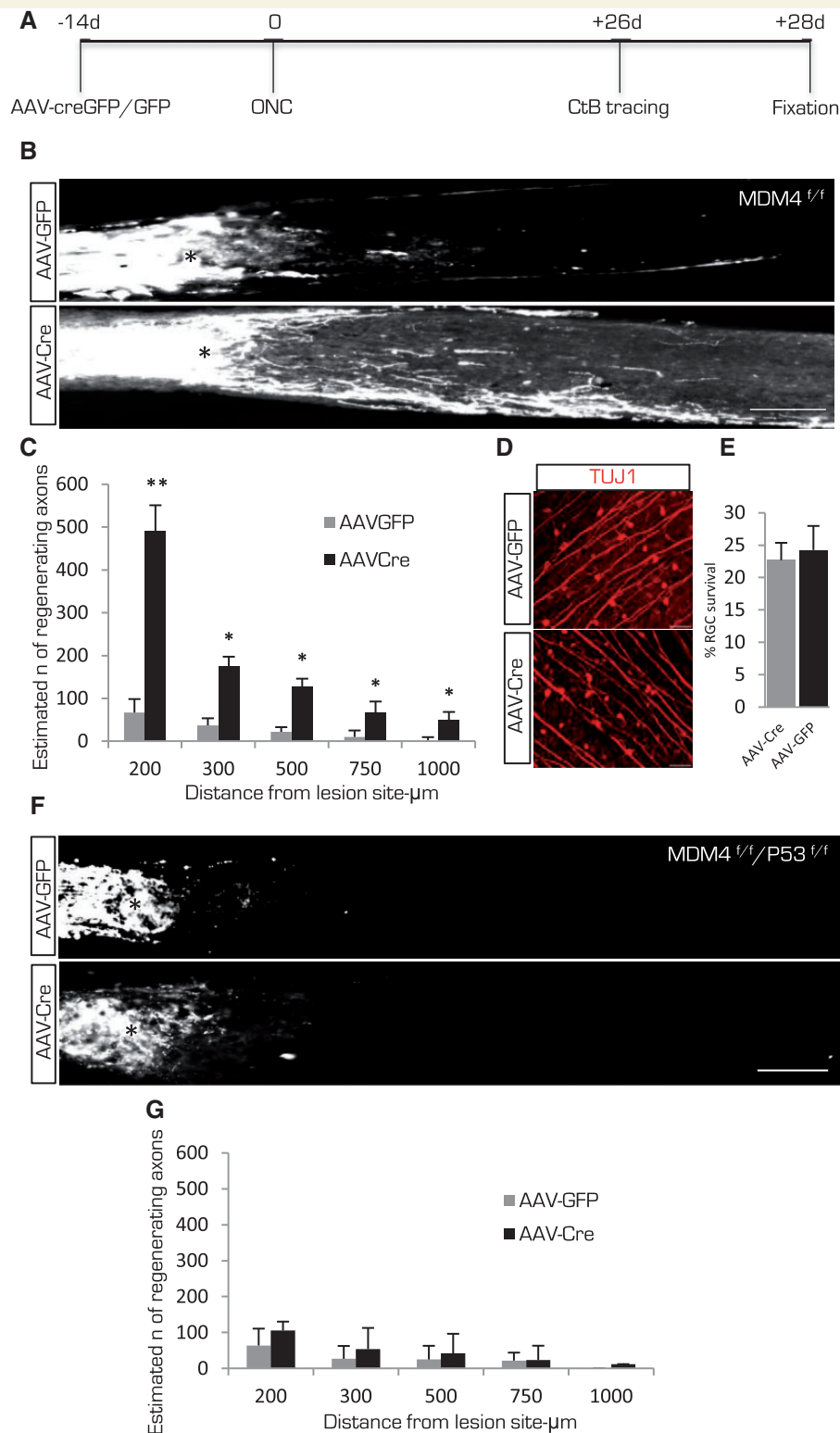


**Figure 1 Conditional deletion of MDM4 in retinal ganglion cells enhances axonal regeneration after optic nerve crush.** (A) Schematic of the experimental design showing AAV-Cre or AAV-GFP intra-vitreous infection of RGC in MDM4<sup>fl/fl</sup> mice 14 days before optic nerve crush. Regenerating axons were traced with CtB. (B) High magnification images of regenerating CtB labelled optic nerve axons 28 days post-crush (asterisk) in MDM4<sup>fl/fl</sup> mice after infection with AAV-Cre or AAV-GFP. Scale bar = 100 μm. (C) Quantification of regenerating optic nerve axons post-crush (shown in B). At least four serial sections were analysed from each animal (Student t-test with ANOVA, \**P* < 0.05 or \*\**P* < 0.01 *n* = 7, each group). (D) Anti-Tuj1 immunofluorescence shows surviving retinal ganglion cells (Tuj1 +) 28 days post-optic nerve crush. Scale bar = 50 μm. (E) Quantification of surviving RGCs as total percentage of surviving cells as compared to the intact contralateral retina (*n* = 7, AAV-Cre infected animals; *n* = 6, AAV-GFP infected animals). (F) Representative images of CtB labelled optic nerve axons from MDM4<sup>fl/fl</sup>/P53<sup>fl/fl</sup> mice infected with AAV-CreGFP/AAV-GFP. No regenerating axons were observed past the lesion site (asterisk). Scale bar = 100 μm. (G) Quantification of CtB-labelled axons regenerating past the lesion site. At least four serial sections were analysed from each animal (Student t-test with ANOVA, *n* = 5, AAV-CreGFP group, *n* = 4, AAV-GFP).

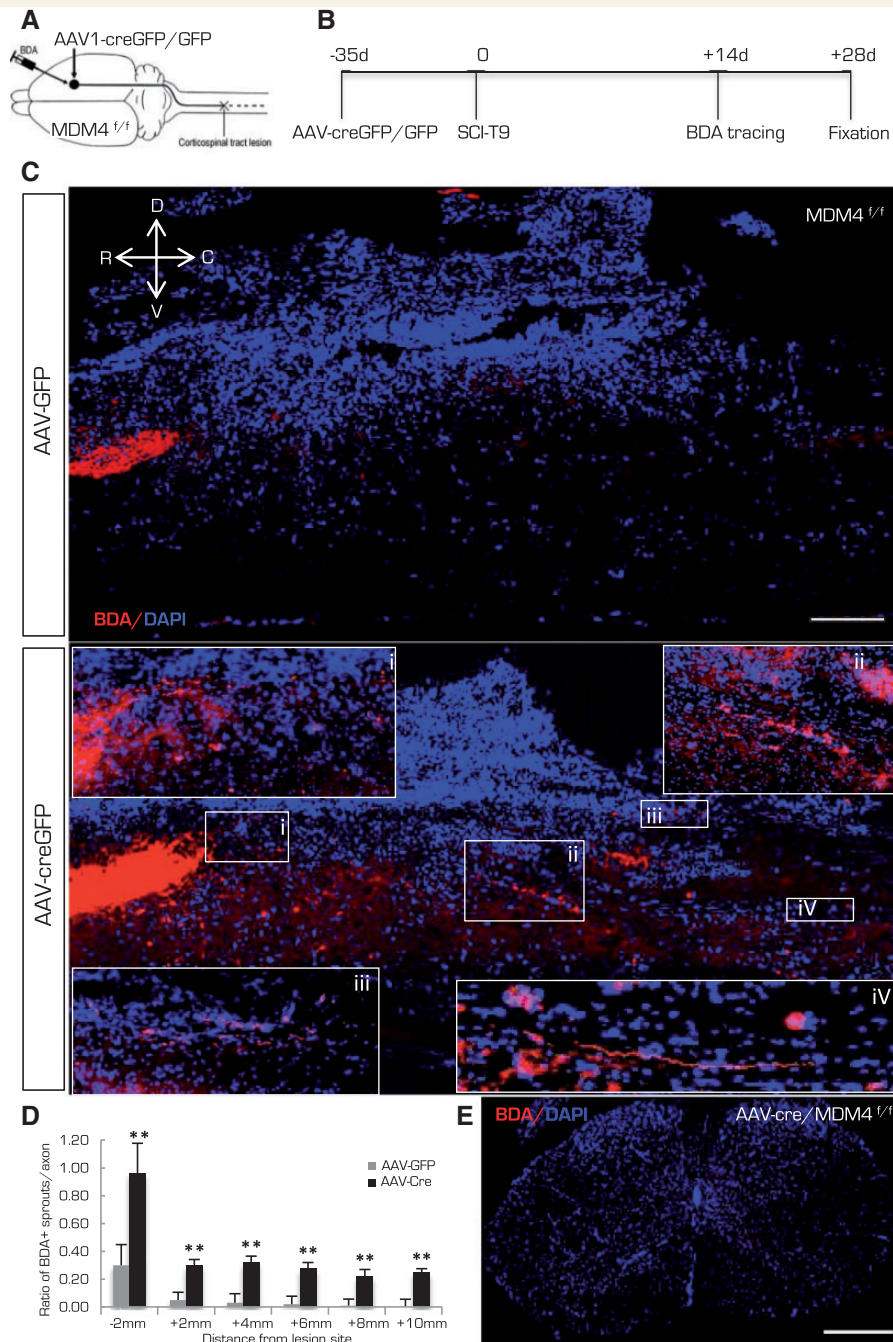


**Figure 2** Conditional deletion of MDM4 in the sensorimotor cortex enhances corticospinal tract sprouting following T9 dorsal hemisection in MDM4<sup>fl/fl</sup> mice. (A and B) Schematic diagrams summarizing the experimental design. AAV-CreGFP/AAV-GFP particles were injected in the sensorimotor cortex of adult MDM4<sup>fl/fl</sup> mice 5 weeks before T9 dorsal hemisection. BDA for corticospinal tract labelling was injected 14 days before sacrificing the animal. (C) Representative images of sagittal sections from MDM4<sup>fl/fl</sup> mice after cortical AAV-GFP/AAV-CreGFP infection. The corticospinal tract was traced by BDA injection (red) in the cortex. Spinal cord sections were also stained with DAPI (blue). High magnification images (insets) show the sprouting axons past the lesion site, in the AAV-CreGFP infected mice. Scale bar = 500  $\mu$ m. (D) Quantification of the BDA-labelled sprouting corticospinal tract in the spinal cord rostral and distal to the lesion site. (Mann Whitney test, \*\* $P < 0.001$ ,  $n = 10$  for AAV-GFP and  $n = 9$  for AAV-CreGFP, number of cords analysed). (E) Coronal section of a spinal cord 15 mm caudal to the lesion site showing completeness of the lesion with lack of BDA positive corticospinal tract labelling after AAV-cre infection in the sensorimotor cortex of MDM4<sup>fl/fl</sup> mice (5 weeks post-spinal cord injury). Scale bar = 500  $\mu$ m.

retinal cells determined by semi-quantitative PCR confirmed MDM4 deletion (Supplementary Fig. 3C). Significantly, MDM4 deletion promoted axonal regeneration of the optic nerve as measured 28 days after optic

nerve crush (Fig. 1); however, it did not affect RGC survival (Fig. 1).

To confirm the generalization of this regenerative phenotype to another clinically relevant CNS fibre tract, we

investigated whether MDM4 conditional deletion may enhance axonal sprouting and regeneration of the corticospinal tract after spinal cord injury. To this end, we performed AAV1-cre-mediated MDM4 conditional deletion in the sensorimotor cortex of MDM4<sup>fl/fl</sup> mice (Fig. 2A and Supplementary Fig. 4A and B) and subsequently performed a spinal thoracic T9 dorsal hemisection, which severs the corticospinal tract in mice. An AAV1-GFP virus was again used as a control. It is important to note that GFP was found highly expressed in the sensorimotor cortex including in layer V neurons (Supplementary Fig. 4C). In line with the data from the optic nerve, we found significant axonal sprouting and regeneration after MDM4 conditional deletion while control-infected mice displayed the typical collapse of the corticospinal tract before reaching the lesion site (Fig. 2C and D and Supplementary Fig. 5). Lack of BDA tracing below the lesion site allowed exclusion of the presence of spared corticospinal tract fibres (Fig. 2E).

In support of the specificity of the *in vivo* axonal regeneration findings, we investigated neurite outgrowth in cultured RGCs and cerebellar granule neurons on both outgrowth permissive and myelin inhibitory conditions. AV-cre or AV-GFP control viruses were employed to infect RGCs or cerebellar granule neuron at the time of plating on poly-D-lysine or myelin and neurite outgrowth was analysed at 72 h and 24 h, respectively. Results showed that MDM4 deletion enhances neurite outgrowth in both RGCs and cerebellar granule neurons on both permissive and inhibitory substrates (Supplementary Fig. 6).

Together, these data suggest that MDM4 conditional deletion significantly lifts the CNS regenerative block thus enhancing axonal regeneration and sprouting after optic nerve and spinal injury in sensory and motor neurons.

#### MDM4 conditional deletion enhances optic nerve regeneration via p53 and is phenocopied by inhibition of the MDM2/p53 interaction

To gain mechanistic insight into the regenerative phenotype observed with MDM4 conditional deletion, we investigated the role of the MDM4 associated proteins, p53 and MDM2. MDM4 typically keeps p53 transactivation under check (Marine and Jochemsen, 2005), as supported by our findings in primary neurons where conditional deletion of MDM4 (Supplementary Fig. 7A) enhances p53-dependent gene targets, including axon growth associated genes (Supplementary Fig. 7B). Therefore, we hypothesized that MDM4 deletion could enhance the regeneration program via p53 transactivation. To this end, we investigated whether double conditional deletion of MDM4 and p53 would block the regenerative phenotype observed with MDM4 deletion. We performed AAV2-cre conditional deletion of MDM4 and p53 in RGCs simultaneously in double MDM4<sup>fl/fl</sup>/p53<sup>fl/fl</sup> mice (Fig. 1) and found that this abolished axonal regeneration induced by MDM4 deletion

alone as the number of axons past the crush site were now similar to AAV2-GFP control infected mice (Fig. 1). This demonstrates that p53 is required for MDM4-dependent axonal regeneration. Next, we further explored the central role of ubiquitin ligase related signalling in this regenerative paradigm. Thus, we asked whether modulation of the MDM4 binding protein and ubiquitin ligase MDM2, also expressed in RGCs (Supplementary Fig. 2E and F), would be phenocopying axonal regeneration as seen upon deletion of MDM4. Given that MDM2 controls p53 protein levels by ubiquitination and proteasome degradation, we inhibited MDM2/p53 interaction by intravitreal injection of the well-characterized small molecule MDM2/p53 antagonist Nutlin-3a (Vassilev *et al.*, 2004). Importantly, Nutlin-3a (100 nM) delivery at the time of optic nerve crush and 7 days later (Fig. 3A) promoted axonal regeneration of the optic nerve to a similar extent as MDM4 deletion without affecting the survival of RGCs 28 days after crush (Fig. 3B, C, E and F). Administration of Nutlin-3a enhanced p53 protein levels in the retina as expected (Fig. 3G). To investigate by a genetic approach whether MDM2/p53 inhibition promotes axonal regeneration specifically via p53, we performed an analogous set of Nutlin-3a experiments, but in p53<sup>-/+</sup> mice that typically retain only 25% of p53 expression; however, do not display aberrant cell metabolism as opposed to p53<sup>-/-</sup> mice (Boehme and Blattner, 2009). This would also address whether a ‘minimum’ threshold p53 expression level is required for axonal regeneration similar to the p53 dosage effect found in cancer (Boehme and Blattner, 2009). Data analysis revealed that axonal regeneration of the optic nerve after crush was significantly reduced in Nutlin-3a p53<sup>-/+</sup> mice as compared to wild-type (Fig. 3B and D), further supporting the overall model that the observed regeneration after either deletion of MDM4 or inhibition of MDM2 is dependent upon p53 transactivation. Indeed, Nutlin-3a delivery in primary neurons enhanced p53 transactivation as shown by quantitative RT-PCR (Supplementary Fig. 8A), without promoting apoptosis (Supplementary Fig. 8B). Genes included as p53-target were previously identified as predicted (promoter analysis correlating with gene expression following p53 modulation) or fully experimentally confirmed p53 targets (including with chromatin immunoprecipitation assays) (Tedeschi *et al.*, 2009; Gaub *et al.*, 2011).

#### Optic nerve axonal regeneration after conditional MDM4 deletion relies upon the IGF1R pathway

The data thus far point to a model where disruption of the MDM4-MDM2/p53 inhibitory protein complex triggers axonal regeneration after optic nerve crush. To explore directly *in vivo* in RGCs whether disruption of this complex via MDM4 deletion would affect the gene expression program supporting the regenerative phenotype, we





performed Affymetrix-based genome wide gene expression arrays from FACS isolated RGCs after optic nerve crush. DiI-positive retrogradely traced RGCs were sorted 3 days following optic nerve crush from MDM4<sup>fl/fl</sup> mice that underwent either AAV2-creGFP or AAV2-GFP control intravitreal injections (Fig. 4A and B). Functional data analysis of statistically significant differentially regulated transcripts was performed with the Ingenuity pathway analysis platform. Unsupervised hierarchical clustering of the gene expression data showed a clear separation of the gene expression profiles between AAV2-cre and AAV2-GFP cells (Fig. 4C). Additionally, Ingenuity pathway analysis revealed that conditional MDM4 deletion was associated with a number of receptor-dependent signalling cascades involved in cell growth and metabolism (Fig. 4D, Table 1, and Supplementary Tables 1 and 2). Highly ranked differentially regulated pathways were p53 and the related GADD45 cascades (Fig. 4D and Supplementary Table 2), supporting our model. Of special interest was the MDM4-deletion dependent activation of insulin and insulin receptor signalling pathways via overexpression of IGF1R, as insulin-dependent pathways have a key role in cell growth and are highly neurotrophic. Careful analysis of IGF1R protein expression in RGCs revealed that in most cells where MDM4 deletion occurred, IGF1R levels were particularly elevated, whereas in control AAV-GFP positive RGCs, IGF1R was lower (Fig. 6E). Next, we asked whether the IGF1R pathway might be critical for the downstream regenerative signalling elicited by conditional deletion of MDM4. Therefore, we decided to inhibit IGF1R signalling after MDM4 deletion and optic nerve crush. We chose to use picropodophyllin, a highly selective and potent inhibitor of IGF1R (IC<sub>50</sub> = 6 nM) that efficiently blocks IGF1R activity and expression *in vivo* without noticeable toxicity. In preparation for the *in vivo* experiment, we performed a dose response analysis of picropodophyllin in primary neurons in permissive growth conditions and monitored toxicity (active cleaved caspase 3-positive neurons) and neurite outgrowth. This allowed identifying a dose between 10 nM and 1 µM that efficiently inhibited neuronal outgrowth without resulting in significant toxicity (Supplementary Fig. 9A and B). After AAV2-cre MDM4 conditional deletion in RGCs of MDM4<sup>fl/fl</sup> mice (Fig. 5A), picropodophyllin 1 µM was delivered both intravitreal and at the site of the nerve crush at the time of optic nerve crush and optic nerve regeneration was evaluated at 28 days post-injury. Indeed, picropodophyllin delivery strongly reduced the expression of IGF1R (Fig. 5B) and drastically inhibited optic nerve regeneration induced by MDM4 deletion, without affecting RGC survival (Fig. 5C–F).

In line with IGF1R loss of function, overexpression of IGF1 in the eye (Fig. 6A and B) led to enhanced axonal regeneration (Fig. 6C and D), whereas it did not affect RGC survival (Fig. 6E and F). Together, these data support

a role for IGF1 signalling in axonal regeneration downstream of MDM4.

## Pharmacological modulation of MDM2/p53/IGF1R axis enhances axonal sprouting and functional recovery after spinal cord injury

Next, we decided to investigate whether pharmacological modulation of the MDM2/p53/IGF1R axis would enhance axonal sprouting and functional recovery after spinal cord injury. To this end, we continuously delivered intrathecally the small molecule Nutlin-3 via an osmotic minipump at the time of spinal cord injury in proximity of the injury site (T9 dorsal hemisection) for 14 days and performed locomotor behavioural tests for 5 weeks post-injury. Importantly, Nutlin-3 triggered the expression of active p53 and of the well-characterized p53 target gene p21 (now known as *CDKN1A*), while it did not enhance active caspase 3, suggesting lack of Nutlin-3 dependent cell death (Supplementary Fig. 10). After sacrifice, we measured axonal regeneration and sprouting of supraspinal descending fibres including the BDA labelled corticospinal tract and the 5-HT raphe-spinal projections, whose sprouting highly correlates with locomotor recovery (Trakhtenberg and Goldberg, 2012). Indeed Nutlin-3 delivery induced significant functional recovery as compared to vehicle as measured by open field Basso Mouse Scale scores and subscores as well as by assessing locomotion ability on a Gridwalk (Fig. 7 and Supplementary Videos 1 and 2). This was paralleled by enhancement in corticospinal tract sprouting (Fig. 7 and Supplementary Fig. 11) and most remarkably in 5-HT fibre sprouting below the lesion site (Fig. 8). No spared fibres below the lesion were found in all the cords included in the analysis. Finally, inhibition of IGF1R signalling via intraperitoneal delivery of picropodophyllin together with Nutlin-3 mini-pump administration strongly reduced sprouting of 5-HT tracts (Fig. 8) as well as Nutlin-3 dependent functional recovery (Fig. 8). Together these data support a novel role for MDM2/p53/IGF1 axis in axonal sprouting and functional recovery after spinal cord injury.

## Discussion

The reasons underlying the lack of a neuronal intrinsic regenerative potential after CNS axonal injury seem to be found in an inhibitory molecular network, which either exists prior to axonal injury or is elicited by it. The present work defines MDM4-MDM2/p53 as a protein complex restricting axonal sprouting and regeneration, whose disruption activates p53 and the axonal regenerative program via IGF1 signalling. Although the effect of MDM4 deletion upon functional recovery after spinal cord injury has not been tested, inhibition of MDM2/p53 interaction led to

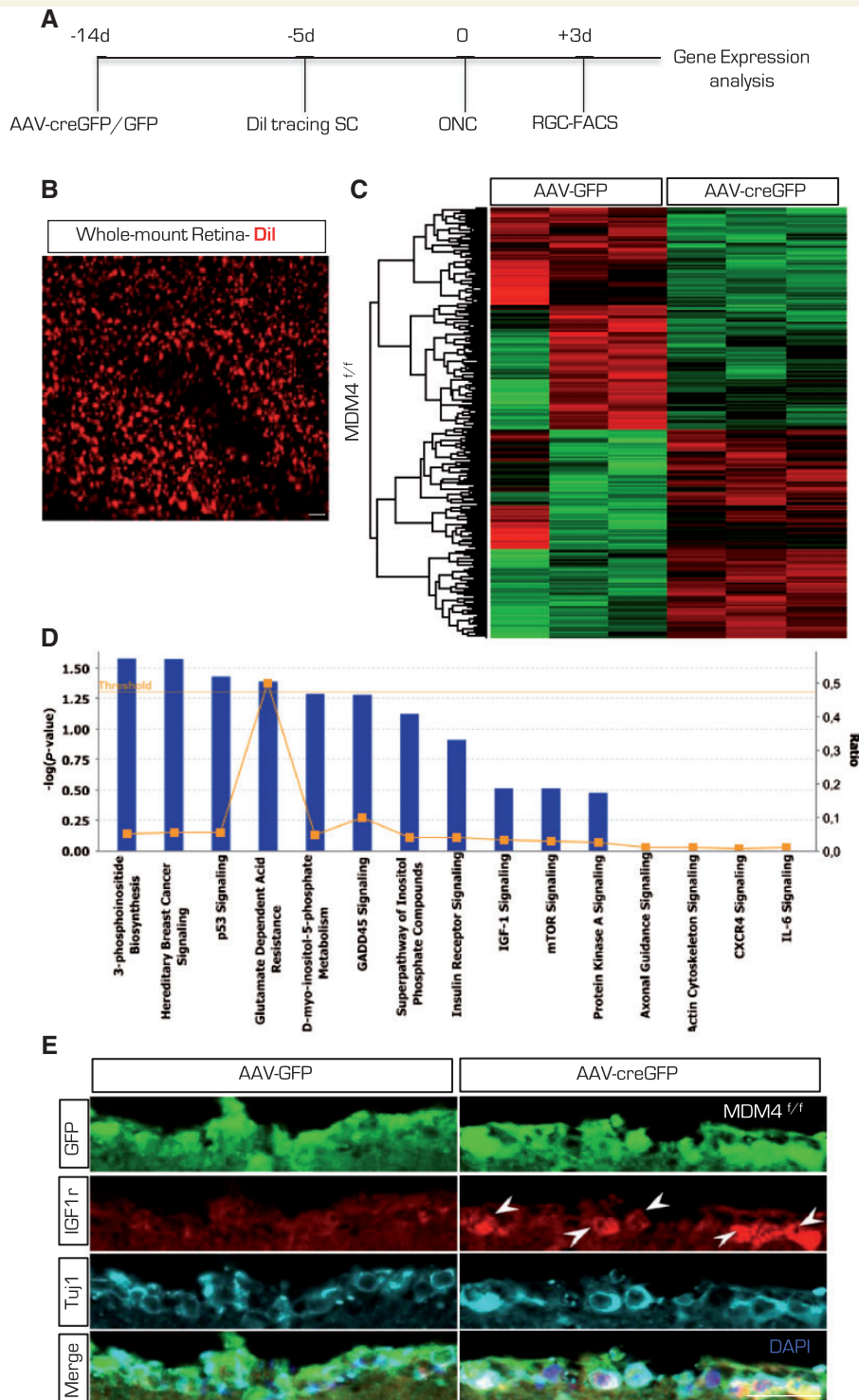


**Figure 4** Genome-wide gene expression analysis in RGCs after conditional MDM4 deletion and sorting by FACS. **(A)** Schematic of the experimental design. MDM4<sup>ff</sup> animals were infected with AAV-CreGFP/AAV-GFP 14 days before the optic nerve crush. Dil was injected in the superior colliculus 7 days before crushing the optic nerve. Dil<sup>+</sup> RGCs were sorted by FACS 3 days following optic nerve crush, and RNA extracted from these samples were used to perform gene expression analysis (Affymetrix). **(B)** Whole mount retina showing highly efficient Dil tracing in the RGC layer. Scale bar = 20  $\mu$ m. **(C)** Heatmap showing clear-cut separation of gene expression levels (green: low; red: high) between AAV-GFP and AAV-creGFP infected RGCs. **(D)** Differentially regulated signalling pathways upregulated in MDM4-deleted RGCs analysed with Ingenuity Pathways Analysis (IPA). These include p53, Gadd45 and IGF1-IGFR signalling pathways. Blue bars represent the relative representation of genes in each pathway. Lack of blue bar shows poorly represented pathways.  $y$ -axis:  $P$ -value: significant below threshold (dotted yellow line). **(E)** Immunofluorescence micrographs showing high IGF1R expression level 3 days after optic nerve crush in retinal ganglion cells (Tuj1<sup>+</sup>) infected with AAV-CreGFP, whereas a faint signal was observed in AAV-GFP + RGCs in MDM4<sup>ff</sup> mice. Retinal ganglion cells are counterstained with Tuj1. Scale bar = 20  $\mu$ m. Arrowheads indicate IGF1r positive cells.

**Table 1** List of selected differentially regulated genes from RGCs after optic nerve crush in MDM4<sup>fl/fl</sup> mice- AAV Cre versus GFP.

Functional class	Fold change (Cre versus GFP)	P-value	Function
<b>Axonal signalling</b>			
IGF1R	2.12	0.0122	Intracellular signalling
CXCR2	2.18	0.0222	Chemoattraction
Klf11	1.764	0.0391	Axonal transport
Cited4	1.69	0.0324	Transcription co-activator
Sprr2b	1.866	0.004	Axon growth
<b>Neuronal morphology and cytoskeleton organization</b>			
DCC	-2.031	0.0476	Axon guidance
GAD1	1.569	0.0365	Glutamate/GABA metabolism
Arf1	3.505	0.02	GTP-bind protein
FCER1A	1.71	0.018	IgE rec
NKX2-2	-1.66	0.014	NeuroD1-cofactor
Nrg1	-1.84	0.006	Neuronal differentiation
Rab23	1.516	0.01	GTPase
Rin2	1.797	0.029	GTPase
Mast3	-1.797	0.043	Microtubule associated kinase
<b>Neuronal development</b>			
GAD1	1.569	0.0365	Glutamate/GABA metabolism
CAMKK2	1.595	0.004	CREB activator
ZIC1	1.632	0.0385	Transcription Activity-Neurogenesis
ZNF423	1.762	0.0226	Smad coactivation-Neurogenesis
LYNX1	2.222	0.0004	Synaptic plasticity
ST8SIA2	1.683	0.02704	NCAM1 binding protein-receptor
DCC	-2.031	0.0476	Axon guidance

significant functional recovery after spinal injury. Therefore, the discovery of the MDM4-MDM2/p53-IGF1 axis clarifies a cause for failed regeneration and provides a target for regenerative therapy after nerve and spinal injury.

MDM4 was first identified as a p53 binding protein in selected cancers where it inhibits p53 transcriptional activity thus promoting tumour progression (Markey, 2011). Similarly, MDM4 regulates cell cycle, survival and apoptosis by forming an inhibitory complex with a selected set of proteins that include MDM2, ASPP1, ASPP2, p300, SMAD1 and SMAD2 (Sabbatini and McCormick, 2002; Wade *et al.*, 2010; Gaub *et al.*, 2011). However, a role for MDM4 and MDM2 in axonal regrowth has, until now, been missing. Here, we show that conditional deletion of MDM4 enhances axonal regeneration and sprouting after optic nerve crush and spinal cord injury, respectively and co-deletion of p53 significantly diminishes the MDM4-deletion dependent regenerative phenotype, while inhibition of MDM2/p53 interaction mimics it. Moreover, pharmacological small molecule mediated disruption of the MDM2/p53 complex enhances axonal sprouting of long spinal descending tracts and promotes significant neurological recovery after spinal cord injury.

We have recently shown that the tumour suppressor and transcription factor p53 is required for neurite outgrowth, axonal sprouting and regeneration both after facial nerve injury and spinal cord hemisection in mice (Di

Giovanni *et al.*, 2006; Tedeschi and Di Giovanni, 2009; Tedeschi *et al.*, 2009a, b; Floriddia *et al.*, 2012). Specifically, transcriptionally active acetylated p53 at K372-3-82 and the acetyltransferases CBP/p300 and P/CAF form a transcriptional complex that occupies promoters of selected pro-regenerative genes, driving neurite outgrowth (Di Giovanni *et al.*, 2006; Tedeschi *et al.*, 2009). p53 integrates numerous stress signals including following axonal injury and it undergoes tight regulation of its protein levels, subcellular localization and of its transcriptional activity by several factors, including the well-defined negatively regulators MDM2 and MDM4 (Lavin and Gueven, 2006). MDM2, an E3 ubiquitin ligase, targets p53 for degradation via the ubiquitin proteasome pathway and negatively regulates p53 cytoplasmic-nuclear shuttling (Toledo and Wahl, 2007). MDM4, although structurally similar to MDM2, is devoid of ubiquitin ligase activity, and rather regulates with MDM2 p53 cytoplasmic-nuclear shuttling and it occupies the p53 transcriptional activation domain thereby inhibiting p53 transactivation (Toledo and Wahl, 2007). MDM4 prevents p53 nuclear translocation in association with MDM2 and competes with the acetyltransferases CBP and p300 for binding to lysines on p53 C-terminus, overall hindering p53 transcriptional activity.

Given the pro-neurite outgrowth and axon regeneration function of the MDM4 interacting proteins p300 and



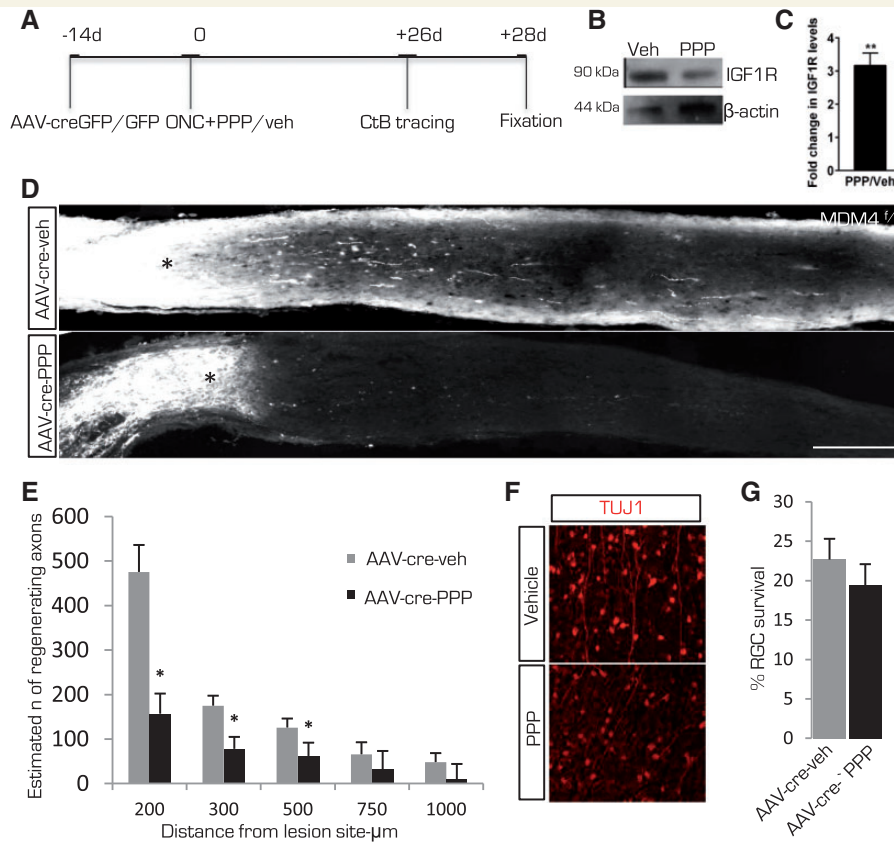


**Figure 5 Regeneration elicited by MDM4 deletion is reduced by inhibition of IGF1R signalling.** (A) Schematic of the experimental design. Conditional MDM4 deletion in MDM4<sup>fl/fl</sup> mice was followed by optic nerve crush and pharmacological inhibition of IGF1R with the antagonist picropodophyllin (PPP). Axonal tracing was performed with CtB. (B) Immunoblotting from retinas 3 days after optic nerve crush and administration of picropodophyllin or vehicle. Shown is a strong reduction in the expression of IGF1R. (C) Bar graphs show densitometry analysis (arbitrary units) expressed as fold change of picropodophyllin versus vehicle ( $n = 3$ ). Student's unpaired two-tailed  $t$ -test  $**P < 0.01$ . (D) Representative images of optic nerves showing regenerating CtB-labelled axons of MDM4<sup>fl/fl</sup> animals after MDM4 conditional deletion and vehicle. Not a significant number of regenerating axons were found after picropodophyllin administration post-optic nerve crush (asterix). Scale bar = 100  $\mu\text{m}$ . (E) Quantification of regenerating optic nerve axons post-crush (shown in D). At least four serial sections were analysed from each animal (Student  $t$ -test with ANOVA,  $P < 0.05$  for each distance,  $n = 6$ , each group). The number of regenerating axons was significantly hampered following AAV-cre-PPP treatment versus AAV-cre-veh. (F) Anti-Tuj1 immunofluorescence shows surviving retinal ganglion cells (Tuj1 +) 28 days post-optic nerve crush. Scale bar = 50  $\mu\text{m}$ . (G) Quantification of surviving RGC as total percentage of surviving cells as compared to the intact contralateral retina ( $n = 6$ ).

Smads (Zou *et al.*, 2009; Gaub *et al.*, 2011; Parikh *et al.*, 2011), it is plausible that p300-dependent acetylation of regenerative promoters as well as TGF $\beta$ -Smad signalling may also contribute to axonal regeneration induced by MDM4 deletion. In support of this, we have recently shown that p300 acetylates p53 in RGCs after optic nerve crush during p300-dependent axonal regeneration, supporting the presence of this signalling network during axonal regeneration (Gaub *et al.*, 2011). Given the axon regenerative/sprouting function of p21 (Tanaka *et al.*, 2004), the previously described inhibitory MDM4 protein complex with p21 (Markey, 2011), which is also a classical p53-target gene, may also play a role in axonal regeneration. Interestingly, we found that MDM4 deletion in primary neurons enhanced p21 gene expression levels along with other classical regeneration

associated genes, supporting the inhibitory role for MDM4 in repressing the regenerative gene expression program.

An extranuclear and non-transcriptional role for p53 in growth cone remodelling and axonal outgrowth has also been described. For example, inhibition of p53 phosphorylation causes growth cone collapse in primary neurons via RhoA kinase activation (Qin *et al.*, 2009). Additionally, when active phosphorylated p53 is truncated by calpain activity following semaphorin 3A-induced growth cone collapse, it results in cytoskeleton reorganization by activating Rho Kinase (ROCK), therefore enhancing growth cone retraction (Qin *et al.*, 2010). This highlights how inhibition of MDM2 and MDM4 may also promote axonal outgrowth via p53 localization and activation in axons and at the growth cone.



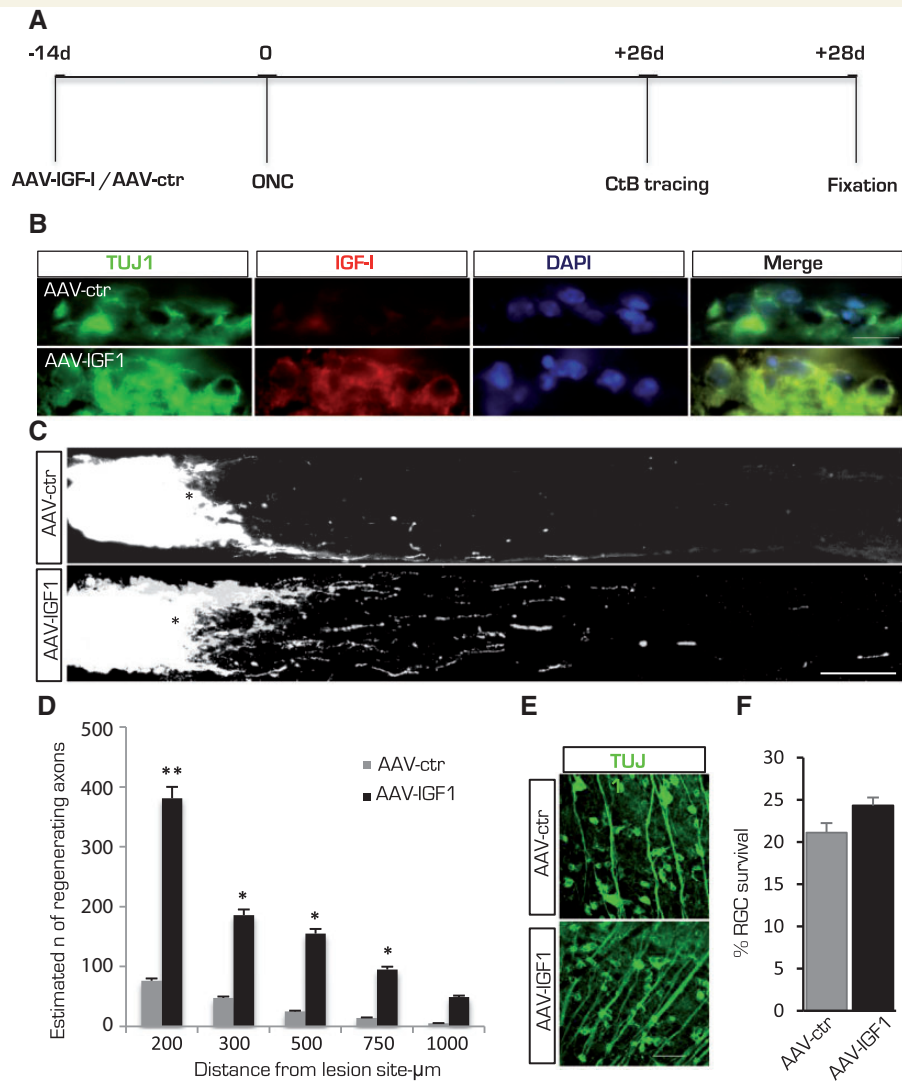


**Figure 6 Overexpression of IGF1 promotes axonal regeneration after optic nerve crush.** (A) Schematic of the experimental design showing AAV-IGF1 or AAV-ctr intra-vitreous infection of RGCs in mice 14 days before optic nerve crush. Regenerating axons were traced with CtB. (B) Immunofluorescence micrographs showing high IGF1 expression level 3 days after optic nerve crush in retinal ganglion cells (Tuj1<sup>+</sup>) infected with AAV-IGF1, while a faint signal was observed in AAV-ctr infected RGCs. RGCs were counterstained with Tuj1. Scale bar = 20 μm. (C) High magnification images of regenerating CtB labelled optic nerve axons 28 days post-crush (asterisk) in MDM4<sup>fl/fl</sup> mice after infection with AAV-IGF1 or AAV-GFP. Scale bar = 100 μm. (D) Quantification of regenerating optic nerve axons post-crush (shown in C). At least four serial sections were analysed from each animal (Student *t*-test with ANOVA, \**P* < 0.05 or \*\**P* < 0.01 *n* = 7, each group). (E) Anti-Tuj1 immunofluorescence shows surviving retinal ganglion cells (Tuj1<sup>+</sup>) 28 days post-optic nerve crush. Scale bar = 50 μm. (F) Quantification of surviving RGCs as total percentage of surviving cells as compared to the intact contralateral retina (*n* = 5, AAV-IGF1 infected animals; *n* = 4, AAV-ctr infected animals).

Further, genome-wide analysis from FACS sorted RGCs after optic nerve crush revealed that MDM4 conditional deletion was associated with the enhancement of transcripts involved in cytoskeleton remodelling, axonal development and signalling, including genes involved in neuronal maturation (Table 1). This pattern of gene expression changes suggests that MDM4 deletion modulates developmentally regulated pathways, which may support axonal regrowth.

Additionally, here we show that IGF1R signalling is required for axonal regeneration of the crushed optic

nerve induced by MDM4 deletion and it is likely downstream of the transcriptional complex formed by MDM4-p53/MDM2. The best-characterized IGF1R targets include PI3K and JAK/STAT3, which are typically activated by IGF1R (Staerk *et al.*, 2005; Serra *et al.*, 2007; Subbiah *et al.*, 2011; Kim *et al.*, 2012). Both PI3K and JAK/STAT3 activation depends upon the phosphorylation status that has been shown to be necessary to promote axonal regeneration following deletion of PTEN or after JAK binding to IL6, respectively (Cao *et al.*, 2006; Shah *et al.*, 2006, Teng and Tang, 2006; Hakkoum *et al.*, 2007;

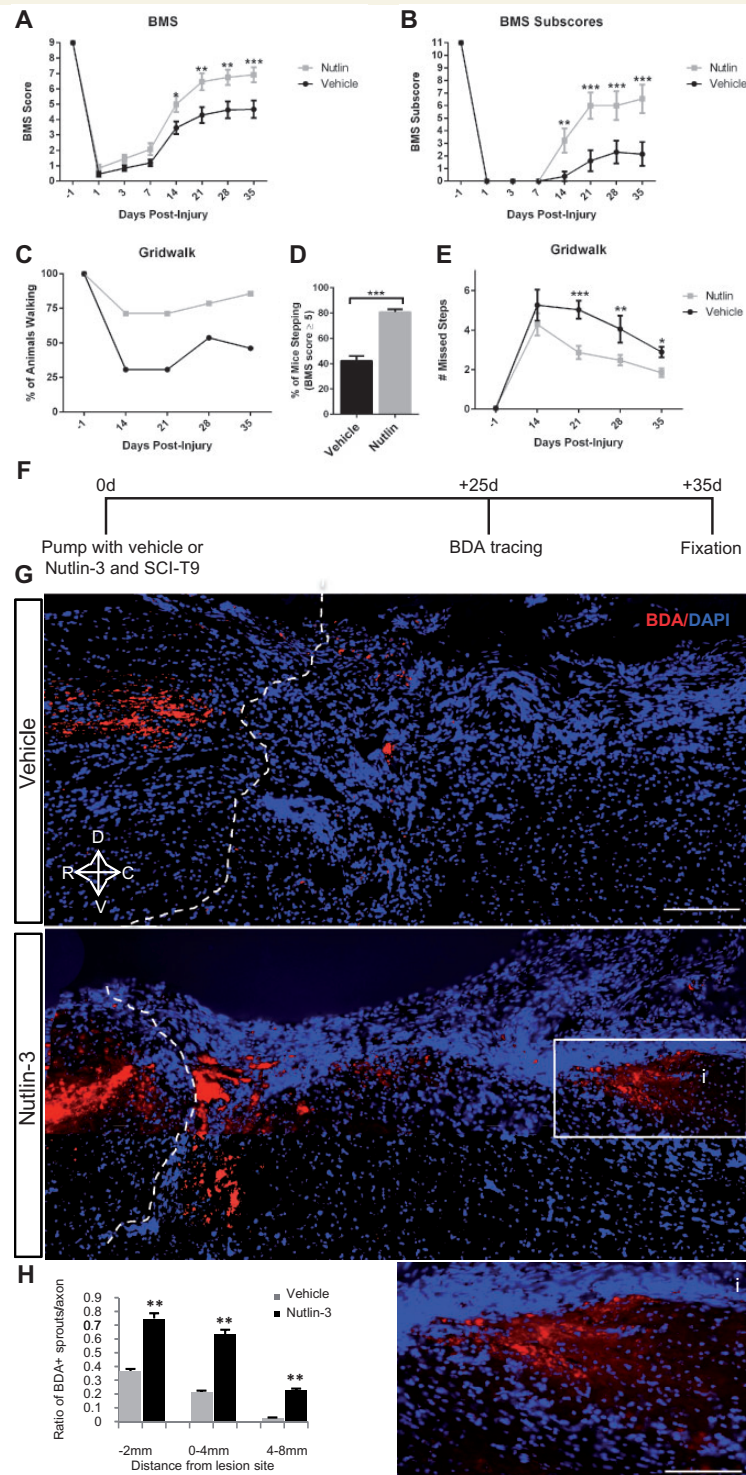


**Figure 7 MDM2/p53 inhibition via Nutlin-3 delivery enhances neurological recovery and corticospinal tract regeneration following T9 dorsal hemisection.** (A) Basso Mouse Scale score and subscore (B) show significant improvement in locomotion in Nutlin-3 treated mice (Nutlin-3 or vehicle) were delivered via osmotic minipump connected to an intrathecal catheter in proximity of a T9 dorsal hemisection for 14 days post-injury). (C) Percentage of mice able to walk on a gridwalk is much higher after Nutlin-3 treatment versus vehicle. (D) Percentage of mice with a Basso Mouse Scale score  $\geq 5$  from 14 days after injury. (E) Number of missteps on a gridwalk is significantly reduced by Nutlin-3 treatment (two-way ANOVA with Sidak's multiple comparisons,  $***P < 0.001$ ;  $**P < 0.01$ ;  $*P < 0.05$ ,  $n = 13$  (vehicle),  $n = 13$  (Nutlin)). (F) Schematic diagram summarizing the experimental design. BDA for corticospinal tract labelling was injected 10 days before sacrifice. SCI = spinal cord injury. (G) Representative images of sagittal cord sections of mice treated with Nutlin-3 or vehicle. The corticospinal tracts were traced by BDA injection (red) in the cortex. Spinal cord sections were also stained with DAPI (blue). Visible are sprouting axons past the lesion site in the Nutlin-3 treated mice. Scale bar = 500  $\mu\text{m}$ . Inset (i) showing sprouting corticospinal tract fibers at higher power. (H) Quantification of the BDA labelled sprouting corticospinal tract axons in the spinal cord rostral and distal to the lesion site. (Mann Whitney test,  $**P < 0.01$   $n = 7$ ).

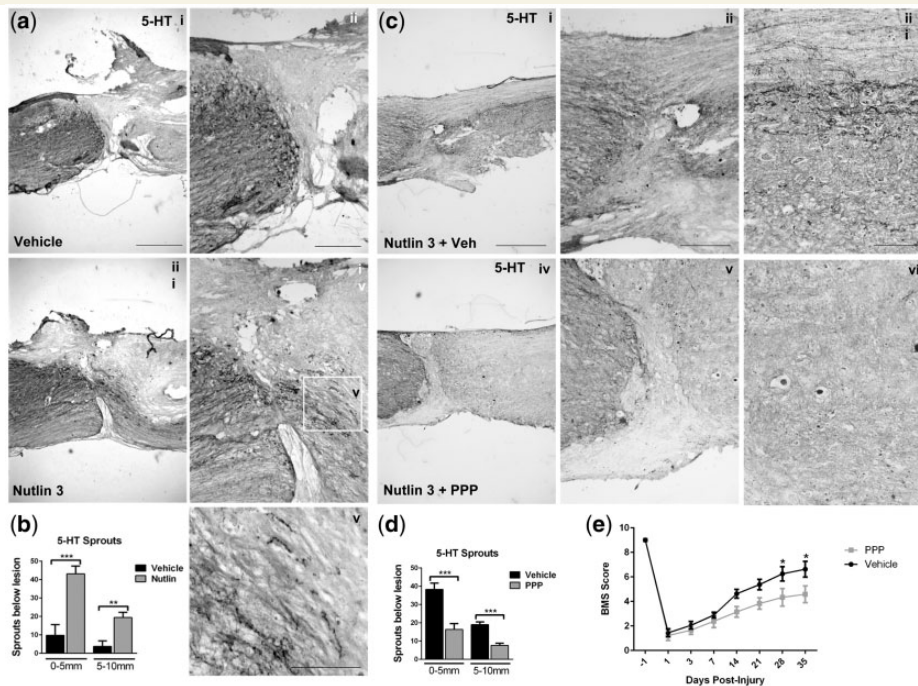


**Figure 8** MDM2/p53 inhibition via Nutlin-3 delivery enhances 5-HT axonal sprouting and functional recovery via IGF1 following T9 dorsal hemisection. (A) Representative images of sagittal cord sections of mice treated with Nutlin-3 or vehicle (Nutlin-3 or vehicle were delivered via osmotic minipump connected to an intrathecal catheter in proximity of a T9 dorsal hemisection for 14 days post-injury). Raphe-spinal fibres were labelled with an anti-5-HT antibody (immunoperoxidase). Visible are parasagittal cord sections with numerous sprouting axons past the lesion site in the Nutlin-3 treated mice (45 days post-injury). (i and iii) Scale bar = 2.5 mm. (ii and iv) Scale bar = 750  $\mu$ m. Inset (v): sprouting fibres at higher power. Scale bar = 50  $\mu$ m. (B) Quantification of the 5-HT-positive fibres in the spinal cord distal to the lesion site. (Unpaired Student's *t*-test, \*\*\**P* < 0.001; \*\**P* < 0.01, *n* = 7). (C) Representative images of sagittal cord sections of mice treated with Nutlin-3 via osmotic mini-pump and intraperitoneal delivery of picropodophyllin (PPP) or vehicle (for 14 days post-spinal injury). Raphe-spinal fibres were labelled with an anti-5-HT antibody (immunoperoxidase). Visible are parasagittal cord sections with numerous sprouting axons past the lesion site in the Nutlin-3 and vehicle treated mice, while only a few are visible after picropodophyllin (35 days post-injury). (i and iv) Scale bar = 2.5 mm; (ii and v) Scale bar = 750  $\mu$ m; (iii and vi) Sprouting fibres at high power. Scale bar = 60  $\mu$ m. (D) Quantification of the 5-HT positive fibres in the spinal cord distal to the lesion site. (unpaired Student's *t*-test, \*\*\**P* < 0.001; \*\**P* < 0.01, *n* = 7). (E) Basso Mouse Scale score shows significant reduction in locomotion performance in Nutlin-3 and picropodophyllin treated mice versus Nutlin-3 and vehicle (two-way ANOVA with Sidak's multiple comparisons, \**P* < 0.05 *n* = 10).

Park *et al.*, 2008). This suggests a likely cross-talk between the MDM4-MDM2/p53-IGF1 signalling and these regenerative pathways, further supporting our findings.

Last but not least, our work shows that MDM2/p53 inhibition via Nutlin-3, a small molecule, significantly enhances axonal sprouting of corticospinal tract and of 5-HT descending fibre tracts as well as functional recovery after spinal cord injury. Importantly, inhibition of IGF1R signalling via picropodophyllin blocks axonal sprouting of the functionally limiting 5-HT tracts as well as Nutlin-3 dependent neurological recovery. This suggests MDM2/p53-IGF1 as a novel regenerative pathway following nerve and spinal injury, including the opportunity of a novel therapeutic target for recovery after spinal trauma.

Given that pharmacological antagonism of MDM2-p53 interaction including with Nutlins have been shown to induce tumour suppression and are currently being explored in the clinic for cancer treatment and have been shown to be safe (Brown *et al.*, 2009), they may represent

viable options for neuroregenerative therapy in the short-term. The recent discovery of specific small molecule inhibitors of MDM4 (Reed *et al.*, 2010; Vogel *et al.*, 2012), which are still awaiting confirmation in multiple studies, may also expand our regenerative therapeutic options.

## Acknowledgements

We are grateful to Marco Benevento for technical support for some of the experiments with neuronal cultures and Anja Wuttke for excellent technical assistance.

## Funding

We would like to thank the Hertie Foundation for financial support (S.D.G.); the DAAD PhD fellowship (M.G.S.); DZNE fellowship (Y.J.); Wings for Life (S.D.G.); ISRT (S.D.G.); the DFG (S.D.G.); the CIN (S.D.G.); CSC



scholarship (L.Z.). Start-up funds-Division of Brain Sciences, Imperial College London (S.D.G.). The research was supported by the National Institute for Health Research (NIHR) Imperial Biomedical Research Centre (S.D.G.). The views expressed are those of the author(s) and not necessarily those of the NHS, the NIHR or the Department of Health.

## Supplementary material

Supplementary material is available at *Brain* online.

## References

- Basso DM, Fisher LC, Anderson AJ, Jakeman LB, McTigue DM, Popovich PG. Basso Mouse Scale for locomotion detects differences in recovery after spinal cord injury in five common mouse strains. *J Neurotrauma* 2006; 23: 635–59.
- Berton O, McClung CA, DiLeone RJ, Krishnan V, Renthal W, Russo SJ, et al. Essential role of bdnf in the mesolimbic dopamine pathway in social defeat stress. *Science* 2006; 311: 864–8.
- Blackmore MG, Wang Z, Lerch JK, Motti D, Zhang YP, Shields CB, et al. Kruppel-like Factor 7 engineered for transcriptional activation promotes axon regeneration in the adult corticospinal tract. *Proc Natl Acad Sci USA* 2012; 109: 7517–22.
- Boehme KA, Blattner C. Regulation of p53—insights into a complex process. *Crit Rev Biochem Mol Biol* 2009; 44: 367–92.
- Bradke F, Fawcett JW, Spira ME. Assembly of a new growth cone after axotomy: the precursor to axon regeneration. *Nat Rev Neurosci* 2012; 13: 183–93.
- Brown CJ, Lain S, Verma CS, Fersht AR, Lane DP. Awakening guardian angels: drugging the p53 pathway. *Nat Rev Cancer* 2009; 9: 862–73.
- Cao Z, Gao Y, Bryson JB, Hou J, Chaudhry N, Siddiq M, et al. The cytokine interleukin-6 is sufficient but not necessary to mimic the peripheral conditioning lesion effect on axonal growth. *J Neurosci* 2006; 26: 5565–73.
- Di Giovanni S, Knights CD, Rao M, Yakovlev A, Beers J, Catania J, et al. The tumor suppressor protein p53 is required for neurite outgrowth and axon regeneration. *EMBO J* 2006; 25: 4084–96.
- Erturk A, Hellal F, Enes J, Bradke F. Disorganized microtubules underlie the formation of retraction bulbs and the failure of axonal regeneration. *J Neurosci* 2007; 27: 9169–80.
- Floriddia EM, Rathore KI, Tedeschi A, Quadrato G, Wuttke A, Lueckmann JM, et al. p53 Regulates the neuronal intrinsic and extrinsic responses affecting the recovery of motor function following spinal cord injury. *J Neurosci* 2012; 32: 13956–70.
- Gaub P, Joshi Y, Wuttke A, Naumann U, Schnichels S, Heiduschka P, et al. The histone acetyltransferase p300 promotes intrinsic axonal regeneration. *Brain* 2011; 134(Pt 7): 2134–48.
- Gaub P, Tedeschi A, Puttagunta R, Nguyen T, Schmandke A, Di Giovanni S. HDAC inhibition promotes neuronal outgrowth and counteracts growth cone collapse through CBP/p300 and P/CAF-dependent p53 acetylation. *Cell Death Differ* 2010; 17: 1392–408.
- Giovanni SD. Molecular targets for axon regeneration: focus on the intrinsic pathways. *Expert Opin Ther Targets* 2009; 13: 1387–98.
- Grieger JC, Choi VW, Samulski RJ. Production and characterization of adeno-associated viral vectors. *Nat Protocols* 2006; 1: 1412–28.
- Grier JD, Xiong S, Elizondo-Fraire AC, Parant JM, Lozano G. Tissue-specific differences of p53 inhibition by Mdm2 and Mdm4. *Mol Cell Biol* 2006; 26: 192–8.
- Hakkoum D, Stoppini L, Muller D. Interleukin-6 promotes sprouting and functional recovery in lesioned organotypic hippocampal slice cultures. *J Neurochem* 2007; 100: 747–57.
- Hill CE, Proschel C, Noble M, Mayer-Proschel M, Gensel JC, Beattie MS, et al. Acute transplantation of glial-restricted precursor cells into spinal cord contusion injuries: survival, differentiation, and effects on lesion environment and axonal regeneration. *Exp Neurol* 2004; 190: 289–310.
- Jensen LJ, Kuhn M, Stark M, Chaffron S, Creevey C, Muller J, et al. STRING 8—a global view on proteins and their functional interactions in 630 organisms. *Nucleic Acids Res* 2009; 37: D412–6.
- Joosten EA, Bar DP. Axon guidance of outgrowing corticospinal fibres in the rat. *J Anat* 1999; 194 (Pt 1): 15–32.
- Kadokia M, Brown TL, McGorry MM, Berberich SJ. MdmX inhibits Smad transactivation. *Oncogene* 2002; 21: 8776–85.
- Kim JG, Kang MJ, Yoon YK, Kim HP, Park J, Song SH, et al. Heterodimerization of glycosylated insulin-like growth factor-1 receptors and insulin receptors in cancer cells sensitive to anti-IGF1R antibody. *PLoS One* 2012; 7: e33322.
- Lavin MF, Gueven N. The complexity of p53 stabilization and activation. *Cell Death Differ* 2006; 13: 941–50.
- Leon S, Yin Y, Nguyen J, Irwin N, Benowitz LI. Lens injury stimulates axon regeneration in the mature rat optic nerve. *J Neurosci* 2000; 20: 4615–26.
- Liu K, Lu Y, Lee JK, Samara R, Willenberg R, Sears-Kraxberger I, et al. PTEN deletion enhances the regenerative ability of adult corticospinal neurons. *Nat Neurosci* 2010; 13: 1075–81.
- Marine JC, Jochemsen AG. Mdmx as an essential regulator of p53 activity. *Biochem Biophys Res Commun* 2005; 331: 750–60.
- Markey MP. Regulation of MDM4. *Front Biosci* 2011; 16: 1144–56.
- Moore DL, Blackmore MG, Hu Y, Kaestner KH, Bixby JL, Lemmon VP, et al. KLF family members regulate intrinsic axon regeneration ability. *Science* 2009; 326: 298–301.
- Parikh P, Hao Y, Hosseinkhani M, Patil SB, Huntley GW, Tessier-Lavigne M, et al. Regeneration of axons in injured spinal cord by activation of bone morphogenetic protein/Smad1 signaling pathway in adult neurons. *Proc Natl Acad Sci USA* 2011; 108: E99–107.
- Park KK, Liu K, Hu Y, Smith PD, Wang C, Cai B, et al. Promoting axon regeneration in the adult CNS by modulation of the PTEN/mTOR pathway. *Science* 2008; 322: 963–6.
- Puttagunta R, Di Giovanni S. Retinoic acid signaling in axonal regeneration. *Front Mol Neurosci* 2011; 4: 59.
- Puttagunta R, Schmandke A, Floriddia E, Gaub P, Fomin N, Ghyselink NB, et al. RA-RAR-beta counteracts myelin-dependent inhibition of neurite outgrowth via Lingo-1 repression. *J Cell Biol* 2011; 193: 1147–56.
- Qin Q, Baudry M, Liao G, Noniyev A, Galeano J, Bi X. A novel function for p53: regulation of growth cone motility through interaction with Rho kinase. *J Neurosci* 2009; 29: 5183–92.
- Qin Q, Liao G, Baudry M, Bi X. Role of calpain-mediated p53 truncation in semaphorin 3A-induced axonal growth regulation. *Proc Natl Acad Sci USA* 2010; 107: 13883–7.
- Reed D, Shen Y, Shelat AA, Arnold LA, Ferreira AM, Zhu F, et al. Identification and characterization of the first small molecule inhibitor of MDMX. *J Biol Chem* 2010; 285: 10786–96.
- Sabbatini P, McCormick F. MDMX inhibits the p300/CBP-mediated acetylation of p53. *DNA Cell Biol* 2002; 21: 519–25.
- Schnell L, Schwab ME. Sprouting and regeneration of lesioned corticospinal tract fibres in the adult rat spinal cord. *Eur J Neurosci* 1993; 5: 1156–71.
- Serra C, Palacios D, Mozzetta C, Forcales SV, Morantte I, Ripani M, et al. Functional interdependence at the chromatin level between the MKK6/p38 and IGF1/PI3K/AKT pathways during muscle differentiation. *Mol Cell* 2007; 28: 200–13.
- Shah M, Patel K, Mukhopadhyay S, Xu F, Guo G, Sehgal PB. Membrane-associated STAT3 and PY-STAT3 in the cytoplasm. *J Biol Chem* 2006; 281: 7302–8.

- Simonen M, Pedersen V, Weinmann O, Schnell L, Buss A, Ledermann B, et al. Systemic deletion of the myelin-associated outgrowth inhibitor nogo-a improves regenerative and plastic responses after spinal cord injury. *Neuron* 2003; 38: 201–11.
- Smith PD, Sun F, Park KK, Cai B, Wang C, Kuwako K, et al. SOCS3 deletion promotes optic nerve regeneration *in vivo*. *Neuron* 2009; 64: 617–23.
- Staerk J, Kallin A, Demoulin JB, Vainchenker W, Constantinescu SN. JAK1 and Tyk2 activation by the homologous polycythemia vera JAK2 V617F mutation: cross-talk with IGF1 receptor. *J Biol Chem* 2005; 280: 41893–9.
- Steward O, Zheng B, Tessier-Lavigne M. False resurrections: distinguishing regenerated from spared axons in the injured central nervous system. *J Comp Neurol* 2003; 459: 1–8.
- Steward O, Zheng B, Tessier-Lavigne M, Hofstadter M, Sharp K, Yee KM. Regenerative growth of corticospinal tract axons via the ventral column after spinal cord injury in mice. *J Neurosci* 2008; 28: 6836–47.
- Subbiah V, Naing A, Brown RE, Chen H, Doyle L, LoRusso P, et al. Targeted morphoproteomic profiling of Ewing's sarcoma treated with insulin-like growth factor 1 receptor (IGF1R) inhibitors: response/resistance signatures. *PloS One* 2011; 6: e18424.
- Sun F, Park KK, Belin S, Wang D, Lu T, Chen G, et al. Sustained axon regeneration induced by co-deletion of PTEN and SOCS3. *Nature* 2011; 480: 372–5.
- Tanaka H, Yamashita T, Yachi K, Fujiwara T, Yoshikawa H, Tohyama M. Cytoplasmic p21(Cip1/WAF1) enhances axonal regeneration and functional recovery after spinal cord injury in rats. *Neuroscience* 2004; 127: 155–64.
- Tedeschi A, Di Giovanni S. The non-apoptotic role of p53 in neuronal biology: enlightening the dark side of the moon. *EMBO Rep* 2009; 10: 576–83.
- Tedeschi A, Nguyen T, Puttagunta R, Gaub P, Di Giovanni S. A p53-CBP/p300 transcription module is required for GAP-43 expression, axon outgrowth, and regeneration. *Cell Death Differ* 2009a; 16: 543–54.
- Tedeschi A, Nguyen T, Steele SU, Feil S, Naumann U, Feil R, et al. The tumor suppressor p53 transcriptionally regulates cGKI expression during neuronal maturation and is required for cGMP-dependent growth cone collapse. *J Neurosci* 2009b; 29: 15155–60.
- Teng FY, Tang BL. Axonal regeneration in adult CNS neurons—signaling molecules and pathways. *J Neurochem* 2006; 96: 1501–8.
- Toledo F, Wahl GM. MDM2 and MDM4: p53 regulators as targets in anticancer therapy. *Int J Biochem Cell Biol* 2007; 39: 1476–82.
- Trakhtenberg EF, Goldberg JL. The role of serotonin in axon and dendrite growth. *Int Rev Neurobiol* 2012; 106: 105–26.
- Vassilev LT, Vu BT, Graves B, Carvajal D, Podlaski F, Filipovic Z, et al. In vivo activation of the p53 pathway by small-molecule antagonists of MDM2. *Science* 2004; 303: 844–8.
- Vogel SM, Bauer MR, Joerger AC, Wilcken R, Brandt T, Veprintsev DB, et al. Lithocholic acid is an endogenous inhibitor of MDM4 and MDM2. *Proc Natl Acad Sci USA* 2012; 109: 16906–10.
- Vuong L, Brobst DE, Saadi A, Ivanovic I, Al-Ubaidi MR. Pattern of expression of p53, its family members, and regulators during early ocular development and in the post-mitotic retina. *Invest Ophthalmol Vis Sci* 2012; 53: 4821–31.
- Wade M, Wang YV, Wahl GM. The p53 orchestra: Mdm2 and Mdmx set the tone. *Trends Cell Biol* 2010; 20: 299–309.
- Yamada T, Yang Y, Bonni A. Spatial organization of ubiquitin ligase pathways orchestrates neuronal connectivity. *Trends Neurosci* 2013; 36: 218–26.
- Yiu G, He Z. Glial inhibition of CNS axon regeneration. *Nat Rev Neurosci* 2006; 7: 617–27.
- Zou H, Ho C, Wong K, Tessier-Lavigne M. Axotomy-induced Smad1 activation promotes axonal growth in adult sensory neurons. *J Neurosci* 2009; 29: 7116–23.

**Supplementary Figure 1. Network pathway analysis and co-immunoprecipitation experiments identify MDM4-p53-MDM2 protein complex in the retina**

**a.** STRING network analysis shows interdependence of a number of key regenerative molecules with ubiquitin ligases and ligase-like proteins. However, a hot spot was found around MDM4-MDM2-p53, due to their highly ranked connections amongst themselves and their central position within the whole network. **b.** Representative co-immunoprecipitation immunoblot and input and co-immunoprecipitation at 72h after optic nerve crush or sham showing p53 and MDM2 co-immunoprecipitation with MDM4. Normal mouse IgG and actin were used as negative controls of the IP,  $n = 3$ .

**Supplementary Figure 2.**

**a.** Representative fluorescent images at 24h and 72h after optic nerve crush showing MDM4 expression in retinal ganglion cells. Retinal ganglion cells were counterstained with Tuj1. MDM4 co-localised with Tuj1. Scale bar 20  $\mu\text{m}$ . **b.** Quantification of the expression level of MDM4 by fluorescence intensity measurement. MDM4 expression level did not change significantly at 24h and 72h following optic nerve crush. At least six sections were analysed from 3 animals in each group. **c.** Representative fluorescent images at 24h and 72h after optic nerve crush showing p53 expression in retinal ganglion cells. Retinal ganglion cells were counterstained with Tuj1. P53 co-localised with Tuj1. Scale bar 20  $\mu\text{m}$ . **d.** Quantification of the expression level of p53 by fluorescence intensity measurement. P53 expression level did not change significantly at 24h and 72h following optic nerve crush. At least six sections were analysed from 3 animals in each group. **e.** Representative fluorescent images at 24h and 72h after optic nerve crush showing MDM2 expression in retinal ganglion cells. Retinal ganglion cells were counterstained with Tuj1. MDM2 co-localised with Tuj1. Scale bar 20  $\mu\text{m}$ . **f.** Quantification of the expression level of MDM2 by fluorescence intensity

measurement. MDM2 expression level did not change significantly at 24h and 72h following optic nerve crush. At least six sections were analysed from 3 animals in each group.

### **Supplementary Figure 3.**

**a.** Representative image of a retina infected with AAV-CreGFP showing specific highly efficient infection in retinal ganglion cells. Scale bar 50  $\mu$ m. **b.** Immunofluorescence of retinal ganglion cells infected with AAV-GFP or AAV-CreGFP showing MDM4 deletion 14d after infection. MDM4 expression could be detected by immunostaining in control AAV-GFP infected samples only (arrowheads). Scale bar 20  $\mu$ m. **c.** Semi quantitative PCR from dissociated retinal ganglion cell culture 3 days after infection with AAV-GFP/AAV-Cre. MDM4 expression was significantly reduced after Cre mediated recombination.

### **Supplementary Figure 4.**

**a.** Shown are GFP and BDA labeling of the sensorimotor cortex after stereotaxic delivery of AAV-GFP or BDA. Inset shows layer V in the sensorimotor cortex. Scale bar 500  $\mu$ m. **b.** Shown are cre-positive cells after anti-cre immunostaining in proximity of the injection site (asterix) of AAV-cre in the sensorimotor cortex. Scale bar 50  $\mu$ m. **c.** Immunostaining for GFP and CTIP2 (layer V neurons marker) show AAV-GFP infection of layer V neurons in the sensorimotor cortex. Scale bar 20  $\mu$ m.

### **Supplementary Figure 5.**

Shown are BDA<sup>+</sup> corticospinal tract sprouting axons (arrowheads) past the lesion site (dashed line) after AAV-cre delivery in the sensorimotor cortex of MDM4f/f mice (5 weeks pre-injury). Sagittal section. Scale bar 500  $\mu$ m.

### **Supplementary Figure 6.**

**a.** Dissociated retinal ganglion cells from MDM4f/f postnatal day 7 mice were cultured on permissive (PDL) and inhibitory substrate (myelin) for 72h following Ad-Cre/Ad-GFP infection. Neurites were traced with Tuj1. **b.** Quantification of neurite outgrowth 72h after AV-GFP/AV-Cre infection. Semi-automatic analysis from more than 500 neurons per condition ( $n = 3$ ) showed a significantly higher outgrowth in the AV-Cre infected group. Student's t-test,  $p < 0.05$ . **c.** Cerebellar granule neurons from MDM4f/f mice were plated on permissive (PDL) and inhibitory (Myelin) substrate and infected with AV-GFP/AV-Cre. AV-Cre infected group showed a significantly higher neurite outgrowth 24h after infection. Neurites were traced with Tuj1. **d.** Quantification of neurite outgrowth of cultured cerebellar granule neuron. Neurites were traced manually from single neurons that were infected with the virus. At least 100 neurons were analysed per condition per group.  $n = 4$ . Student's t-test,  $p < 0.05$ .

### **Supplementary Figure 7.**

**a.** Semiquantitative PCR mice from MDM4f/f cerebellar granule neuron (cerebellar granule neuron) cultures after infection with AV-Cre or AV-GFP. MDM4 expression was significantly reduced after Cre mediated recombination. **b.** Real time quantitative PCR from MDM4f/f cerebellar granule neuron cultures 24h after infection with AV-GFP or AV-Cre showed enhanced expression of several p53-target genes. P53 expression was not altered due to MDM4 deletion.

### **Supplementary Figure 8.**

**a.** Quantitative RTPCR from cerebellar granule neuron treated with Nutlin-3a or vehicle (24h). Shown is enhanced expression of axon growth associated and p53 target genes with



Nutlin-3a 100nM versus vehicle. 18S RNA was used for normalization.  $n = 3$ . (Student t-test,  $*p < 0.05$  or  $**p < 0.01$ ). **b.** Apoptosis was evaluated 24h after administration of Nutlin-3a or vehicle in cerebellar granule neuron. Pyknotic cells were identified with DAPI staining.  $n = 3$ . (Student t-test,  $*p < 0.05$  or  $**p < 0.01$ ).

### **Supplementary Figure 9.**

**a.** Dose response of picropodophyllin (picropodophyllin, IGF1R antagonist) in cerebellar granule neurons was determined by counting the number of Cleaved Caspase 3 positive cells in a dose response curve. picropodophyllin 1 $\mu$ M or above showed significant cell death as compared to vehicle control.  $n = 3$ . Student's t-test,  $p < 0.05$ . **b.** Cells extending neuritis in response to picropodophyllin treatment (dose response) were counted. Cells treated with picropodophyllin 10nM or above showed reduced number of cells extending neurites.  $n = 3$ . Student's t-test,  $p < 0.05$ .

### **Supplementary Figure 10.**

**a.** Representative immunoblotting from a spinal cord 72 hours after Nutlin-3 or vehicle delivery with osmotic minipump and spinal cord T9 hemisection. Shown is enhancement of active acetylated p53 (p53ac) and of the prototypical p53 target gene p21 after Nutlin-3 versus vehicle. Classical cell death pathways were also not induced by Nutlin-3 as shown by cleaved caspase 3 expression. **b.** Bar graphs show densitometry analysis (arbitrary units) expressed as fold change of Nutlin-3 versus vehicle.  $n = 3$ . Student's unpaired two-tailed t-test  $**p < 0.01$  or  $***p < 0.001$ .

### **Supplementary Figure 11.**

Shown are BDA+ corticospinal tract sprouting axons past the lesion site (dashed line) after Nutlin-3 administration (for 14 days after T9 spinal cord hemisection) 45 days post-injury.

Scale bar 250  $\mu$ m.

### **Supplementary Table 1.**

List of dysregulated genes. Genes differentially expressed were selected based upon a 2 fold change cut-off and significant statistical difference between AAV GFP and AAV cre infected RGC (ANOVA with Bonferroni correction).

### **Supplementary Table 2.**

Ingenuity canonical pathways from dysregulated genes between AAV GFP and AAV cre infected RGC.

### **Supplementary Table 3.**

Details about our spinal cord injury experimental design and criteria according to the Minimal Information about a Spinal Cord Injury Experiment reporting standards.

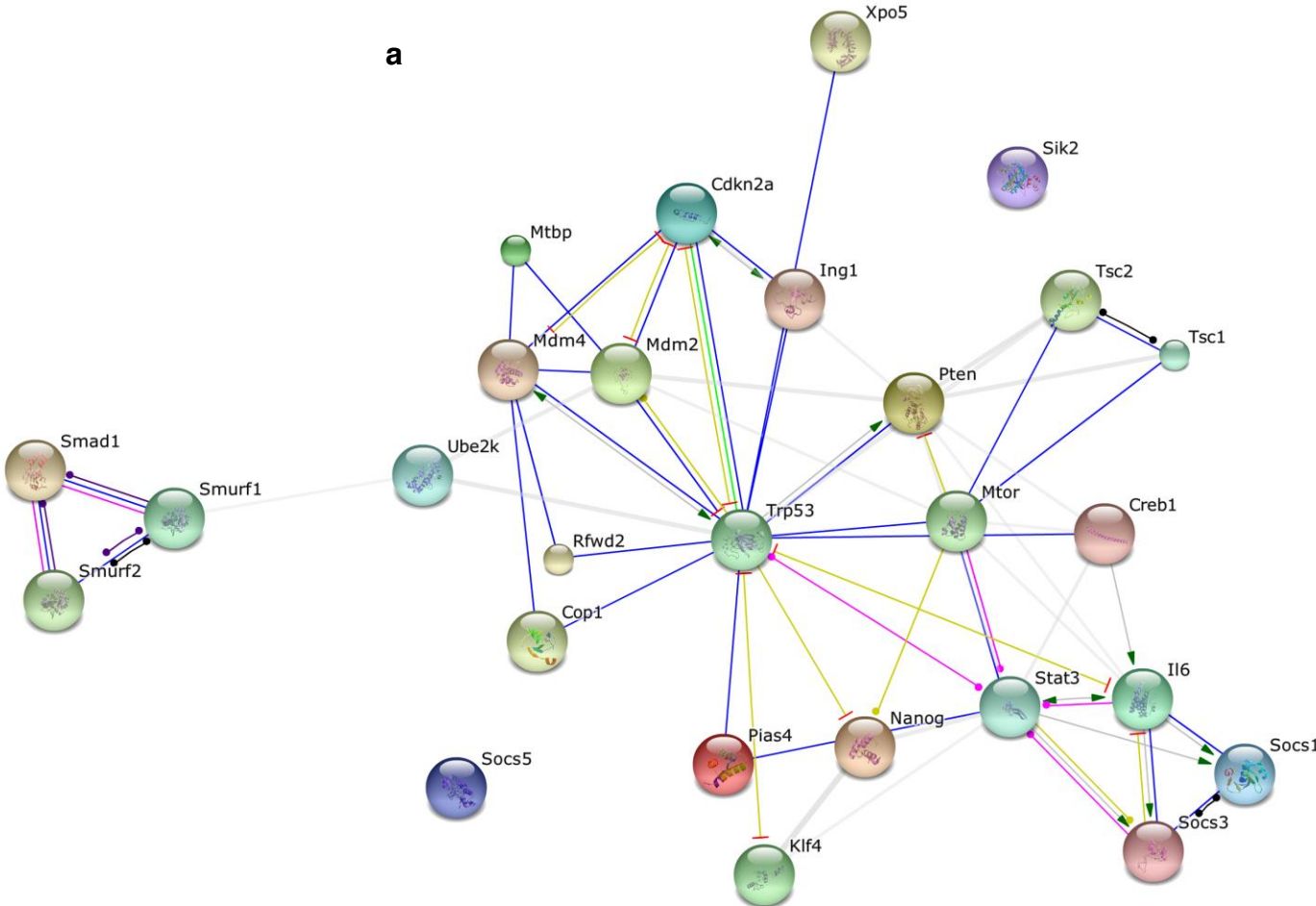
### **Supplementary Table 4.**

Details about our optic nerve crush experimental design and criteria according to the Minimal Information about a Spinal Cord Injury Experiment reporting standards.

### **Supplementary movies.**

Shown are representative runs on the grid walk 35 days after spinal cord injury and vehicle **(a)** versus Nutlin-3 administration **(b)**. The number and severity of missteps is significantly reduced after Nutlin-3 treatment.

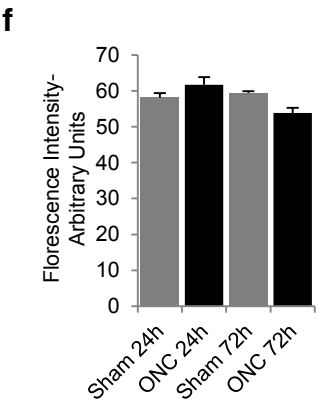
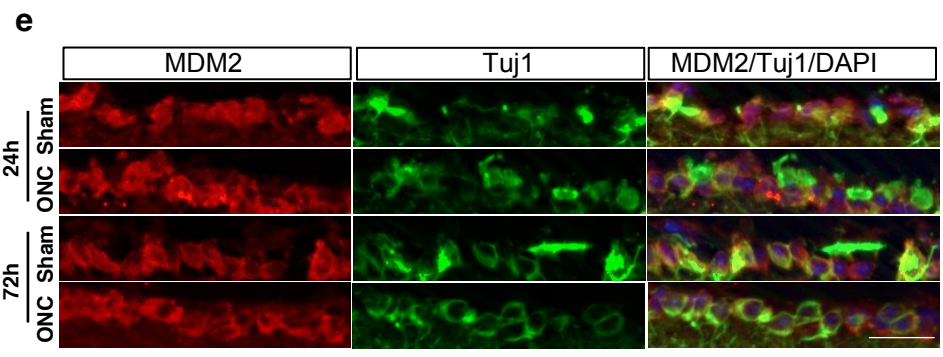
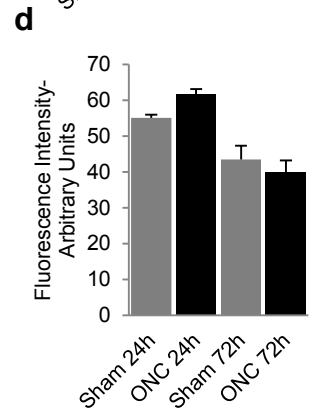
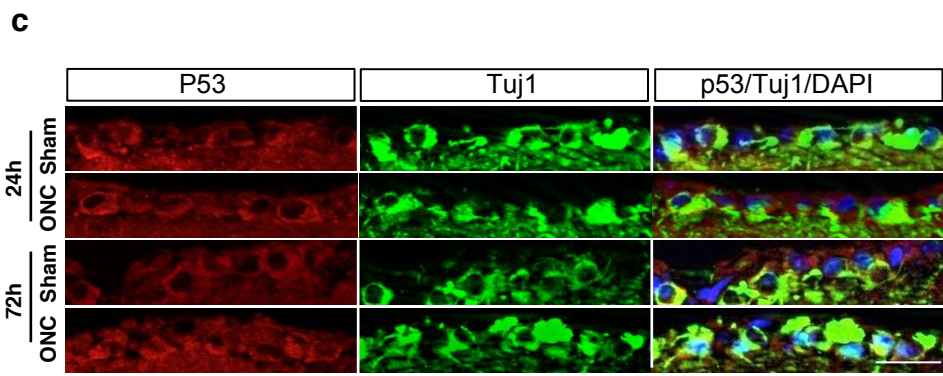
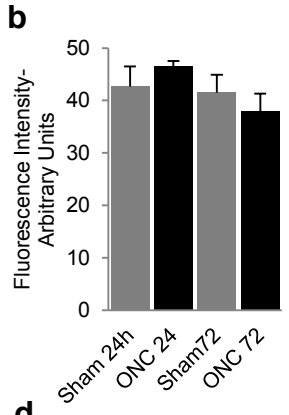
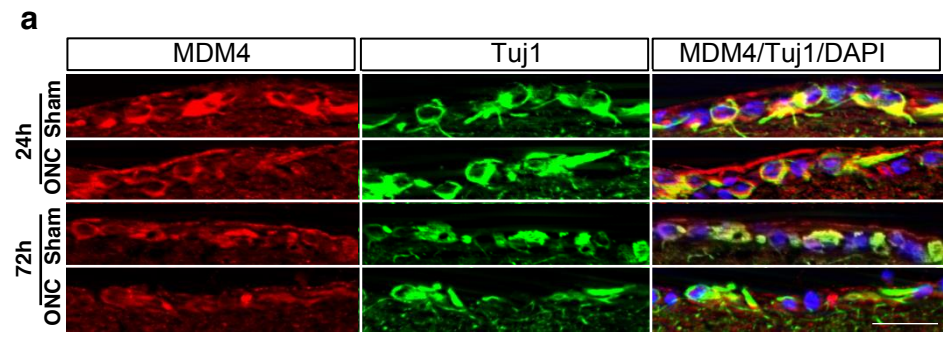
**a**



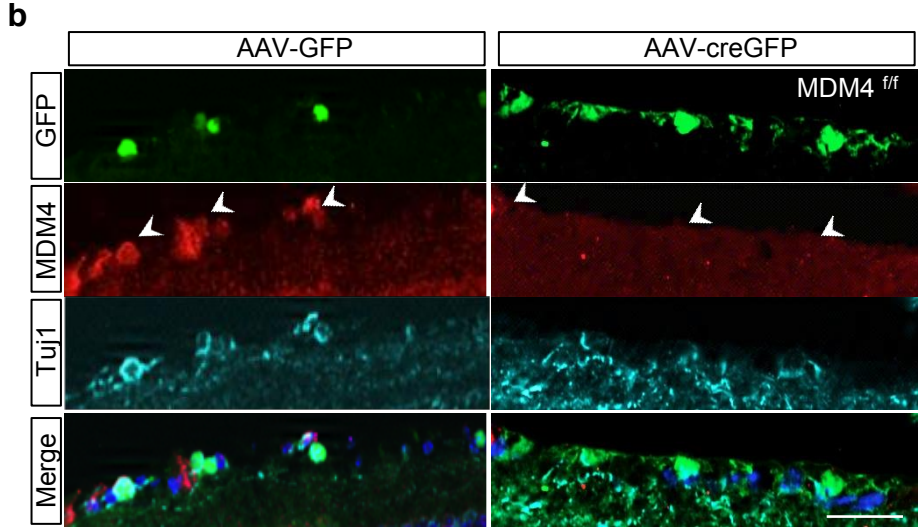
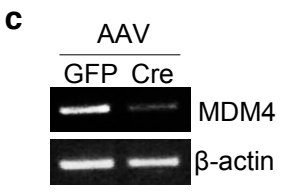
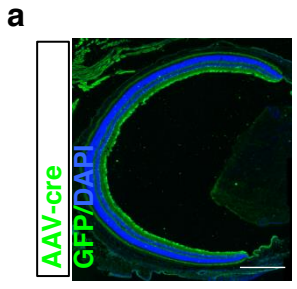
**b**

	MDM4 IP		IgG		Input		
	Sham	ONC	Sham	ONC	Sham	ONC	
72 kDa							MDM4
53 kDa							p53
90 kDa							MDM2
44 kDa							β-actin

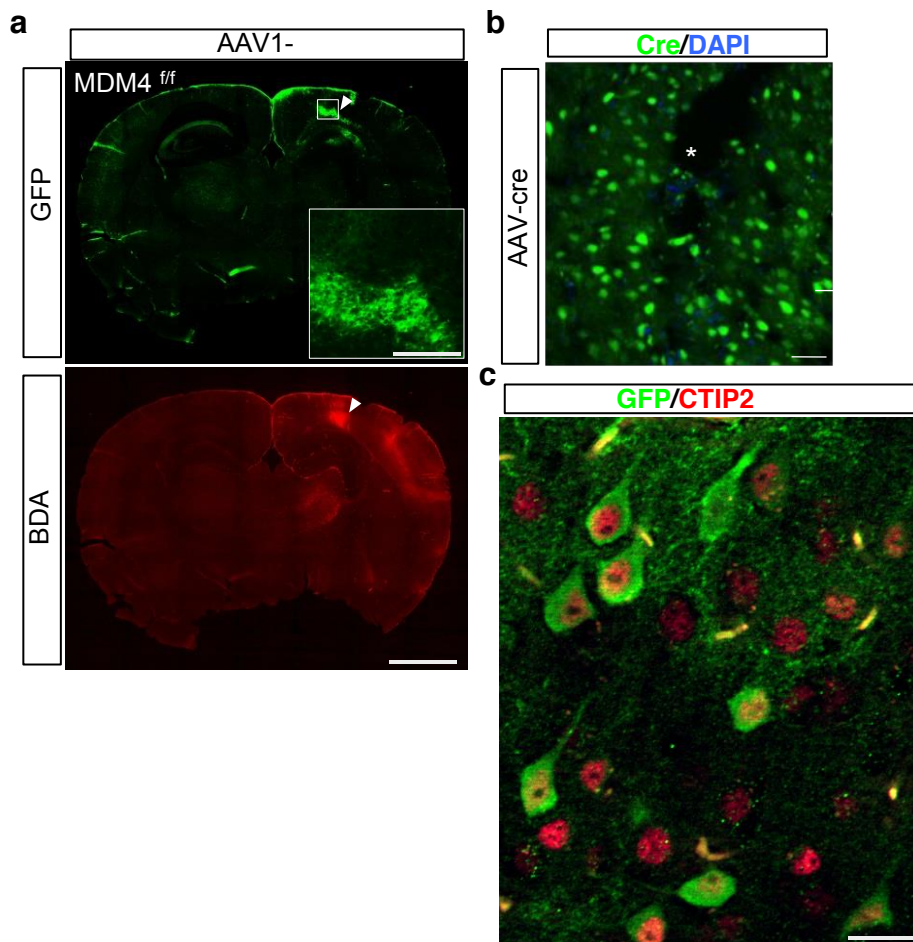
Supp. Figure 2



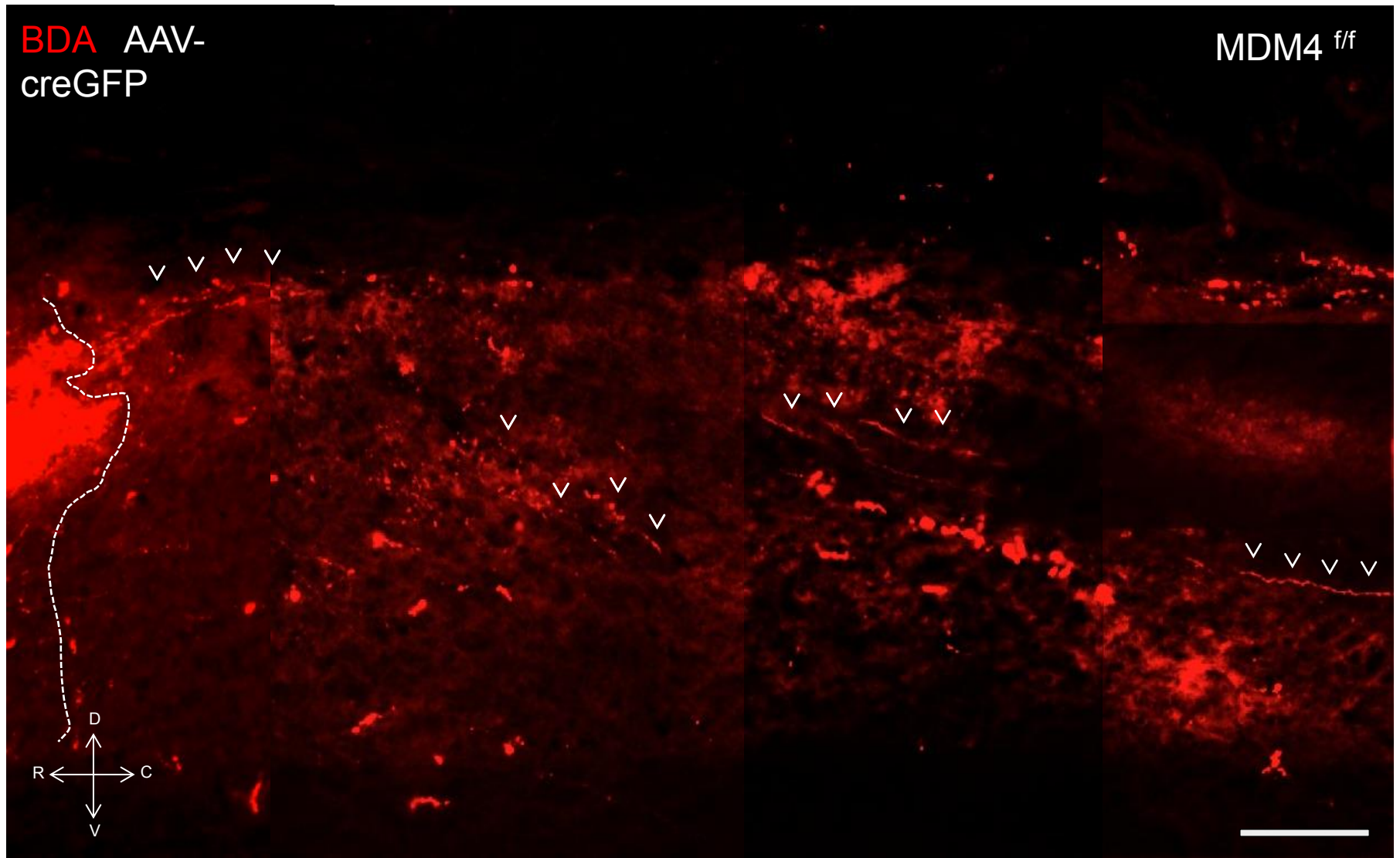
Supp. Figure 3

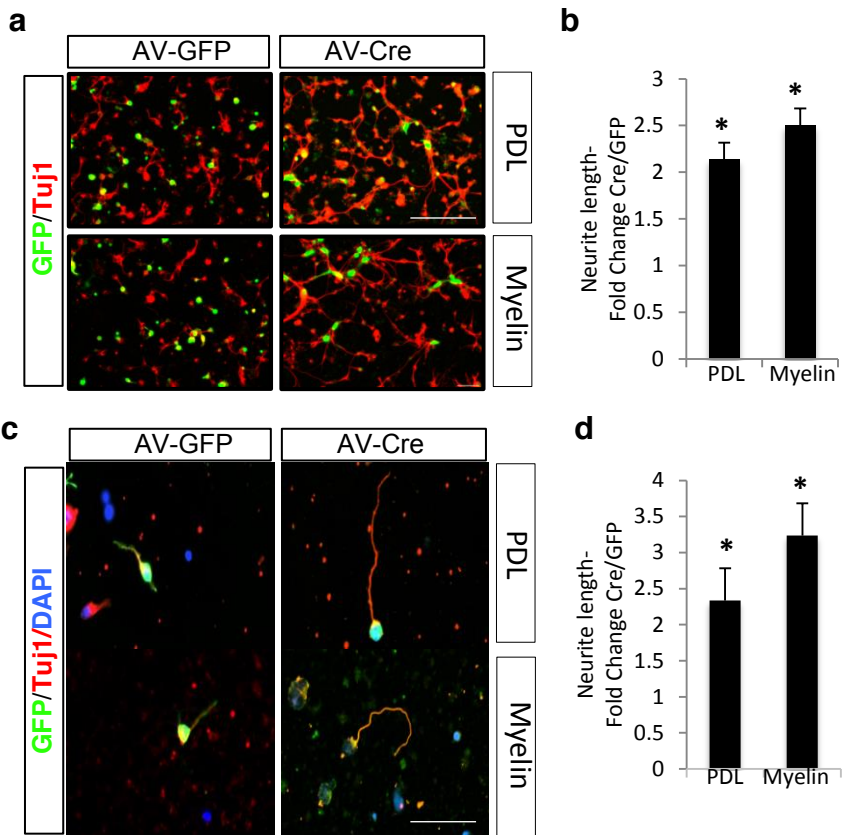


Supp. Figure 4

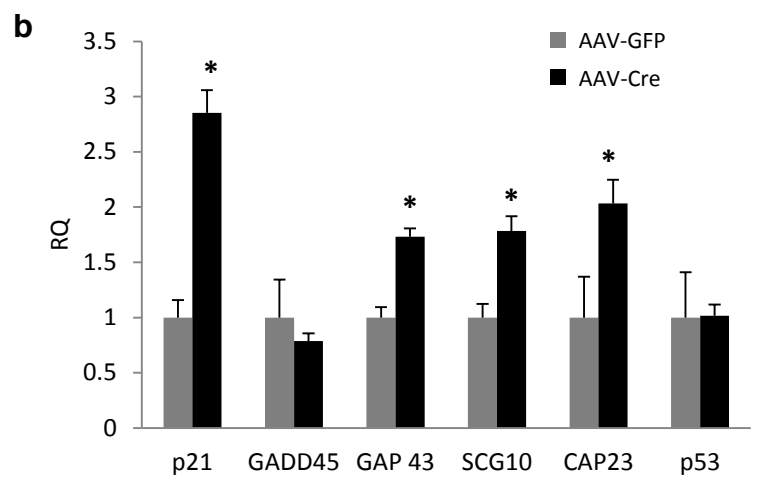
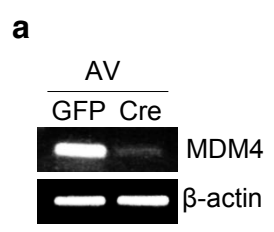




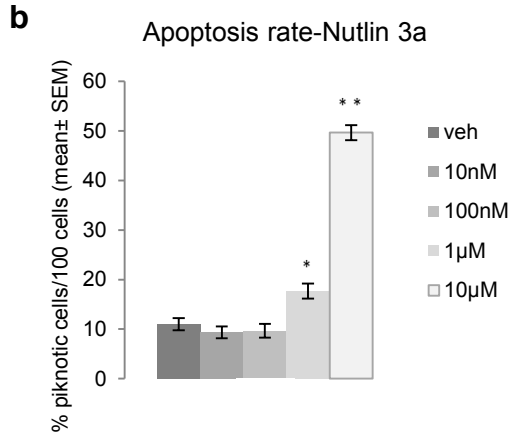
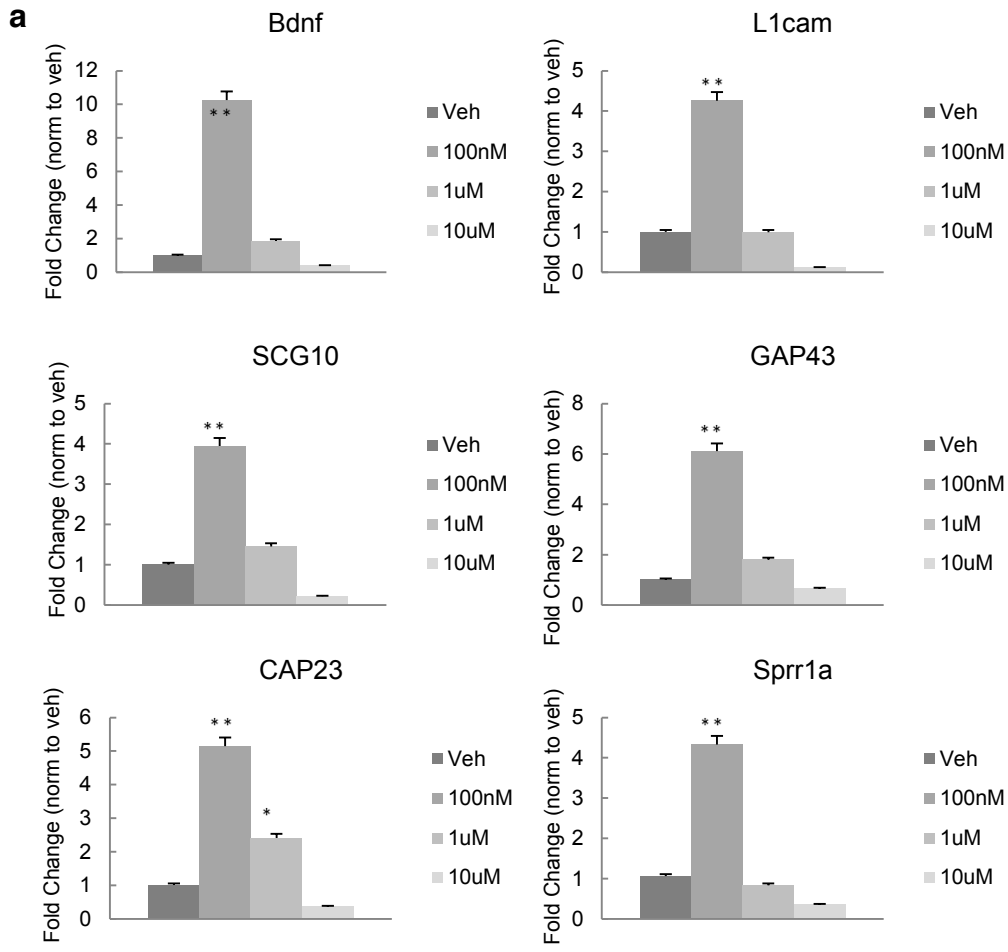




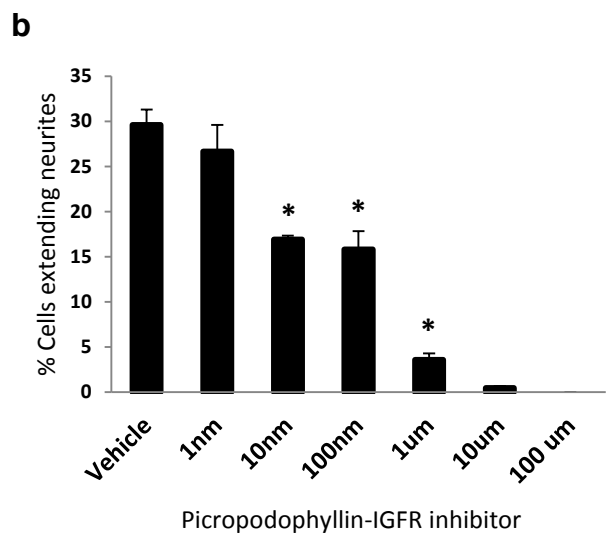
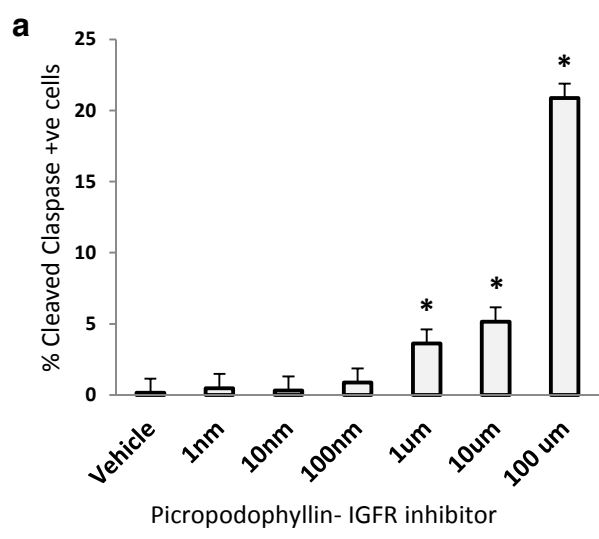




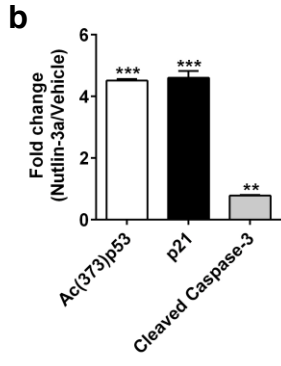
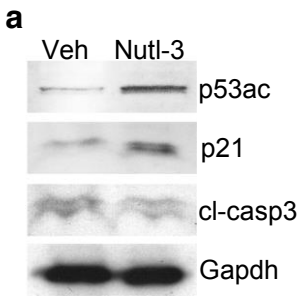
Supp. Figure 8



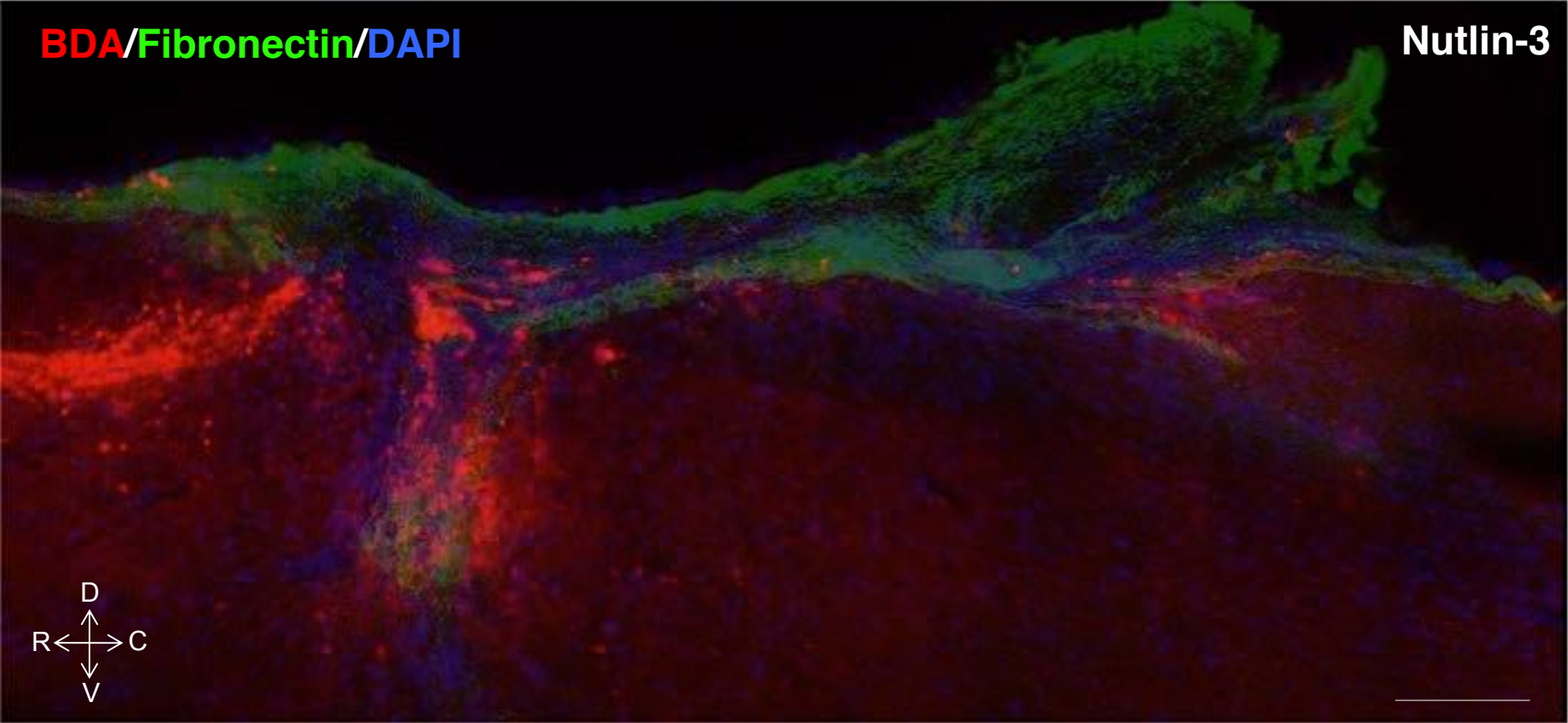
Supp. Figure 9



Supp. Figure 10



Supp. Figure 11



## Supplementary Table 3

## Minimum Information About a Spinal Cord Injury experiment\*

ORGANISM	Nutlin experiments	Nutlin + PPP experiment	MDM4 f/f experiments
Binomial systematic name (genus and species)	Mus musculus	Mus musculus	Mus musculus
Phenotype	Wild type	Wild type	Wild type
Genotype	None	None	Mdm4 f/f
How was genotype confirmed?	Not applicable	Not applicable	PCR (primer sequences in MM)
Source/Vendor	Charles River, Sulzfeld, Germany	Charles River, Sulzfeld, Germany	Obtained from J.C. Marine Lab
Organism Vendor Cat #	B6NSIMA	B6NSIMA	
Strain	C57BL/6	C57BL/6	C57BL/6
Number of generations backcrossed	Not applicable	Not applicable	
Sex	Male	Male	M&F
PubMed Reference	Not applicable	Not applicable	Not available
Het vs. homozygote	Not applicable	Not applicable	Homozygote
Propagation strategy	Not applicable	Not applicable	
Age at sacrifice	19 weeks	19 weeks	13 weeks
Weight at surgery	24-30 g	25-30 g	19-29 g
Was Tamoxifen administered?	No	No	No
If yes, at what age?	Not applicable	Not applicable	Not applicable
If yes, when relative to injury?	Not applicable	Not applicable	Not applicable
<b>HOUSING</b>			
Group vs. Single	Group	Group	Group
Light/Dark Cycle	12-12	12-12	12-12
When tested relative to Light/Dark cycle?	Light (morning)	Light (morning)	Not applicable
Enrichment	Yes	Yes	Yes
Exercise opportunities	Nestlets	Nestlets	Nestlets
Food	Milk+moistured food+dry food until 3 <sup>rd</sup> DPO, moistured food+dry food until recovery of surgery weight, fruit crunchies ad libitum	Milk+moistured food+dry food until 3 <sup>rd</sup> DPO, moistured food+dry food until recovery of surgery weight, fruit crunchies ad libitum	Moistured food+dry food ad libitum
Supplemental Nutrical	Yes, daily until sacrifice	Yes, daily until sacrifice	No

\*Lemmon VP et al. (2014) Minimum Information about a Spinal Cord Injury Experiment: A Proposed Reporting Standard for Spinal Cord Injury Experiments. *J Neurotrauma* 31:1354–1361.

<b>SURGERY</b>	<b>Nutlin experiments</b>	<b>Nutlin + PPP experiment</b>	<b>MDM4 f/f experiments</b>
<b>Anesthetics</b>			
<b>Systemic Anesthetics</b>			
Anesthetic 1	<b>Ketamin 10%</b>	<b>Ketamin 10%</b>	<b>Ketamin 10%</b>
Source/Company	WDT	WDT	WDT
Catalogue number	F0637-04	F0637-04	F0637-04
Amount	100 mg/Kg	100 mg/Kg	100 mg/Kg
Solvent	0,9% saline	0,9% saline	0,9% saline
Delivery method	Intraperitoneal	Intraperitoneal	Intraperitoneal
Anesthetic 2	<b>Sedaxylan (Xylazin 20 mg/ml)</b>	<b>Sedaxylan (Xylazin 20 mg/ml)</b>	<b>Sedaxylan (Xylazin 20 mg/ml)</b>
Source/Company	WDT	WDT	WDT
Catalogue number	Ch. B. EM43	Ch. B. EM43	Ch. B. EM43
Amount	10 mg/Kg	10 mg/Kg	10 mg/Kg
Solvent	0,9% saline	0,9% saline	0,9% saline
Delivery method	Intraperitoneal	Intraperitoneal	Intraperitoneal
<b>Local Anesthetics</b>	<b>Xylocain 2%</b>	<b>Xylocain 2%</b>	<b>Xylocain 2%</b>
Source/Company	Astra Zeneca	Astra Zeneca	Astra Zeneca
Catalogue number	PZN#1313764	PZN#1313764	PZN#1313764
Amount	1 drop	1 drop	1 drop
Solvent	not diluted	not diluted	not diluted
Delivery method	local on the dura mater	local on the dura mater	local on the dura mater
<b>Surgical details</b>			
Concealed allocation: were experimenters blinded to treatments?	Yes	Yes	Yes
Does the phenotype of a transgenic animal make its genetic status obvious?	Not applicable	Not applicable	No
Injury Level	T9	T9	T9

<b>SURGERY</b>	<b>Nutlin experiments</b>	<b>Nutlin + PPP experiment</b>	<b>MDM4 f/f experiments</b>
Surgery duration	1 hour	1 hour	20 minutes
Surgery time of day	Morning and afternoon	Morning and afternoon	Morning and afternoon
Batching method / method of randomization	Randomized	Randomized	Randomized
Number of surgeons in project	1	1	1
<b><i>Injury Method</i></b>			
<b>Contusion</b>	<b>No</b>	<b>No</b>	<b>No</b>
<b>Hemisection</b>	<b>Yes</b>	<b>Yes</b>	<b>Yes</b>
If yes, provide details	T9 dorsal hemisection until the central canal	T9 dorsal hemisection until the central canal	T9 dorsal hemisection until the central canal
Neurochemical	No	No	No
Crush	No	No	No
Compression	No	No	No
Vascular occlusion	No	No	No
Transection	No	No	No
<b><i>Reporters</i></b>			
Axon labeling method	BDA anterograde tracing and 5-HT immunostaining	5-HT immunostaining	BDA anterograde tracing
<b><i>Post Surgery Care</i></b>			
<b>Analgesic 1</b>	<b>Buprenorphine (Temgesic) 0,3 mg/ml injection solution</b>	<b>Buprenorphine (Temgesic) 0,3 mg/ml injection solution</b>	
Source	Schering-Plough	Schering-Plough	
Catalogue number	PZN 345928	PZN 345928	
Amount	0,05-0,1 mg/Kg 12/12 h until 3rd DPO	0,05-0,1 mg/Kg 12/12 h until 3rd DPO	
Solvent	0,9% saline	0,9% saline	
Delivery method	Subcutaneous	Subcutaneous	



<b>SURGERY</b>	<b>Nutlin experiments</b>	<b>Nutlin + PPP experiment</b>	<b>MDM4 f/f experiments</b>
<b>Analgesic 2</b>	<b>Carprofen (Carprieve) 50 mg/ml injection solution</b>	<b>Carprofen (Carprieve) 50 mg/ml injection solution</b>	
Source	Norbrook	Norbrook	
Catalogue number	VM#10999/102/1	VM#10999/102/1	
Amount	5 mg/Kg once day, 4th-7th DPO	5 mg/Kg once day, 4th-7th DPO	
Solvent	0,9% saline	0,9% saline	
Delivery method	Subcutaneous	Subcutaneous	
<b>Hydration</b>			
Solution	0,9% saline	0,9% saline	0,9% saline
Volume	2 ml or 1 ml	2 ml or 1 ml	2 ml or 1 ml
Delivery method	Subcutaneous	Subcutaneous	Subcutaneous
Frequency	1 ml 12/12 h until 2 <sup>nd</sup> DPO, 1 ml once daily 3 <sup>rd</sup> -5 <sup>th</sup> DPO. 1 ml daily if signs of bladder infection (i.e. purulent or bloody urine)	1 ml 12/12 h until 2 <sup>nd</sup> DPO, 1 ml once daily 3 <sup>rd</sup> -5 <sup>th</sup> DPO. 1 ml daily if signs of bladder infection (i.e. purulent or bloody urine)	1 ml 12/12 h until 2 <sup>nd</sup> DPO, 1 ml once daily 3 <sup>rd</sup> -5 <sup>th</sup> DPO. 1 ml daily if signs of bladder infection (i.e. purulent or bloody urine)
<b>Antibiotics</b>	<b>Enrofloxacin (Baytril) 2,5% injection solution</b>	<b>Enrofloxacin (Baytril) 2,5% injection solution</b>	
Source	Bayer	Bayer	
Catalogue number	PZN 3543238	PZN 3543238	
Volume	5 mg/Kg (prophylactic) or 10 mg/Kg (therapeutic)	5 mg/Kg (prophylactic) or 10 mg/Kg (therapeutic)	
Delivery method	Subcutaneous	Subcutaneous	
Frequency	<u>Prophylactic</u> : once daily at surgery day and 1 <sup>st</sup> -5 <sup>th</sup> DPO. <u>Therapeutic</u> : 10-14 days at chronic phase (+8 DPO) if signs of bladder infection (i.e. purulent or bloody urine)	<u>Prophylactic</u> : once daily at surgery day and 1 <sup>st</sup> -5 <sup>th</sup> DPO. <u>Therapeutic</u> : 10-14 days at chronic phase (+8 DPO) if signs of bladder infection (i.e. purulent or bloody urine)	

<b>SURGERY</b>	<b>Nutlin experiments</b>	<b>Nutlin + PPP experiment</b>	<b>MDM4 f/f experiments</b>
<b>Bladder expression</b>			
Frequency	Twice a day	Twice a day	Twice a day
Timing relative to behavioral testing	Always before	Always before	Not applicable
<b>Animal Attrition</b>			
Exclusion criteria	Animals were excluded from analysis in the case of spared fibers or when we observed a total transection with the fibronectin positive scar spanning the entire depth of the spinal cord. These animals were rejected from analysis by someone blinded to their treatment allocation.	Animals were excluded from analysis in the case of spared fibers or when we observed a total transection with the fibronectin positive scar spanning the entire depth of the spinal cord. These animals were rejected from analysis by someone blinded to their treatment allocation.	Animals were excluded from analysis in the case of spared fibers, poor CST tracing or when we observed a total transection with the fibronectin positive scar spanning the entire depth of the spinal cord. These animals were rejected from analysis by someone blinded to their treatment allocation.
Were exclusion criteria established before the study was initiated	Yes		
<b>Health Outcomes</b>			
Number of animals excluded for any reason	7	0	6
Why were animals excluded?	Total transection		CST tracing was poor
Survival time after surgery	45 days	35 days	28 days

PERTURBAGEN	Nutlin experiments	Nutlin + PPP experiment	MDM4 f/f experiments
<b>Adapted from MIACA 080404</b>			
<b><i>Perturbagen Name 1</i></b>	<b>Nutlin-3a</b>	<b>Nutlin-3a</b>	<b>Virus</b>
Perturbagen Type	Drug	Drug	AAV1-GFP and AAV1-Cre-GFP
Perturbagen Sequence/Composition: of cDNA/siRNA/shRNA; structure/'smile'/CHEBI if compound	Not applicable	Not applicable	Not applicable
Perturbagen manufacturer	Cayman	Cayman	SignaGen Laboratories
Perturbagen Catalogue #	18585	18585	SL100803 (AAV1-GFP) and SL100805 (AAV1-Cre-GFP)
Perturbagen Lot #	Batch#0441705-7	Batch#0441705-7	AAV616714 (AAV1-GFP) and AAV616731 (AAV1-Cre-GFP)
Perturbagen Target Species: e.g. if siRNA	Not applicable	Not applicable	Not applicable
Perturbagen Stock Concentration	2 mM	2 mM	
Perturbagen Solvent	100% pure ethanol	100% pure ethanol	
Solvent Final concentration	8,6% (in PBS)	8,6% (in PBS)	
Stock storage condition	-20 °C	-20 °C	-80 °C
If perturbagen is a compound, is any information available about its biodistribution?	Yes (Zhang F et al. Drug Metab Dispos. 39:15-21, 2011)	Yes (Zhang F et al. Drug Metab Dispos. 39:15-21, 2011)	
<b>If Perturbagen 1 is part of a library</b>			
Library Name	PubChem	PubChem	
Library Type	Compound	Compound	
Library manufacture	U.S. National Library of Medicine	U.S. National Library of Medicine	
Library Catalogue #	CID 11433190	CID 11433190	

PERTURBAGEN	Nutlin experiments	Nutlin + PPP experiment	MDM4 f/f experiments
<b><i>Perturbagen Name 2</i></b>		<b>Picropodophyllin</b>	
Perturbagen Type		Drug	
Perturbagen Sequence/Composition: of cDNA/siRNA/shRNA; structure/'smile'/CHEBI if compound		Not applicable	
Perturbagen manufacturer		Medkoo Biosciences	
Perturbagen Catalogue #		205812	
Perturbagen Lot #		BP40711	
Perturbagen Target Species: e.g. if siRNA		Not applicable	
Perturbagen Stock Concentration		100 mM	
Perturbagen Solvent		DMSO	
Solvent Final concentration		10% (in cottonseed oil)	
Stock storage condition		-20 °C	
If perturbagen is a compound, is any information available about its biodistribution?		Yes (Yin S et al. Neuro Oncol. 12(1):19-27, 2010)	
<b>If Perturbagen 2 is part of a library</b>			
Library Name		PubChem	
Library Type		Substance	
Library manufacture		U.S. National Library of Medicine	
Library Catalogue #		SID 53787335	
<b><i>If Perturbagen is virus:</i></b>			
Virus Type			AAV
Virus isotype			AAV1
Virus Titer			4,4 x 10 <sup>9</sup> GC/μl (AAV1-GFP) and 3,1 x 10 <sup>9</sup> GC/μl (AAV1-Cre-GFP)
Titration method			Real-time PCR
Promoter driving protein/miRNA expression			CMV
IRIS/2A peptide/Dual Promoter			Not applicable

<b>PERTURBAGEN</b>	<b>Nutlin experiments</b>	<b>Nutlin + PPP experiment</b>	<b>MDM4 f/f experiments</b>
<i>Transfection Reagents</i>	Not applicable		
<i>Timing of perturbagen 1 delivery relative to injury</i>	Immediately after	Immediately after	5 weeks prior to injury
<i>Timing of perturbagen 2 delivery relative to injury</i>		At the surgery day ( $\leq$ 8 hours after surgery)	
<b><i>Treatment Delivery (Perturbagen 1)</i></b>	<b>Nutlin-3a</b>	<b>Nutlin-3a</b>	<b>AAV</b>
Rate	0,5 $\mu$ l/h	0,5 $\mu$ l/h	
Location	Minipump subcutaneous, catheter intrathecal	Minipump subcutaneous, catheter intrathecal	Right sensorimotor cortex
Method & route (i.p., i.v., minipump)	Alzet minipump (model 2002, Lot#10285-12)+intrathecal catheter (polyethylene, 32G, ReCathCo)	Alzet minipump (model 2002, Lot#10285-12)+intrathecal catheter (polyethylene, 32G, ReCathCo)	Stereotaxic-coordinated micro-injections with 5 $\mu$ l Hamilton syringe
Dosage (mg/kg)	0,04 mg/Kg/day (14 days)	0,04 mg/Kg/day (14 days)	0,32 $\mu$ l
Acute / chronic	Acute and chronic	Acute and chronic	
Convection based	Not applicable	Not applicable	Not applicable
<b><i>Treatment Delivery (Perturbagen 2)</i></b>		<b>Picropodophyllin</b>	
Rate		Not applicable	
Location		Not applicable	
Method & route (i.p., i.v., minipump)		I.P.	
Dosage (mg/kg)		20 mg/Kg 12/12 h (14 days)	
Acute / chronic		Acute and chronic	
Convection based		Not applicable	

<b>HISTOLOGY</b>	<b>Nutlin experiments</b>	<b>Nutlin + PPP experiment</b>	<b>MDM4 f/f experiments</b>
<b>Fixation Method</b>			
Method	Pump	Pump	Pump
Anesthetic	Ketamine+Xylazine	Ketamine+Xylazine	Ketamine+Xylazine
Prerinse	Yes	Yes	Yes
Buffer	PBS	PBS	PBS
Volume	10 ml	10 ml	10 ml
Temperature	0 °C	0 °C	0 °C
Fixative	4% PFA	4% PFA	4% PFA
Buffer	PBS	PBS	PBS
Volume	10 ml	10 ml	10 ml
Temperature	0 °C	0 °C	0 °C
<b>Tissue Processing</b>			
Sectioning method	Cryostat, embedded in OCT, 18 µm	Cryostat, embedded in OCT, 18 µm	Cryostat, embedded in OCT, 18 µm
Normalization method for shrinkage	None	None	None
Lesion volume/size	≈2mm (length) X 1 mm (wide) x 0,5 mm (depth)	≈2mm (length) X 1 mm (wide) x 0,5 mm (depth)	≈2mm (length) X 1 mm (wide) x 0,5 mm (depth)
White matter/Gray matter sparing	Both	Both	Both
<b>Axonal tracing methods</b>			
Traditional tracer	BDA	No	BDA
Genetic tracer	No	No	No
Viral tracer	No	No	No
Where tracer injected	Sensorimotor cortex		Sensorimotor cortex
When tracer injected relative to injury	5 weeks after injury		2 weeks after injury
Survival time after injection of tracer	10 days		14 days

<b>Histology</b>	<b>Nutlin experiments</b>	<b>Nutlin + PPP experiment</b>	<b>MDM4 f/f experiments</b>
<b>Characterization of injury</b>			
Measures of sprouting	Yes	Yes	Yes
Measures of regeneration	No	No	No
Measures of spanning	No	No	No
Clearing method	None	None	None
Cell counts	No	No	No

<b>IMMUNOHISTOCHEMISTRY</b>	<b>Nutlin Experiments</b>	<b>Nutlin + PPP experiment</b>	<b>MDM4 f/f experiments</b>
<b>Neurons identified</b> Marker used	No	No	Yes Ctip2 (Brain)
<b>Neurites identified</b>	No	No	
<b>Axons identified</b> Marker used	Yes BDA and 5-HT	Yes 5-HT	Yes BDA
<b>Dendrites identified</b>	No	No	No
<b>Growth Cones identified</b>	No	No	No
<b>Synapses identified</b>	No	No	No
<b>Astrocytes identified</b> Markers used	Yes GFAP	No	Yes GFAP
<b>Oligodendrocytes identified</b>	No	No	No
<b>Schwann cells identified</b>	No	No	No
<b>Microglia identified</b>	No	No	No



Immunohistochemistry	Nutlin Experiments	Nutlin + PPP experiment	MDM4 f/f experiments
<b>Primary antibodies</b>			
Antigen / Target	Fibronectin	5-HT	Ctip2
Vendor	Sigma-Aldrich	Immunostar	Abcam
Catalogue number	F3648	20080	AB18465
Species	Rabbit	Rabbit	Rat
Clonality	Polyclonal	Polyclonal	Monoclonal
lot #		1131001	
Antigen / Target	GFAP		GFAP
Vendor	Millipore		Millipore
Catalogue number	AB5804		AB5804
Species	Rabbit		Rabbit
Clonality	Polyclonal		Polyclonal
lot #	NG1817590		NG1817590
Antigen / Target	5-HT		
Vendor	Immunostar		
Catalogue number	20080		
Species	Rabbit		
Clonality	Polyclonal		
lot #	1131001		

<b>IMAGING</b>	<b>Nutlin experiments</b>	<b>Nutlin + PPP experiment</b>	<b>MDM4 f/f experiments</b>
Live Cell Imaging	No	No	No
Immunostaining	Yes	Yes	Yes
Imaging Format:	.zvi	.zvi	.zvi
Imaging method:	Fluorescence and bright field	Fluorescence and bright field	Fluorescence
<b>Microscope Manufacture</b>	<b>Zeiss</b>	<b>Zeiss</b>	<b>Zeiss</b>
Microscope Name	Axioplan 2 with Axiophot 2	Axioplan 2 with Axiophot 2	Axioplan 2 with Axiophot 2
Microscope model	Light microscope	Light microscope	Light microscope
Were constant image acquisition standards used	Yes	Yes	Yes
<b>Camera Manufacture 1</b>	<b>Zeiss</b>	<b>Zeiss</b>	<b>Zeiss</b>
Camera type	CCD	CCD	CCD
Camera Model	AxioCam MRm	AxioCam MRm	AxioCam MRm
Pixel binning	Yes	Yes	Yes
<b>Camera Manufacture 2</b>	<b>MBF Bioscience</b>		<b>MBF Bioscience</b>
Camera Type	Legacy with IIDC interface protocol		Legacy with IIDC interface protocol
Camera Model	MBF CX9000		MBF CX9000
Pixel binning	No		No
<b>Microscope Incubator</b>	<b>Not applicable</b>	<b>Not applicable</b>	<b>Not applicable</b>

<b>IMAGING</b>	<b>Nutlin experiments</b>	<b>Nutlin + PPP experiment</b>	<b>MDM4 f/f experiments</b>
<i>Imaging</i>			
Observer blinded to treatment?	Yes	Yes	
<b>Image Analysis 1</b>	<b>AxioVision</b>	<b>AxioVision</b>	<b>AxioVision</b>
Software Vendor	Zeiss	Zeiss	Zeiss
Software Package Name	AxioVision 4.8.1 (11-2009)	AxioVision 4.8.1 (11-2009)	AxioVision 4.8.1 (11-2009)
Software Package release Number	AxioVs40 V 4.8.1.0	AxioVs40 V 4.8.1.0	AxioVs40 V 4.8.1.0
Parameters Captured	CST-labelled and 5HT-stained axons and sprouts/GFAP labelled astrocytes/amorphous substance labelled with fibronectin at the injury site	5HT-stained axons and sprouts	CST-labelled axons and sprouts
Features studied	Axons and sprouts/injury site area and morphology	Axons and sprouts/injury site area and morphology	Axons and sprouts
Neurite length, #, branching, density	Not applicable	Not applicable	Not applicable
Velocity of neurite growth or retraction	No	No	No
Varicosities in synapse formation	No	No	No
Neurite thickness	No	No	No
Criteria of cell selection/analysis		Morphology: axons above the lesion are homogeneous and run parallel to each other in the tract; sprouts follow an irregular and random course.	
Biased/unbiased	Unbiased	Unbiased	
Sholl Analysis	No	No	No
Are neurites touching?	Not applicable	Not applicable	Not applicable
<b>Image Analysis 2</b>	<b>Stereo Investigator</b>		<b>Stereo Investigator</b>
Software Vendor	MBF Bioscience		MBF Bioscience
Software Package Name	Stereo Investigator 7		Stereo Investigator 7
Software Package release Number	Stereo Investigator 7.50.4		Stereo Investigator 7.50.4
Parameters Captured	CST axons and sprouts		CST axons and sprouts
Features studied	Axons and sprouts counted live		Axons and sprouts counted live

<b>IMAGING</b>	<b>Nutlin experiments</b>	<b>Nutlin + PPP experiment</b>	<b>MDM4 f/f experiments</b>
Neurite length, #, branching, density	Not applicable		Not applicable
Velocity of neurite growth or retraction	No		No
Varicosities in synapse formation	No		No
Neurite thickness	Not applicable		Not applicable
Criteria of cell selection/analysis	Morphology: axons above the lesion are homogeneous and run parallel to each other in the tract; sprouts follow an irregular and random course.		Morphology: axons above the lesion are homogeneous run and parallel to each other in the tract; sprouts follow an irregular and random course.
Criteria of cell selection/analysis			
Biased/unbiased			
Biased/unbiased	Unbiased		Unbiased
Sholl Analysis	No		No
Are neurites touching?	Not applicable		Not applicable

<b>BEHAVIOR</b>	<b>Nutlin experiments</b>	<b>Nutlin + PPP experiment</b>
History of Training	Animal handling once a day for 7 days. Animal acclimatization once a day for another 7 days.	Animal handling once a day for 7 days. Animal acclimatization once a day for another 7 days.
Frequency of testing	1 day before injury, then 1, 3, 7, 14, 21, 18 and 35 days after injury	1 day before injury, then 1, 3, 7, 14, 21, 18 and 35 days after injury
Devices	Basso open field platform for BMS, grid walk	Basso open field platform for BMS
Time of day	Morning	Morning
Observers blinded to treatments?	Yes	Yes
<b>Analgesics</b>	Yes	Yes
Kind of analgesic	Opioid or NSAID	Opioid or NSAID
Dose	0,05-0,1 mg/Kg or 5 mg/Kg, respectively	0,05-0,1 mg/Kg or 5 mg/Kg, respectively
Frequency	12/12 h or once day, respectively	12/12 h or once day, respectively
When relative to testing	Always after testing	Always after testing
<b>Hydration administered during behavioral testing</b>	Yes	Yes
Kind	0,9% saline solution	0,9% saline solution
Amount	1 ml	1 ml
Frequency	1 ml 12/12 h until 2 <sup>nd</sup> DPO, 1 ml once daily 3 <sup>rd</sup> -5 <sup>th</sup> DPO. 1 ml daily if signs of bladder infection (i.e. purulent or bloody urine)	1 ml 12/12 h until 2 <sup>nd</sup> DPO, 1 ml once daily 3 <sup>rd</sup> -5 <sup>th</sup> DPO. 1 ml daily if signs of bladder infection (i.e. purulent or bloody urine)
When relative to testing	Always after testing	Always after testing
<b>Antibiotics</b>	Yes	Yes
Kind	Fluoroquinolone	Fluoroquinolone
Amount	5 mg/Kg (prophylactic) or 10 mg/Kg (therapeutic)	5 mg/Kg (prophylactic) or 10 mg/Kg (therapeutic)
Frequency	Once a day	Once a day
When relative to testing	Always after testing	Always after testing

<b>Behavior</b>	<b>Nutlin experiments</b>	<b>Nutlin + PPP experiment</b>
<i>Motor</i>		
<b>Basso, Beattie, Bresnahan Locomotor Rating Scale (BBB) for rats</b>	<b>No</b>	<b>No</b>
<b>Basso Mouse Scale</b>	<b>Yes</b>	<b>Yes</b>
BMS subscore	Yes	Yes
<b>Raters</b>		
Paired	Yes	Yes
Discussion	Yes	Yes
Interrater correlation	Not calculated	Not calculated
Training certification	Yes	Yes
If certified, when relative to testing	One year before the tests were started	One year before the tests were started
<i>Gait Analysis</i>	<b>No</b>	<b>No</b>
<i>Sensory</i>	<b>No</b>	<b>No</b>
<i>Cognitive</i>	<b>No</b>	<b>No</b>
<i>Autonomic</i>	<b>No</b>	<b>No</b>

EXPERIMENTAL DESIGN, DATA ANALYSIS, STATISTICS	Nutlin experiments	Nutlin + PPP experiment	MDM4 f/f experiments
How and when were investigators blinded to experimental treatments?	The surgeon, the behavior raters and the researchers that performed histological analysis were blinded to the pump content (i.e. Nutlin-3a or vehicle)	The surgeon, the behavior raters and the researchers that performed histological analysis were blinded to the syringe content (i.e. PPP or vehicle)	
<b>Number of independent experiments for a study</b>	3	3	2
What does independent mean?	Different days	Different days	Different days
<b>Technical replicates</b>	1	None	1
What is a technical replicate?	Different animals and days		Different animals and days
Was primary outcome measure set prior to start of study?	Yes	Yes	Yes
Describe the prospective analysis plan	To study a continuous response variable such as behavioral testing (BMS and grid walk) from matched pairs with prior data indicating a standard deviation 1, we will need to study 13 pairs of subjects to be able to reject the null hypothesis that this response difference is zero with probability (power) 0,9 and a significant p-value of 0,05 for a mean difference of 1. Performed with the software PS Power and Sample Size Calculations 3.1.2 ( <a href="http://biostat.mc.vanderbilt.edu/PowerSampleSize">http://biostat.mc.vanderbilt.edu/PowerSampleSize</a> ).	To study a continuous response variable such as behavioral testing (BMS) from matched pairs with prior data indicating a standard deviation 1, we will need to study 7 pairs of subjects to be able to reject the null hypothesis that this response difference is zero with probability (power) 0.9 and a significant p-value of 0.05 for a mean difference of 1.5. Performed with the software PS Power and Sample Size Calculations 3.1.2 ( <a href="http://biostat.mc.vanderbilt.edu/PowerSampleSize">http://biostat.mc.vanderbilt.edu/PowerSampleSize</a> ).	To study a variable such as histological sprouting from matched pairs with prior data indicating a standard deviation 0,75, we will need to study 4 pairs of subjects to be able to reject the null hypothesis that this response difference is zero with probability (power) 0,9 and a significant p-value of 0,05 for a mean difference of 2. Performed with the software, PS Power and Sample Size Calculations 3.1.2 ( <a href="http://biostat.mc.vanderbilt.edu/PowerSampleSize">http://biostat.mc.vanderbilt.edu/PowerSampleSize</a> ).

Experimental Design, Data Analysis, Statistics	Nutlin experiments	Nutlin + PPP experiment	MDM4 f/f experiments
Statistical tests: what tests were used	Two-way ANOVA with Sidak multiple comparison post-tests (behavior) and One-way ANOVA with multiple comparison Tukey post-tests (histology/sprouting fibers).	Two-way ANOVA with Sidak multiple comparison post-tests (behavior) and One-way ANOVA with multiple comparison Tukey post-tests (histology/sprouting fibers).	One-way ANOVA with multiple comparison Tukey post-tests (sprouting fibers).
Normalization methods	The number of corticospinal tract sprouts was normalized to the number of labeled axons rostral to the lesion.		The number of corticospinal tract sprouts was normalized to the number of labeled axons rostral to the lesion.
Positive and negative controls	Negative controls: 8,6% pure ethanol in PBS	Negative controls: 10% DMSO in cottonseed oil	Negative controls: AAV1-GFP virus injected in the sensorimotor cortex



<i>Primers sequences</i>		
Gene	Primer forward	Primer Reverse
p21	CGGTGGAACCTTTGACTTCGT	AGAGTGCAAGACAGCGACAA
GADD45	CAGGGGAGGGACTCGCACTT	CGGGGTCTACGTTGAGCAGC
GAP43	AAGCTACCACTGATAACTCCCC	CTT CTTTACCCTCATCCTGTCTG
SCG10	AGACTCCTCTCTCGCTCTCTCCGC	AGCCTCTTGAGACTTTCTTCGCTCCTC
CAP23	GGCGGCAGCGCTCCAACCTCG	CCGCCTGGGGTTTCGCTCTCC
p53	AGAGACCGCCGTACAGAAGA	CTGTAGCATGGGCATCCTTT
MDM4	CAGCTAGGAGGGGGAGCGACT	GCAGTTTTGGCCGCACCTGACTAA
$\beta$ -actin	CTCTCSGCTGTGGTGGTGAA	AGCCATGTACGTAGCCATCC
L1CAM	ATGCTGCGGTACGTGTGGCCCT	CCACTTGGGGGCACCCTCGG
BDNF	AGTCTCCAGGACAGCAAAGC	TCGTCAGACCTCTCGAACCT
Sprr1a	CCCCTCAACTGTCACTCCAT	CAGGAGCCCTTGAAGATGAG
18S RNA	CTCAACACCGGGAAACCTCAC	CGCTCCACCAACTAAGAACG
$\beta$ -actin	CTCTCSGCTGTGGTGGTGAA	AGCCATGTACGTAGCCATCC
RPL13a	GGCTGAAGCCTACCAGAAAG	TTCTCCTCCAGAGTGGCTGT

**Supplementary Table 5.** List of primer sequences

ARTICLE

Received 13 Dec 2013 | Accepted 27 Feb 2014 | Published 1 Apr 2014

DOI: 10.1038/ncomms4527

# PCAF-dependent epigenetic changes promote axonal regeneration in the central nervous system

Radhika Puttagunta<sup>1,\*</sup>, Andrea Tedeschi<sup>2,\*</sup>, Marilia Grando Sória<sup>1,3</sup>, Arnau Hervera<sup>1,4</sup>, Ricco Lindner<sup>1,3</sup>, Khizr I. Rathore<sup>1</sup>, Perrine Gaub<sup>1,3</sup>, Yashashree Joshi<sup>1,3,5</sup>, Tuan Nguyen<sup>1</sup>, Antonio Schmandke<sup>1</sup>, Claudia J. Laskowski<sup>2</sup>, Anne-Laurence Boutillier<sup>6</sup>, Frank Bradke<sup>2</sup> & Simone Di Giovanni<sup>1,4</sup>

Axonal regenerative failure is a major cause of neurological impairment following central nervous system (CNS) but not peripheral nervous system (PNS) injury. Notably, PNS injury triggers a coordinated regenerative gene expression programme. However, the molecular link between retrograde signalling and the regulation of this gene expression programme that leads to the differential regenerative capacity remains elusive. Here we show through systematic epigenetic studies that the histone acetyltransferase p300/CBP-associated factor (PCAF) promotes acetylation of histone 3 Lys 9 at the promoters of established key regeneration-associated genes following a peripheral but not a central axonal injury. Furthermore, we find that extracellular signal-regulated kinase (ERK)-mediated retrograde signalling is required for PCAF-dependent regenerative gene reprogramming. Finally, PCAF is necessary for conditioning-dependent axonal regeneration and also singularly promotes regeneration after spinal cord injury. Thus, we find a specific epigenetic mechanism that regulates axonal regeneration of CNS axons, suggesting novel targets for clinical application.

<sup>1</sup>Laboratory for NeuroRegeneration and Repair, Center for Neurology, Hertie Institute for Clinical Brain Research, University of Tübingen, 72076 Tübingen, Germany. <sup>2</sup>Department of Axonal Growth and Regeneration, German Center for Neurodegenerative Disease, 53175 Bonn, Germany. <sup>3</sup>Graduate School for Cellular and Molecular Neuroscience, University of Tübingen, 72076 Tübingen, Germany. <sup>4</sup>Division of Brain Sciences, Department of Medicine, Imperial College London, Hammersmith Campus, London W12 0NN, UK. <sup>5</sup>DZNE, German Center for Neurodegenerative Diseases, D-72076 Tübingen, Germany. <sup>6</sup>Laboratoire de Neurosciences Cognitives et Adaptatives (LNCA), Université de Strasbourg-CNRS, GDR CNRS, Strasbourg 67000, France. \*These authors contributed equally to this work. Correspondence and requests for materials should be addressed to R.P. (email: radhika.puttagunta@medizin.uni-tuebingen.de) or to S.D.G. (email: s.di-giovanni@imperial.ac.uk).

The regenerative response initiated following axonal injury in the peripheral nervous system (PNS) versus the central nervous system (CNS) leads to differential growth capacities and repair. In fact, the lack of pro-neuronal growth gene expression and glial inhibitory signals leads to regenerative failure following CNS but not PNS injury<sup>1–4</sup>. Immediately after a peripheral nerve injury, rapid ion fluxes increase, followed by a rise in cAMP levels, axonal translation occurs, phosphorylation retrograde cascades activate transcription factors, gene expression is induced and finally regeneration occurs<sup>5,6</sup>. However, the final link between axonal injury-induced retrograde signalling and the regulation of essential regenerative gene expression remains elusive. The dorsal root ganglia (DRG) sensory neurone system has a central as well as a peripheral axonal branch departing from a single cell body. This allows for bimodal injury inputs with differing regenerative capacities into one central transcriptional hub. Interestingly, the lack of regeneration of injured ascending sensory fibres in the spinal cord can be partially enhanced by an injury to the peripheral branch (conditioning lesion) of DRG neurones<sup>7</sup>. In search of key regulatory mechanisms that may clarify the molecular nature of this regenerative gene expression programme, we hypothesized that as an ‘orchestrator of gene regulation’ epigenetic changes would direct expression of genes crucial for regeneration only in the presence of pro-regenerative signalling following peripheral but not central damage.

Identification of a specific regulatory mechanism shared by several essential genes may lead to novel molecular strategies recapitulating the conditioning effect, thus non-surgically enhancing axonal regeneration in the CNS. To this end, we employed the first systematic approach to understand the epigenetic environment in DRG neurones. We examined both DNA methylation and various key histone modifications with regards to gene regulation following axonal injury. We found that p300/CBP-associated factor (PCAF)-dependent acetylation of histone 3 lysine 9 (H3K9ac), paralleled by a reduction in methylation of H3K9 (H3K9me2), occurred at the promoters of select genes only after PNS axonal injury. In addition, we observed that extracellular signal-regulated kinase (ERK) axonal retrograde signalling is required for PCAF-dependent acetylation at these promoters and for their enhancement in gene expression. Finally, we established that PCAF is required for regeneration following a conditioning lesion and PCAF overexpression promotes axonal regeneration similar to that of a conditioning lesion after CNS injury in spinal ascending sensory fibres. Our results show the first evidence of immediate retrograde signalling leading to long-term epigenetic reprogramming of gene expression of select genes whose modulation leads to axonal regeneration in the hostile spinal environment.

## Results

**Histone codes are shaped by a peripheral not by a central lesion.** Given that epigenetic changes are a rapid and dynamic way to translate external stimuli into targeted and long-lasting gene regulation, such has been observed in learning and memory, seizures, stroke and neuronal differentiation<sup>8–11</sup>, we hypothesized that retrograde signals following axonal injury could lead to an epigenetic environmental shift facilitating the expression of genes critical to regeneration. We believed that a positive retrograde signal initiated by PNS injury could relax the chromatin environment surrounding specific promoters and allow for gene expression; however, a negative signal following CNS injury may restrict promoter accessibility and inhibit gene expression. Following equidistant CNS (dorsal column axotomy, DCA) or PNS (sciatic nerve axotomy, SNA) axotomies, from L4–L6 DRG we assessed both high-throughput promoter

and CGI DNA methylation (DNA methylation microarrays) and histone modifications (quantitative chromatin immunoprecipitation (ChIP) assays) at the proximal promoters of genes previously established to be critical to regeneration such as growth-associated protein 43 (GAP-43)<sup>12</sup>, Galanin<sup>13</sup> and brain-derived neurotrophic factor (BDNF)<sup>14,15</sup> (Fig. 1a).

DNA methylation arrays showed a modest number of genes differentially methylated between injuries (Supplementary Fig. 1a–e); however, none of the genes associated with regeneration displayed significant levels of methylation nor were they differentially methylated between SNA and DCA (Supplementary Fig. 2a). More importantly, and as opposed to a recent study investigating folate and its DNA methylation after sciatic and spinal injury<sup>16</sup>, quantitative RT-PCR analysis of the differentially methylated genes, and DNA methyltransferases did not show a consistent correlation between DNA methylation levels and gene expression (Supplementary Figs 2b–e and 3). Therefore, promoter and CGI DNA methylation does not appear to be a key factor in the differential regenerative response between CNS and PNS injuries in the DRG system.

Next, we investigated whether key histone modifications would be specifically enriched on established critical genes for the regenerative programme in DRG neurones. Of all histone modifications that correlate with active gene transcription (H3K9ac, H3K18ac, H3K4me2)<sup>17</sup> or gene repression (H3K9me2 and H3K27me3)<sup>17</sup> that were screened, H3K9ac, H3K9me2 and H3K27me3 were enriched compared with IgG on most promoters; however, only H3K9ac and H3K9me2 were found to be differentially enriched at *GAP-43*, *Galanin* and *BDNF* promoters, consistently correlating with early and sustained increased expression following SNA (1–7 days; Figs 1b,c and 2a–d; Tables 1 and 2). Additionally, these three genes presented common promoter motifs in CpG content as well as transcription-binding sites that together with increased H3K9ac at their promoters suggest common transcriptional regulation (Fig. 1b,c). H3K9ac and the H3K9ac-specific acetyltransferase, PCAF, are typically found in the proximity of transcriptional start sites of actively transcribing genes<sup>17</sup>, and accordingly PCAF was also enriched at these promoters (Fig. 1c). Interestingly, H3K9me2, which is associated with gene silencing<sup>17</sup>, was found to be decreased at these promoters and inversely correlated to gene expression following SNA (Fig. 1c). In contrast, *SCG-10*, whose gene expression is unaltered after 24 h and only modestly increased following 3- and 7-day SNA (Fig. 1b), did not show an enhancement of H3K9ac or PCAF at its promoter (Fig. 1c). Given that a preconditioning lesion (SNA preceding DCA) activates the regenerative capacity of the CNS<sup>7</sup>, we questioned whether a PNS epigenetic signal overrides a CNS signal. We observed an increase in the gene expression of these genes following preconditioned DCA versus DCA alone, which correlated with an increase in PCAF at these promoters (Fig. 1d,e). Furthermore, a broader picture of post-axotomy gene expression profiles and H3K9ac promoter enrichment is depicted by regeneration-associated (*Chl1*, *L1cam*, *SPRR1a*)<sup>18</sup>, axonal growth (*ATF3* and *Bcl-xL*)<sup>19,20</sup> housekeeping (*ribosomal unit 18S*) genes and axonal structure (*NF-L*) genes<sup>21</sup> (Fig. 2a,b). Importantly, these experiments show that H3K9ac, a marker of actively transcribing genes, is selectively enriched on the promoters of *GAP-43*, *Galanin* and *BDNF*, but not on the promoters of other SNA-induced genes such as *SPRR1a*, *ATF3* and *HSP27* (Fig. 2a–d; Table 1), suggesting that their common regulation maybe linked to their importance in regeneration.

**NGF-MEK-ERK signalling regulates PCAF and H3K9ac.** Next, we turned our attention to understanding whether retrograde signalling following SNA plays a role in this positive chromatin

remodelling. Immediately following peripheral injury, pERK levels rise in the injured axon and ERK signalling modules are retrogradely transported to the DRG cell body<sup>22,23</sup>, where we show that global PCAF and H3K9ac levels rise (Fig. 3a–c). In adult primary DRG neuronal cultures, nerve growth factor (NGF), an activator of ERK signalling and neurite outgrowth<sup>24</sup>, increased the expression of PCAF and H3K9ac, while the ERK kinase (MEK) inhibitor, PD98059 (PD), prevented PCAF and H3K9ac induction<sup>25</sup> (Fig. 4a,b). NGF induces PCAF expression, nuclear localization and activation of acetyltransferase activity specifically by threonine phosphorylation at its histone acetyltransferase domain<sup>26</sup>. In L4-L6 DRG, SNA induced the expression of nuclear PCAF and PCAF threonine but not serine

phosphorylation (Fig. 4c,d). This correlated with an increase in pERK in DRG, as well as nuclear PCAF translocation and acetylation of H3K9, all of which are dependent on ERK activation following SNA (Fig. 4e–i). As predicted, inhibition of ERK activation following SNA decreased gene expression as well as PCAF and H3K9ac at the promoters of *GAP-43*, *Galanin* and *BDNF* (Fig. 4j–l). However, in conjunction with our theory of specificity of regulation, H3K9ac did not correlate with gene expression at other promoters following inhibition of ERK activation (Supplementary Fig. 4a,b). Remarkably, cAMP signalling in adult DRG neuronal cultures did not induce nuclear PCAF translocation (Supplementary Fig. 5), suggesting that cAMP-mediated mechanisms only partially supporting

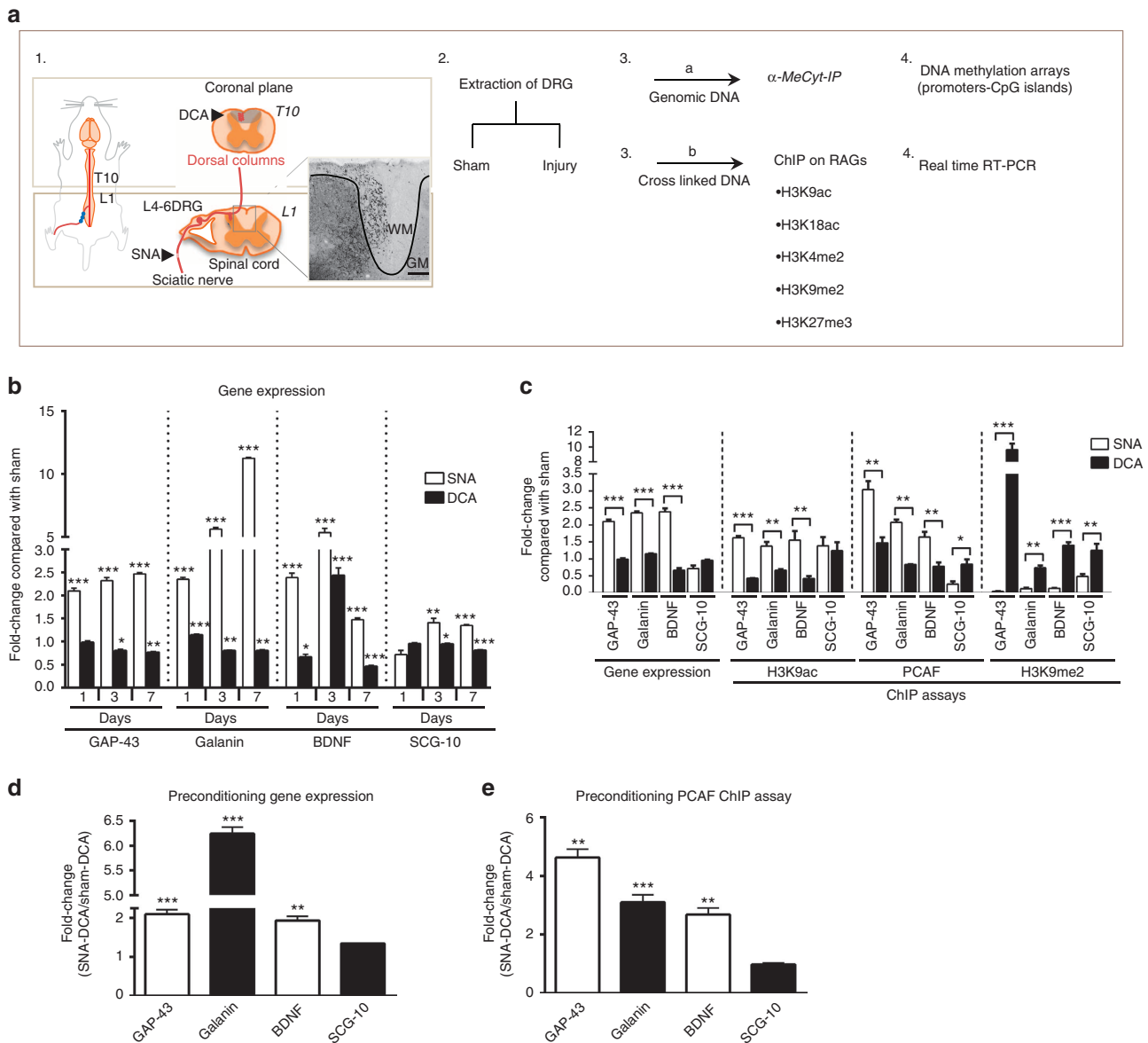


**Figure 1 | H3K9ac and PCAF involvement in the regulation of regeneration genes.** (a) Schematic diagram of SNA and DCA injury models used for epigenetic screens involving DNA methylation arrays and quantitative ChIP assays from L4-L6 DRG. Scale bar, 100  $\mu$ m. (b) Fold change increases observed in *GAP-43*, *Galanin* and *BDNF* gene expression at 1, 3 and 7 days post SNA but not DCA and at 3 and 7 days for *SCG-10*. (c) Increased gene expression, H3K9ac, PCAF and decreased H3K9me2 at *GAP-43*, *Galanin* and *BDNF*, but not *SCG-10* (*SCG-10* had decreased H3K9me2 enrichment to a lesser extent) promoters following 1 day post-SNA versus DCA. (d) A preconditioning lesion performed 1 week before DCA still induced 24 h later gene expression of *GAP-43*, *Galanin* and *BDNF* but not *SCG-10*. (e) This correlated with an increase in PCAF at the promoters of activated regeneration genes. Q-PCR. (b,c)  $N = 3$  per group; ChIP assays (c–e)  $N = 6$  per group, Student's  $t$ -test, error bars, s.e. \* $P < 0.05$ , \*\* $P < 0.01$ , \*\*\* $P < 0.001$ . All experiments were performed in triplicate.

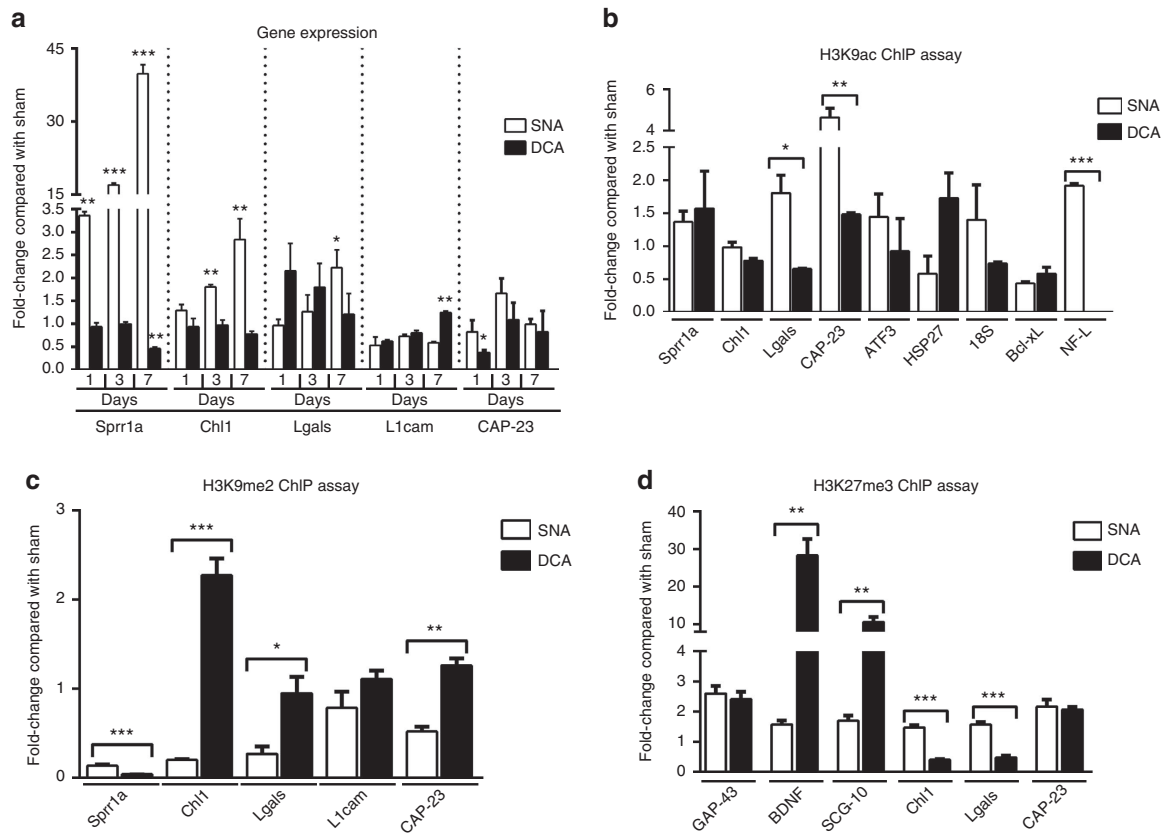


**Figure 2 | Histone modifications that do not correlate with gene expression.** (a) Gene expression of genes associated with regeneration found to be induced (*Sprr1a* and *Chl1*) or not changed (*Lgals*, *L1cam* and *CAP-23*) at various timepoints. (b) H3K9ac ChIP assays at the promoters of several genes previously found to be either induced (*Sprr1a*, *HSP27* and *ATF3*), unchanged (*Chl1* and *18S*) or repressed (*Bcl-xL* and *NF-L*) in gene expression 24 h post SNA only showed a correlation between expression and H3K9ac promoter occupancy for *Bcl-xL*. No enrichment to IgG was found for *L1cam* promoter. (c) ChIP assay for H3K9me2 24 h post SNA and DCA compared with Shams shows no correlation with 24-h gene expression time point for *Sprr1a*, *Chl1*, *Lgals* and *CAP-23*, but for *L1cam* there is no change observed, which is in agreement with no change in gene expression. (d) No consistent pattern of correlation with gene expression was found with H3K27me3 24 h post SNA by ChIP assay. No enrichment was found compared with IgG for *L1cam* and *Galanin*. (ChIP assays,  $N = 6$  per group, performed in triplicate). Error bars, s.e. (a,c,d) Student's  $t$ -test, \* $P < 0.05$ , \*\* $P < 0.001$  and \*\*\* $P < 0.001$ .

**Table 1 | Correlation between gene expression and H3K9ac ChIP data.**

		H3K9ac at promoters		
		Increase	No change	Decrease
Gene expression	Increase	BDNF, Galanin, GAP-43		<i>Sprr1a</i>
	No change	CAP-23		<i>SCG-10</i> , <i>Chl1</i> , <i>L1cam</i> , <i>18S</i> , <i>Lgals</i>
	Decrease	NF-L		<i>Bcl-xL</i>

BDNF, brain-derived neurotropic factor; ChIP, chromatin immunoprecipitation; H3K9ac, acetylation of histone 3 lysine 9. A table displaying our gene expression data for genes associated with regeneration or known data for control genes and our H3K9ac ChIP data at their promoters, showing a clear correlation between increased gene expression and H3K9ac at the promoters of the genes BDNF, Galanin and GAP-43.

**Table 2 | Enrichment of histone modifications over IgG.**

Histone modifications	Enrichment compared with IgG
H3K9ac	Yes
H3K18ac	No
H3K4me2	No
H3K9me2	Yes
H3K27me3	Yes

Of the histone modifications examined, those shown in the table in white are inducers and those in grey are repressors of gene expression. Two of the histone modifications screened for this study, H3K18ac and H3K4me2, did not show enrichment compared with IgG for any of the genes examined.

conditioning-dependent axonal regeneration<sup>27</sup> operate independently from pERK-induced epigenetic PCAF-mediated long-term mechanisms. These data present the first link between retrogradely transported PNS-injury-related signals and epigenetic modifications at the promoters of specific established regenerative genes.

**PCAF supports axonal regeneration mimicking a conditioning lesion.** As a preconditioning lesion is able to induce neurite outgrowth in primary adult DRG neurones cultured on permissive (laminin) or non-permissive (myelin) substrates<sup>28</sup>, we tested whether increased PCAF expression by adeno-associated virus



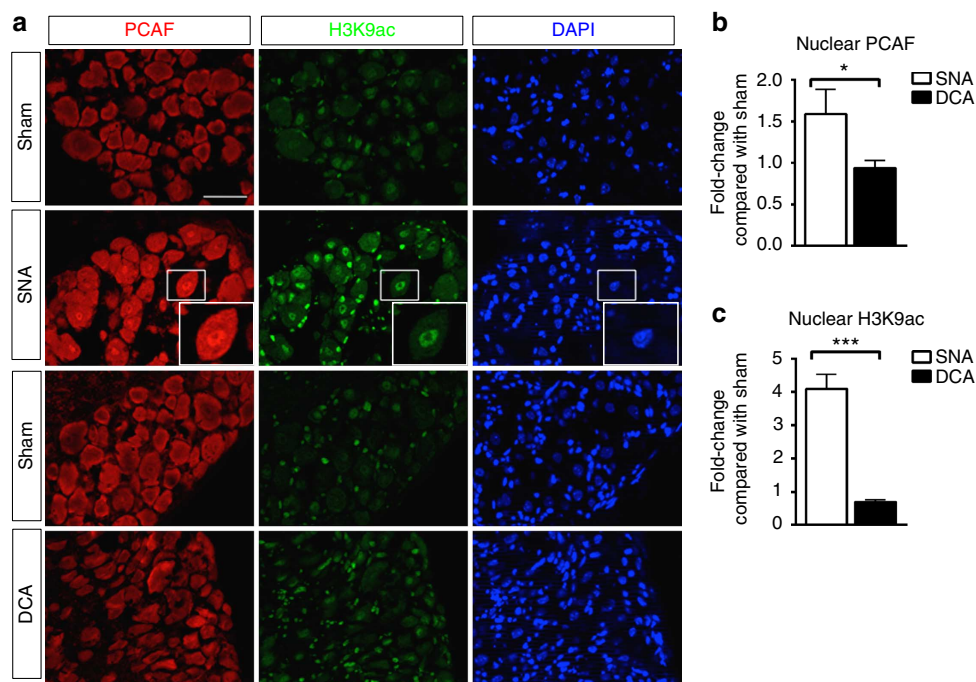


**Figure 3 | Increased nuclear PCAF and H3K9ac following SNA but not DCA.** (a) IHC co-staining with PCAF and H3K9ac of L4-L6 DRG following Sham/SNA or Sham/DCA. Insert shows high nuclear expression of PCAF and H3K9ac after SNA. Scale bar, 50  $\mu$ m. (b) IHC intensity density analysis reveals an increase in nuclear PCAF following SNA/Sham but not DCA/Sham. (c) Intensity density analysis of IHC stained with H3K9ac reveals a significant fold increase following SNA but not DCA when compared with respective Sham. Student's *t*-test, error bars, s.e., \**P* < 0.05, \*\*\**P* < 0.001, *N* = 3 per group, performed in triplicate.

(AAV, Supplementary Fig. 6a–c) could also drive neurite outgrowth. Indeed, neurite outgrowth increased on laminin and myelin by PCAF overexpression in DRG (Fig. 5a,b) as well as another CNS primary culture, cerebellar granule neurones (CGN, Supplementary Fig. 7a). In CGN (employed for its ease of culture and greater cell number for use in immunoblotting, ChIP and transfections for luciferase assays) there was a significant decrease in H3K9ac when plated on myelin (Supplementary Fig. 7b,c) and a reduction of H3K9ac at select promoters, which was reverted to permissive levels with overexpression of PCAF (Supplementary Fig. 7d). Likewise, PCAF overexpression reversed myelin repression of select genes in DRGs (Fig. 5c). Furthermore, the drug Garcinol (5  $\mu$ M), which inhibits PCAF acetyltransferase activity<sup>29</sup>, reduced neurite outgrowth in DRG (Fig. 5d,e) and CGN (Supplementary Fig. 7e,f), decreased the luciferase expression of a *GAP-43* promoter luciferase construct in CGN (Supplementary Fig. 7g) and decreased select gene expression in DRG (Fig. 5f). In *ex vivo* experiments, the inhibition of PCAF activity by Garcinol was able to significantly limit neurite outgrowth on both laminin and myelin as well as repress H3K9ac induced by SNA (Fig. 5g–i). Correspondingly, *PCAF*<sup>−/−</sup> mice provided full abolishment of neurite outgrowth induced by SNA in *ex vivo* cultured DRG neurones (Fig. 5j,k). Additionally, SNA-dependent neurite outgrowth in *ex vivo* cultured DRG neurones was blocked by ERK inhibition via delivery of PD at the nerve stump (Fig. 6a–c), phenocopying PCAF loss of function experiments.

Thus far our data suggest that PCAF is integral to the signalling involved following PNS injury leading to regeneration by altering the epigenetic landscape and stimulating intrinsic competence through crucial gene expression. To validate these observations *in vivo*, we studied regeneration of ascending sensory fibres following a preconditioning lesion (SNA 7 days before DCA) in the absence of PCAF and found that PCAF is required for

regeneration induced by a conditioning lesion and for the expression of *GAP-43*, *Galanin* and *BDNF* in DRG (Fig. 7a–g). Importantly, axonal tracing in SCI experiments in a cohort of *PCAF*<sup>−/−</sup> mice and strain-matched controls showed that *PCAF*<sup>−/−</sup> mice did not display any abnormalities or overt phenotype in axonal tracing or regarding the lesion site (Fig. 7a).

Next, we wondered whether PCAF overexpression alone would mimic regeneration induced by a conditioning lesion and enhance regeneration of ascending sensory fibres in the spinal cord following dorsal column lesion. Indeed, similar to that previously reported for a preconditioning lesion<sup>7,30</sup>, PCAF overexpression (Supplementary Fig. 8) significantly increased the number of regenerating fibres across the lesion and up to a distance of 1 mm rostral of the lesion site (Fig. 8a–c and Supplementary Fig. 9). Important to note, the depth of the lesion (Supplementary Fig. 10) and lack of tracing rostral to the lesion site (Supplementary Fig. 11) allowed excluding the presence of spared fibres. Furthermore, the introduction of the AAV directly into the sciatic nerve is in and of itself a PNS injury that does induce minimal sprouting towards the lesion in the GFP control.

## Discussion

Our work demonstrates that PCAF is required for conditioning-dependent spinal regeneration and that PCAF overexpression alone is able to promote regeneration of sensory fibres across the injured spinal cord and beyond similarly to previously established conditioning paradigms. Furthermore, PCAF-induced regeneration correlated with a significant increase in the expression of H3K9ac, *GAP-43*, *Galanin* and *BDNF* in the L4-L6 DRG. The definition of regeneration-associated genes (RAGs) is genes differentially induced between the regenerating PNS and non-regenerating CNS systems; however, this does not validate the

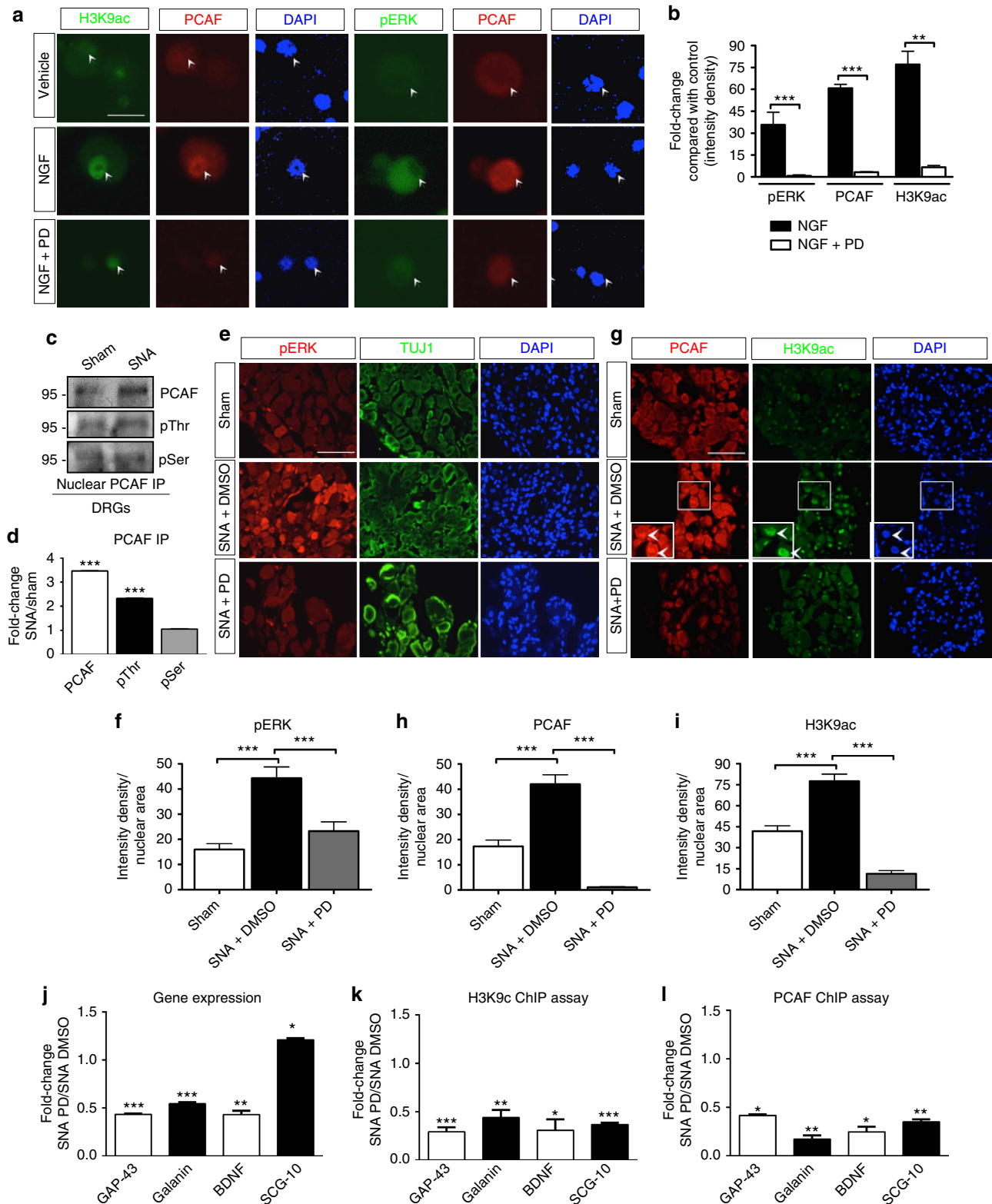


**Figure 4 | ERK retrograde signalling controls PCAF activation.** (a,b) NGF stimulates pERK, PCAF and H3K9ac expressions in adult DRG cultures after 3-h treatment, which is abrogated by the ERK kinase inhibitor PD98059 (PD), ICC (a) and fold change analysis of intensity density (b). Scale bar, 20  $\mu$ m,  $N=3$  per group, performed in triplicate. (c,d) Nuclear PCAF immunoprecipitation from *in vivo* L4-L6 DRG 24 h following Sham or SNA reveals an increase in PCAF expression and threonine phosphorylation following SNA but not serine phosphorylation, immunoblot (c) and fold change of density analysis (d).  $N=5$  per group, performed in triplicate. (e-i) In L4-L6 DRG, 24 h following SNA we observe an increase in pERK (e,f), PCAF (g,h) and H3K9ac (g,i) expression, which is significantly decreased by ERK inhibition with PD at the nerve stump. Insert shows high nuclear expression of PCAF and H3K9ac after SNA. Scale bars, 75  $\mu$ m,  $N=3$  per group, performed in triplicate. (j-l) PD also inhibits gene expression (Q-PCR,  $N=3$  per group) (j) as well as H3K9ac (k) and PCAF (l) at the promoters of GAP-43, Galanin and BDNF 24 h following SNA (ChIPs).  $N=6$  per group, performed in triplicate. Error bars, s.e. (b,f,h,i)  $P<0.0001$ , ANOVA, Bonferroni *post hoc* tests, \*\* $P<0.001$  and \*\*\* $P<0.001$ , (d,j-l) Student's *t*-test, \* $P<0.05$ , \*\* $P<0.001$  and \*\*\* $P<0.001$ . Original immunoblot images are shown in Supplementary Fig. 12.

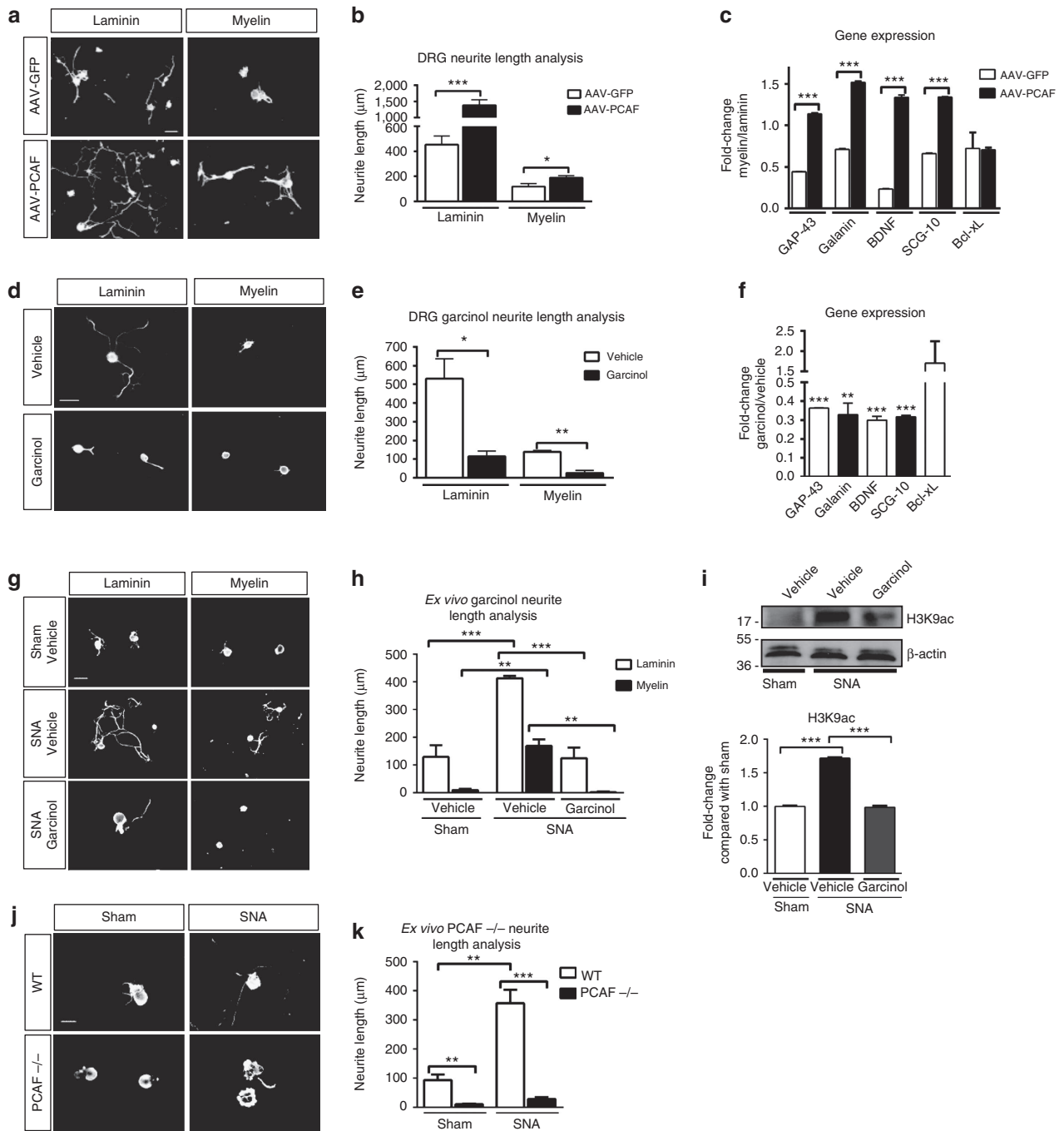


**Figure 5 | PCAF promotes neurite outgrowth *in vitro* and *ex vivo* following SNA. (a,b)** On both laminin and myelin substrates, adult DRG infected with AAV-PCAF (48 h) showed an increase in neurite outgrowth compared with AAV-GFP-infected DRG, ICC ( $\beta$ III Tubulin) **(a)** and average neurite length analysis **(b)**. Scale bars, 100  $\mu$ m. **(c)** Q-PCR fold changes of myelin/laminin 48-h post-AAV infection reveals inhibitory myelin-dependent reduction in gene expression of regeneration genes, which was restored by PCAF overexpression. **(d-f)** On laminin and myelin substrates, the PCAF activity inhibitor Garcinol (24 h) represses neurite outgrowth as well as the gene expression of regeneration genes, ICC ( $\beta$ III Tubulin) Scale bars, 50  $\mu$ m **(d)**, average neurite length analysis **(e)** and Q-PCR **(f-i)** Garcinol when applied intrathecally compared with Vehicle at the time of a conditioning lesion significantly repressed neurite outgrowth of the given lesion 24 h later in *ex vivo* cultures on both laminin and myelin substrates as well as the acetylation of H3K9, ICC ( $\beta$ III Tubulin). Scale bars, 50  $\mu$ m **(g)**, average neurite length analysis **(h)** and western blot and intensity analyses **(i)**. **(j,k)** In addition, neurite outgrowth in *ex vivo* cultures from PCAF  $-/-$  mice showed PCAF to be required for neurite outgrowth induced by a conditioning lesion, ICC ( $\beta$ III Tubulin). Scale bars, 50  $\mu$ m **(j)**, average neurite length analysis **(k)**. Error bars, s.e. **(b,c,e,h,i,k)**  $P < 0.0001$ , ANOVA, Bonferroni *post hoc* tests,  $*P < 0.05$ ,  $**P < 0.001$  and  $***P < 0.001$ . **(f)** Student's *t*-test,  $**P < 0.001$  and  $***P < 0.001$ ,  $N = 3-6$ , performed in triplicate. Original immunoblot images are shown in Supplementary Fig. 13.

entire class of genes as essential for immediate and sustained axonal regeneration. In support of this, our data show that PCAF-dependent regulation of *GAP-43*, *Galantin* and *BDNF* is at the essential core of the regenerative programme.

An immediate response to the external stimulus of a peripheral axonal injury is to seal the wound. This is followed by electrical impulses and calcium fluxes that are the first messages relayed from the lesion site to the cell body requesting assistance. Next, is



a rise in cAMP levels and phosphorylation signalling by multiple players involved in transmitting further information to the cell body<sup>5,6</sup>. Recently, it has been shown that calcium influx ejects histone deacetylase 5 (HDAC5) from the DRG nucleus correlating to increased global H3ac and gene expression<sup>31</sup>. It has been hypothesized that merely shifting the balance from a deacetylated to a globally acetylated chromatin environment by inhibition of HDACs could recapitulate the conditioning lesion and could lead to regeneration. However, recent experimental evidence<sup>32</sup> and our own work using HDAC class I and HDAC class I and II inhibitors<sup>33</sup> has proven this to be insufficient in producing post-lesion regeneration of sensory fibres following a spinal or optic nerve injury and therefore unlikely the key to unlocking the molecular mechanisms of regeneration. While our work here describes that specific epigenetic codes are induced endogenously following a conditioning lesion that leads to CNS regeneration, it is also consistent with previous findings from our laboratory that showed the presence of a transcriptional complex formed by p53, p300 and PCAF in the proximity of several RAGs including *GAP-43*, *Coronin 1b* and *Rab13* in primary neurones as well as facial motor neurones in a PNS facial nerve axotomy model<sup>34–36</sup>. Additionally, we found that the histone acetyltransferase p300 (which may form a complex with PCAF) is developmentally regulated in retinal ganglion cells and whose overexpression drives axonal regeneration of the injured optic nerve<sup>33</sup>.

While it is known that signals are sent via retrograde transport machinery<sup>23,37–39</sup>, how they are decoded into the gene expression of key axonal regeneration players for growth towards re-innervation of the lost target has not been known until now. Here, we have shown the first systematic study of various epigenetic modifications revealing specifically that increased H3K9ac and PCAF as well as decreased H3K9me2 at the promoters of *GAP-43*, *Galanin* and *BDNF* are due to retrogradely induced pERK activation of PCAF leading to essential gene activation, which is sufficient to mimic the regenerative response assembled by a conditioning lesion, thus driving regeneration in the CNS.

The fundamentals of decoding the regenerative retrograde signal by understanding the specific epigenetic changes that occur to chromatin surrounding essential genes is paramount in our ability to recapitulate this mechanism when the signal is lacking, such as after spinal cord injury (SCI). Here we take the first steps in this understanding that may lead to the design of epigenetic-related regenerative therapies for SCI patients.

## Methods

**Reagents.** PD 98059 (Calbiochem), Garcinol (Sigma-Aldrich), NGF (BD Biosciences) and dbcAMP (Enzo Life Sciences) were purchased from respective companies. The following antibodies were purchased and utilized, rabbit anti-PCAF (ab12188, Abcam), mouse anti-PCAF (E8, sc-13124, Santa Cruz Biotechnology), rabbit anti-AcH3K9 (no. 9671, Cell Signalling), rabbit anti-H3K9me2 (no. 9753, Cell Signalling), mouse anti-H3K27me3 (ab6002, Abcam), mouse anti-H3K4me2 (no. 9726, Cell Signalling), rabbit anti-H3K18ac (ab15823, Abcam), mouse anti-NeuN (MAB 377, Millipore), rabbit anti-phospho-Erk 1/2 (no. 9101, Cell Signalling), mouse anti-βIII tubulin (no. G712A, Promega), mouse β-actin (A2228, Sigma), rabbit anti-Phospho-Threonine (no. 600-403-263, Rockland), rabbit anti-Phospho-Serine (no. ADI-KAP-ST2103-E, Enzo Life Sciences), rabbit anti-MAP2 (sc20172, Santa Cruz Biotechnology), rat anti-Glial fibrillary acidic protein (GFAP) (no. 13-0300, Invitrogen), rabbit anti-BDNF (sc-546, Santa Cruz Biotechnology), rabbit anti-Galanin (T-4334, Bachem Peninsula Laboratories) and sheep anti-GAP-43 (no. NBP1-41123, Novus Biologicals).

**Mice.** All mice used for this work were treated according to the Animal Welfare Act and to the ethics committee guidelines of the University of Tübingen. Equally distributed male and female C57Bl6/J (bred from Charles River Laboratories), CD1 or CD1 PCAF  $-/-$  (generated in Dr Boutillier's laboratory) mice ranging from 6 to 8 weeks of age were used for all experiments. C57Bl6/J were used for all studies except those specifying PCAF null mice. For surgeries, mice were anesthetized with ketamine (100 mg kg<sup>-1</sup> body weight) and xylazine (10 mg kg<sup>-1</sup> body weight). For all experiments, we employed a target for the appropriate expected power calculation linked to an *ad hoc* statistical test.

**Dorsal column axotomy.** Surgeries were performed as previously reported<sup>40</sup>. Briefly, mice were anesthetized and a T10 laminectomy was performed (~20 mm from the L4-L6 DRGs), the dura mater was removed, taking care of not damaging the spinal cord. A dorsal hemisection until the central canal was performed with a microknife (FST). For the control laminectomy surgery, the dura mater was removed but the dorsal hemisection was not performed.

**Sciatic nerve axotomy.** Mice were anesthetized. At ~20 mm far from L4-L6 DRG, a 10-mm incision was performed on the gluteal region and muscles were displaced to expose the sciatic nerve for a complete transection with spring micro-scissors. For the PD study 30 s before transection, 2.5 μl of 100% DMSO or 2.0 μl of PD 98059 were slowly pipetted on the nerve. Finally, skin was closed with two suture clips. The nerve fibre was left uninjured in sham surgery.

**Methylated DNA immunoprecipitation from DRG ex vivo.** For each of the three time points (1, 3 and 7 days post SNA or DCA and naive), L4-L6 DRG were collected from two mice per time point and condition in triplicate for injury samples and naive, and in duplicate for shams. Frozen tissue was ground and digested with 0.2 mg ml<sup>-1</sup> Proteinase K. The lysate was then sonicated to average size of 700 bp and cleared of remaining tissue by centrifugation. Genomic DNA was extracted from the lysate via standard phenol-chloroform extraction and DNA precipitation protocols. MeDIP was then performed according to the manufacturer's protocol for the ChIP Kit from Upstate/Millipore. A total of 10 μg

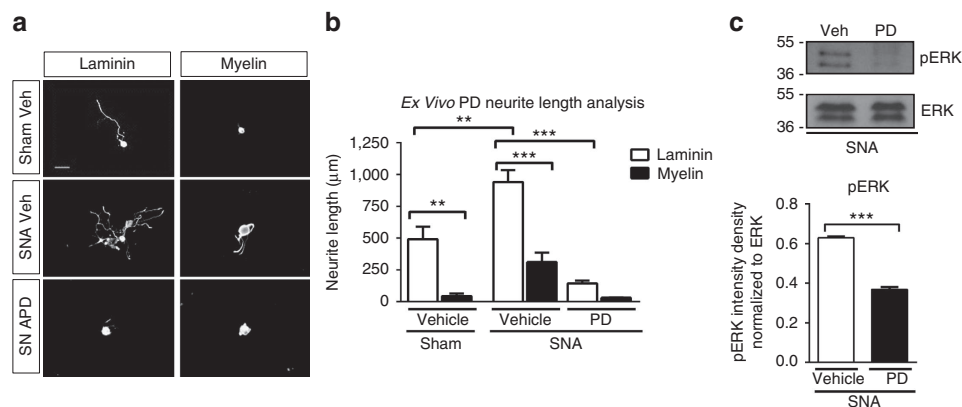


**Figure 6 | ERK kinase inhibition blocks neurite outgrowth after conditioning lesion.** (a–c) PD98059 when applied at the nerve stump compared with Vehicle at the time of a conditioning lesion or in Sham significantly repressed neurite outgrowth 12 h later in *ex vivo* cultures on both laminin and myelin substrates, ICC (βIII Tubulin). Scale bars, 50 μm (a), average neurite length analysis (b) and western blot and intensity analysis showing significant reduction in pERK after PD98059 delivery (c). (b)  $P < 0.0001$ , ANOVA, Bonferroni post hoc tests,  $**P < 0.001$  and  $***P < 0.001$ . (c) Student's *t*-test,  $***P < 0.001$ ,  $N = 3–6$ , performed in triplicate. Original immunoblot images are shown in Supplementary Fig. 14.

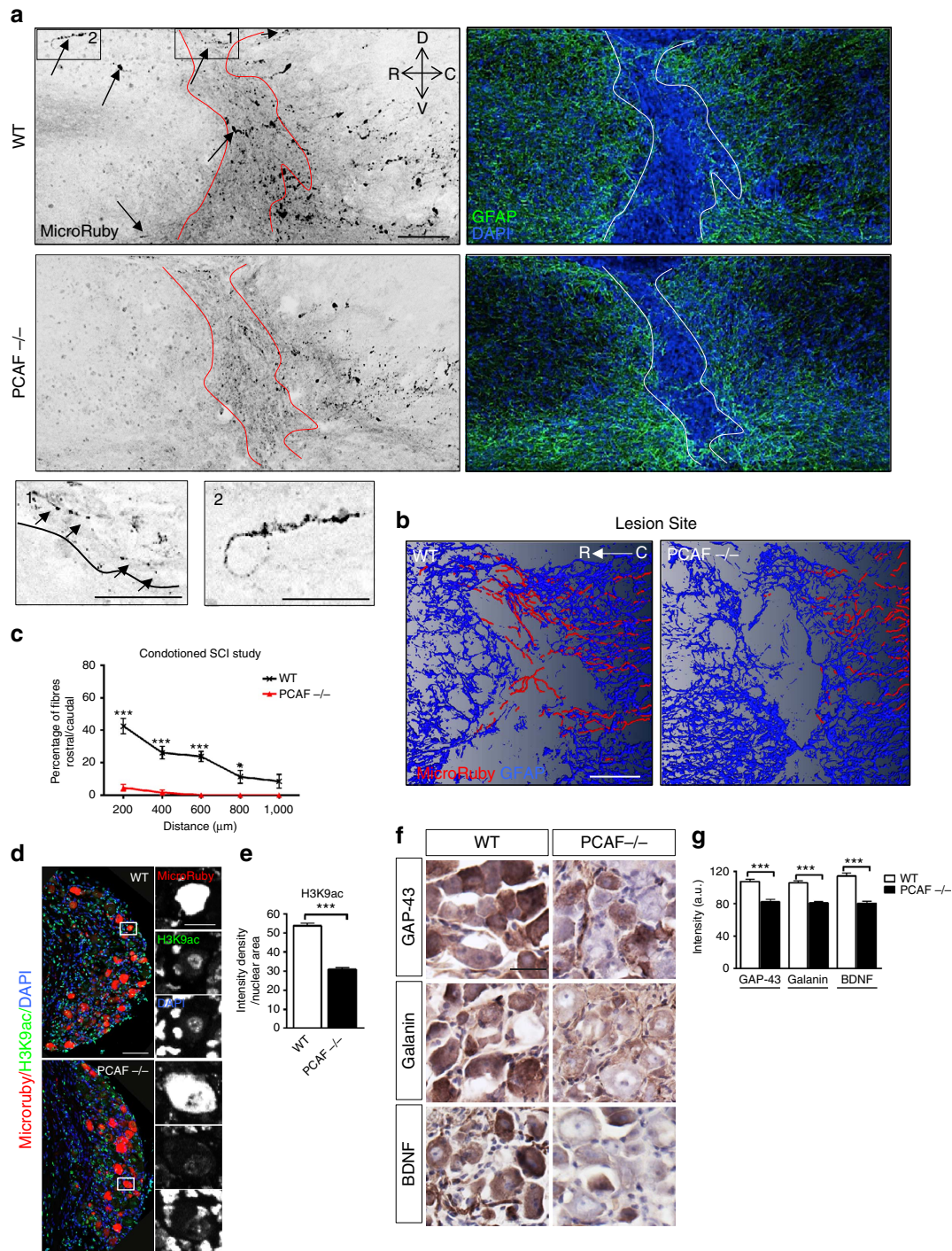


**Figure 7 | PCAF is required for conditioning-dependent axonal regrowth after SCI.** (a) MicroRuby tracing of the dorsal columns shows regenerating fibres invading into and past the lesion site (upper) in WT but not in PCAF<sup>-/-</sup> (lower) after conditioning injury (SNA followed by DCA; left panels). The red dotted lines indicate the lesion site. Insets (1 and 2) show higher magnification of regenerating axons. D-R-C-V: anatomical coordinates, dorsal-rostral-caudal-ventral. Right panels show the lesion site. Arrows indicate axonal sprouts. Scale bar, 100 µm. (b) Amira 3D reconstruction of regenerating dorsal column axons and glial scar in a sagittal projection (~25 µm) of the lesion site from WT and PCAF<sup>-/-</sup> mice. (c) Quantification of regenerating axons, N=6 (WT), N=6 (PCAF<sup>-/-</sup>), Welch's *t*-test, \**P*<0.05 and \*\*\**P*<0.001. (d,e) Lack of CNS regeneration correlates with a significant decrease in H3K9ac expression in L4-L6 PCAF<sup>-/-</sup> traced DRG neurones when compared with WT, IHC (d), bar graphs (e). Inset shows high nuclear expression of H3K9ac in WT but not PCAF<sup>-/-</sup> traced DRG neurones. Student's *t*-test, error bars, s.e., \*\*\**P*<0.001, N=6, performed in triplicate. (f,g) IHC and 3,3'-Diaminobenzidine (DAB) intensity analysis of L4-6 DRG neurones shows a decrease in GAP-43, BDNF and Galanin expression in PCAF<sup>-/-</sup> DRG neurones when compared with WT after SNA followed by SCI. Scale bar, 25 µm. Student's *t*-test, \*\*\**P*<0.001, N=4 per group, performed in triplicate.



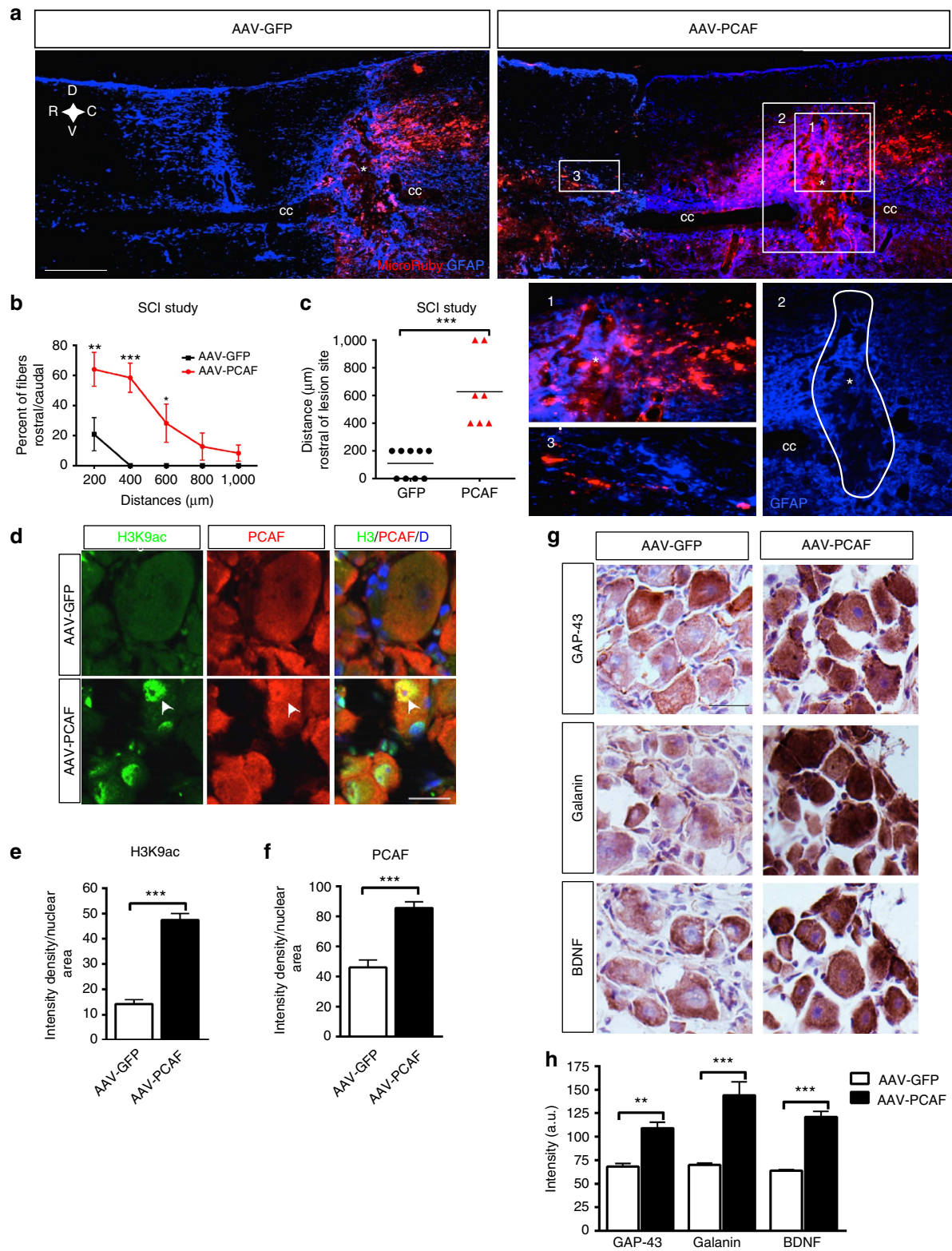


**Figure 8 | PCAF overexpression induces spinal axonal regeneration.** (a) MicroRuby tracing of the dorsal columns shows regenerating fibres invading into and past the lesion site after AAV-PCAF overexpression (upper right) versus a control AAV-GFP virus (upper left). Insets show higher magnification of regenerating axons. D-R-C-V: anatomical coordinates, dorsal-rostral-caudal-ventral. cc: central canal. Scale bar, 250  $\mu\text{m}$ . (b) Quantification of regenerating axons,  $N = 9$  (AAV-GFP),  $N = 7$  (AAV-PCAF). (c) Quantification of longest regenerating axon per animal. (d-f) Overexpression of AAV-PCAF in the SCI study promotes H3K9ac (8 weeks post infection; arrowheads) as shown by IHC (d). Nuclear intensity density analysis of H3K9ac (e) and PCAF (f) show enhanced PCAF and H3K9ac after PCAF overexpression. (g,h) GAP-43, Galanin and BDNF IHC analysis of corresponding L4-L6 DRG from infected AAV-PCAF and AAV-GFP animals show an increase in GAP-43, Galanin and BDNF expression, IHC (g) and DAB intensity analysis (h). Scale bars, 25  $\mu\text{m}$ . Error bars, s.e., (b) Welch's  $t$ -test,  $*P < 0.05$ ,  $**P < 0.01$  and  $***P < 0.001$ . (c,h)  $P < 0.0001$ , ANOVA, Bonferroni *post hoc* tests,  $**P < 0.01$  and  $***P < 0.001$ , (e,f) Student's  $t$ -test,  $***P < 0.001$ ,  $N = 3$ , performed in triplicate.

of genomic DNA and 5 µg of a 5-methyl-Cytosine antibody (Eurogentec, BI-MECY-0100) were added to immunoprecipitate methylated DNA fragments. The Whole Genome Amplification Kit (Sigma-Aldrich) was applied to amplify 20 ng of genomic samples to a maximum yield of 3–7 µg, followed by subsequent column purification using the GenElute PCR Clean-Up Kit (Sigma). MeDIP efficiency was tested with previously published primers for methylated H19 ICR<sup>41</sup>.

**DNA methylation microarray.** Whole-genome amplified, high-quality<sup>42</sup> samples (input genomic DNA, immunoprecipitated methylated DNA or no-antibody control) were sent to Roche/NimbleGen for DNA methylation microarray analysis. NimbleGen processed the samples as described in its ‘NimbleChip Arrays User’s Guide for DNA Methylation Analysis’. A ‘2007-02-27 MM8 CpG Island Promoter (385K RefSeq)’ tiling microarray, covering proximal promoter regions and CGIs by close-set oligonucleotide probes. Fluorescence intensity raw data were obtained from scanned images of the tiling arrays using the NimbleScan extraction software. For each spot on the array, Cy5/Cy3 ratios were normalized and calculated to obtain log<sub>2</sub> values. Then, the bi-weight mean of log<sub>2</sub> ratios of a certain region was subtracted from each data point; this procedure is similar to mean normalization of each channel.

**Promoter CGI analysis.** Several known RAGs and of differentially methylated genes that emerged from the DNA methylation microarray analysis within this study were analyzed for CpG islands (CGIs). The complete genomic region, together with the promoter region (5,000 bp upstream of the transcription start site (TSS)), was analysed with the *EMBOSS CpGPlot* online tool from EMBL-EBI. Characteristic parameters of reported CGIs were used.

**Gene-regulatory region bioinformatics analysis.** We performed a MatInspector (Genomatix) and UCSD genome browser-based bioinformatics analysis of the regulatory regions of RAG genes (*GAP-43*, *Galanin*, *BDNF*, *SCG-10*, *Spr1a*, *Ch11*, *Lgals*, *L1cam* and *CAP-23*) spanning 1,000 bp upstream and 1,500 bp downstream of the TSS. These regions overlap and further extend what we studied for DNA methylation (500 bp upstream and 1,500 bp downstream of the TSS). Significant transcription-binding sites displayed at least two of the three classically required criteria: a *P*-value < 0.05, matrix similarity > 0.8 and core similarity > 0.8. Additionally, CGI and DNA methylation were examined in these regions for all of the RAGs investigated with the EMBO DNA methylation analysis online software. Results of the combined analysis suggested that *GAP-43*, *Galanin* and *BDNF* had common gene regulatory regions with low levels of DNA methylation and absence of typical CpG islands, presented transcriptional-binding sites for transcription factors that are typically acetylated and active in the proximity of acetylated histones, including, *Klf*, *NfκB*, *Srf*, *p53*, *YY1*, *CREB* and *c-jun*.

**Quantitative real-time RT-PCR analysis.** RNA was extracted using PeqGOLD TriFast reagent (peqlab), cDNA was synthesized from 1 µg of total RNA using both oligodT and random hexamers from the SuperScript II Reverse Transcriptase kit (Invitrogen) and a real time RT-PCR was performed using Absolute QPCR SYBR low ROX master mix (Thermo Scientific). Quantities and fold changes were calculated following the manufacturer’s instructions (ABI 7,500) and as previously reported<sup>35,43</sup>. Primer sequences are shown in Supplementary Table 1. *RPL13A*, *GAPDH* or  $\beta$ -actin were used for normalization.

**Quantitative chromatin immunoprecipitation.** The SimpleCHIP Enzymatic Chromatin IP Kit with magnetic beads (Cell Signalling) was used according to previously published methods<sup>44</sup>. Antibodies used were H3K9ac, PCAF (rabbit), H3K9me2, H3K27me3, H3K4me3 and H3K18ac. Real-time Q-PCR was run using Absolute QPCR SYBR low ROX master mix (Thermo Scientific). Quantities and fold changes were calculated following the manufacturer’s instructions (ABI 7,500) and as previously reported<sup>35,43</sup>. Primers were designed in proximity (within 500 bp upstream) of the TSS. Primer sequences are shown in Supplementary Table 2.

**Immunohistochemistry.** DRG were fixed in 4% paraformaldehyde (PFA) and transferred to 30% sucrose. The tissue was embedded in OCT compound (Tissue-Tek), frozen at –80 °C and sectioned at 10-µm thickness. DRG sections underwent antigen retrieval with 0.1 M citrate buffer (pH 6.2) at 98 °C and were incubated with 120 µg ml<sup>-1</sup> goat anti-mouse IgG (Jackson ImmunoResearch). They were blocked for 1 h with 8% BSA, 1% PBS-TX100 or 0.3% PBS-TX100, respectively, and then incubated with NeuN (1:100), PCAF (mouse, 1:500) and AcH3K9 (1:500) antibodies or phospho-Erk 1/2 (1:500) and  $\beta$ III tubulin (1:1,000) antibodies O/N. This was followed by incubation with Alexa Fluor 568-conjugated goat anti-mouse and Alexa Fluor 488-conjugated goat anti-rabbit or Alexa Fluor 568-conjugated goat anti-rabbit and Alexa Fluor 488-conjugated goat anti-mouse (1:1,000, Invitrogen), respectively. Slides were counterstained with DAPI (1:5,000, Molecular Probes). Photomicrographs were taken with an Axio Imager.Z1/Apotome (Zeiss) microscope as 0.800 µm Z-stacks at  $\times 40$  magnification and processed with the software AxioVision (Zeiss). In order to determine the nuclear intensity density (ID) of pixels, Image J (Fiji) was used. Each neuronal nuclear

area was selected in the DAPI channel (about 25 nuclei/picture). The same selection was then used to delineate the nuclei in the other channels. The threshold of the nuclear area was set for each different channels, and based on that the pixel ID of the nucleus was determined and divided by its nuclear area. Triplicates of each treatment were analysed.

**Immunoblotting and immunoprecipitation.** For whole-cell extract immunoblotting, DRG or CGN were collected, lysed on ice in RIPA lysis buffer containing protease inhibitors (Complete Mini; Roche Diagnostics), sonicated briefly, centrifuged and the supernatant collected. The NE-PER Nuclear and Cytoplasmic Extraction Reagents (Thermo Scientific) was used according to the manufacturer’s instructions for nuclear enriched fractions. H3K9ac (1:1,000), PCAF (rabbit, 1:500),  $\beta$ -actin (1:1,000) and  $\beta$ III Tubulin (1:1,000) were employed as primary antibodies. Quantitation of protein expression was performed by densitometry (Image J) of the representative bands of the immunoblots and normalized to the respective levels of loading controls.

For immunoprecipitation, the nuclear enriched fractions were bound to rabbit PCAF antibody (8 µg), pulled down with Protein G magnetic beads, washed with low and high salt buffers (ChIP kit, Cell Signalling) and was eluted with loading buffer (Thermo Scientific). The IP was stained with PCAF (rabbit, 1:500), Phospho-Threonine (1:1,000) or Phospho-Serine (1:1,000).

**DRG culture.** Adult DRG were dissected and collected in Hank’s balanced salt solution on ice. DRGs were transferred to a digestion solution (5 mg ml<sup>-1</sup> Dispase II (Sigma), 2.5 mg ml<sup>-1</sup> Collagenase Type II (Worthington) in DMEM (Invitrogen)) and incubated at 37 °C for 35 min with occasional mixing. Following which DRGs were transferred to media containing 10% heat-inactivated fetal bovine serum (Invitrogen), 1  $\times$  B27 (Invitrogen) in DMEM:F12 (Invitrogen) mix and were briefly triturated with a Sigma-cote (Sigma) fire-polished pipette to manually dissociate the remaining clumps of DRG. After which the single cells were spun down, resuspended in media containing 1  $\times$  B27 and Penicillin/Streptomycin in DMEM:F12 mix and plated at 4,000–5,000 per coverslip. The culture was maintained in a humidified atmosphere of 5% CO<sub>2</sub> in air at 37 °C. Neurones were infected with either AAV-GFP or AAV-PCAF (1  $\times$  10<sup>12</sup> ml<sup>-1</sup>) a few hours post-plating and fixed with 4% PFA 48 h later. For the Garcinol study, cells were exposed to Vehicle (5% EtOH) or Garcinol (5 µM per well, Sigma-Aldrich) for 24 h and fixed. For the ERK/PD study, the day following plating DRG were exposed for 1 h to PD 98059 (50 µM per well), then to NGF (100 ng ml<sup>-1</sup>) for 3 h and fixed.

**CGN culture.** CGNs were prepared from the cerebellum of 7-day-old C57Bl/6J mice following standard procedures<sup>45</sup>. These disassociated CGNs were plated on either PDL (with or without 5 µM Garcinol) or myelin for 24 h in a humidified atmosphere of 5% CO<sub>2</sub> in air at 37 °C. Neurones were infected at the time of plating with a CMV promoter AV-GFP or AV-PCAF (1  $\times$  10<sup>10</sup> ml<sup>-1</sup>).

**Immunocytochemistry.** Glass coverslips were coated with 0.1 mg ml<sup>-1</sup> PDL, washed and coated with mouse Laminin (2 µg ml<sup>-1</sup>; Millipore). For myelin experiments, they were additionally coated with 4 µg cm<sup>-2</sup> rat myelin. Cells were plated on coated coverslips for 24 or 48 h, at which time they were fixed with 4% PFA/4% sucrose. Immunocytochemistry was performed as previously reported<sup>45</sup> using  $\beta$ III Tubulin (1:1,000), MAP2 (1:100), PCAF (mouse, 1:400), AcH3K9 (1:1,000) or pErk1/2 (1:500). This was followed by incubation with Alexa Fluor 568-conjugated goat anti-mouse and Alexa Fluor 488-conjugated goat anti-rabbit (1:1,000, Invitrogen). To visualize the nucleus, we stained the cells with DAPI (1:5,000, Molecular Probes).

**Image analysis for immunocytochemistry.** DRG pictures were taken at  $\times 20$  magnification with an Axioplan 2 (Zeiss) microscope and processed with the software AxioVision (Zeiss). Using Image J, a threshold was set. On the basis of the threshold, for each picture the ID of pixels was calculated in each channel and then divided by its respective number of cells (about 225 cells per picture). This was carried out in triplicate.

**Neurite length analysis.** Immunofluorescence was detected using an Axiovert 200 microscope (Zeiss) and pictures were taken as a mosaic at  $\times 10$  magnification using a CDD camera (AxioCam MRm, Zeiss). Neurite analysis and measurements were performed using the NeuroLucida software (MicroBrightField) in triplicate with 50 cells per triplicate.

**Luciferase assays.** Experiments were performed in CGN using electroporation with the rat neurone nucleofactor kit (Amaxa Biosystems) according to the provided protocol. Briefly, five million neurones were used for each cuvette, with 2–4 µg of total DNA (*GAP-43-Luc reporter*<sup>46</sup> and 25 ng of *pRL-TK-Renilla-luciferase* (Promega)). Neurones were plated in 24-well plates at a density of 0.4 million cells per well with or without 5 µM Garcinol and incubated for a total



of 24 h. Cells were harvested and lysed with 100  $\mu$ l of passive lysis buffer, and luciferase activities were determined using the Dual-Luciferase kit (Promega).

**Ex vivo DRG culture.** Intrathecal (i.t.) injection was performed using the Wilcox technique<sup>47</sup>. Mice were briefly anaesthetized with isoflurane (2%), and a lumbar cutaneous incision (1 cm) was made. I.t. injections were performed with 30-gauge 15-mm needles mated to a 5- $\mu$ l luer tip syringe (Hamilton, Reno, NV, USA). The needle was inserted into the tissue between the L5 and L6 spinous processes and inserted  $\sim$ 0.5 cm with an angle of 20°. Vehicle (10% DMSO in 0.9% NaCl) or Garcinol (80  $\mu$ M) was slowly injected in a final volume of 5  $\mu$ l. Directly after i.t. injection of Vehicle or Garcinol, mice underwent Sham or SNA surgeries. Twenty-four hours after surgery, mice were killed and L4–L6 DRG were collected and cultured for 24 h, and were then fixed and stained. We used three animals per group and plated in triplicate. L4–L6 DRG were also collected for total protein extraction for western blot analysis of H3K9ac.

For PCAF null *ex vivo* study, WT or PCAF<sup>-/-</sup> mice (generated in Dr Boutilier's laboratory) underwent Sham or SNA surgeries. Twenty-four hours after surgery, mice were killed and L4–L6 DRG were collected and cultured for 18 h, and were then fixed and stained. We used three animals per group and the DRG were plated in triplicate.

### SCI study

**AAV-GFP/PCAF injection.** All experimental procedures were performed in accordance with protocols approved by the University of Tübingen. PCAF expression plasmid was obtained from Addgene (Plasmid 8941). AAVs were prepared as described previously<sup>48</sup>. Mice were anaesthetized and left sciatic nerve was injected with 1.5–2  $\mu$ l of either AAV-GFP or AAV-PCAF ( $1 \times 10^{12}$  ml<sup>-1</sup>) using a glass-pulled micropipette. Standardized randomization and blinding strategies were adopted. Randomization of samples was performed by random assignment and labelling of control and test groups while between one to three experimenters were blind to the groups for each experiment performed.

**Spinal cord injury.** Two weeks after AAV injection, a T9–10 laminectomy was performed and the dorsal half of the spinal cord was crushed with no. 5 forceps (Dumont, Fine Science Tools) for 2 s (ref. 49). The forceps were deliberately positioned to sever the dorsal column axons completely. Four weeks after the spinal cord lesion, dorsal column axons were traced by injecting 2  $\mu$ l of Microruby tracer (3,000 molecular weight, 10%, Invitrogen) into the left sciatic nerve<sup>50</sup>. Mice were kept for an additional 2 weeks before termination. CD1 WT and PCAF<sup>-/-</sup> mice underwent the same spinal cord surgery as above. Additionally, they received a conditioning sciatic nerve lesion 1 week before the spinal surgery. One week after the spinal cord lesion, dorsal column axons were traced by injecting 2  $\mu$ l of Microruby tracer (3,000 molecular weight, 10%, Invitrogen) into the left sciatic nerve<sup>50</sup>. These mice were kept for an additional 2 weeks before termination. Animals were deeply anaesthetized and were perfused transcardially. Spinal cords were dissected and post-fixed in 4% PFA in phosphate-buffered saline (PBS) at 4 °C for 2 h and 30% sucrose O/N. Then the tissue was embedded in Tissue-Tek OCT compound, frozen at  $-80$  °C and cut in 18- $\mu$ m-sagittal and coronal sections (3 mm caudal and 5 mm rostral to the lesion were taken to confirm the completeness of the lesion and to quantify tracing efficiency among experimental groups). Brain stem from each cord was also dissected, and sections of the nuclei gracilis and cuneatus were generated to monitor tracing from spared fibres. Mice with incomplete lesions were excluded. Staining for GFAP (1:2,000) was performed following the standard protocols<sup>40</sup>. Confocal laser scanning microscopy was performed using a Zeiss LSM700. Semi-automatic skeletonization of regenerating axons was performed on confocal scans using the three-dimensional (3D) imaging software Amira (FEI Visualization Sciences Group). An isosurface was applied to the GFAP signal.

**Quantification of axonal regeneration.** For each spinal cord after dorsal column crush, the number of fibres caudal to the lesion and their distance from the lesion epicentre were analysed in four to six sections per animal with a fluorescence Axioplan 2 (Zeiss) microscope and with the software StereoInvestigator 7 (MBF bioscience). The lesion epicentre (GFAP) was identified in each section at a  $\times 40$  magnification. The sum total number of labelled axons rostral to the lesion site was normalized to the total number of labelled axons caudal to the lesion site counted in all the analysed sections for each animal, obtaining an inter-animal comparable ratio considering the individual tracing variability. Sprouts and regrowing fibres were defined following the anatomical criteria reported by Steward *et al.*<sup>51</sup> Samples falling short of standard quality for each specific experiment or altered by clear experimental flaw were excluded from the analysis.

**DAB immunostaining.** Peroxidase activity was blocked in 0.3% H<sub>2</sub>O<sub>2</sub>, followed by incubation in 8% bovine serum albumin (BSA) and 0.3% TBS-TX-100. BDNF (1:500), Galanin (1:2,000) or GAP-43 (1:500) antibodies in 2% BSA and 0.2% TBS-TX100 were used. Labelled cells were visualized using the ABC system

(Vectastain Elite; Vector Laboratories) with DAB as chromogen. The sections then were counterstained with haematoxylin (Vector Laboratories).

**Statistical analysis.** Data are plotted as the mean  $\pm$  s.e. All experiments were performed in triplicate. Asterisks indicate a significant difference analysed using analysis of variance with Bonferroni *post hoc* tests, Student's *t*-test, Welch's *t*-test or two-way analysis of variance as indicated (\**P* < 0.05; \*\**P* < 0.01; \*\*\**P* < 0.001).

### References

- Skene, J. H. Axonal growth-associated proteins. *Annu. Rev. Neurosci.* **12**, 127–156 (1989).
- Schmitt, A. B. *et al.* Identification of regeneration-associated genes after central and peripheral nerve injury in the adult rat. *BMC Neurosci.* **4**, 8 (2003).
- Stam, F. J. *et al.* Identification of candidate transcriptional modulators involved in successful regeneration after nerve injury. *Eur. J. Neurosci.* **25**, 3629–3637.
- Starkey, M. L. *et al.* Expression of the regeneration-associated protein SPRR1A in primary sensory neurons and spinal cord of the adult mouse following peripheral and central injury. *J. Comp. Neurol.* **513**, 51–68 (2009).
- Hanz, S. & Fainzilber, M. Retrograde signaling in injured nerve—the axon reaction revisited. *J. Neurochem.* **99**, 13–19 (2006).
- Rishal, I. & Fainzilber, M. Retrograde signaling in axonal regeneration. *Exp. Neurol.* **223**, 5–10 (2010).
- Neumann, S. & Woolf, C. J. Regeneration of dorsal column fibers into and beyond the lesion site following adult spinal cord injury. *Neuron* **23**, 83–91 (1999).
- Maurice, T. *et al.* Altered memory capacities and response to stress in p300/CBP-associated factor (PCAF) histone acetylase knockout mice. *Neuropsychopharmacology* **33**, 1584–1602 (2008).
- Tsankova, N. M., Kumar, A. & Nestler, E. J. Histone modifications at gene promoter regions in rat hippocampus after acute and chronic electroconvulsive seizures. *J. Neurosci.* **24**, 5603–5610 (2004).
- Qureshi, I. A. & Mehler, M. F. Emerging role of epigenetics in stroke: part 1: DNA methylation and chromatin modifications. *Arch. Neurol.* **67**, 1316–1322 (2010).
- Lunyak, V. V. *et al.* Corepressor-dependent silencing of chromosomal regions encoding neuronal genes. *Science* **298**, 1747–1752 (2002).
- Basi, G. S., Jacobson, R. D., Virag, L., Schilling, J. & Skene, J. H. Primary structure and transcriptional regulation of GAP-43, a protein associated with nerve growth. *Cell* **49**, 785–791 (1987).
- Skofitsch, G. & Jacobowitz, D. M. Immunohistochemical mapping of galanin-like neurons in the rat central nervous system. *Peptides* **6**, 509–546 (1985).
- Lindsay, R. M. Nerve growth factors (NGF, BDNF) enhance axonal regeneration but are not required for survival of adult sensory neurons. *J. Neurosci.* **8**, 2394–2405 (1988).
- Geremia, N. M. *et al.* Endogenous BDNF regulates induction of intrinsic neuronal growth programs in injured sensory neurons. *Exp. Neurol.* **223**, 128–142 (2010).
- Iskandar, B. J. *et al.* Folate regulation of axonal regeneration in the rodent central nervous system through DNA methylation. *J. Clin. Invest.* **120**, 1603–1616 (2010).
- Wang, Z. *et al.* Combinatorial patterns of histone acetylations and methylations in the human genome. *Nat. Genet.* **40**, 897–903 (2008).
- Liu, K., Tedeschi, A., Park, K. K. & He, Z. Neuronal intrinsic mechanisms of axon regeneration. *Annu. Rev. Neurosci.* **34**, 131–152 (2011).
- Seiffers, R., Mills, C. D. & Woolf, C. J. ATF3 increases the intrinsic growth state of DRG neurons to enhance peripheral nerve regeneration. *J. Neurosci.* **27**, 7911–7920 (2007).
- Kretz, A., Kugler, S., Happold, C., Bahr, M. & Isenmann, S. Excess Bcl-XL increases the intrinsic growth potential of adult CNS neurons in vitro. *Mol. Cell Neurosci.* **26**, 63–74 (2004).
- Julien, J. P., Meyer, D., Flavell, D., Hurst, J. & Grosfeld, F. Cloning and developmental expression of the murine neurofilament gene family. *Brain Res* **387**, 243–250 (1986).
- Hanz, S. & Fainzilber, M. Integration of retrograde axonal and nuclear transport mechanisms in neurons: implications for therapeutics. *Neuroscientist* **10**, 404–408 (2004).
- Perlson, E. *et al.* Vimentin-dependent spatial translocation of an activated MAP kinase in injured nerve. *Neuron* **45**, 715–726 (2005).
- Averill, S. *et al.* Nerve growth factor modulates the activation status and fast axonal transport of ERK 1/2 in adult nociceptive neurones. *Mol. Cell Neurosci.* **18**, 183–196 (2001).
- Alessi, D. R., Cuenda, A., Cohen, P., Dudley, D. T. & Saltiel, A. R. PD 098059 is a specific inhibitor of the activation of mitogen-activated protein kinase kinase *in vitro* and *in vivo*. *J. Biol. Chem.* **270**, 27489–27494 (1995).
- Wong, K. *et al.* Nerve growth factor receptor signaling induces histone acetyltransferase domain-dependent nuclear translocation of p300/CREB-binding protein-associated factor and hGCN5 acetyltransferases. *J. Biol. Chem.* **279**, 55667–55674 (2004).

27. Blesch, A. *et al.* Conditioning lesions before or after spinal cord injury recruit broad genetic mechanisms that sustain axonal regeneration: superiority to camp-mediated effects. *Exp. Neurol.* **235**, 162–173 (2012).
28. Qiu, J. *et al.* Spinal axon regeneration induced by elevation of cyclic AMP. *Neuron* **34**, 895–903 (2002).
29. Balasubramanyam, K. *et al.* Polyisoprenylated benzophenone, garcinol, a natural histone acetyltransferase inhibitor, represses chromatin transcription and alters global gene expression. *J. Biol. Chem.* **279**, 33716–33726 (2004).
30. Ylera, B. *et al.* Chronically CNS-injured adult sensory neurons gain regenerative competence upon a lesion of their peripheral axon. *Curr. Biol.* **19**, 930–936 (2009).
31. Cho, Y., Sloutsky, R., Naegle, K. M. & Cavalli, V. Injury-induced HDAC5 nuclear export is essential for axon regeneration. *Cell* **155**, 894–908 (2013).
32. Finelli, M. J., Wong, J. K. & Zou, H. Epigenetic regulation of sensory axon regeneration after spinal cord injury. *J. Neurosci.* **33**, 19664–19676 (2013).
33. Gaub, P. *et al.* The histone acetyltransferase p300 promotes intrinsic axonal regeneration. *Brain* **134**, 2134–2148 (2011).
34. Di Giovanni, S. *et al.* The tumor suppressor protein p53 is required for neurite outgrowth and axon regeneration. *EMBO J.* **25**, 4084–4096 (2006).
35. Tedeschi, A., Nguyen, T., Puttagunta, R., Gaub, P. & Di Giovanni, S. A p53-CBP/p300 transcription module is required for GAP-43 expression, axon outgrowth, and regeneration. *Cell Death Differ.* **16**, 543–554 (2009).
36. Gaub, P. *et al.* HDAC inhibition promotes neuronal outgrowth and counteracts growth cone collapse through CBP/p300 and P/CAF-dependent p53 acetylation. *Cell Death Differ.* **17**, 1392–1408 (2010).
37. Hanz, S. *et al.* Axoplasmic importins enable retrograde injury signaling in lesioned nerve. *Neuron* **40**, 1095–1104 (2003).
38. Yudin, D. *et al.* Localized regulation of axonal RanGTPase controls retrograde injury signaling in peripheral nerve. *Neuron* **59**, 241–252 (2008).
39. Shin, J. E. *et al.* Dual leucine zipper kinase is required for retrograde injury signaling and axonal regeneration. *Neuron* **74**, 1015–1022 (2012).
40. Floriddia, E. M. *et al.* p53 regulates the neuronal intrinsic and extrinsic responses affecting the recovery of motor function following spinal cord injury. *J. Neurosci.* **32**, 13956–13970 (2012).
41. Weber, M. *et al.* Chromosome-wide and promoter-specific analyses identify sites of differential DNA methylation in normal and transformed human cells. *Nat. Genet.* **37**, 853–862 (2005).
42. Komashko, V. M. *et al.* Using ChIP-chip technology to reveal common principles of transcriptional repression in normal and cancer cells. *Genome Res.* **18**, 521–532 (2008).
43. Tedeschi, A. *et al.* The tumor suppressor p53 transcriptionally regulates cGKI expression during neuronal maturation and is required for cGMP-dependent growth cone collapse. *J. Neurosci.* **29**, 15155–15160 (2009).
44. Floriddia, E., Nguyen, T. & Di Giovanni, S. Chromatin immunoprecipitation from dorsal root ganglia tissue following axonal injury. *J. Vis. Exp.* **20** pii 2803 (2011).
45. Puttagunta, R. *et al.* RA-RAR-beta counteracts myelin-dependent inhibition of neurite outgrowth via Lingo-1 repression. *J. Cell Biol.* **193**, 1147–1156 (2011).
46. Nguyen, T. *et al.* NFAT-3 is a transcriptional repressor of the growth associated protein 43 during neuronal maturation. *J. Biol. Chem.* **284**, 18816–18823 (2009).
47. Hylden, J. L. & Wilcox, G. L. Intrathecal morphine in mice: a new technique. *Eur. J. Pharmacol.* **67**, 313–316 (1980).
48. Park, K. K. *et al.* Promoting axon regeneration in the adult CNS by modulation of the PTEN/mTOR pathway. *Science* **322**, 963–966 (2008).
49. Liu, K. *et al.* PTEN deletion enhances the regenerative ability of adult corticospinal neurons. *Nat. Neurosci.* **13**, 1075–1081 (2010).
50. Parikh, P. *et al.* Regeneration of axons in injured spinal cord by activation of bone morphogenetic protein/Smad1 signaling pathway in adult neurons. *Proc. Natl Acad. Sci. USA* **108**, E99–107 (2011).
51. Steward, O., Zheng, B. & Tessier-Lavigne, M. False resurrections: distinguishing regenerated from spared axons in the injured central nervous system. *J. Comp. Neurol.* **459**, 1–8 (2003).

## Acknowledgements

This work was supported by funds granted by the Hertie Foundation, by the Wings for Life Spinal Cord Research Foundation, by the DFG-DI 140731 and DFG-DI 149741 (all granted to Simone Di Giovanni), the DAAD PhD fellowship (granted to Marilia Grando Soria) and a DZNE PhD fellowship (granted to Yashashree Joshi). We would like to thank Bernd Knöll for Galanin antibody and for discussion of our work, Torsten Plosch and Philipp Kahle for giving us feedback on the manuscript and for providing phospho-antibodies, and Marlies Knipper for BDNF antibody. We would also like to thank Yingchun Ni for discussion on AAV production and purification, and Giorgia Quadrato for discussion on immunohistochemistry.

## Author contributions

S.D.G. designed the project; R.P., A.T., M.G.S., A.H., R.L., K.I.R., P.G., Y.J., T.N., A.S. and C.J.L. performed the experiments; R.P., A.T., M.G.S., A.H. and R.L. analysed data, A.-L.B. provided mice, F.B. provided support and feedback, R.P. and S.D.G. supervised the research as well as co-wrote the paper. A.T. contributed to editing the manuscript.

## Additional information

**Accession code:** DNA methylation microarray data have been deposited in the NCBI Gene Expression Omnibus (GEO) database under the accession number GSE55514.

**Supplementary Information** accompanies this paper at <http://www.nature.com/naturecommunications>

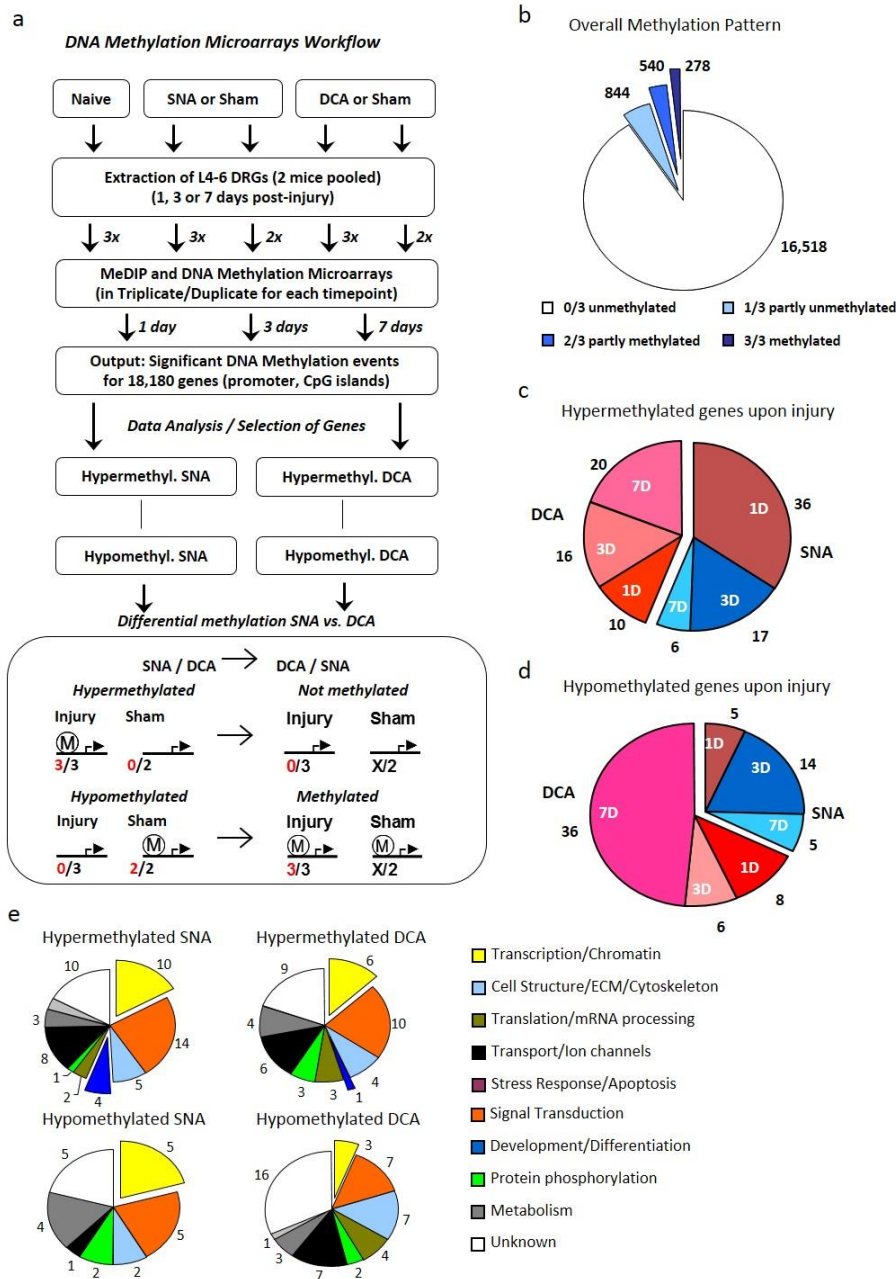
**Competing financial interests:** The authors declare no competing financial interests.

**Reprints and permission** information is available online at <http://npg.nature.com/reprintsandpermissions/>

**How to cite this article:** Puttagunta, R. *et al.* P/CAF-dependent epigenetic changes promote axonal regeneration in the central nervous system. *Nat. Commun.* 5:3527 doi: 10.1038/ncomms4527 (2014).

## Supplementary Information

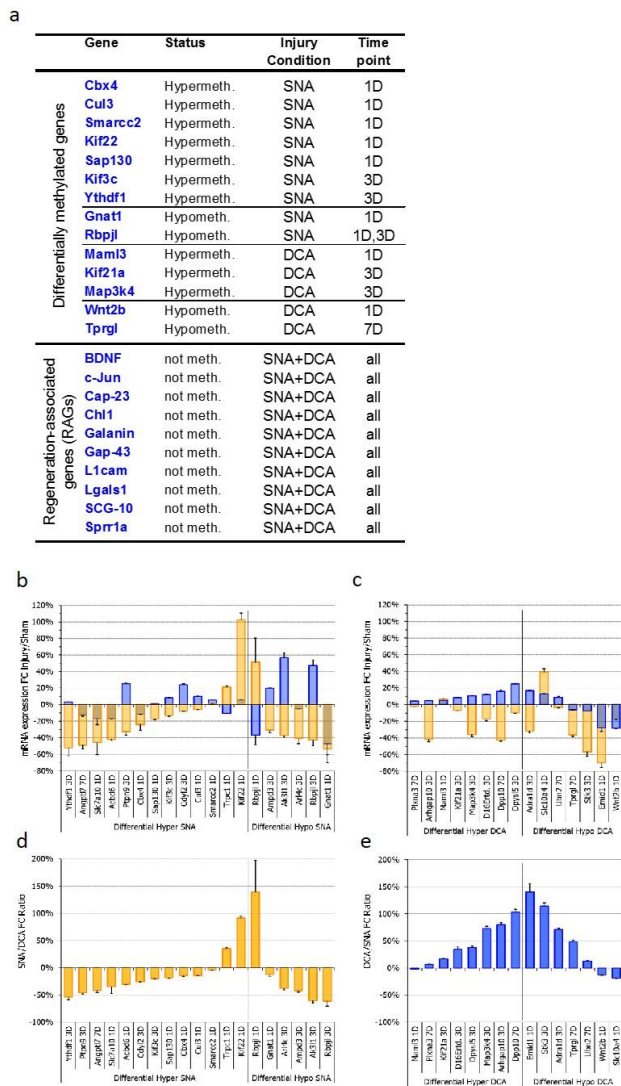
Supplementary Figure 1



### Supplementary Figure 1 Promoter and CpG island DNA methylation arrays

**a**, Schematic diagram summarizing the experimental design of promoter and CpG island DNA methylation arrays from L4-L6 DRGs after SNA and DCA. **b**, Pie chart summarizing the overall number of methylated genes irrespective of injury, showing only a minority of methylated genes. **c**, Pie charts showing the number of fully hypermethylated or hypomethylated genes (3/3) after either SNA or DCA in comparison with Shams. **e**, Pie charts showing the limited number and respective functional classes of differentially methylated genes (comparison to Shams) after SNA and DCA.

Supplementary Figure 2

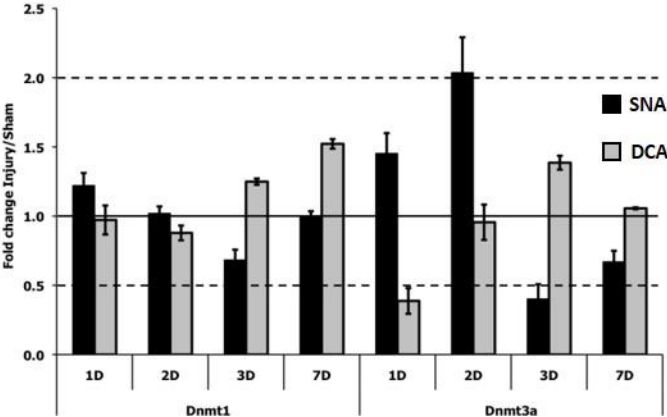


### Supplementary Figure 2 Methylation of genes and correlation with expression

**a**, Table shows a selection of differentially methylated genes belonging to chromatin remodelling and retrograde signalling functional classes and the lack of methylation of RAGs after axonal injury. Relative mRNA expression fold changes upon SNA or DCA for a subset of differentially methylated genes do correlate with methylation status, but not as a general rule. **b-e**, For each differentially methylated gene, mRNA levels were detected for the relevant time point for SNA and DCA samples (injury and sham). Most differentially hypermethylated genes upon SNA exhibit decreased mRNA expression levels (injury/sham fold change, in orange), while levels upon DCA varied (blue). In contrast to the hypothesis, most differentially hypomethylated genes upon SNA are downregulated, except for *Rbpjl* (**b**). Upon DCA, some differentially hypomethylated genes are upregulated while differentially hypermethylated genes were marginally upregulated as well (**c**). To investigate the correlation between gene expression and DNA methylation, the SNA/DCA FC ratio was calculated, showing lack of correlation between promoter and CpG island methylation and gene expression (**d, e**). Error bars, s.e.m.

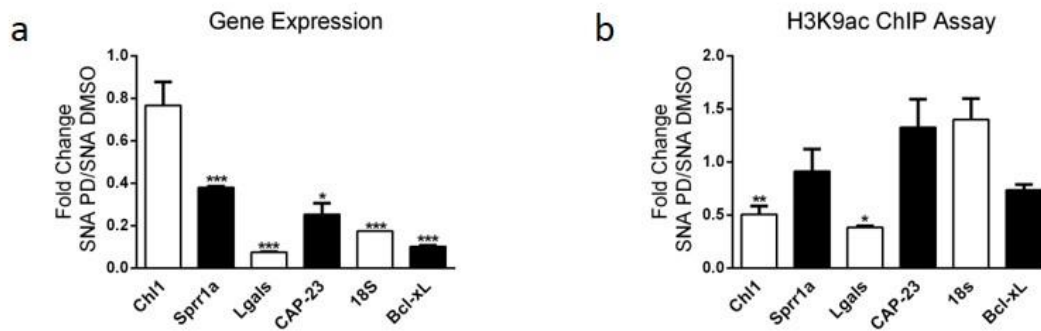


Supplementary Figure 3



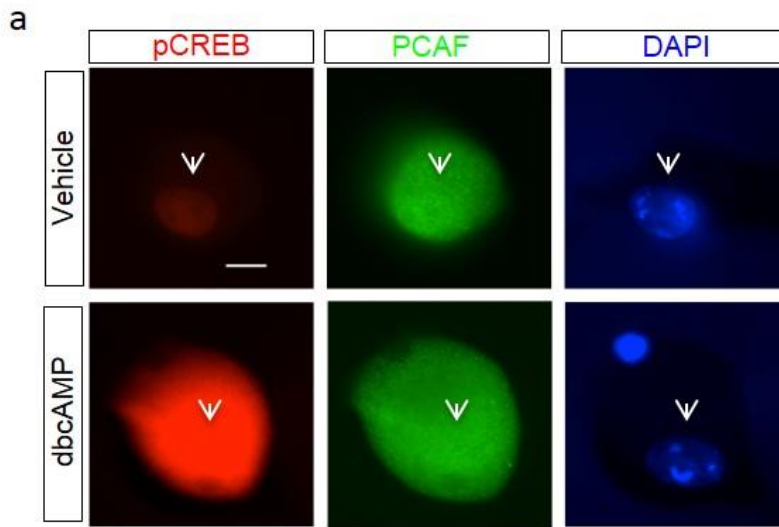
**Supplementary Figure 3 DNMT 1 and 3a gene expression after SNA and DCA**  
Quantitative RT-PCR shows a modest change in gene expression for DNMT1 and DNMT3a after SNA and DCA. All values are fold changes to Shams, N = 3, triplicate experiments. Error bars, s.d.

## Supplementary Figure 4



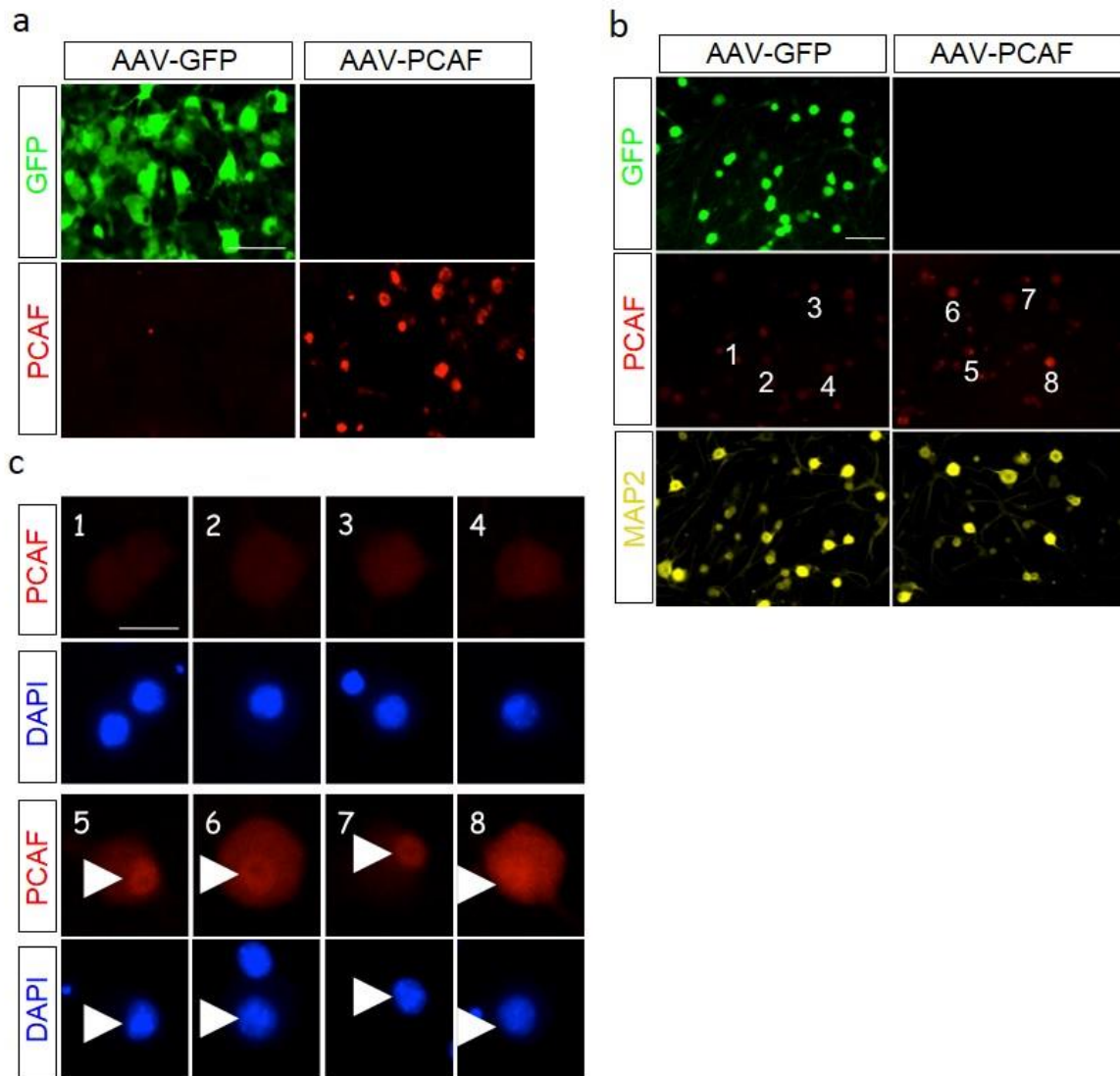
**Supplementary Figure 4 Inhibition of ERK on gene expression and promoters** **a**, One day following SNA with PD treatment showed a decrease in gene expression of most genes tested compared to SNA with DMSO (Quantitative RT-PCR, N = 3 per group). **b**, No correlation with H3K9ac at the promoters of these genes was found except for Lgals (ChIPs). N = 6 per group, performed in triplicate. Error bars, s.e.m. (a,b) Student's *t*-test, \*P<0.05, \*\*P<0.001 and \*\*\*P<0.001.

## Supplementary Figure 5



**Supplementary Figure 5 dbcAMP does not alter PCAF in cultured DRG neurons**  
**a**, dbcAMP (1 mM) delivered at the time of plating enhances pCREB expression as expected (24 h), but does not alter expression level nor localization of PCAF. N = 3. Arrow head shows selected cell and nuclear localization. (Scale bar: 10  $\mu$ m)

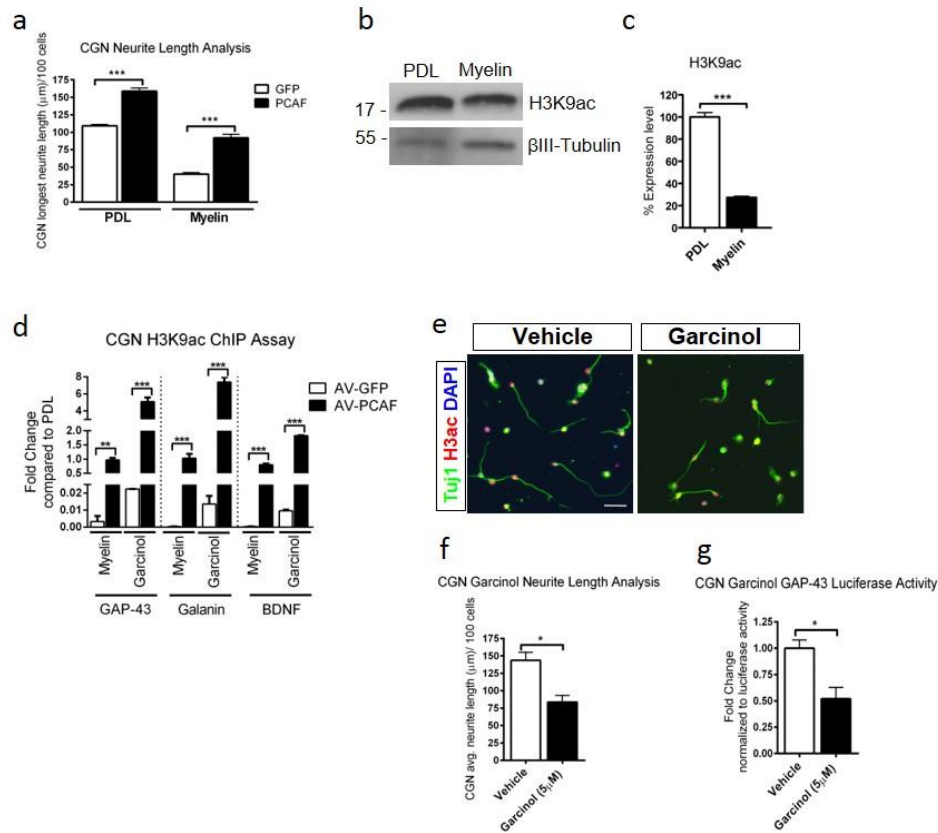
## Supplementary Figure 6



### Supplementary Figure 6 AAV overexpression leads to enhanced PCAF levels

**a**, HEK cells infected with AAV-GFP or AAV-PCAF for 48 h. Scale bar, 100  $\mu$ m. **b**, Cultured DRG neurons from adult mice were infected with AAV-GFP or AAV-PCAF for 48 h. Scale bar, 100  $\mu$ m. **c**, High magnification of numbered PCAF positive cells in **(b)** showing nuclear accumulation after PCAF overexpression. Scale bar, 25  $\mu$ m.

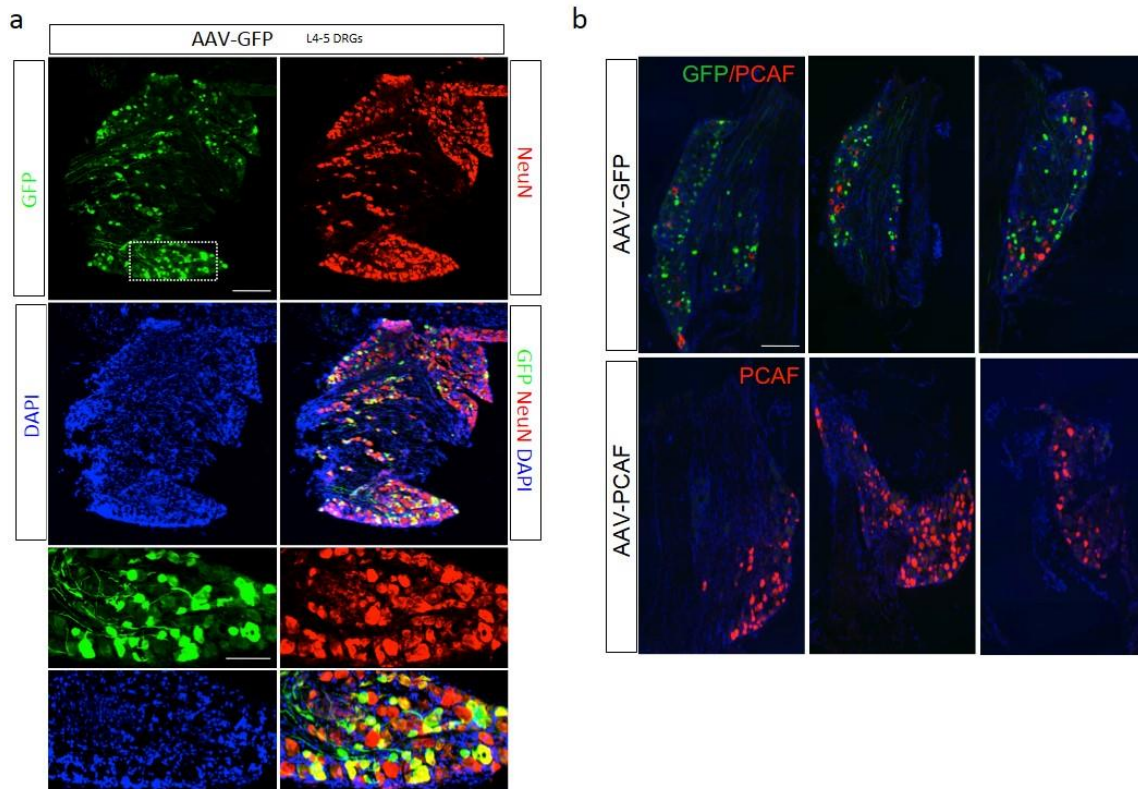
## Supplementary Figure 7



### Supplementary Figure 7 PCAF overexpression in CGN

**a**, CGN electroplated with PCAF for 24 h showed an increase in neurite length on PDL and myelin. **b, c**, Immunoblot (**b**) shows decreased H3K9ac expression in CGN following 24 h of plating on myelin, intensity analysis (**c**). **d**, Myelin significantly decreases H3K9ac at the promoters of RAGs, which is restored by AV-PCAF overexpression (24 h) in CGN. **e, f**, CGN plated for 24 h and treated with 5 μM of the PCAF inhibitor Garcinol showed a decrease in neurite outgrowth on PDL, ICC (**e**) and neurite length analysis (**f**). Scale bars, 50 μm. **g**, GAP-43 proximal promoter luciferase construct shows decreased expression after 24h treatment with 5 μM Garcinol. Error bars, s.e.m., (a, d)  $P < 0.0001$ , ANOVA, Bonferroni post-hoc tests, \* $P < 0.05$ , \*\* $P < 0.001$  and \*\*\* $P < 0.001$  (c, f, g) Student's *t*-test, \* $P < 0.05$ , \*\* $P < 0.001$  and \*\*\* $P < 0.001$ ,  $N = 3-6$ , performed in triplicate. Original immunoblot images are shown in Supplementary Figure 15.

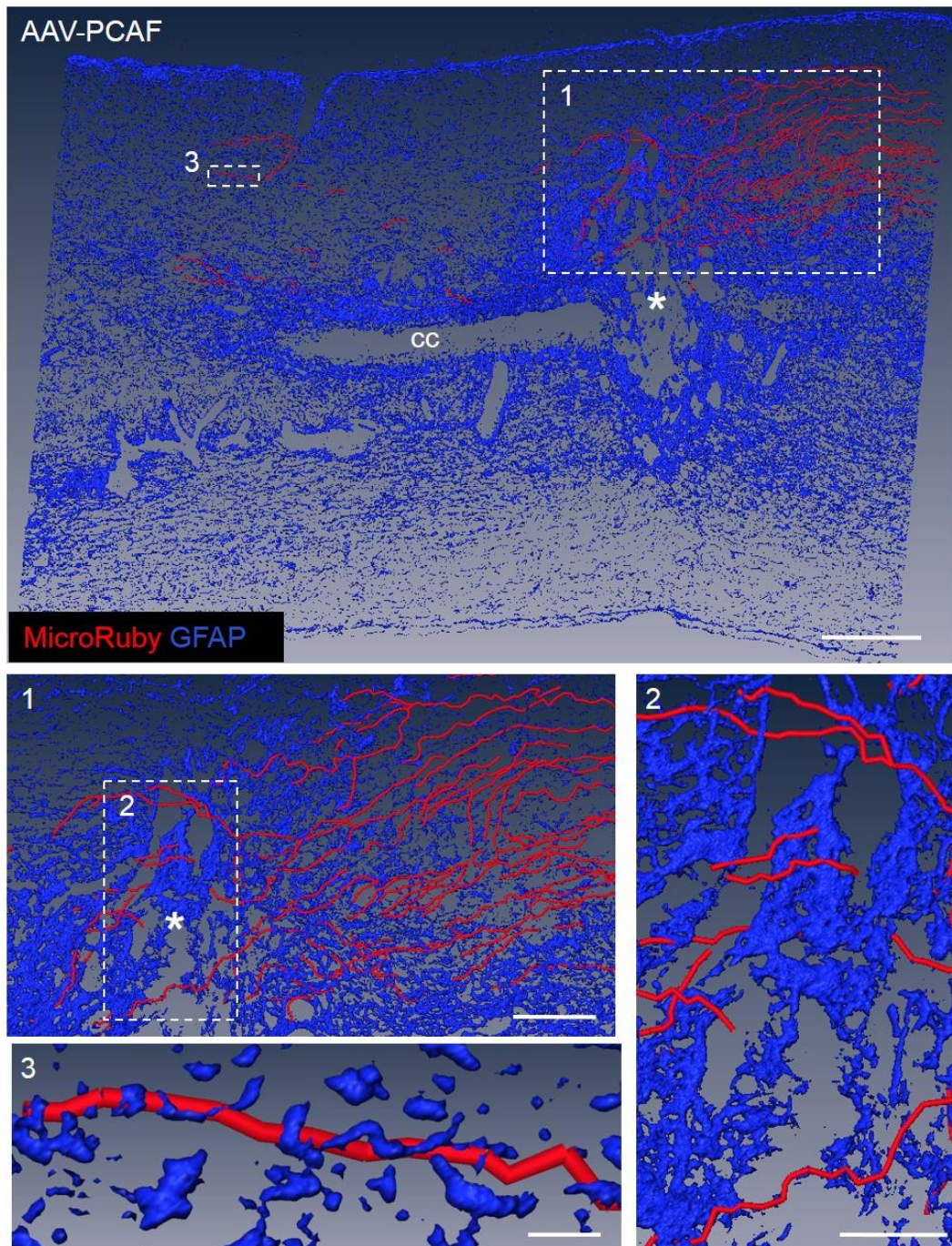
Supplementary Figure 8



**Supplementary Figure 8 Infection efficiency of AAV in DRGs from SCI study**  
**a**, AAV injected in the sciatic nerve specifically targets DRG neurons (8 weeks post-infection) as seen by the overlap in GFP expression and NeuN staining. Scale bars, 250 and 100  $\mu\text{m}$  respectively. **b**, Sciatic nerve injected AAV-GFP and AAV-PCAF shows infection and expression of PCAF protein levels in the L4-L6 DRGs (8 weeks post-infection). Scale bar, 250  $\mu\text{m}$ .



Supplementary Figure 9

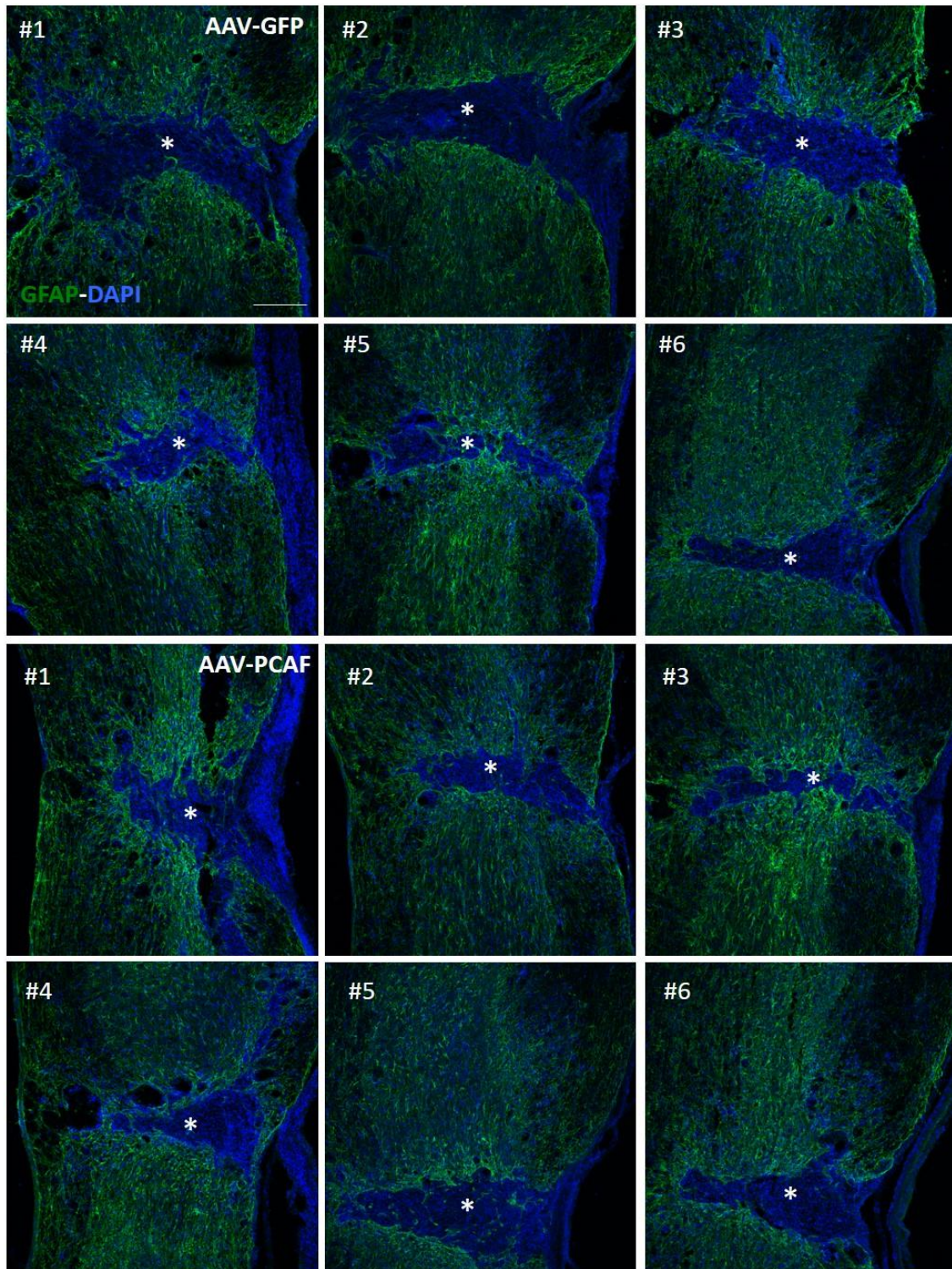


**Supplementary Figure 9 3D visualization of regenerating axons**

Amira 3D reconstruction of regenerating dorsal column axons and glial scar in a sagittal projection (~25  $\mu\text{m}$ ) of the spinal cord after PCAF overexpression. \* Lesion site. cc: central canal. Scale bars, 200  $\mu\text{m}$  (top panel), 100  $\mu\text{m}$  (1), 50  $\mu\text{m}$  (2) and 10 $\mu\text{m}$  (3).



Supplementary Figure 10

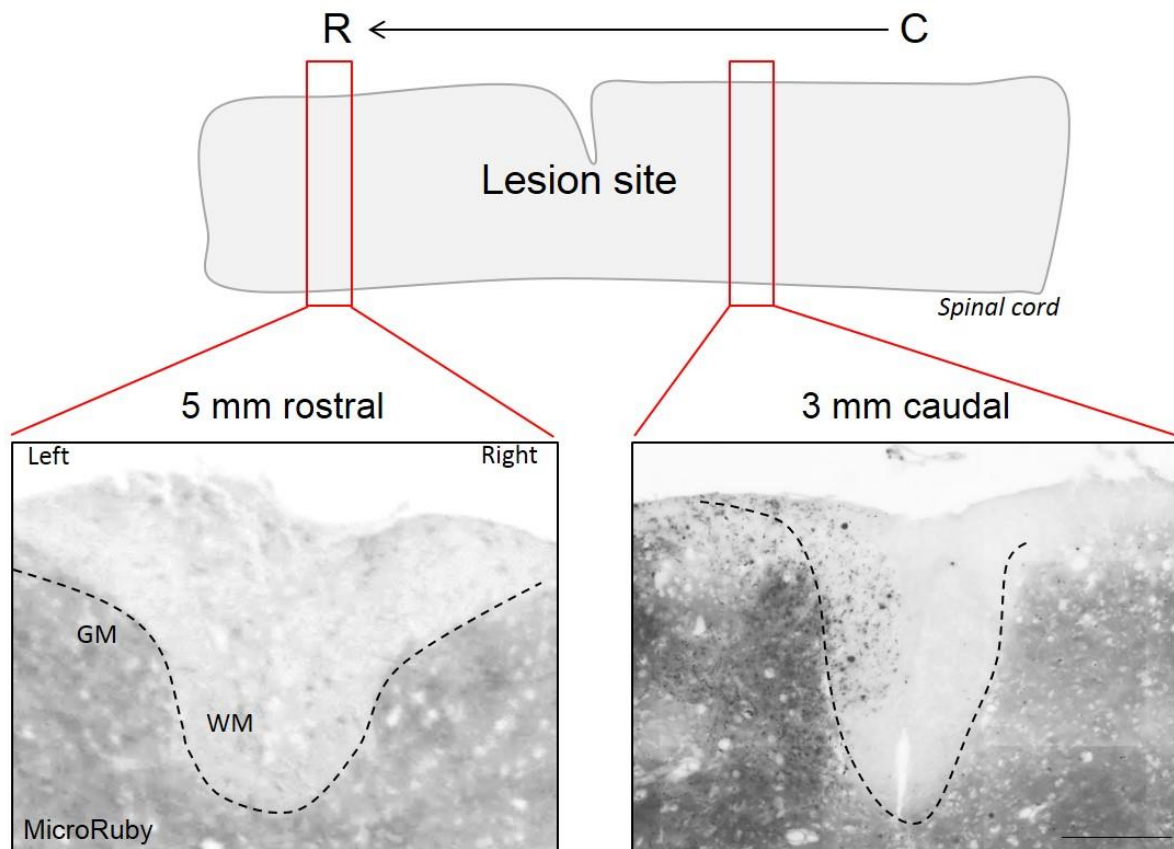


**Supplementary Figure 10 Lesion sites after SCI**

Micrographs show spinal cord lesion sites from individual mice (#1,2, etc...) after SCI as indicated in Figure 8. Asterisk indicates the lesion site. Scale bar, 250  $\mu$ m. 40X Scale bar: 250  $\mu$ m



Supplementary Figure 11

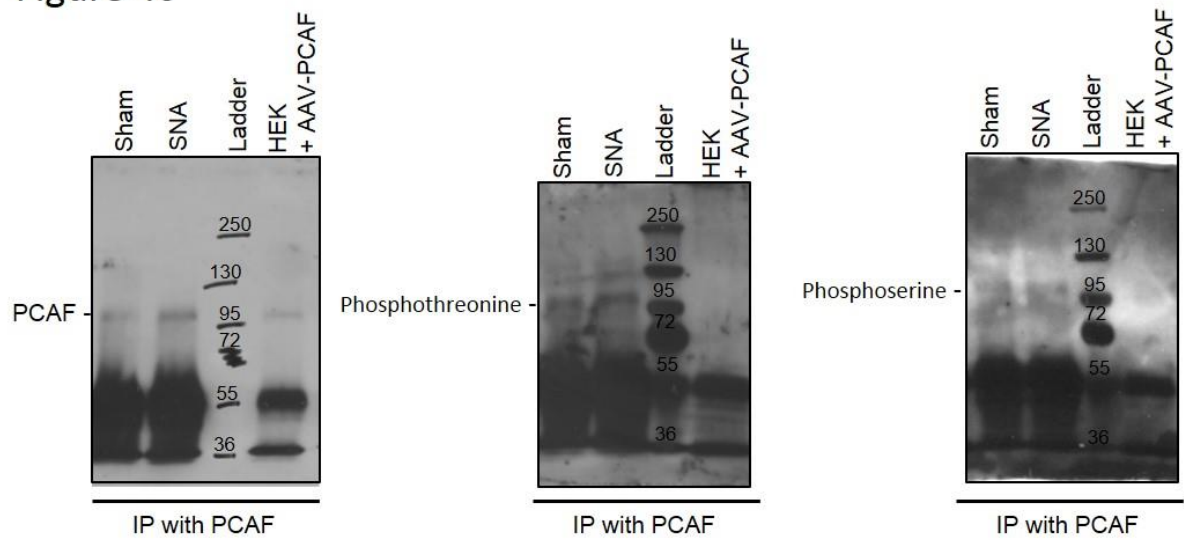


**Supplementary Figure 11 Tracer in the dorsal columns after SCI**

Micrographs show tracing in representative coronal sections of the dorsal columns after SCI cord. The dotted line indicates dorsal columns. Tracer is visible 3 mm caudal to the lesion site (right panel), but not 5 mm rostral to it (left panel). Scale bar, 150  $\mu$ m.

## Supplementary Figure 12

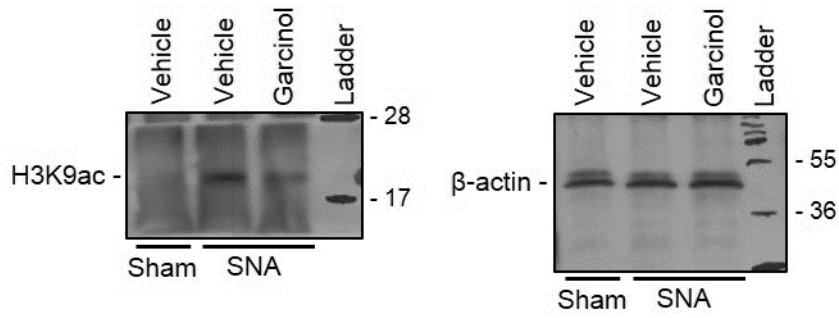
### Figure 4c



Supplementary Figure 12 Full scan images of western blot data in Figure 4

## Supplementary Figure 13

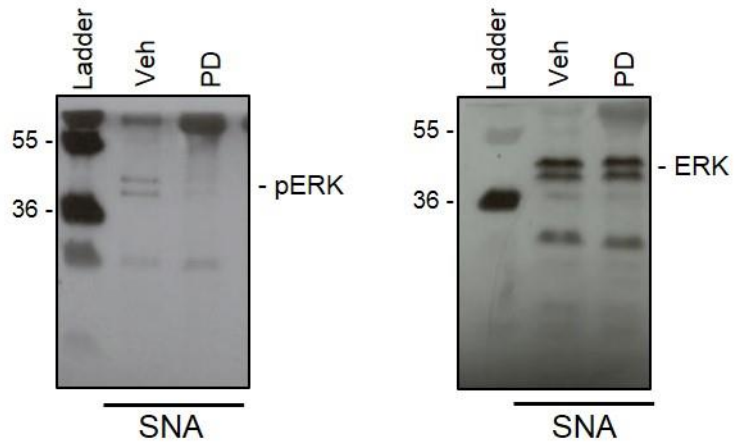
Figure 5i



Supplementary Figure 13 Full scan images of western blot data in Figure 5i

## Supplementary Figure 14

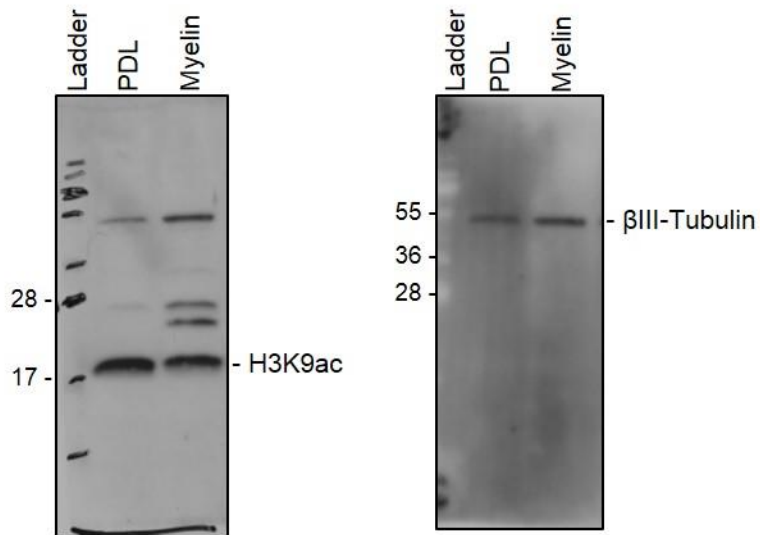
### Figure 6c



Supplementary Figure 14 Full scan images of western blot data in Figure 6c

## Supplementary Figure 15

### Supplemental Figure 7b



Supplementary Figure 15 Full scan images of western blot data in Supplemental Figure 7

## Supplementary Table 1

### Quantitative-RT-PCR Primers

Gene	Forward Primer	Reverse Primer
<b>GAP-43</b>	5'-CTTCTTTACCCTCATCCTGTCG-3'	5'- CAGGAAAGATCCCAAGTCCA-3'
<b>Galanin</b>	5'- GTGACCCTGTCAGCCACTCT -3'	5'- GGTCTCCTTTCCTCCACCTC-3'
<b>BDNF</b>	5'- AGTCTCCAGGACAGCAAAGC-3'	5'- TCGTCAGACCTCTCGAACCT -3'
<b>SCG-10</b>	5'- GCAATGGCCTACAAGGAAAA -3'	5'- GGTGGCTTCAAGATCAGCTC-3'
<b>L1cam</b>	5'-GGGTGAGTGGAATCTGGCTA-3'	5'- TGGCTCTAGCACATGGTGTC-3'
<b>Sprr1a</b>	5'-CCCCTCAACTGTCACTCCAT-3'	5'-CAGGAGCCCTTGAAGATGAG-3'
<b>CAP-23</b>	5'-GGGAGAGAGAGAGCCTTTGC-3'	5'-CTTCGGCCTTCTTGTCTTTG-3'
<b>Lgals</b>	5'-TCAAACCTGGGGAATGTCTC-3'	5'-ATGCACACCTCTGTGATGCT-3'
<b>Chl1</b>	5'-ATTGCGGCTAACAATTCAGG-3'	5'-GAGGGTTGCAGGGTAAGACA-3'
<b>Bcl-xL</b>	5'- CTGGTGGTTGACTTTCTCTCC-3'	5'- CAAGGCTCTAGGTGGTCATTC-3'
<b>18S</b>	5'-CGGCTACCACATCCAAGGAA-3'	5'-GCTGGAATTACCGCGGCT-3'
<b>Dnmt1</b>	5'- GTGGTGTCTGTGAGGTCTGTC-3'	5'- AAGTTAGGACACCTCCTCTTGAG-3'
<b>Dnmt3a</b>	5'- AGGGAGGCTGAGAAGAAAGC-3'	5'- GGCTGCTTTGGTAGCATTCT-3'
<b>Dnmt3b</b>	5'- AGTTTCCGGCTACCAGGTCT-3'	5'- TGTGCTGTCTCCATCTCTGC -3'
<b>RPL13A</b>	5'-CCCTCCACCCTATGACAAGA-3'	5'-CCTTTCCTTCCGTTTCTCC-3'
<b>GAPDH</b>	5'-ACCCTGTTGCTGTAGCCGTATCA-3'	5'- TCAACAGCAACTCCCCTCTCCA-3'
<b>β-actin</b>	5'-GAACGGAACATTGCACACAC-3'	5'-ACAGCTTCACCACCACAGCTGA-3'

## Supplementary Table 2

### ChIP Primers

Gene	Forward Primer	Reverse Primer
<b>GAP-43</b>	5'- CTGCGCGTAAAATCTAATGG-3'	5'- TGGAGAGATTGGATGGAACA-3'
<b>Galanin</b>	5'- TACACCTCCGGTCCTGAGAC-3'	5'- GGTAGGGAAGCTGCAGTCAC-3'
<b>BDNF</b>	5'- GGAGACTAGCGCCGATCTTC-3'	5'- CGAGCCACTAGTTGCCACACA-3'
<b>SCG-10</b>	5'- AAGGAGGCTTCCAGGCTAAG-3'	5'- GCTCAAGCAGATTGGCTCTC-3'
<b>CAP-23</b>	5'-GTCCCCCAACTTCTCTCCAC-3'	5'-GGGCGTGTAAGGAGGGAATA-3'
<b>Sprr1a</b>	5'-TCCCCTAGTTCACCTCTGA-3'	5'-AGGACCACTTCAACCTCCT-3'
<b>Lgals</b>	5'-CTGACTGGTCACCTCTGCTC-3'	5'-CAGTCAGAAGACTCCACCCGA-3'
<b>Ch11</b>	5'-TGTCCCCTTTCGCGGTTTTTC-3'	5'-TGAAGGCTCGATGCCCAAGT-3'
<b>L1cam</b>	5'-GCTGCACCATCCACTCTCTT-3'	5'-TCACGACCATCTTGCTGTCAG-3'
<b>Bcl-xL</b>	5'- CGACATCGAAAGGAAAAAGC -3'	5'-ATCGAGACATGGGAGAGCAG-3'
<b>NF-L</b>	5'-CAGGGAAGTTATGGGGTCT -3'	5'-TTATACGCCGGGACTCTGAC-3'
<b>HSP27</b>	5'-TTGCTCCCAGGAGATACAC-3'	5'-GATTCCCCTGTCGGGTTTA-3'
<b>ATF3</b>	5'-GCTGGTCAAAGAAGGCACAT-3'	5'-ATCTCTCCCTCCGCTAGGTT-3'
<b>18S</b>	5'-GGCCGAACCGGAAGTTATAG-3'	5'-AAGAGAGAGCGGAAGTGACG-3'

## APPENDIX – Calculations of Nutlin-3a mass rate infusion and concentration

The calculation of the concentration of Nutlin-3a to be infused daily was based on the manufacturer instructions, available at [http://www.alzet.com/products/guide\\_to\\_use/formulating.html](http://www.alzet.com/products/guide_to_use/formulating.html). Accordingly, the mass rate of drug infusion is governed mathematically by:

$$K_0 = Q \times C_d,$$

where  $K_0$  = mass delivery rate ( $\mu\text{g/hr}$ ),  $Q$  = volume delivery rate ( $\mu\text{l/hr}$ ) of the solution from the pump,  $C_d$  = concentration ( $\mu\text{g}/\mu\text{l}$ ) of the agent in the vehicle. Considering that for the osmotic pump Alzet model 2002, **Lot.#10285-12<sup>1</sup>**,  $Q = 0,43 \mu\text{l/hr}$  and the mean fill volume is  $242,8 \mu\text{l}$  (considered as **240  $\mu\text{l}$**  for practical purposes); taking also in account that the solubility of Nutlin-3a is **0,1 mg/ml in 1:10 ethanol:PBS** (Catalog#18585, Cayman, USA), then the maximum Nutlin-3a mass ( $m$ ) per pump is:

$$0,1 \frac{\text{mg}}{\text{ml}} = \frac{100 \mu\text{g}}{1000 \mu\text{l}} = \frac{x \mu\text{g}}{240 \mu\text{l}}$$

$$m = 24 \mu\text{g}$$

With **24  $\mu\text{g}$**  of Nutlin per pump:

$$C_d = \frac{24\mu\text{g}}{240\mu\text{l}} = 0,1 \mu\text{g}/\mu\text{l}$$

$$K_0 = 0,43 \frac{\mu\text{l}}{\text{h}} \times 0,1 \frac{\mu\text{g}}{\mu\text{l}} = 0,043 \mu\text{g}/\text{hr}$$

In 24h:

$$0,043 \frac{\mu\text{g}}{\text{h}} \times 24\text{h} = 1,032 \mu\text{g}/\text{day}$$

---

<sup>1</sup>  $Q$  and the **mean fill volume** vary among pumps from different production lots. To rule out variability, I always employed the same lot of pumps for all experimental groups.



Having in account that the pump content diffuses into the cerebrospinal fluid (CSF) of the mouse, we need to consider the total volume of CSF produced daily to determine the concentration of Nutlin-3a that is going to be daily delivered into the CSF. According to the pump manufacturer, the CSF production rate in the mouse is 18  $\mu\text{l}/\text{h}$ , therefore in 24 hours it produces a total of **432  $\mu\text{l}$ . 1,032  $\mu\text{g}$**  of Nutlin-3a (molecular weight = **581,5 g/mol**) in **432  $\mu\text{l}$**  of CSF corresponds to:

$$\text{Concentration} \left( \frac{\text{mol}}{\text{L}} \right) = \frac{\text{mass (g)}}{\text{volume (L)} \times \text{Molecular Weight} \left( \frac{\text{g}}{\text{mol}} \right)}$$

$$\text{Concentration} = \frac{0,001032}{0,000432 \times 581,5}$$

$$\text{Concentration} = 0,0041 \text{ M} \approx \mathbf{4 \mu\text{M}}$$

Because of the limited Nutlin-3a solubility (0,1mg/ml), the maximal concentration we could reach with an osmotic minipump, considered all the available models for mice that deliver for two weeks, was about **4  $\mu\text{M}$  daily**.

Finally, considering that the concentration of Nutlin-3a in the stock solution in pure ethanol is **2mM**, the volume of stock solution to have 24  $\mu\text{g}$  of Nutlin-3a was calculated by:

$$\text{Volume (L)} = \frac{\text{mass (g)}}{\text{Concentration} \left( \frac{\text{mol}}{\text{L}} \right) \times \text{Molecular weight} \left( \frac{\text{g}}{\text{mol}} \right)}$$

$$\text{Volume} = \frac{0,000024}{0,002 \times 581,5}$$

$$\text{Volume} = 0,0000206 \text{ L} = \mathbf{20,6 \mu\text{L}}$$

Therefore, 20,6  $\mu\text{l}$  Nutlin-3a in pure ethanol were diluted in 240  $\mu\text{l}$  PBS or **8,6% ethanol/PBS**.

## AKNOWLEDGMENTS

A dream can be dreamed alone, but it is only possible to realize it with the help and support of others. Many people were involved to make this dream reality. And I would like sincerely to thank all of you.

I am very grateful for my advisor Prof. Simone Di Giovanni, who gave me the opportunity to work and grow in his team, for sharing his knowledge, providing support and direction. I am also thankful to Dr. Radhika Puttagunta, who has always been very supportive and worked with me during all this period. Moreover, I want to express my gratitude to the DAAD, who granted me with a full scholarship for doctoral studies in Germany, and recommended me to attend the "64<sup>th</sup> Lindau Nobel Laureate Meeting", which was a singular and remarkable opportunity.

Furthermore, I would like to thank Prof. Burkhard Schlosshauer and PD Dr. Andrea Wizenmann, members of my Advisory Board Committee, for your attention and insightful advices. I am also grateful for the support of Prof. Horst Herbert and Dr. Tina Lampe from the Graduate Training Centre of Neuroscience, who have always been willing to help.

I would like to take this opportunity to thank all my colleagues for your friendship, support and the willingness to share your knowledge with me.

I also cannot forget to mention all my friends, the old and the new, and thank them for caring and cheering.

Very specially, I would like to thank Alexander and his family for the patience, care, encouragement and support.

At last but not least, I dedicate this thesis to my parents Nuelita and Miguel and my brother Felipe, who believed in my dream, never measured efforts to support me and have been decisive in all the steps of this endeavor.

Marília Grando Sória

---

## MARÍLIA GRANDO SÓRIA, M.D.

mgsoria@gmail.com

Tübingen Germany

### EDUCATION

- 2011 - current      Ph.D. Student, Hertie Institute for Clinical Brain Research, University Eberhard-Karls of Tübingen, Germany.  
Thesis title: **Promoting Regeneration and Functional Recovery following SCI through Transcriptional Regulation.** Supervisor: Prof. Dr. Simone Di Giovanni.
- 2003 - 2009      Graduation in Medicine, Federal University of Paraná (Universidade Federal do Paraná – UFPR), Curitiba, Brazil.

### EXPERIENCE

- 06/2011 – 08/2015      **Neuroscientist, University Eberhard-Karls of Tübingen, Germany**
- Designed *in vitro* and *in vivo* studies.
  - Optimized and performed a high-skilled microsurgical technique to implant an osmotic minipump/intrathecal catheter system in mice.
  - Designed and established an animal care protocol for spinal cord-injured mice according to the guidelines of the SCITP (Ohio State University, 2012) that increased the survival of mice up to 100% after surgeries.
  - Optimized immunohistochemistry protocols.
  - Created a protocol for nuclear fluorescence quantification of dorsal root ganglia.
  - Trained Ph.D. and M.Sc. students in animal surgery and handling, behavior assessments, immunohistochemistry and imaging analysis.
- 08/2003 - 07/2009      **Medical Student**
- 01/2009 - 04/2009      ○ Internship in Neurosurgery, University Eberhard-Karls of Tübingen, Germany; supervision of Prof. Marcos Soares Tatagiba, M.D., Ph.D.  
*Attended interdisciplinary meetings, visited patients with the medical team, assisted surgeries, participated in academic activities.*
- 06/2005 - 06/2009      ○ Internship in Neurology and Neurosurgery, *Instituto de Neurologia de Curitiba* (INC), Brazil; supervision of Prof. Ricardo Ramina, M.D., Ph.D.  
*Attended interdisciplinary meetings, visited patients with the medical team, helped residents with clinical work, assisted surgeries, participated in academic activities.*
- 08/2004 - 02/2005      ○ Internship in Neuroanatomy, Federal University of Paraná; supervision of Prof. Murilo Sousa de Meneses, M.D., Ph.D.  
*Prepared expository lectures with human brain and spinal cord cadaveric specimens and taught Neuroanatomy to medical students.*

## SKILL SET

- **Research *in vivo*:** rodent microsurgeries (spinal cord injury, sciatic nerve injury, pudendal nerve injury, stereotaxic injections), animal handling, locomotion assessments (BBB, BMS, Catwalk and grid walk).
- **Research *in vitro*:** cell culture and drug assays.
- **Basic research techniques:** *post-mortem* dissection, histology, immunoblotting, qRT-PCR, bright field and fluorescence microscopy, stereology.
- Experimental design, planning and execution.
- Team coordination, support and collaboration.
- Anatomical illustration.
- **Softwares:** MS Office, Fiji (Image J), AxioVision, Stereo Investigator, Ingenuity Pathway Analysis, GraphPad Prism, Adobe Illustrator, Adobe Photoshop.
- **Operational systems:** Mac OS X and Windows.

## AWARDS

- 2014 Participation at the 64<sup>th</sup> Lindau Nobel Laureate Meeting, Lindau, Germany.
- 2011 Full scholarship for doctoral studies from the German Academic Exchange Service (DAAD).

## CERTIFICATIONS

- 2012 Rodent spinal cord injury research. NINDS-funded Spinal Cord Injury Training Program (SCITP), The Ohio State University College of Medicine, Columbus, USA.
- 2009 First Instructional Spine Course Tübingen. Certified by the Department of Neurosurgery, University Eberhard-Karls of Tübingen, Germany.

## LECTURE

- 2011 Cell Therapy in Spinal Cord Injury In: „Cell Therapy: Facts and Fantasy“ course for the Molecular Medicine Master students, University Albert-Ludwig of Freiburg, Germany.

## CONFERENCE PRESENTATIONS

- 2015 Invited to share my impressions on the 64<sup>th</sup> Lindau Nobel Laureate Meeting at the *Deutscher StiftungsTag 2015*, Karlsruhe, Germany.
- 2014 Sória MG. Modulation of the ubiquitin ligase MDM2 promotes functional recovery after spinal cord injury in mice In: Master Class „Biology in the Service of Medicine“, moderated by Nobel Laureate Prof. Aaron Ciechanover, 64<sup>th</sup> Lindau Nobel Laureate Meeting, Lindau, Germany.
- 2009 Sória MG, Feigl GC, Pereira CU, Tatagiba MS. Facial Nerve Reconstruction after Vestibular and Facial Schwannoma Resection: Technical Report of Facial-Sural Anastomosis In: *XIII Congresso da Academia Brasileira de Neurocirurgia*, Curitiba, Brazil.

## SELECTED PUBLICATIONS

Joshi Y\*, **Sória MG\***, Quadrato G, Inak G, Zhou L, Hervera A, Rathore KI, Elnaggar M, Magali C, Marine JC, Puttagunta R, Di Giovanni S. The MDM4/MDM2-p53-IGF1 axis controls axonal regeneration, sprouting and functional recovery after CNS injury. *Brain* 138(Pt 7):1843-1862, 2015.

\* These authors contributed equally to this work.

Puttagunta R<sup>§</sup>, Tedeschi A<sup>§</sup>, **Sória MG**, Hervera A, Lindner R, Rathore KI, Gaub P, Joshi Y, Nguyen T, Schmandke A, Laskowski CJ, Boutillier AL, Bradke F, Di Giovanni S. PCAF-dependent epigenetic changes promote axonal regeneration in the central nervous system. *Nat Commun* 5:3527, 2014.

§ These authors contributed equally to this work.

Puttagunta R, Tedeschi A, **Sória MG**, Lindner R, Hervera A,, Rathore K, Gaub P, Joshi Y, Bradke F, Di Giovanni S. PCAF-dependent epigenetic changes promote axonal regeneration in the central nervous system. 831.22/LL1, Annual Meeting of the Society for Neuroscience, San Diego (USA), 2013.

Joshi Y, Quadrato G, Inak G, **Sória MG\***, Puttagunta R, Rathore K, Wuttke A, Elnaggar M, Marine JC, Di Giovanni S. Modulation of MDM4/MDM2 signaling promotes axonal regeneration in the CNS. 341.15/AA2, Annual Meeting of the Society for Neuroscience, San Diego (USA), 2013.

Lepski G, Honegger J, Liebsch M, **Sória MG**, Narischat P, Ramina KF, Nägele T, Ernemann U, Tatagiba M. Safe resection of arteriovenous malformations in eloquent motor areas aided by functional imaging and intraoperative monitoring. *Neurosurgery* 70(2 Suppl Operative):276-288, 2012.

Munhoz RP, Kowacs PA, **Sória MG**, Ducci RD, Raskin S, Teive HA. Catamenial and oral contraceptive-induced exacerbation of chorea in chorea-acanthocytosis: case report. *Mov Disord* 24:2166-2167, 2009.

Almeida DB, Mattei TA, **Sória MG**, Prandini MN, Leal AG, Milano JB, Ramina R. Transitional lumbosacral vertebrae and low back pain: diagnostic pitfalls and management of Bertolotti's syndrome. *Arq Neuropsiquiatr* 67:268-272, 2009.

Ramina R, Mattei TA, **Sória MG**, da Silva EB Jr, Leal AG, Neto MC, Fernandes YB. Surgical management of trigeminal schwannomas. *Neurosurg Focus* 25:E6, 2008.

## LANGUAGE SKILLS

Portuguese	Mother tongue
English	Fluent
German	Advanced
Spanish	Advanced
Italian	Intermediary